Thesis for the Degree of Doctor of Philosophy

Adaptive model-based battery management

Predicting energy and power capability

Björn Fridholm

Department of Electrical Engineering
Chalmers University of Technology
Göteborg, Sweden 2019

Adaptive model-based battery management
Predicting energy and power capability
Björn Fridholm
ISBN: 978-91-7905-119-8

Doktorsavhandlingar vid Chalmers tekniska högskola
Ny serie nr 4586
ISSN 0346-718X

Department of Electrical Engineering
Chalmers University of Technology
SE–412 96 Göteborg
Sweden

Telephone: +46 (0)31 – 772 1000

Typeset by the author using LaTeX.

Chalmers Reproservice
Göteborg, Sweden 2019

With all my love to Jarl and Elin

Abstract

The battery is the limiting system for automotive electrification due to cost, size, and uncertain degradation. To be competitive the battery must therefore be used optimally. This thesis address the on-line battery management problem, with primary objectives to (i) enable optimal usage of the battery by providing accurate estimates of its power and energy capability, while (ii) ensuring durability by keeping the battery inside predefined operating limits at all times. This means translating measurable information of current, voltage, and temperature into cell related quantities such as state-of-charge (SOC) and state-of health (SOH), and vehicle related quantities such as power capability and available energy.

The main difficulty of battery management is that battery cells have complex, non-linear dynamics that changes with both operating conditions, usage history, and age. This thesis and the appended papers proposes a system of adaptive algorithms for on-line battery estimation. Several aspects are considered, from modelling and parameter estimation to estimation of SOC, energy, and power. Recursive algorithms are proposed for estimation of parameters and SOC, while power and energy are estimated using algebraic expressions derived from equivalent circuit battery models. The algorithms are evaluated on lithium-ion battery cell data collected laboratory tests. For the cell chemistries considered, the evaluation indicates that accuracy within 2% can be achieved for both SOC and power, also in cases with limited prior information about the cell.

Keywords: Battery management, lithium-ion batteries, state estimation, parameter estimation, state-of-charge estimation.

Acknowledgements

I started this journey back in 2012, which means that I have been a PhD student for most of my sons life. I have tried to keep the research out of my private life, but that is of course not always possible and therefore, my first thanks goes to my family and friends. The academic work could not have been done without the help of my main supervisor Prof. Torsten Wik, who is not only an excellent researcher but also a fantastic person. Thank you for all the support and interesting discussions! On the industrial side Hannes Veen provided me with many relevant topics and several of the appended papers are direct results of our discussions. As a new researcher the help from my co-supervisor Magnus Nilsson was invaluable. Other important collaborators that deserves special mention are Anton Klintberg, Changfu Zou, Marcus Hedegärd, and Faisal Altaf. Thank you for the discussions, input, and support! There were also more people who influenced this work than can be mentioned here, and therefore I direct a huge thanks to all my friends and colleagues at Volvo Cars, Chalmers, AB Volvo, and RISE Viktoria. Finally the financial support from Energimyndigheten, Volvo Cars, AB Volvo, and Intertek is greatly appreciated.

Björn Fridholm
Göteborg, May 2019

List of publications

This thesis is based on the following appended papers:

Paper 1

B. Fridholm, M. Nilsson and T. Wik, "Robustness comparison of battery state of charge observers for automotive applications", *19th IFAC World Congress 2014*, August 2014, Cape Town, South Africa.

Paper 2

B. Fridholm, T. Wik, and M. Nilsson, "Kalman filter for adaptive learning of look-up tables with application to battery ohmic resistance estimation", *Control Engineering Practice*, 48, 2016.

Paper 3

B. Fridholm, T. Wik, and M. Nilsson, "Robust recursive impedance estimation for automotive lithium-ion batteries", *Journal of Power Sources*, 304, 2016.

Paper 4

B. Fridholm, T. Wik, H. Kuusisto, and A. Klintberg, "Estimating power capability of aged lithium-ion batteries in presence of communication delays", *Journal of Power Sources*, 383, 2018.

Paper 5

B. Fridholm, T. Wik, C. Zou, and A. Klintberg, "Long-term voltage prediction for lithium-ion batteries using an extended equivalent circuit model and moving horizon estimation", *Submitted for publication in Journal of Power Sources.*

Paper 6

B. Fridholm, M. Hedegärd, and T. Wik, "An analytic estimate of available battery energy considering thermal effects", *Submitted for publication in Journal of Power Sources*.

Other publications

In addition to the appended papers, the following papers by the thesis author are also related to the topic of the thesis:

T. Wik, **B. Fridholm**, and H. Kuusisto, "Implementation and robustness of an analytically based battery state of power", *Journal of Power Sources*, 287, 2015.

A. Klintberg, T. Wik, and **B. Fridholm**, "Theoretical bounds on the accuracy of state and parameter estimation for batteries", *Proceedings of the American Control Conference 2017*, May 2017, Seattle, USA.

A. Klintberg, E. Klintberg, **B. Fridholm**, H. Kuusisto, and T. Wik, "Statistical modeling of OCV-curves for aged battery cells", *Proceedings of the IFAC World Congress 2017*, July 2017, Toulouse, France.

C. Zou, A. Klintberg, Z. Wei, **B. Fridholm**, T. Wik, and B. Egardt, "Power capability prediction for lithium-ion batteries using economic nonlinear model predictive control", *Journal of Power Sources*, 396, 2018.

H. Ekström, **B. Fridholm**, and G. Lindbergh, "Comparison of lumped diffusion models for voltage prediction of a lithium-ion battery cell during dynamic loads", *Journal of Power Sources*, 402, 2018.

A. Klintberg, C. Zou, **B. Fridholm**, and T. Wik, "Kalman filter for adaptive learning of two-dimensional look-up tables applied to OCV-curves for aged battery cells", *Control Engineering Practice*, 84, 2019.

Contents

Part I

Introductory Chapters

Chapter 1

Introduction

Batteries are passive systems and it is therefore easy to dismiss the problem of battery management as being trivial from an automatic control perspective. In fact, to develop a fully functioning battery management system is not that complex as long as the battery is operated well within its performance limits. Still, this thesis is centred around the deceptively simple question:

Question 1. *How much power and energy can the battery pack deliver without violating cell level constraints?*

As will be seen, however, this becomes a quite complex question once you scratch the surface.

1.1 Motivation and scope

Market analysts predicts a boom in sales for electric vehicles (EVs) in the coming years [1]. As an example, Volvo Car Corporation has announced that all their vehicles will be electrified from 2019, either as hybrid electric vehicles (HEV), plug-in hybrids (PHEV) or fully battery electric vehicles (BEV). This increase in sales is fuelled by legislations and incentives by governments, improved performance, and reduced cost of batteries.

Despite the rapid increase in battery performance in recent years [2], the battery system is still limiting for electrification in terms of:

- **Cost**: The battery is by far the most expensive system of an EV. Analysts estimate that the battery contributes to almost half of the production cost of Tesla Model S [3]. While costs are expected to decrease, a rapid increase in volumes may affect supply and thereby impact profit margins of the vehicle manufacturers [2, 4].

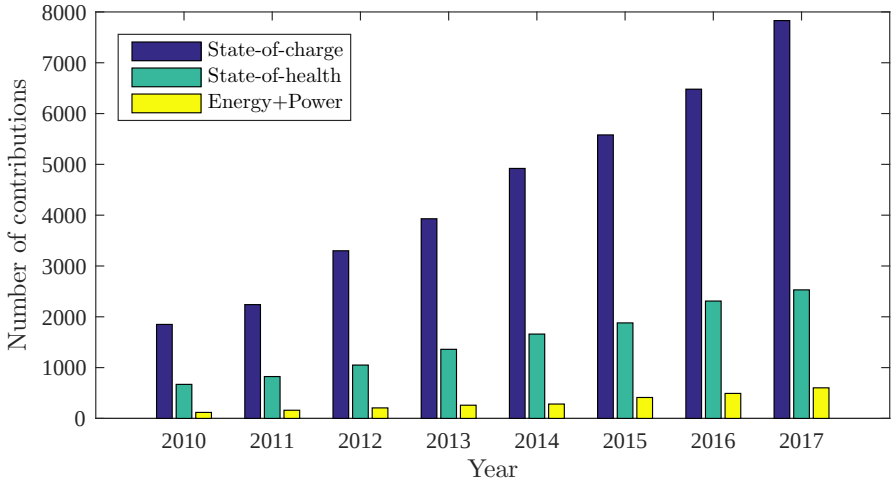

Figure 1.1: Number of contributions to the field of battery management per year according to Google Scholar. The bars for Energy+power combines several search-terms. This is by no means a thorough investigation, but still gives a clear indication as to where the main focus of battery management is within the academic field.

- **Size and weight**: On pack level the energy density is typically below 150–200Wh/l and 100–150Wh/kg, which means that the battery for a 500 km range BEV containing around 80kWh can have a volume of over 300l and weigh more than 500kg.
- **Life-time**: Batteries may degrade faster than intended if they are used too aggressively, which is a major concern for both customers and vehicle manufacturers.

This signifies the importance of using the installed battery capacity as much as possible while addressing the trade-off between short-term performance and long-term degradation.

In the academic community battery management has been more or less synonymous with state-of-charge estimation, as indicated in Figure 1.1, which shows the number of results in a Google Scholar search using different keywords related to battery management. The aim of this thesis is to widen the scope according to Question 1, which can be illustrated as in Figure 1.2. Without going into details of the internal workings of lithium-ion batteries, they need to be operated in some safe region to avoid side-reactions that lead to accelerated degradation. The boundary of the safe operating region, i.e. when side-reactions start, depends on internal dynamics that are not measurable on production-ready cells. In fact, even in laboratory conditions, specially prepared three-electrode cells are needed to get cell internal

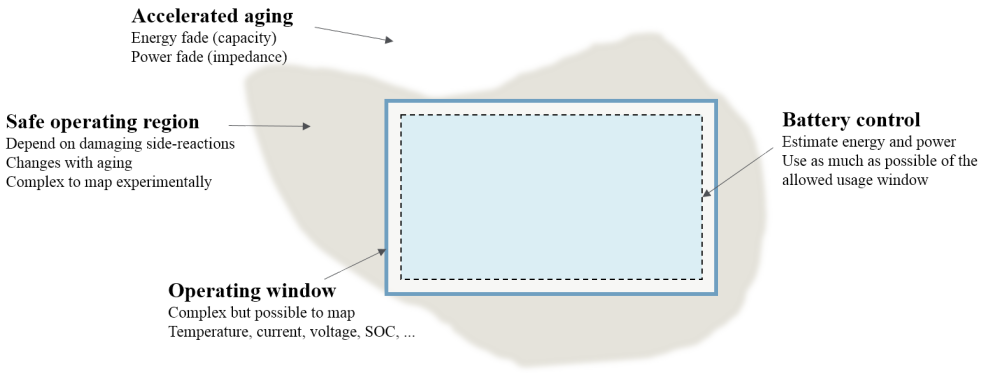

Figure 1.2: A highly simplified view on battery control.

measurements (see e.g. [5]). To handle this problem, an operating window can be defined in terms of measurable quantities (current, voltage, and temperature) together with some estimated quantities such as state-of-charge (SOC). This constrains the battery cell to be in the safe region, but the operating window is still described in terms of cell related quantities. The vehicle on the other hand needs information about the energy and power that the pack can deliver, and the battery management system (BMS) must therefore understand how all these quantities are related. Question 1 can thereby be broken down into two main problems:

Problem 1. *Ensure durability of the battery by keeping operation inside the operating window at all times.*

Problem 2. *Enable optimal usage of the battery for other controllers of the vehicle by providing accurate estimates of power and energy capability of the battery.*

There are several impacts of poor estimates. In terms of energy capability, the accuracy is directly related to range prediction. The main issues are, however, found on the shorter time-scales where over-estimating the power capability can lead to accelerated degradation if cells are used outside the usage window, or to poor drivability if power is suddenly reduced to stay inside (or get back into) the operating window. Under-estimating the power capability can on the other hand lead to poor performance since the potential performance is not utilized.

The difficulty in estimating power and energy capability is that battery cells have complex and non-linear dynamics that change with both operating conditions and age. This means that the models must handle changes on several time-scales, from milliseconds to years. Many unmeasurable internal states of the cells are needed, such as SOC, concentration gradients (or

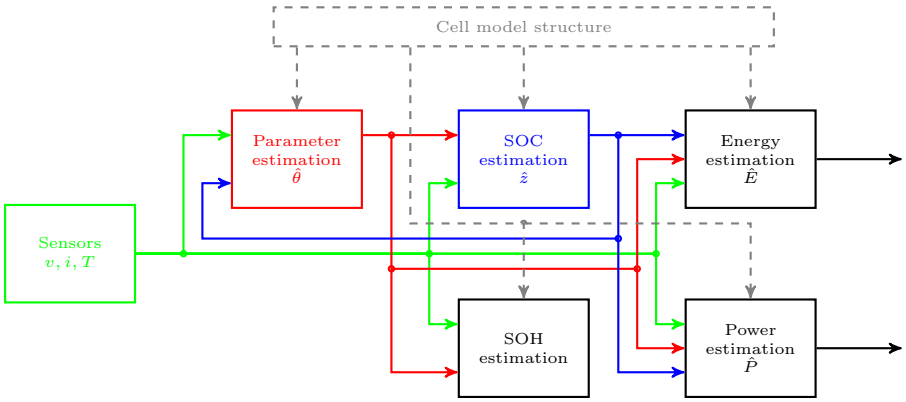

Figure 1.3: Overview of the adaptive estimation system investigated in the thesis. The choice of model structure impacts all algorithms which is indicated by grey arrows.

polarization voltages), and state-of-health (SOH). Furthermore, automotive battery packs are complex systems containing hundreds of cells (all needing individual monitoring), cooling system, cabling, etc. (see Section 2.3), and therefore computationally efficient algorithms are needed.

The scope of this thesis is to investigate the problem of tracking battery capability on-line in the BMS. Several aspects of the resulting estimation problem are covered with focus on robust algorithms that can be implemented on typical automotive control units.

1.2 Contributions

An overview of the set-up investigated in the thesis is illustrated in Figure 1.3. In itself this is not an outcome of the thesis; several others have proposed similar set-ups (see e.g. [6, 7, 8]). However, there are novel contributions to each part of this system of algorithms, as described in the following.

Cell model structure

All proposed algorithms for battery estimation are based on a cell model that relates the current and voltage of the cell to each other. Since the algorithms are to be run on-line in the BMS, the model structure needs to be fairly simple (i.e. few states). Most of this work is based on equivalent circuits (which is the most common model structure for BMS found in the literature). However, one contribution to battery modelling is found in Paper 5, where an extension to the equivalent circuit to improve volt-

age prediction at low temperatures and high discharge power operation is proposed.

Parameter estimation

The characteristics of the battery changes with operating conditions and to maintain accuracy of the battery model, its parameters must be updated during operation. Since the battery model contains both static (purely resistive) and dynamic parts, for which the excitation conditions are quite different, the accuracy of the parameter estimation is improved by separating the estimation task into different algorithms, as described in Paper 3. The resistance of the cell is then estimated using a recursive least-squares algorithm, while the parameters for the dynamics are estimated using an adaptive Kalman filter.

SOC estimation

Tracking SOC on-line is one of the most covered topics of battery management in the literature. There are two contributions to this in the thesis. The first is found in Paper 1, where three different algorithms are compared to assess their accuracy and robustness for SOC estimation. The main result is that the best choice of algorithm depends on both cell characteristics and intended vehicle application. The second contribution is found in Chapter 5 where an extended Kalman filter from Paper 1 is combined with the parameter estimation from Paper 3 and tested on experimental laboratory cell data. The results show that SOC can be estimated to an accuracy within 2% also with very limited prior knowledge of the cell.

SOH estimation

Estimating SOH is also well covered in the literature. It is often calculated as a reduction in capacity and/or increase of resistance of the cell. The thesis contribution to this area, found in Paper 2, proposes a novel application of the Kalman filter to update look-up tables also in areas of the table not being visited. This way changes of battery resistance due to ageing can be separated from changes due to operating conditions (temperature, SOC, etc.).

Power estimation

Power capability estimation is important for vehicle operation. There are two contributions to this in the thesis, both found in Paper 4. Firstly, a

thorough validation of an adaptive power estimation algorithm is performed on aged cells in a wide temperature range. Secondly, power estimation turns into a closed-loop controller of the battery power when the cell is operated at the limit of its capability. An analysis of the robustness of this closed-loop shows that time-delays in the controller network may cause the power limitation algorithm to become unstable if the bandwidth of the closed-loop is not constrained.

Energy estimation

Energy estimation is important for range predictions of the vehicle. The thesis contribution here is a novel analytic expression of available energy that considers the thermal trajectory of the battery pack during discharge, which is presented in Paper 6.

1.3 Outline

Part I of this thesis serves as an introduction and provides background information on adaptive battery management. Chapter 2 presents the automotive battery system, and its most important components. Chapter 3 gives an overview of methods and theory used throughout the thesis work. In Chapter 4 the most common ways of modelling lithium-ion batteries are presented. Chapter 5 presents the adaptive battery state estimation problem. Chapter 6 discuss how to translate the state information to predictions/estimations of the battery capability. Chapter 7 summarizes the appended papers, and finally, Chapter 8 closes Part I with concluding remarks and possible future research directions. Part II contains full text versions of the papers that this thesis is based on.

Chapter 2

Automotive battery systems

This chapter provides an introduction to automotive battery systems.

2.1 Definitions

There are several measures, parameters, and states referred to both in this thesis and in battery management literature in general. Many of them are also used in slightly different form in cell related research, which can cause confusion. Therefore, their use in the context of this work is defined here.

Definition 1. *The current (i) is positive for charging and negative for discharging.*

Definition 2. *The **operating window** ($\mathcal{W}$) is the region where the cell is allowed to be used, described in terms of measurable (current, voltage, temperature) and estimated (SOC, power, energy) quantities.*

Definition 3. *The **C-rate** is the current scaled to the capacity of the cell such that a current of 1C will (dis)charge the cell in one hour.*

Definition 4. *The **open-circuit voltage** (v_{oc}) is the equilibrium voltage of a cell.*

Definition 5. *A cell is **fully charged** when $v_{\mathrm{oc}} = V_{\max}$.*

Definition 6. *A cell is **fully discharged** when $v_{\mathrm{oc}} = V_{\min}$.*

Definition 7. *A cell is **1C discharged** when the terminal voltage $v_{\mathrm{cell}} = V_{\min}$ with 1C constant current discharge.*

Definition 8. *The **nominal capacity** (Q_{nom}) of the cell is the number of ampere-hours between a fully charged and a fully discharged cell.*

Definition 9. *The **1C capacity** (Q_{1C}) of the cell is the number of ampere-hours between a fully charged and a 1C discharged cell.*

Remark. Q_{1C} is popular for cell characterization since it approximates the usable capacity in different operating conditions. For on-line BMS applications, Q_{nom} is preferable since it is approximately constant for all operating conditions, but changes with age.

Definition 10. *The **state-of-charge** (z) is the ratio of remaining capacity to the nominal capacity of the cell.*

Definition 11. *The **nominal energy** (E_{nom}) is the energy stored in the cell.*

Definition 12. *The **available energy** (E_{avail}) is the energy in the cell that can be used.*

Definition 13. *The **available charge power** (P_{max}) is the maximum power that can be charged into the cell without violating constraints set by the cell usage window.*

Definition 14. *The **available discharge power** (P_{min}) is the maximum power that can be discharged from the cell without violating constraints set by the cell usage window.*

2.2 Lithium-ion cells

Lithium-ion cells are currently the dominating battery type in the automotive industry [9]. There are several combinations of materials used to tailor the cell to different requirements, such as energy content, power capability, or life-time. This section summarizes some common characteristics of lithium-ion batteries.

2.2.1 Working principles of lithium-ion batteries

Lithium-ion cells consists of four basic parts; positive and negative electrodes, a separator, and electrolyte (see Figure 2.1). The negative electrode is most often of graphite, while the positive electrode can be of different materials. The separator is electrically insulating while letting lithium-ions through.

When the cell is discharged, lithium-ions leave the negative electrode and enters the positive electrode by a process called intercalation. At the same time, electrons move in an outer circuit producing electric work. Charging

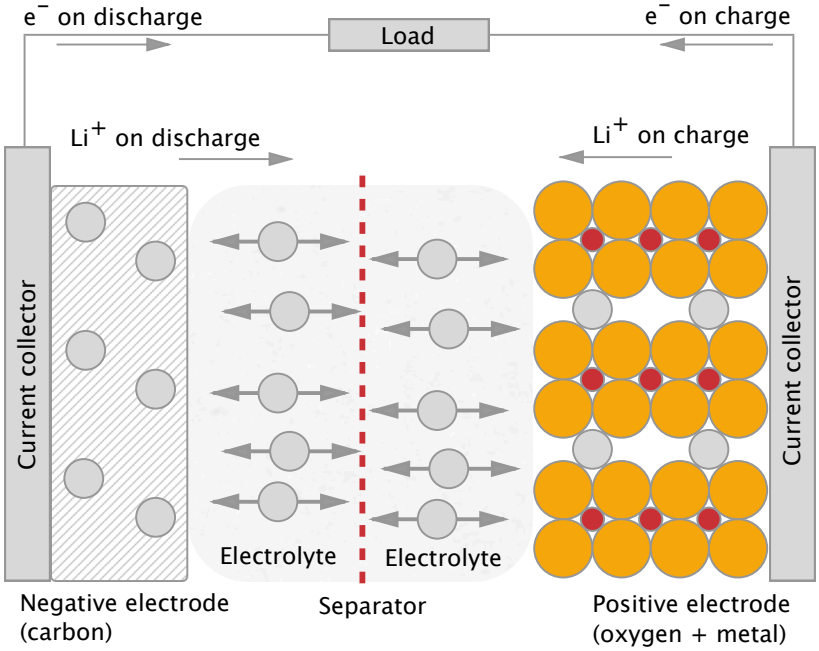

Figure 2.1: Schematic view of a lithium-ion cell.

reverses the process. Most of the work in the thesis uses a cell of lithium nickel manganese cobalt oxide (NMC) type, for which the negative electrode reaction is

$$\mathrm{LiC_6} \rightleftharpoons \mathrm{C_6} + \mathrm{Li^+} + e^-,$$

while the positive electrode reaction is

$$\mathrm{Ni_{1/3}Mn_{1/3}Co_{1/3}O_2} + \mathrm{Li^+} + e^- \rightleftharpoons \mathrm{LiNi_{1/3}Mn_{1/3}Co_{1/3}O_{1/3}}.$$

Remark. In Paper 1 also a lithium iron phosphate (LFP) cell is used.

The energy of the cell depends on the difference between the energy states of the lithium intercalated in the positive and negative electrode. At rest these potentials are called open circuit potentials (OCP) and gives rise to a potential difference referred to as the open circuit voltage (OCV). During use, the voltage depends on concentration gradients built up inside the cell, caused primarily by diffusion in the solid particles, charge transfer resistance, and mass transport in the electrolyte. For more details on battery electro-chemistry, see [10, 11, 12].

2.2.2 Ageing

Apart from the main process of moving lithium-ions between the electrodes, there are unwanted parasitic side-reactions that can occur inside the cell.

Table 2.1: Summary of important ageing factors of lithium-ion batteries with carbon based anode [16].

Ageing mechanism	**Enhanced by**	**Result**
Growth of solid electrolyte interface (SEI), changes in surface porosity	low SOC, high C-rate	impedance increase
Loss of active surface	high temperature, high SOC	impedance increase
Electrode and binder dissolution	high temperature, high SOC	impedance increase, capacity loss
Lithium plating	low temperature, high C-rate	impedance increase, capacity loss
Active mass particles loss of contact	low SOC, high C-rate	capacity loss
Cracking of graphite	over-charging	capacity loss
Conductor corrosion	over-discharging, low SOC	impedance increase

The occurrence and rate of these side-reactions depend on internal dynamics that by existing technology are not measurable on production-ready cells. Experimental studies of these have to be conducted using cells with reference electrodes or on "half cells" [5]. Side-reactions do not originate from one single cause, but from a number of various processes and their interactions [13, 14, 15]. Some general ageing mechanisms, common to most lithium-ion battery chemistries with graphite negative electrodes, are listed in Table 2.1 (see [16] for details).

On cell level, the effect of degradation is normally described in terms of capacity loss and impedance increase. For the vehicle, this translates to energy fade (i.e. reduced range), power fade due to increased losses, and increased heat generation (thus requiring more cooling).

2.2.3 Current–voltage characteristics

Since the important internal dynamics are not directly measurable in normal battery management applications, it is important to relate the existing measurement information to the states of the cell. The most fundamental relationship is that between current and voltage, and all models and algorithms described in later chapters rely on this.

Different chemical compositions of lithium-ion batteries affect details in their characteristics. However, for the chemistries considered here, the current–voltage response can be divided into equilibrium and transient re-

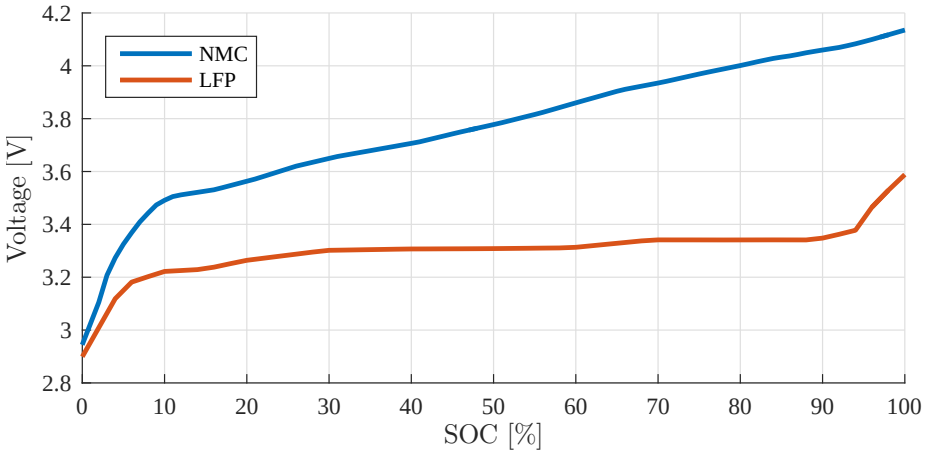

Figure 2.2: Open circuit voltage as a function of SOC for an NMC and an LFP cell.

sponse. For some chemistries hysteresis effects must be considered.

Equilibrium voltage

The equilibrium voltage of the cell at rest (v_{oc}), often referred to as open circuit voltage (OCV), is related to SOC by

$$v_{\text{oc}}(t) = h_{\text{ocv}}(z(t)), \tag{2.1}$$

where $h_{\text{ocv}} : \mathbf{R} \to \mathbf{R}$ is a non-linear function that maps SOC (z) to OCV (see Figure 2.2).

There are slight variations in the OCV depending on temperature [17], but this effect was tested to be very small on the cells used in this work and is therefore neglected (see Figure 2.3). The OCV also changes with degradation since ageing effects normally are not equal on both electrodes [18].

Transient voltage response

When current is fed through the cell its voltage differs from equilibrium due to electrical resistance and concentration gradients. There are two main chemical processes that determine the dynamic voltage response of lithium-ion batteries; diffusion and double-layer effects [19]. Diffusion is caused by concentration gradients within the cell. It is a slow effect, typically on the time-scale of seconds to minutes. The double-layer effects are faster (typically below 1s) and comes from charge zones that are created between the electrode and electrolyte and have a behaviour similar to a capacitance.

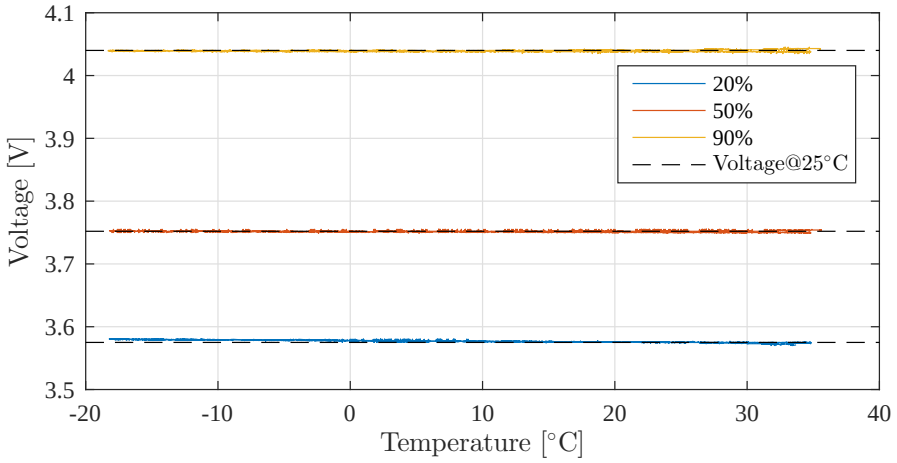

Figure 2.3: Voltage at constant SOC levels when sweeping the temperature of an NMC cell. Temperature dependency of the OCV manifests as a change in voltage during the sweep. The maximum change observed here is for 20% SOC where the maximum difference is around 5mV, which corresponds to less than 0.5% in SOC, and was therefore considered negligible.

The double-layer effect occurs in parallel to the charge transfer resistance. There are also even faster dynamics caused by electric and magnetic effects. However, these occur on a millisecond time-scale, which means that for a BMS application they can be regarded as purely resistive losses. Figure 2.4 displays a typical voltage response to a current pulse.

Hysteresis

Hysteresis is to a varying degree present in all types of lithium-ion chemistries, and its main causes are strain and thermodynamic effects [20]. The consequence is that the OCV at the same SOC will be different depending on if it was reached after charging or discharging. The asymptotic OCV is typically higher if the cell has been charged than if it has been discharged. Results from [21] indicate that hysteresis is a difficult phenomenon to model. Plett, [22], models hysteresis using a dynamic system in SOC, while Tang et al., [23], indicates that the hysteresis converges to its boundaries quickly enough to be modelled as a two-state switch. The lack of consensus in the literature may be related to the fact that it is hard to measure the dynamic behaviour of the hysteresis, since even small currents also triggers other dynamic effects. Hysteresis is mainly important to model if its size is large compared to the derivative of the OCV curve, since it will then have a significant impact on SOC estimation. Based on the OCV curves in Figure 2.2 it can

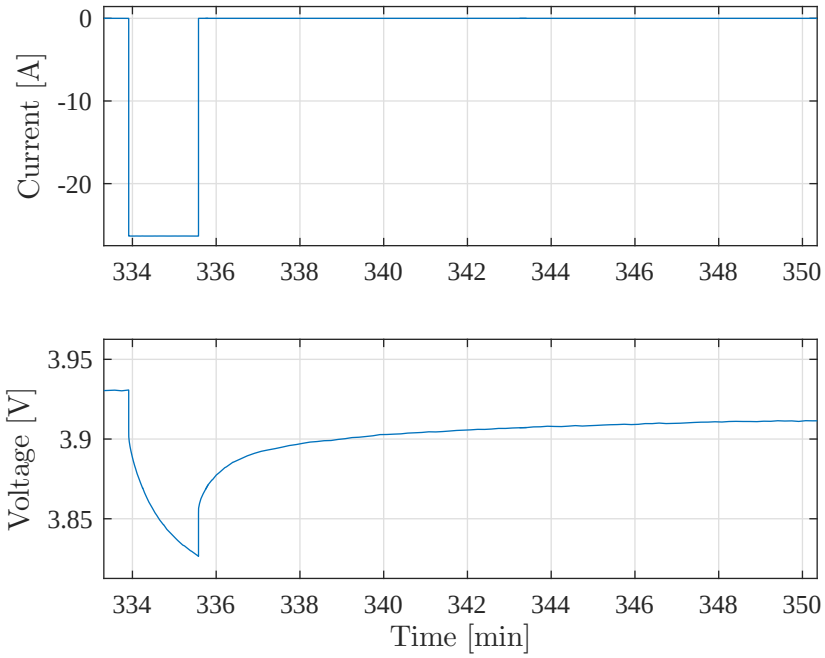

Figure 2.4: Voltage response to a current discharge pulse on an NMC cell.

be assumed that hysteresis modelling is more important for the LFP cell than for the NMC cell.

For the NMC cells used in this work, hysteresis was small and therefore did not need to be considered in the models.

2.3 Automotive battery packs

An automotive battery pack is a complex system [24, 25, 26]. Apart from the battery cells and sensors, the pack must also contain cooling, cabling, insulation, and a protective enclosure (see Figure 2.5). While the power and/or energy capability of the pack is often discussed, many more considerations are required when designing a battery pack for series production. Some examples are design of the mechanical construction to handle crash safety, high-voltage electrical distribution to handle high currents, low-voltage sensors with sufficient accuracy, a thermal system to keep the cells within specified temperatures, and so on.

The nominal pack voltage is typically around 400V for passenger cars, which means that around 100 battery cells must be placed in series. Depending on which cell is chosen, there might be a need to have more energy in the pack than what 100 series connected cells provide. Then several cells

may be placed in parallel to increase the pack energy without changing the nominal voltage. An extreme example of this is Tesla that uses over 40 cells in parallel to reach the required energy levels. To handle flexibility and to simplify production and service, the cells are built into modules. All manufacturers uses different configurations and the choice is primarily a trade-off between flexibility and over-head in terms of weight, volume, and material cost.

A cooling system is normally used to keep the cells in their preferred temperature range. These can be either based on cooling using ambient air directly, or by a liquid system where water is cooled using either ambient air or an AC compressor. In some systems, particularly for battery electric vehicles, the liquid cooling system can also be used to heat the battery in cold temperatures. Both systems using heat generated from other components of the vehicle, such as electric machines, or systems with dedicated heaters are used.

The SOC of the cells of the battery pack may slowly drift unevenly due to current leakages in the electrical system, uneven ageing, production variability causing differences in self discharge, etc. Since the series connected cells will then reach their fully charged state at different times, and since the system is limited by the cell that first becomes fully charged, this will limit the available energy of the pack. To remedy this, the cells can normally be balanced individually. The most common solution is that each cell can be discharged with a small current to reduce its SOC. This balancing method has the drawback that the energy to balance away is dissipated as heat, and thereby lost. There are also systems where energy can be moved between cells or where individual cells can be bypassed from the series string to control their charge levels individually. The benefit of this is that no additional energy is lost, but this kind of system is unfortunately expensive.

2.4 Battery management systems

The battery pack requires an advanced monitoring system [27, 28, 29, 30]. The main functionalities can be divided into four parts; (i) monitor, (ii) protect, (iii) control, and (iv) estimate.

Monitor

There is normally one sensor measuring the current through each series connected string of cells, i.e. normally one sensor per battery pack. The voltage is monitored for each cell since it is highly correlated to safety issues. For temperature, there are normally at least some sensors in each module

Figure 2.5: An example of an automotive battery pack from a Volvo XC90 T8 plug-in hybrid electric vehicle.

to get measurements of the warmest and coldest cell of the pack, since they are potentially limiting the performance. For safety of the battery pack also other sensors, measuring pressure, gases, etc. may be included.

Protect

Safety is a crucial aspect of battery management. Normally these functions are certified according to automotive safety standards, which in practice limit the use of advanced control functions in favour of simpler logics. Many of the instantly dangerous conditions are also actually measurable. Examples of potentially hazardous situations are over-charging, which may lead to thermal runaway and explosion [31], and too high currents which can cause excessive heating of cells, cabling and other parts of the pack and must therefore be avoided. Since the battery system is passive from a power delivery perspective, the only action that is possible in a hazardous situation is to disconnect the affected parts of the battery from the rest of the electrical system of the vehicle, and for this there are switches controlled by the BMS.

Control

An important task of the BMS is to control the thermal system to keep the battery cells in optimal temperature range for both performance and durability. This is a major energy consumer of an electric vehicle, and therefore one of the primary objectives is to achieve energy efficient thermal strategies.

The BMS controls the balancing circuit mentioned in the previous section. The main objective is to make sure that the energy available from the system is not reduced by unbalanced cells. Depending on the balancing circuit configuration, the control strategies will be different [32, 33, 34].

While there is normally another system controlling charging, the BMS is responsible for determining the charging current. Therefore, this can also be seen as a control problem where the main objective is to charge as fast as possible while not degrading the battery faster than necessary. There are several contributions in the literature to optimal charging strategies, see e.g. [35, 36].

Estimate

Several internal states and attributes of the battery pack cannot be measured directly and must therefore be estimated. Examples are SOC level, health status, and power and energy capability, which are main topics of the

upcoming chapters. Although not covered here, estimations are also needed for temperature of cells without dedicated temperature sensing, charging time, and remaining useful battery life, to name a few.

Chapter 3

Methods

To solve the diverse set of problems encountered in battery management, a set of model structures and estimation algorithms are used. This chapter is mainly aimed at readers unfamiliar with the field of automatic control, and provides an introduction to the methods used and why one method may be preferred over the other for some specific tasks.

3.1 Research approach

The work presented here has been done in close collaboration with industry and, hence, most investigations were derived from actual problems found in battery management system development. The typical approach has been to start by analysing a problem and reviewing existing research on the topic. Laboratory experiments on cell level that reveals specific aspects of the problem were then performed to use for model and algorithm development. Final results were, when applicable, evaluated in a rapid prototyping test rig on physical cells.

3.2 Modelling

The starting-point for most methods for analysis and synthesis in automatic control is that the system is described in some generic format. Depending on the task, different formulations are preferred and in this work three types of models have been used:

- State-space models for synthesis of state estimators
- Input-output models for synthesis of parameter estimators
- Transfer function models for analysis

All these models can be described in both continuous and in discrete time. In the following text, we will refer to these generic models as model structures.

3.2.1 State-space models

State-space models are common in control and estimation synthesis both for linear and nonlinear systems. They collect a system of first order ordinary differential equations (ODE) into a generic structure. Dynamic, as opposed to static, systems have a behaviour that depends on its history. This memory of the system is contained in the state vector x. In this work, focus is most often on systems described in discrete time, where the most general form used can be written as:

$$x_{k+1} = f\left(x_k, u_k, w_k, \theta_k\right) \tag{3.1}$$
$$y_k = h\left(x_k, u_k, v_k, \theta_k\right), \tag{3.2}$$

where $x \in \mathbf{R}^{n_x}$ are the states, $u \in \mathbf{R}^{n_u}$ are the inputs, $y \in \mathbf{R}^{n_y}$ are the outputs, $\theta \in \mathbf{R}^{n_\theta}$ are the parameters, $w \in \mathbf{R}^{n_w}$ and $v \in \mathbf{R}^{n_v}$ are unmeasurable disturbances, and f and g are (non)linear functions of appropriate dimensions.

Batteries can often be described as linear parameter varying systems (LPV) by the generic model

$$x_{k+1} = A(p)x_k + B(p)u_k + w_k \tag{3.3}$$
$$y_k = C(p)x_k + D(p)u_k + v_k, \tag{3.4}$$

where p is a scheduling parameter (possibly a vector). Then f and g in (3.1–3.2) are consequently defined by matrices A, B, C, and D of appropriate dimensions and parametrised by θ. The rest of the variables are as defined above.

State-space models are the most common models for use in state estimators. However, they can also be used for parameter estimation, and then it is common to model the parameters as random walks, i.e.

$$\theta_{k+1} = \theta_k + e_k, \tag{3.5}$$

where $e \sim \mathcal{N}(0, \sigma_\theta)$ is Gaussian white noise with standard deviation σ_θ. The parameters can then be redefined as additional states in the models above.

3.2.2 Linear input-output models

Linear input-output (IO) models are particularly useful for estimating parameters. The reason is that the parameters describing the system enter linearly and they can therefore be estimated using, for instance, least-squares techniques. Identification of IO models use sampled data from the system, but the models and parameters estimated can be for systems described in both continuous and discrete time.

The output of a linear IO model without noise can be described by the regression model

$$y(k) = \theta^T \varphi(k), \tag{3.6}$$

where $\varphi \in \mathbf{R}^{n_\theta}$ is the regression vector.

Remark. The notation $y_k \equiv y(k)$ is used interchangeably throughout this work to enhance readability.

The model (3.6) is often extended with a noise model. There are several alternatives, but here only ARX and ARMAX models are considered for on-line estimation of battery model parameters. For a thorough description of linear IO models, the reader is referred to [37].

ARX models

Auto-regressive models with exogenous inputs (ARX) are described by

$$A(q)y(k) = B(q)u(k) + e(k), \tag{3.7}$$

where q is the time-shift operator ($q^{-m}u(k) \equiv u(k-m)$), and

$$A(q) = 1 + a_1 q^{-1} + \cdots + a_{n_a} q^{-n_a} \tag{3.8}$$

$$B(q) = b_0 + b_1 q^{-1} + \cdots + b_{n_b} q^{-n_b} \tag{3.9}$$

are polynomials with parameters a_i and b_i, respectively.

Equations (3.7–3.9) can be rewritten as

$$y(k) = [1 - A(q)]y(k) + B(q)u(k) + e(k), \tag{3.10}$$

or as the linear regression

$$y(k) = \theta_{\text{arx}}^T \varphi_{\text{arx}}(k) + e(k) \tag{3.11}$$

with

$$\theta_{\text{arx}} = \begin{bmatrix} -a_1 \\ \vdots \\ -a_{n_a} \\ b_0 \\ \vdots \\ b_{n_b} \end{bmatrix} \text{ and } \qquad \varphi_{\text{arx}} = \begin{bmatrix} y(k-1) \\ \vdots \\ y(k-n_a) \\ u(k) \\ \vdots \\ u(k-n_b) \end{bmatrix},$$

where $\theta_{\text{arx}}, \varphi_{\text{arx}} \in \mathbf{R}^{n_a+n_b+1}$ are the parameter and regression vectors, respectively.

ARMAX models

Auto-regressive moving average models with exogenous inputs (ARMAX) use a noise model according to

$$A(q)y(k) = B(q)u(k) + C(q)e(k), \tag{3.12}$$

where

$$\begin{aligned} A(q) &= 1 + a_1 q^{-1} + \cdots + a_{n_a} q^{-n_a} \\ B(q) &= b_0 + b_1 q^{-1} + \cdots + b_{n_b} q^{-n_b} \\ C(q) &= 1 + c_1 q^{-1} + \cdots + c_{n_c} q^{-n_c}. \end{aligned}$$

As for the ARX model, this can be rewritten as

$$y(k) = [1 - A(q)]y(k) + B(q)u(k) + C(q)e(k),$$

where we notice that this can no longer be described by a linear regression since the sequence $e(k)$ is unknown. One way to overcome this problem is to approximate $e(k)$ by the prediction error $\varepsilon(k) = y(k) - \hat{y}(k)$ and write this as

$$\hat{y}(k) = [1 - A(q)]y(k) + B(q)u(k) + [C(q) - 1]\varepsilon(k), \tag{3.13}$$

which can be written as a pseudo-linear regression

$$\hat{y}(k) = \theta_{\text{armax}}^T \varphi_{\text{armax}}(k) \tag{3.14}$$

with

$$\theta_{\text{armax}} = \begin{bmatrix} -a_1 \\ \vdots \\ -a_{n_a} \\ b_0 \\ \vdots \\ b_{n_b} \\ c_1 \\ \vdots \\ c_{n_c} \end{bmatrix} \quad \text{and} \quad \varphi_{\text{armax}} = \begin{bmatrix} y(k-1) \\ \vdots \\ y(k-n_a) \\ u(k) \\ \vdots \\ u(k-n_b) \\ \varepsilon(k-1) \\ \vdots \\ \varepsilon(k-n_c) \end{bmatrix}, \tag{3.15}$$

where $\theta_{\text{armax}}, \varphi_{\text{armax}} \in \mathbf{R}^{n_a+n_b+n_c+1}$ are the parameter and regression vectors, respectively.

An ARMAX model is, for example, proposed for estimating the dynamics of the battery model in Paper 3.

3.2.3 Transfer function models

Analysis of linear closed loop systems can often be conducted using transfer function models. In this work, only transfer functions in continuous time are used, which can be formulated as

$$Y(s) = G(s)U(s),$$

where s is the Laplace variable, $Y(s) = \mathcal{L}\{y(t)\}$, $U(s) = \mathcal{L}\{u(t)\}$, and

$$G(s) = \frac{b_0 + b_1 s + \cdots + b_{n_b} s^{n_b}}{1 + a_1 s + \ldots a_{n_a} s^{n_a}},$$

where a_i and b_i are system parameters.

More information on transfer function models can be found in any textbook on linear systems, e.g. [37]. The battery is described by a transfer function when analysing closed loop properties for power prediction in Paper 4.

3.3 State and parameter estimation

In general, all algorithms for state and parameter estimation considered here are based on using the difference between measured and estimated/predicted output of the system to find states and/or parameters that are optimal in some sense. Depending on the assumptions of the system and in what way the solution should be optimal, the algorithms looks different. In some cases the optimal solution can be found analytically, by e.g. recursive least squares and Kalman filters for unconstrained linear systems. In other cases, approximate solutions, such as the extended Kalman filter for unconstrained non-linear systems, or optimization based algorithms such as moving horizon estimation must be used.

3.3.1 Recursive least squares

The least squares solution to an over-determined set of equations determines the parameter vector $\hat{\theta}$ that minimizes the squared error between the measured output and the output predicted by the model (3.6), i.e.

$$\hat{\theta}(k) = \arg\min_{\theta} \frac{1}{2} \sum_{i=1}^{k} \lambda^{k-i} \left(y(i) - \varphi^T(i)\theta\right)^2, \tag{3.16}$$

where $0 \ll \lambda \leq 1$ is a forgetting factor introduced to weigh recent data more than old. This minimization problem has an analytic solution that

can be implemented as a recursive algorithm:

$$\hat{\theta}(k) = \hat{\theta}(k-1) + K(k)\left(y(k) - \varphi^T(k)\hat{\theta}(k-1)\right) \tag{3.17}$$

$$K(k) = P(k-1)\varphi(k)\left(\lambda + \varphi^T(k)P(k-1)\varphi(k)\right)^{-1} \tag{3.18}$$

$$P(k) = \left(I - K(k)\varphi^T(k)\right)P(k-1)/\lambda, \tag{3.19}$$

where K is the estimator gain and P is the covariance estimate.

In the literature, there are several versions of recursive least squares (RLS) estimators [37, 38, 39]. By simplifications, reformulations of the cost function or avoiding estimation of the covariance estimate, they can be tailored to different system requirements. In this work, the regular RLS algorithm with exponential forgetting factor (3.17)–(3.19) is used for parameter estimation in Paper 3. In the battery estimation field, RLS is also used for parameter estimation in e.g. [40, 41].

3.3.2 Kalman filters

A common approach to state estimation is to use a Kalman filter. Although originally for linear systems, Kalman filters can be used for non-linear systems using either extended (EKF) or unscented (UKF) transformations, both of which will be introduced shortly. The basic idea of the Kalman filter is to use a model of the system to provide an *a priori* estimate of the states and then correct this estimate using measured data of the process output. Given that the model structure and parameters are correct and that the noise covariance probability distributions are white and Gaussian, the Kalman filter is the optimal estimator, in the sense that it is unbiased and minimizes the estimation error variance [39]. Also in cases when the noises are not Gaussian, the Kalman filter will still be the linear estimator with minimum variance. However, the performance of the Kalman filter cannot be guaranteed if these prerequisites are not met. An illustrative example of this was presented by Ljung in [42], where the EKF is used for parameter estimation. Recommended reading for Kalman filters are otherwise [43, 44].

Extended Kalman filter

The EKF treats the non-linearities by linearising the state space representation (3.1–3.2) at each time step. It is a two-stage procedure where the *a priori* state ($\hat{x}^-$) and covariance (P^-) estimates are first calculated using the state-space model. Based on the predicted and measured system output, the estimates are then corrected by the *Kalman gain* K to form the *a posteriori* estimates, $\hat{x}^+$ and P^+. This can be formed in a recursive

algorithm according to

$$\hat{x}_k^- = f\left(\hat{x}_{k-1}^+, u_{k-1}, \bar{w}_{k-1}\right) \tag{3.20}$$
$$P_k^- = \hat{A}_{k-1} P_{k-1}^+ \hat{A}_{k-1}^T + Q \tag{3.21}$$
$$\hat{y}_k = h\left(\hat{x}_k^-, u_k, \bar{v}_k\right) \tag{3.22}$$
$$K_k = P_k^- \hat{C}_k^T \left[\hat{C}_k P_k^- \hat{C}_k^T + R\right]^{-1} \tag{3.23}$$
$$\hat{x}_k^+ = \hat{x}_k^- + K_k\left(y_k - \hat{y}_k\right) \tag{3.24}$$
$$P_k^+ = \left(I - K_k \hat{C}_k\right) P_k^- \tag{3.25}$$

where $Q \in \mathbf{R}^{n_x}$ and $R \in \mathbf{R}^{n_y}$ are the noise covariance matrices for the model (w_k) and measurements (v_k), respectively, and can be regarded as tuning matrices that weigh uncertainties in the model to those of the measurements, while $\hat{A}_k$ and $\hat{C}_k$ are the Jacobian matrices

$$\hat{A}_k = \frac{\partial f\left(x_k, u_k, w_k\right)}{\partial x_k}\Big|_{x_k = \hat{x}_k^+}$$
$$\hat{C}_k = \frac{\partial h\left(x_k, u_k, v_k\right)}{\partial x_k}\Big|_{x_k = \hat{x}_k^-}.$$

It should be noted that implementing the EKF according to Eq. (3.20–3.25) may result in an algorithm with poor numerical properties because of recursive propagation of the error covariances from one time-step to the next [45]. To improve the numerical properties, there are several versions of the Kalman filter that propagates the square root of the error covariance instead. Algebraically the implementations are equivalent, but the numerical properties can be significantly improved. For a description and in-depth derivation of the square-root algorithm, the reader is referred to [46].

Uncented Kalman filter

The UKF uses a similar predict/correct procedure as the EKF, but rather than using the Jacobians to linearise the system, the UKF lets several perturbed versions of the state vector, called sigma points, pass the non-linear system (3.1–3.2). The estimated state is then calculated as a weighted average of the outputs for each sigma-point. For strong non-linearities, the UKF theoretically provides a better approximation of the output probability distribution than the EKF [44].

The recursive algorithm is more complex than the EKF. First, an augmented state vector x^a and an augmented covariance matrix P_k^a are defined

by

$$\hat{x}_k^a = \left[\hat{x}_k^T, w_k^T, v_k^T\right]^T \in \mathbf{R}^n$$
$$P_k^a = \text{diag}\left(P_k, Q, R\right) \in \mathbf{R}^{n\times n},$$

where $n = 2n_x + n_y$. Next, the matrix of sigma points $\chi \in \mathbf{R}^{n\times 2n+1}$ is updated in each time-step by

$$\chi_{k-1}^{a,+} = \left\{\hat{x}_{k-1}^{a,+}, \hat{x}_{k-1}^{a,+} + \gamma\sqrt{P_{k-1}^{a,+}}, \hat{x}_{k-1}^{a,+} - \gamma\sqrt{P_{k-1}^{a,+}}\right\}.$$

Note that the rows are related to the augmented state vector and each column corresponds to one sigma point where the state vector is shifted based on the covariance estimate $P_{k-1}^{a,+}$. By indexing the columns as $\chi_{k,i}^a$, we define $\chi_{k,i}^x$, $\chi_{k,i}^w$, and $\chi_{k,i}^v$ as the rows of column i that are related to x, w, and v, respectively. Then the update of the state and covariance estimates are given by

$$\chi_{k,i}^{x,-} = f\left(\chi_{k-1,i}^{x,+}, u_{k-1}, \chi_{k-1,i}^{w,+}\right)$$
$$\hat{x}_k^- = \sum_{i=0}^{2n} \alpha_i^{(m)} \chi_{k,i}^{x,-}$$
$$P_k^- = \sum_{i=0}^{2n} \alpha_i^{(c)} \left(\chi_{k,i}^{x,-} - \hat{x}_k^-\right)\left(\chi_{k,i}^{x,-} - \hat{x}_k^-\right)^T.$$

An estimate of the output is calculated from the predicted state using the same weights as for the states

$$\mathcal{Y}_{k,i} = h\left(\chi_{k,i}^{x,-}, u_k, \chi_{k-1,i}^{v,+}\right)$$
$$\hat{y}_k = \sum_{i=0}^{2n} \alpha_i^{(m)} \mathcal{Y}_{k,i}.$$

The gain of the estimator is

$$\Sigma_{\tilde{y},k} = \sum_{i=0}^{2n} \alpha_i^{(c)} \left(\mathcal{Y}_{k,i} - \hat{y}_k\right)\left(\mathcal{Y}_{k,i} - \hat{y}_k\right)^T$$
$$\Sigma_{\tilde{x}\tilde{y},k}^- = \sum_{i=0}^{2n} \alpha_i^{(c)} \left(\chi_{k,i}^{x,-} - \hat{x}_k^-\right)\left(\mathcal{Y}_{k,i} - \hat{y}_k\right)^T$$
$$K_k = \Sigma_{\tilde{x}\tilde{y},k}^- \Sigma_{\tilde{y},k}^{-1}.$$

Finally, the state and covariance estimates are corrected according to

$$\hat{x}_k = \hat{x}_k^- + K_k\left(y_k - \hat{y}_k\right)$$
$$P_k^+ = P_k^- - K_k \Sigma_{\tilde{y},k} K_k^T.$$

Table 3.1: Weighting parameters of the unscented Kalman filter. α, β, and κ are tuning parameters.

λ	$\alpha^2 (n + \kappa) - n$
γ	$\sqrt{n + \lambda}$
$\alpha_0^{(m)}$	$\frac{\lambda}{n+\lambda}$
$\alpha_k^{(m)}$	$\frac{1}{2(n+\lambda)}$
$\alpha_0^{(c)}$	$\frac{\lambda}{n+\lambda} + 1 - \alpha^2 + \beta$
$\alpha_k^{(c)}$	$\frac{1}{2(n+\lambda)}$

The tuning parameters γ, $\alpha_i^{(m)}$, and $\alpha_i^{(c)}$ can be selected in different ways. For the UKF, values according to Table 3.1 shall be selected. A thorough background to the unscented transformation and derivation of the UKF can be found in [44]. For SOC estimation, UKF is used in [47, 48], and in Paper 1 it is compared to the EKF.

Tuning of Kalman filters

In theory the covariances R and Q of the EKF and UKF are determined by the noise models. In practice they are, however, often treated as tuning parameters. Finding a tuning that provides good performance of the filter can be a time consuming task, and therefore automatic calibration procedures have been proposed in robot navigation applications, see [49] for EKF and [50] for UKF. These procedures are more or less directly transferable to SOC estimation, and they are also used in Paper 1 to get a fair comparison of the estimators. In the battery SOC estimation field, there were no previous examples of automatic tuning of Kalman filters found in a literature review for Paper 1, seeming that mostly a trial-and-error approach had been used.

3.3.3 H_∞ filters

H_∞ filters have close similarities to Kalman filters, as pointed out in [44]. They are, just like Kalman filters, originally derived for linear systems, but can also be used for non-linear systems by extended [51] and unscented [52] transformations. In the SOC estimation field, Yan et al. [53] promotes the use of the H_∞ filter, based on the fact that it does not require any information on noise characteristics.

In [54], the sub-optimal H_∞ filtering problem is formulated as that of finding an estimate $\hat{x}$ such that

$$\sup_{x_0, w \in H_2, v \in H_2} \frac{\|L_k x_k - L_k \hat{x}_k\|_2^2}{\|x_0 - \hat{x}_0\|_{P_0^{-1}}^2 + \|w_k\|_2^2 + \|v_k\|_2^2} < \gamma^2 \tag{3.26}$$

for some predefined error bound γ and state weight matrix L. A solution to the problem is given by the recursion

$$\begin{aligned}
\hat{x}_k^- =& f\left(\hat{x}_{k-1}^+, u_{k-1}, \bar{w}_{k-1}\right) \\
R_k =& \begin{bmatrix} I & 0 \\ 0 & -\gamma^2 I \end{bmatrix} + \begin{bmatrix} \hat{C}_k \\ L_k \end{bmatrix} P_{k-1} \begin{bmatrix} \hat{C}_k^T L_k^T \end{bmatrix} \\
P_k =& \hat{A}_k P_{k-1} \hat{A}_k^T + \hat{W}_k \hat{W}_k^T \\
& - \hat{A}_k P_{k-1} \begin{bmatrix} \hat{C}_k^T & L_k^T \end{bmatrix} R_k^{-1} \begin{bmatrix} \hat{C}_k \\ L_k \end{bmatrix} P_{k-1} \hat{A}_k^T \\
K_k =& P_k \hat{C}_k^T \left[\hat{V}_k \hat{V}_k^T + \hat{C}_k P_k \hat{C}_k^T\right]^{-1} \\
\hat{x}_k^+ =& \hat{x}_k^- + K_k \left(y_k - h\left(\hat{x}_k^-, u_k, \bar{v}_k\right)\right).
\end{aligned}$$

For the solution to actually solve the sub-optimal H_∞ filtering problem, the following condition must also hold:

$$P_k^{-1} + \hat{C}_k^T \hat{C}_k - \gamma^{-2} L_k^T L_k > 0. \tag{3.27}$$

The H_∞-filter is compared to UKF and EKF in Paper 1.

3.3.4 Moving horizon estimation

Moving horizon estimation (MHE) is an optimization-based method that uses a receding time-horizon covering a limited number of past measurements. A dynamic optimization problem is repeatedly solved on-line in each time-step. Disturbances in the form of unknown and slowly time-varying parameters can be estimated along with the states in a consistent way by adding them as single degrees of freedom to the optimization problem. Letting k be present time, N be the time horizon, and defining $L = k - N$, the MHE considering states (x), parameters (θ) and state noise (w) can be described by

$$\begin{aligned}
\min_{x_j, w_j, \theta} \quad & \left\| \begin{matrix} x_L - \bar{x}_L \\ \theta - \bar{\theta}_L \end{matrix} \right\|_{P_L^{-1}}^2 + \sum_{j=L}^{k} \left\| y_j - h(x_j, u_j, \theta) \right\|_R^2 + \sum_{j=L}^{k-1} \left\| w_j \right\|_Q^2 \\
\text{s.t.} \quad & x_{j+1} = f(x_j, u_j, \theta) + w_j, \ j = L, \ldots, k-1 \\
& \theta \in \mathcal{P}, x_j \in \mathcal{X}, w_j \in \mathcal{W}, \ j = L, \ldots, k,
\end{aligned}$$

where the notation $\|a\|_A^2 = a^T A a$ is used, $\bar{x}_L$ and $\bar{\theta}_L$ are initial estimates based on the previous iteration, $P_L \in \mathbf{R}^{n_x + n_\theta}$, $R \in \mathbf{R}$, and $Q \in \mathbf{R}^{n_x}$ are positive definite weighting matrices, and $\mathcal{P}$, $\mathcal{X}$, and $\mathcal{W}$ define constraints on parameters, states, and noise, respectively.

There are three parts of the objective function, (i) the arrival cost, (ii) the prediction error, and (iii) the state noise, all having their individual weighting matrices. The prediction error and state noise can be given static weights while the arrival cost is used to sum up information prior to the present time window and must therefore be updated in each iteration. In general, the exact arrival cost cannot be calculated but there are numerous approximations available (see e.g. [55, 56]). One strategy for computing an approximate arrival cost is to use a first-order Taylor expansion around the trajectory of past estimates. This is equivalent to applying an EKF recursion for the covariance update [57, 58].

Moving horizon estimation is used in Paper 5 for joint estimation of parameters and states.

3.3.5 Other observers

There are several other observers that can be used for the estimation task. In this work, also Luenberger and sliding mode observers were considered, but never used in any of the appended papers.

Luenberger observer

The overall structure of the Luenberger observer is similar to that of the Kalman filter and its background is also from linear systems theory. The main difference compared to the Kalman filter is the way the gain is chosen. In the Kalman filter it is the statistically optimal balance of the model and observation in terms of the noise covariances. The Luenberger observer choose the gain based on desired closed-loop properties of the error dynamics instead, i.e. the difference between measured and predicted output. Hu et al. [59] implements an adaptive Luenberger observer for battery SOC estimation that manages to handle both initial errors and noise.

Sliding mode observer

As described by Misawa and Hedrick in [60], sliding mode observers are basically Luenberger observers and, hence, does not rely on perfect models or Gaussian noise processes. To improve robustness to modelling errors and uncertainties compared to the normal Luenberger observer, the sliding mode observer adds a switching term. Using Lyapunov theory, design parameters of the observer are chosen so that the error dynamics are asymptotically stable, i.e. the difference between the estimated and real states go to zero as time goes to infinity.

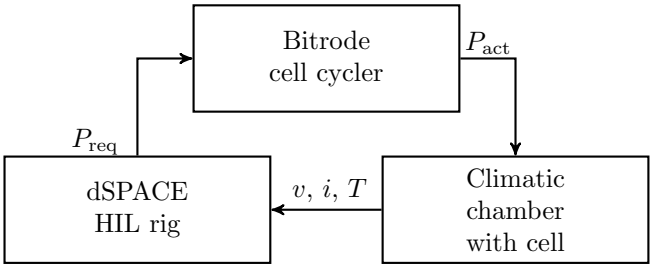

Figure 3.1: Schematics of the rapid prototyping setup used for algorithm development. The signal flow is such that the HIL rig sends out a power request that the cell cycler actuates. The resulting cell voltage, current, and temperature are measured using the same sensors as in Volvo XC90 T8 vehicles and are fed back to the HIL rig.

Kim [61] presents a sliding mode observer for SOC estimation that is within 3% accuracy compared to lab data using a simple model. Unfortunately, the experiments lack robustness analysis, even though that is where this observer design theoretically should prove its strength.

3.4 Rapid prototyping environment

A rapid prototyping environment (schematically illustrated in Figure 3.1) was set up for testing the algorithms proposed in the upcoming chapters. The BMS algorithms and a vehicle model are executed in real-time on a hardware-in-the-loop (HIL) rig, which sends power requests that the cell cycler actuates. The test object is a lithium-ion cell of NMC type used in Volvo XC90 T8 plug-in hybrids, and it is located in a temperature chamber where the ambient temperature can be varied between -20 and $+50$°C. The current, voltage, and temperature of the cell are measured using the same sensors as in Volvo vehicles and are sent to the HIL rig.

Chapter 4

Battery modelling

Model-based BMS algorithms often use the current–voltage characteristics to estimate internal states of the cell. As with all mathematical modelling of physical systems, the correct choice of model depends on the intended application. Aspects to consider when selecting a model for BMS are:

- Battery packs can contain hundreds of cells, each potentially requiring their own cell model, which means that the computational load grows rapidly with model complexity.

- To be able to track degradation effects, parameters and states should preferably be observable from current and voltage measurements.

- The model will be used for prediction rather than simulation.

The battery models considered here can be divided into two categories; physical models of the electro-chemistry of the cells, and empirical models based on equivalent circuits. A short introduction to these two types of models follows next.

4.1 Physics-based modelling

Physical models start from the reactions inside the cell, as described in Section 2.2.1. Electrode and electrolyte potentials and concentrations are calculated to capture cell behaviour. These models can explain internal dynamics of the cell, but that comes at the price of computational complexity. Therefore, electro-chemical models are most common in off-line simulations, where details on a low level are needed.

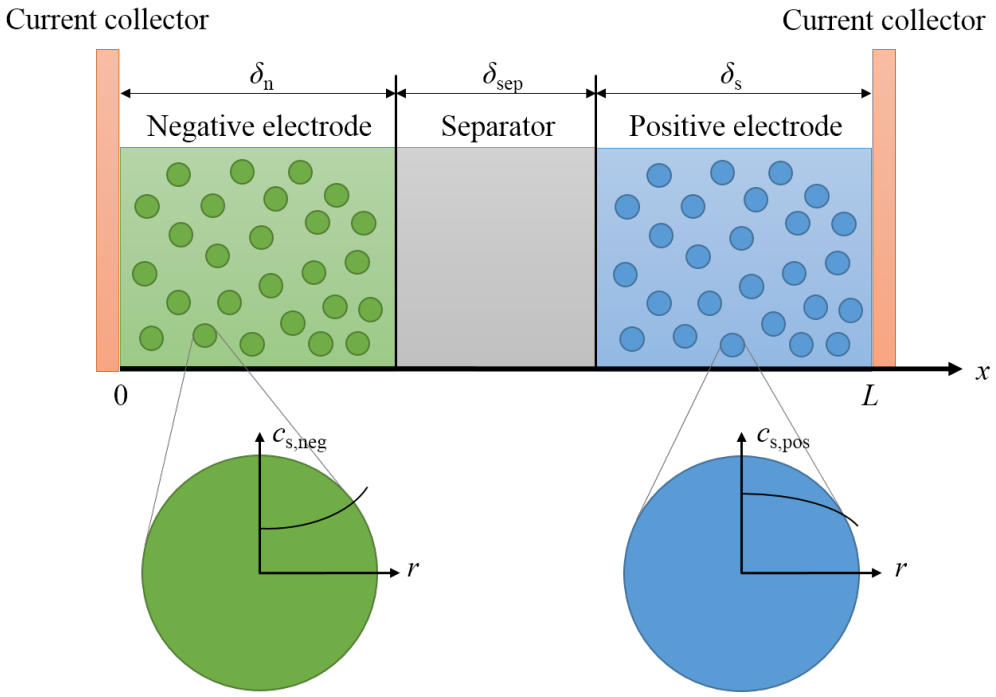

Figure 4.1: Schematic figure of a lithium-ion cell with dimensions used in the P2D model.

4.1.1 The Newman model

Most physical models of lithium-ion batteries are versions of the Newman model [62], sometimes called pseudo 2D (P2D) since it contains one dimension for the particle and one for the electrolyte. Figure 4.1 illustrates a schematic view of the cell as defined in the P2D model. The model consists of a set of partial differential equations (PDEs) and algebraic equation for each electrode [11, 62, 63, 64].

Assuming that the particles are homogeneous and that the transport of ions follow Fick's law of diffusion, conservation of lithium in solid phase gives

$$\frac{\partial c_s}{\partial t} = \frac{D_s}{r^2}\frac{\partial}{\partial r}\left(r^2\frac{\partial c_s}{\partial r}\right),$$

where $c_s(t, r, x)$ is the solid phase lithium concentration, r is the particle radial distance, and D_s is the solid phase diffusion coefficient.

Analogous, conservation of lithium in electrolyte phase gives

$$\frac{\partial}{\partial t}\varepsilon_e c_e = \frac{\partial}{\partial x}\left(D_e\frac{\partial}{\partial x}c_e\right) + (1 - t_+)\frac{j_f}{F},$$

where ε_e is the electrolyte volume fraction, $c_e(t, x)$ is the electrolyte lithium concentration, D_e is the electrolyte ionic diffusion coefficient, t_+ is the

lithium ion transference number, $j_f(t,x)$ is the volumetric transfer current density, and F is the Faraday's constant.

Charge balance in the solid phase yields

$$\frac{\partial}{\partial x}\left(\sigma\frac{\partial}{\partial x}\phi_s\right) - j_f = 0,$$

where σ is the electrode electronic conductivity and $\phi_s(t,x)$ is the solid phase potential. The boundary condition is linked to the cell current i as

$$-\sigma\frac{\partial}{\partial x}\phi_s(t,0) = \sigma\frac{\partial}{\partial x}\phi_s(t,L) = \frac{i(t)}{A},$$

where A is the electrode surface area.

Charge balance in the electrolyte phase gives

$$\frac{\partial}{\partial x}\left(\kappa\frac{\partial}{\partial x}\phi_e\right) + \frac{\partial}{\partial x}\left(\kappa_D\frac{\partial}{\partial x}\ln c_e\right) + j_f = 0,$$

where $\phi_e(t,x)$ is the electrolyte potential, κ is the electrolyte ionic conductivity, and κ_D is the electrolyte diffusional conductivity.

The current density is a function of over-potential, $\eta(t,x)$, and is described by the Butler-Volmer equation

$$j_f = 2a_s i_0 \sinh\left(\frac{F}{2RT}\eta\right),$$

where a_s is the solid/electrolyte interface area, i_0 is exchange current, R is the universal gas constant, and T is absolute temperature. The over-potential is described by

$$\eta = \phi_s - \phi_e - U_{\text{ocp}} - \frac{R_{\text{sei}}}{a_s}j_f, \tag{4.1}$$

where $U_{\text{ocp}}(c_s(t,r_s,x))$ is the open circuit potential, r_s is the particle radius, and R_{sei} is the solid/electrolyte film resistance.

The terminal voltage of the cell can then be described by the potential difference between the electrodes as

$$v(t) = \phi_s(t,L) - \phi(t,0). \tag{4.2}$$

More information about the above equations together with the complete set of boundary conditions can be found in [64, 65].

4.1.2 Single particle models

Single particle models (SPM) are simplifications to the P2D model to address the high computational load. They neglect current distribution in the electrodes as well as concentration gradients in the electrolyte, which means that all particles in one electrode behave in the same way. Thus, each electrode can be represented by one single, spherical particle. Several versions of the SPM have been proposed for SOC estimation (see e.g. [11, 63, 66, 67]). However, even if SPMs are simplifications of the underlying physics, they are still described by systems of non-linear PDEs, and for use in on-line applications, further simplifications are needed. Several different model order reduction techniques have been suggested in the literature [68, 69, 70, 71]. Usually these techniques manages to reduce the models down to ODEs with four to six states while maintaining reasonable accuracy. Compared to an equivalent circuit model, which often contains only two states, trade-off between accuracy and complexity must, however, still be assessed. Also, the combination of estimating parameters and states together may pose a problem since they model individual electrodes, while measurement information is aggregated to the cell (i.e. difference between electrodes).

4.2 Empirical modelling

Empirical models aims to mimic the current–voltage characteristics of the battery as described in Section 2.2.3. One of the most commonly used models is the equivalent circuit model (ECM) that uses electrical components such as resistors and capacitors to describe the relationship between current and voltage in a battery. There are several versions of the equivalent circuit model presented in the literature. In most cases, the model will be based on a circuit like the one in Figure 4.2. Sometimes incorporating more RC pairs in series and sometimes non-linearities, such as hysteresis. The parameters in the models may be varying with SOC, temperature and current.

One drawback with this type of "grey-box" models is that the circuit elements only have limited relation to the physical reactions inside the cell. This may limit the validity of the model in applications far from equilibrium, such as extreme temperatures and currents. The benefit is their simple structure, which means that they simulate fast and that their parameters are easier to estimate on-line than for electrochemical models.

There are several papers on battery modelling using equivalent circuits, see e.g. [72, 73, 74]. In [72], twelve different equivalent circuit models are compared to experimental data. Considering the trade-off between accuracy and complexity, these results show that a first-order RC model often is

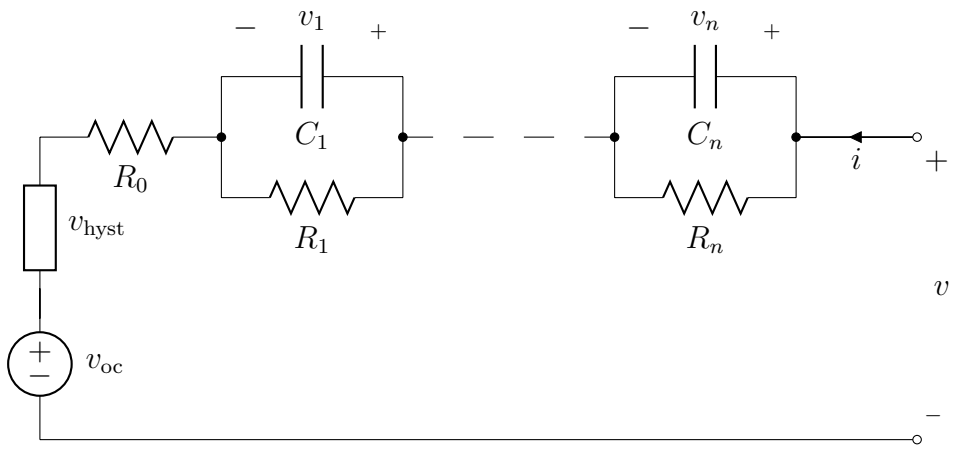

Figure 4.2: Thevenin equivalent circuit model with n RC-pairs and hysteresis.

sufficient. It should be noted that these results are mainly for +22°C. Our work has verified these results for room temperature, but at colder temperatures, more advanced models were needed to handle slower relaxation and non-linear effects.

4.2.1 Dual RC model

The ECM in Figure 4.3 can be described by the following state-space model (see Section 3.2.1) in discrete time

$$\begin{bmatrix} v_1(k+1) \\ v_2(k+1) \\ z(k+1) \end{bmatrix} = \begin{bmatrix} e^{-\frac{\Delta t}{\tau_1}} & 0 & 0 \\ 0 & e^{-\frac{\Delta t}{\tau_2}} & 0 \\ 0 & 0 & 1 \end{bmatrix} \begin{bmatrix} v_1(k) \\ v_2(k) \\ z(k) \end{bmatrix} + \begin{bmatrix} R_1\left(1-e^{-\frac{\Delta t}{\tau_1}}\right) \\ R_2\left(1-e^{-\frac{\Delta t}{\tau_2}}\right) \\ \frac{\eta_i \Delta t}{Q_{\text{nom}}} \end{bmatrix} i(k) \quad (4.3)$$

$$v(k) = h_{\text{ocv}}(z(k)) + v_1(k) + v_2(k) + R_0 i(k) \quad (4.4)$$

where h_{ocv} is the non-linear OCV curve, and v_1, v_2, R_0, R_1, R_2, $\tau_1 = R_1C_1$, and $\tau_2 = R_2C_2$ are the voltages, resistances, and time constants of the RC network, Δt is the sampling time, Q_{nom} is the nominal capacity and η_{i} is the Coulombic efficiency (set to 1 in all coming models).

With constant parameters, the ECM is only valid for narrow operating conditions (SOC and temperature). There are different approaches to extend the validity range. In this work, mainly two alternatives were used:

- Off-line parametrisation of the model from laboratory data using methods of system identification. Parameters are then typically stored in look-up tables for use in the BMS (see e.g. [75, 76]).

- On-line estimation of model parameters from current and voltage measurements. The methods found in the literature can be categorised as, model-based *recursive* and *non-recursive* methods, and data-driven *machine learning* methods. A comprehensive review of methods and references can be found in [6].

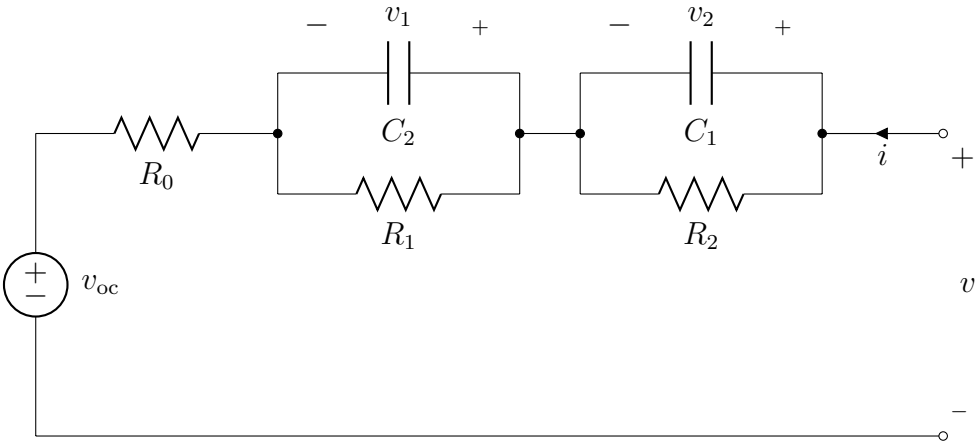

Figure 4.3: Equivalent circuit model with two RC-pairs.

4.2.2 An extended equivalent circuit model

In some cases the ECM cannot capture the voltage response of the cell. An example is provided in Paper 5, where a cell is subject to high-power discharge in cold temperature. To handle this problem, an extension to the ECM is proposed that is based on comparison of the voltage model of the ECM (4.4) with that of SPMs, which can normally be described by

$$v(t) = U_p(c_p^{(s)}(t)) - U_n(c_n^{(s)}(t)) + \eta_p(t) - \eta_n(t) + R_0 i(t), \tag{4.5}$$

where $c_p^{(s)}$ and $c_n^{(s)}$ are the surface concentrations in the positive and negative electrodes, U_p and U_n are non-linear material dependent scalar functions that maps the surface concentrations to potentials, η_p and η_n are over-potentials, and R_0 is a lumped resistive term.

As described in [77], a major conceptual difference between the two is the use of open circuit voltage (OCV) based on cell average SOC versus individual open circuit potential (OCP) based on surface concentration. This means that the polarization voltages v_j in the ECM will have to account for the over-potentials as well as the diffusion dynamics in the solid phase. This simplification will work well as long as the OCV curve is relatively

linear, but in areas where the derivative changes, such as below 10% SOC in Figure 2.2, the ECM needs to compensate for the effect by using a different set of parameters. However, this may not be sufficient if the non-linear effects are too strong, or if the non-linearity depends on a dynamic state.

The proposed extended ECM (XECM) instead introduces an additional state to model the electrode surface SOC (z_s) that is fed through the OCV function. The XECM of first order can be written as

$$\begin{aligned} v_1(k+1) &= \alpha_1 v_1(k) + \beta_1 i(k) \\ \Delta z_1(k+1) &= \alpha_2 \Delta z_1(k) + \beta_2 i(k) \\ z(k+1) &= z(k) + \Delta t Q_{\text{nom}}^{-1} i(k) \\ v(k) &= h_{\text{ocv}}\left(z(k) + \Delta z_1(k)\right) + v_1(k) + R_0 i(k), \end{aligned}$$

where the algebraic equation for surface SOC z_s was introduced to enhance readability. This model is described in more detail in Paper 5.

4.3 Thermal model

Some algorithms, such as energy estimation, also requires a thermal model of the battery. Assuming that the heat is only generated in the resistances of Figure 4.3, a lumped mass model can be described by

$$mc\dot{T}(t) = R(T(t))i^2(t) + P_{\text{cool}}(t), \tag{4.6}$$

where R is the total resistance, m is the thermal mass, c is the specific heat capacity, and P_{cool} is the cooling power applied to the battery [75, 76, 78]. The total resistance will be cycle dependent and contain R_0 plus some portions of R_1 and R_2 that depends on the load-cycle (i.e. current). For further details on this, see Paper 6.

Chapter 5

Adaptive battery state estimation

The main objective of battery state estimation is to relate measurements of current, voltage, and temperature to the cell operating window $\mathcal{W}$ over the complete operating range and life-time of the battery.

This can be divided into three parts:

- Selecting a model-structure that relates measurements to internal states of the cell.
- Parametrisation of the selected model.
- Estimation of internal states of the cell using the parametrised model.

In this chapter, an adaptive estimation system is proposed and demonstrated on laboratory data.

5.1 Combined estimation of parameters and states

In the context of this work, adaptive battery state estimation refers to combined estimation of model parameters and states on-line during operation. This is often handled by either *joint estimation* where they are estimated in the same algorithm, or by *dual estimation* where the tasks are separated.

In joint estimation it is common to use state-space formulations and then augment the state vector with the unknown parameters that are modelled as random walks, i.e.

$$\begin{bmatrix} x_{k+1} \\ \theta_{k+1} \end{bmatrix} = \begin{bmatrix} f(x_k, u_k, \theta_k) \\ \theta_k \end{bmatrix} + \begin{bmatrix} w_{x,k} \\ w_{\theta,k} \end{bmatrix}.$$

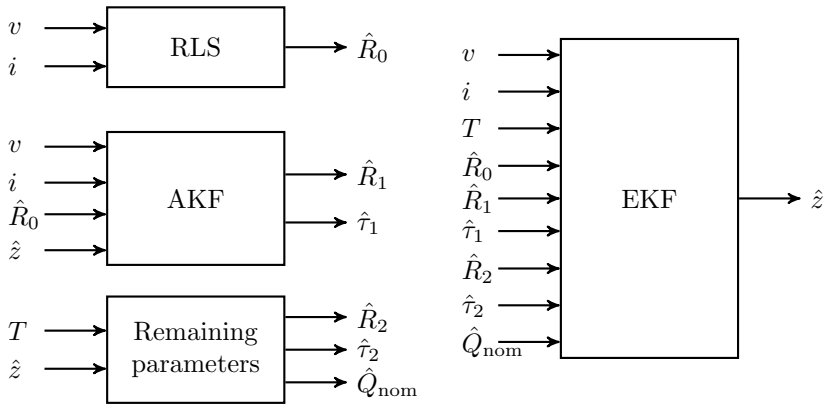

Figure 5.1: Overview of the dual estimator proposed in this thesis. The parameters R_2, τ_2 and Q are not estimated on-line in the upcoming tests and are therefore simply stated as "remaining parameters".

The algorithms presented in Chapter 3.3 can then be applied to estimate the augmented state vector. The main benefit of joint estimation is that it is easy to implement since it only involves adding the unknown parameters to the states. Joint estimation has been proposed in the literature for battery estimation by e.g. [79, 80, 81]. In practice there are several pitfalls to consider when using this approach. During the course of this work it was found that the combination of uncertainties in model-structure, parameters, and states requires accurate initial values and slow adaptation to guarantee convergence of the joint estimator. The main reasons identified were that

- parameters and states vary on very different time-scales.
- excitation requirements of the parameters and states are not the same.

In Paper 5, MHE is used for joint estimation of the extended ECM. The algorithm is able to handle the task for the purpose of the article, but future work is proposed to separate estimation of parameters and states for the reasons just mentioned.

In dual estimation the parameters and states are estimated by different algorithms. The main benefits are that tailored algorithms, excitation conditions, and sampling-times can be used to attack different properties of each sub-problem. Based on the results of Papers 1 and 3, the algorithm system illustrated in Figure 5.1 is proposed. It is based on the dual RC model of Section 4.2.1 and all included parts will be further described in the upcoming sections.

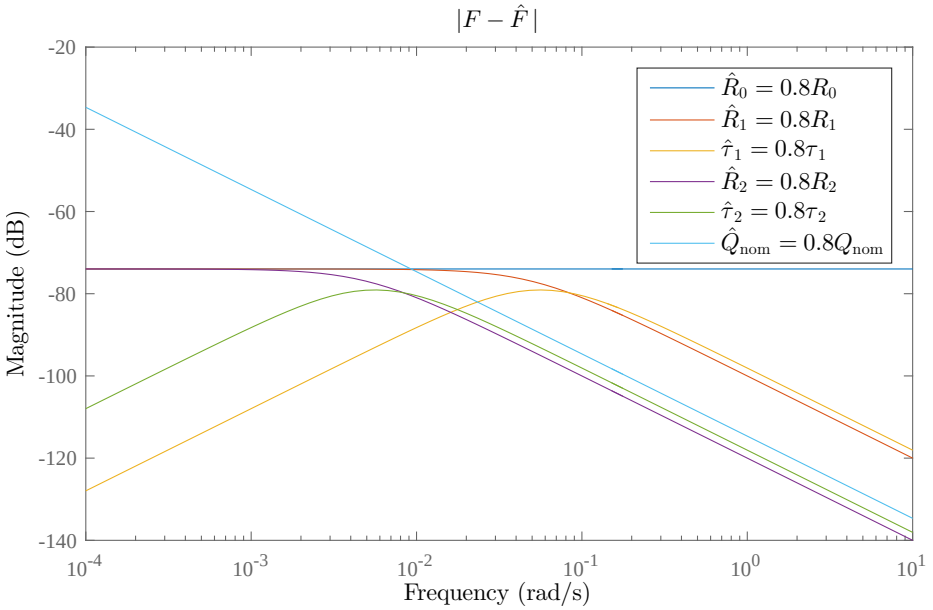

Figure 5.2: Illustration of how parameter errors impacts voltage prediction errors for of the ECM. Note that Q_{nom} dominates the low frequencies while R_0 dominates for high frequencies. R_1 and τ_1 dominate in the middle frequency range if the error in R_0 is small. Finally, R_2 and τ_2 are only dominant if all other errors are small.

5.2 Parameter estimation

Parameter estimation is related to tracking battery characteristics on-line. This work focus on model-based recursive methods using the ECM (4.3–4.4) with parameters R_0, R_1, τ_1, R_2, τ_2 and Q_{nom}. Some common algorithms used in the literature are the Recursive Least Squares (RLS) [40, 41], the Kalman filter [82, 83] or parameter adaptation laws based on Lyapunov theory [84].

Figure 5.2 illustrates how the model parameters impacts voltage prediction by plotting $|F(s) - \hat{F}(s)|$, where

$$F(s) = \left(\frac{\kappa}{Q_{\text{nom}} s} + \frac{R_1}{1 + \tau_1 s} + \frac{R_2}{1 + \tau_2 s} + R_0 \right) I(s) \tag{5.1}$$

is a transfer function version of the linearised ECM, κ is the derivative of the OCV curve, and $\hat{F}$ is the corresponding transfer function where one of the parameters is set incorrectly.

First, it can be noted that errors in R_0 are visible for all frequencies, and totally dominant for high frequencies, while Q_{nom} dominates at lower frequencies. For the parameters related to R_1 and τ_1 we see that they are

dominating in the middle frequency range, but only if there are no errors in R_0. Finally, note that R_2 and τ_2 are not dominant in any region, unless all other parameters are correct. These observations together with the analysis found in Paper 3 motivates a division of the estimation task into separate estimators, as described next.

Estimation of R_0

Accurate estimation of R_0 is crucial for SOC estimation (and for capability estimations in the next chapter). The good news is that R_0 turns out to be relatively easy to estimate based on the observation that (4.4) for sampling instants $k-1$ and k are

$$\begin{aligned} v(k-1) &= v_{\text{oc}}(k-1) + v_1(k-1) + v_2(k-1) + R_0 i(k-1) \\ v(k) &= v_{\text{oc}}(k) + v_1(k) + v_2(k) + R_0 i(k), \end{aligned}$$

where $v_{\text{oc}} = h_{\text{ocv}}(z(k))$. If the sampling-time is short enough, v_{oc}, v_1, and v_2 remains approximately constant and therefore

$$\Delta v(k) \approx R_0 \Delta i(k),$$

with $\Delta v(k) = v(k) - v(k-1)$ and $\Delta i(k) = i(k) - i(k-1)$.

The RLS algorithm (3.17-3.19) with exponential forgetting factor is proposed for estimation of R_0 based on results presented in Paper 3.

Estimation of R_1 and τ_1

Accurate estimation of R_1 and τ_1 is important for model accuracy in use-cases where significant polarisation of the cell is expected (see Paper 6, where R_1 contribution to overall resistance is investigated). Typical examples are during charging and in depleting drive-cycles.

R_1 and τ_1 affects the polarization voltage v_1. Since the estimation of the resistance R_0 assumed that the sampling-time was short enough to consider v_1 constant, it cannot be estimated in the same algorithm as R_1 and τ_1. The time-constant τ_1 is typically in the order of 20-40s for the cells used in this work, and a rule of thumb is to sample at 10 times per the expected dynamics (see [37]). Thereby a sampling-time of $\sim 2-4$s is suggested for estimation of R_1 and τ_1.

A negative side-effect of separating the estimation of R_1 and τ_1 from that of R_0 is that uncertainties in both R_0 and v_{oc} may impact performance. Especially errors in v_{oc} can be interpreted as a long time-constant. To improve accuracy and robustness an ARMAX model together with an adaptive Kalman filter, which was found to be less sensitive to excitation than other tested algorithms, is proposed in Paper 3.

Estimation of R_2 and τ_2

When the dual RC model is used also R_2 and τ_2 are needed. However, they turn out to be hard to estimate robustly on-line using recursive algorithms. The main reason is that τ_2 found in off-line parametrisation is in the order of 100-200s, and the effect is therefore hard to distinguish from changes in SOC. Since the impact of R_2 and τ_2 on other algorithms was found to be minor they were parametrised off-line and stored in look-up tables over SOC and temperature.

Estimation of Q_{nom}

The capacity of the battery must also be tracked since it changes with ageing. For this task existing literature was considered sufficient and there were no additional results derived in the thesis work. The simplest concept (see e.g. [85]) is to use Coulomb counting

$$z(t) = z(0) + \frac{1}{Q_{\text{nom}}} \int_0^t i(\tau) d\tau,$$

which can be rewritten as

$$Q_{\text{nom}} = \frac{\int_0^t i(\tau) d\tau}{z(t) - z(0)}$$

to get a measurement of the capacity. Here it is important to use SOC measured from the OCV rather than estimated SOC. Since capacity is the most important parameter for SOC estimation, the combined parameter and state estimator may otherwise fail to converge. The measured capacity can be corrupted by noise due to the integration of a noisy current over a possibly long period of time. To improve accuracy, a Kalman filter can be used to estimate capacity based on several measurements. There are also more sophisticated capacity estimators proposed in the literature (see e.g. [86, 87, 88]).

5.3 State-of-charge estimation

Tracking the cell SOC on-line is a well-covered topic of battery management in the literature. Some examples of proposed algorithms are EKF [83], UKF [47], Luenberger Observers [59], Sliding Mode Observers [61], and H_∞ observers [53].

The difficulty in SOC estimation is strongly related to the OCV curve of the cell, since a weak correlation between SOC and voltage leads to

poor observability. As an example, the flat OCV of LFP cells depicted in Figure 2.2 makes them significantly more difficult to track than NMC cells.

The performances of EKF, UKF, and H_∞ are compared in a simulation study in Paper 1, which shows that the appropriate choice of observer algorithm depends on both cell chemistry and intended vehicle application. The EKF provides a good compromise between accuracy and complexity, and is therefore used for SOC estimation in the rest of the thesis. Klintberg et al. [89] also confirmed that the EKF provides close to optimal results for NMC cells modelled as ECMs by studying the Cramer-Rao lower bound.

5.4 State-of-health estimation

SOH is normally defined as the ratio of capacity and/or resistance of an aged cell compared to a new cell. Based on the definitions of Section 2.1, the capacity remains relatively unaffected by operating conditions and the approach to capacity estimation presented in Section 5.2 can therefore be used. For resistance, however, the effect of operating conditions (particularly temperature) can be significantly larger than the changes due to ageing, and these two effects must therefore be distinguished from one another. Variations with age are, typically, much slower than changes with operating conditions [19], which motivates handling these two types of variations separately.

Handling temperature dependency of resistance

Parameter variations due to operating conditions can be mapped in look-up tables [75, 76, 82, 90]. As the battery ages, these look-up tables must then be updated to reflect the changes in characteristics. It is difficult to find algorithms for updating look-up tables in the battery community. In other fields there have been previous work on updating look-up tables at operating points close to the present operating conditions using Kalman filters [91, 92] and recursive least squares [93]. This means that the parameter estimate in operating points that have not been visited for a long time may be far from the true value, which can cause problems. As an example, under-estimating the resistance of the battery leads to errors in the estimation of available power, which in turn may result in problems starting the vehicle [94].

In Paper 2, a novel use of the Kalman filter for updating complete look-up tables based on measurement information in the currently active operating conditions is presented. In particular this was applied to the mapping of R_0 w.r.t. temperature. The proposed method is, however, more general,

and was in later work extended to two-dimensions and applied to adapt the OCV w.r.t. SOC and age [95].

5.5 Coordinating dual estimators

To improve robustness, the dual estimators for parameters and states are coordinated based on the following heuristics about the prediction error of the adaptive model:

- Errors in different parameters have different effects over the frequency range, where R_0 dominates in high frequencies, R_1 and τ_1 in mid frequencies, and SOC in the low frequency range, see Figure 5.2.
- The model should be correct after some time with low current, since the polarization voltages converges to zero and SOC thereby can be updated from the OCV.

These observations are used to automatically recalibrate the estimators. Future work is needed to formalize this procedure and prove properties of the dual estimator.

5.6 Verification

The proposed dual estimator was implemented in Simulink and tested on real cells using a rapid prototyping environment (see Section 3.4). A test cycle from typical usage of a plug-in hybrid vehicle was used, where the battery starts from fully charged ($\sim$90% SOC) and is then discharged down to approximately 15% SOC. In the literature, SOC estimation accuracy is often evaluated by studying convergence from an initial error. This is, however, not a probable case in a real battery application since SOC can be measured by OCV when the cell is at rest. The tests therefore focus on handling uncertain parameters of the battery model instead. All parameters were given initial errors, and R_0, R_1, and τ_1 were then estimated on-line together with SOC. Test cases were run for several temperatures, but here only results from -10 to $+25$°C are reported. The results, which are previously unpublished, are promising, with SOC estimation accuracy within 2% compared to reference SOC calculated using sensors in laboratory equipment.

The first test, illustrated in Figure 5.3–5.4, examines accuracy of the SOC estimation when the capacity is uncertain, which means that SOC estimated by Coulomb counting will drift over time. Three tests are shown where the capacity is set to Q_{nom} (i.e. nominal capacity determined from

reference test), $0.95Q_{\text{nom}}$, and $1.05Q_{\text{nom}}$ respectively. Note that noise on the BMS current sensor causes additional drift in the Coulomb counting compared to the laboratory equipment, which is most visible in Figure 5.3 where also the use of Q_{nom} results in over 4% error in Coulomb counting. The EKF still manages to correct SOC, and the error compared to the reference is within $\pm 2\%$ for all cases in $+25°\text{C}$. In $-10°\text{C}$, the results are similar but the maximum error is slightly larger than 2% at some occasions.

Figure 5.5–5.6 show the adaptation of R_0, R_1, and τ_1 from three different starting values. The performance is evaluated in terms of the voltage prediction error, which is typically within $\pm 50\text{mV}$ at $+25°\text{C}$, while the accuracy deteriorates in the low SOC region, which can be seen in the test at $-10°\text{C}$. Note that the larger spikes in the prediction error come from inconsistencies in the data that were intentionally introduced to test robustness of the algorithms. It can be seen that R_0 rapidly converges to the same values for all cases. Also R_1 and τ_1 seems to converge to the same value, but the adaptation is not fast enough to converge during the cycle.

Summarizing the results, it can be concluded that the SOC accuracy is consistent also in cases with limited prior information about cell characteristics (i.e cell model parameters). Similar results should thus be possible for the entire battery life-time.

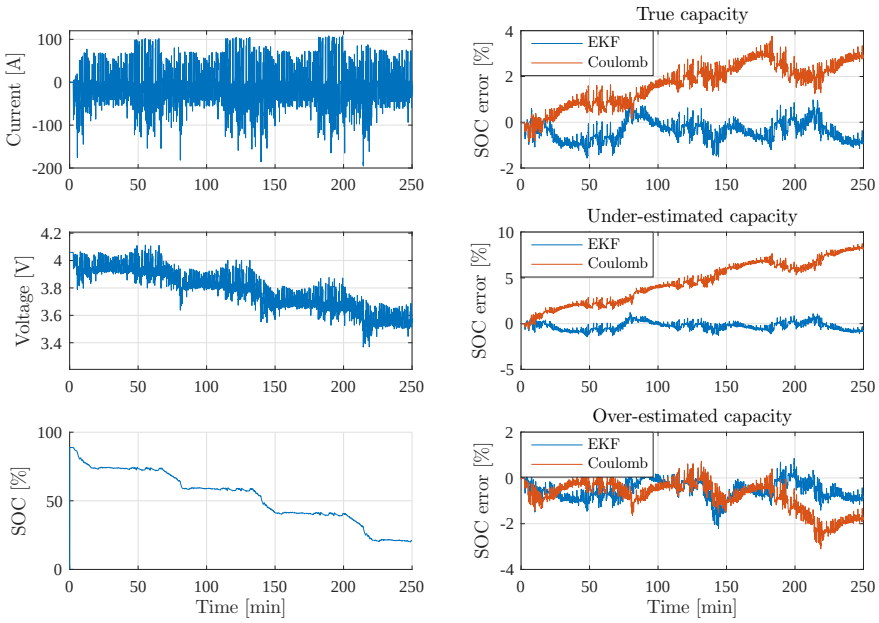

Figure 5.3: SOC estimation accuracy at +25°Cwith error in capacity. Reference SOC is calculated by Coulomb counting using laboratory equipment, while the "Coulomb" signal is integration of the current measured by the BMS sensor.

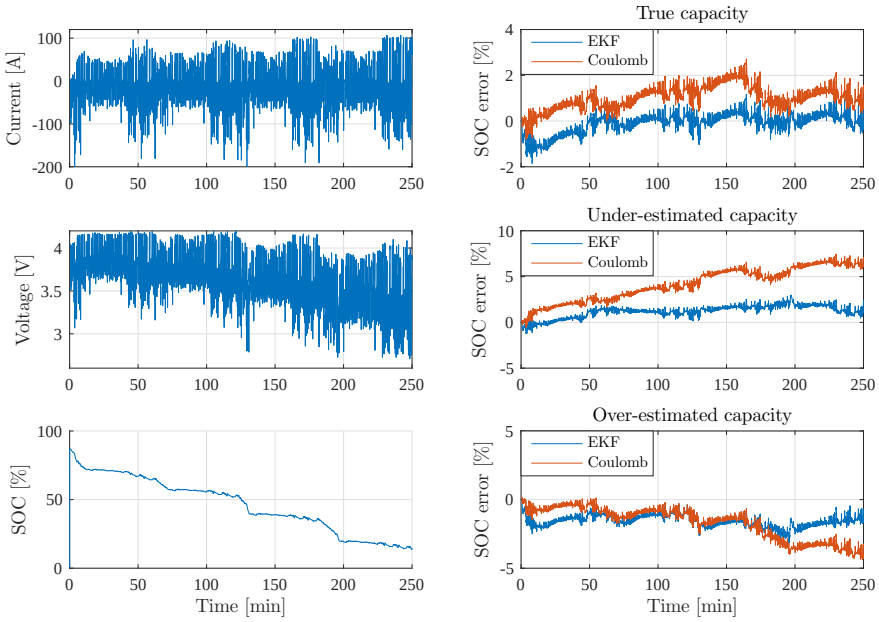

Figure 5.4: SOC estimation accuracy at -10°Cwith error in capacity.

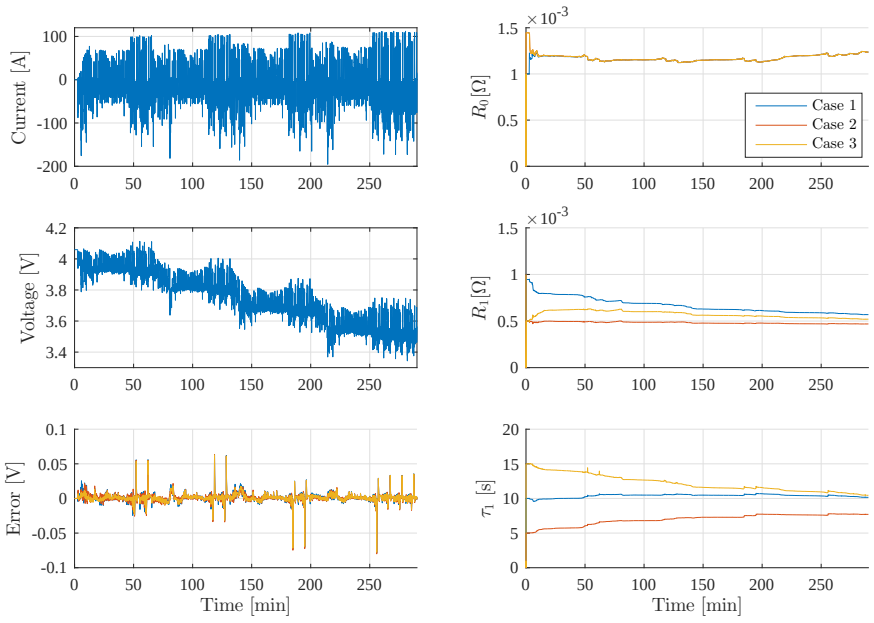

Figure 5.5: Parameter adaptation for three different parameter initialization at +25°C. It can be seen that R_0 rapidly converges to the same value for all initialization values. Also R_1 and τ_1 seem to converge to the same values. The adaptation is, however, not fast enough to converge during the cycle, but they all approach the same value slowly. Note the "spikes" in the voltage prediction error. They are caused by inconsistencies in the data that were intentionally added to test robustness to sensor errors.

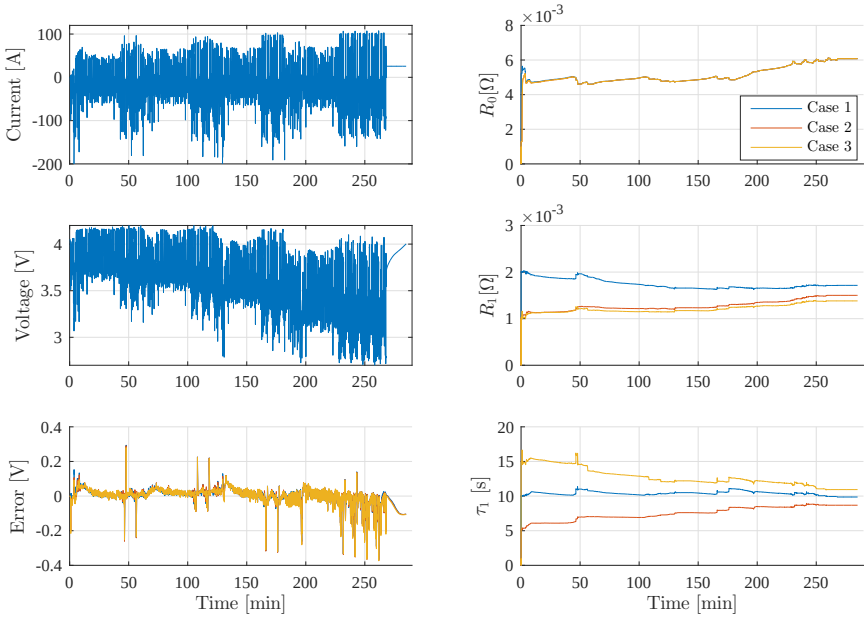

Figure 5.6: Parameter adaptation at -10°C.

Chapter 6

Estimating battery capability

It is now time to address Question 1, which boils down to estimating the battery capability to deliver power and energy without violating constraints set by the operating window $\mathcal{W}$. Optimal operation of the electrified vehicle requires information about the battery capability in different time-scales, from short-term maximum power (typically seconds) up to remaining energy that is available until the battery is drained. From the adaptive battery model of the previous chapter, analytic expressions can be derived for both energy and power estimations.

6.1 Estimating available energy

In the literature, energy estimation is often treated similarly to SOC estimation (see e.g. [96, 97, 98]). By comparing the energy stored in the battery at present time to the energy of a fully charged battery, the state-of-energy (SOE) is estimated. When considering not only the energy stored in the battery, but how much energy that can actually be used by the vehicle there is, however, a major difference between SOC and energy estimation that is not handled explicitly in the existing SOE formulations. SOC and SOE only depends on the present conditions while the available energy also depends on the future driving profile. To see this, start by noting that the energy delivered from the battery over a drive cycle can be calculated by integrating the power, i.e.

$$E_{\text{avail}}(t) = \int_t^{t_{\text{end}}} v(\tau) i(\tau) d\tau, \tag{6.1}$$

where t_{end} is the time when the battery is fully discharged (see Section 2.1).

To simplify expressions, we discard the dynamics of the polarization and consider a purely ohmic battery model

$$v(t) = v_{\text{oc}}(t) + R(T(t))i(t), \tag{6.2}$$

where $R(T(t))$ is a temperature dependent resistive term (see Paper 6 for how this resistance can be derived from an ECM). The power integral can then be rewritten

$$\begin{aligned} E_{\text{avail}}(t) &\approx \int_t^{t_{\text{end}}} v_{\text{oc}}(z(\tau))i(\tau) + R(T)i^2(\tau)d\tau \\ &= \underbrace{\int_t^{t_{\text{end}}} v_{\text{oc}}(z(\tau))i(\tau)d\tau}_{E_{\text{nom}}(t)} + \underbrace{\int_t^{t_{\text{end}}} R(T)i^2(\tau)d\tau}_{E_{\text{loss}}(t)} \end{aligned} \tag{6.3}$$

where E_{nom} is the energy stored in the battery, and E_{loss} is a resistive loss-term.

E_{nom} can be solved by parameter substitution and depends only on battery capacity and SOC. E_{loss} on the other hand depends on the future drive profile. A common solution in the literature to overcome the problem of dependency on future driving profile for SOE is to implicitly include it by using 1C capacity, $Q_{1\text{C}}$ (see Section 2.1). $Q_{1\text{C}}$ depends on both temperature and current, which means that the available energy can be estimated, but only for well defined cycles. It will, however, not handle cases when the temperature changes. To overcome this, an energy estimation based on solving (6.3) is presented in Paper 6, where statistical information about the future driving profile is assumed to be known. A thermal model is then used to handle the temperature trajectory of the battery during the cycle.

6.2 Estimating power capability

To ensure safety and durability, batteries must remain inside the operation window $\mathcal{W}$ at all times. $\mathcal{W}$ is normally defined by bounds on voltage, current, temperature, and SOC, and this means that the power that the battery can provide is limited. For optimal operation of an electrified vehicle, the BMS must give an accurate estimation of how these limitations impact the power capability of the battery in both short (less than 2s) and long term ($\sim$30s).

Maximum power capability

The maximum power capability, which must be considered both for charging and discharging, is used to keep the battery inside the operating window. It can be defined as the maximum constant power that can be handled on a short time-horizon, typically a few second. Since power is non-linear (product of current and voltage), the problem is often simplified by estimating

maximum constant current rather than constant power. The short time-horizon means that slower dynamics, such as SOC and temperature, can usually be considered constant and thereby no predictions are needed for them. The difficult part is instead to predict how the power is affected by current and voltage limits.

There are several existing approaches on the topic of power estimation:

- Analytic expressions based on an equivalent circuit model (see [99, 100])
- Kalman filter based estimation (see [7, 97, 101])
- Particle filter based estimation (see [102])
- Neural networks (see [103]).

The method proposed here is based on an analytic expression and was developed in collaborative work [99]. In Paper 4 it is connected to the adaptive model from Chapter 5 and validated on aged cells in laboratory.

Continuous power capability

A battery cannot be operated at maximum power for extended periods of time. Firstly, due to voltage sometimes dropping rapidly at discharge, and secondly because this puts additional stress on the cell. This means that maximum power may have to be rapidly reduced in some cases, which may introduce issues with drive-ability. To handle this, maximum power can be calculated also for longer time-horizons to provide strategic information to the energy management system of the vehicle.

Theoretically, the same function as for maximum power capability can be used. However, there are some more problems to consider, firstly, also the slower dynamics may become limiting (also temperature and SOC changes during the time-horizon must be considered in the calculations). Secondly, the models are sometimes not accurate for long discharge powers. An example of this for high power discharge in cold temperatures is treated in Paper 6, where an extended ECM is proposed to handle the voltage prediction.

6.3 Limiting power

In addition to estimating power capability, the BMS must also limit the power if the vehicle demands more than the battery can deliver. In the limiting case, e.g. when the battery is operated at the voltage limit, a closed-loop

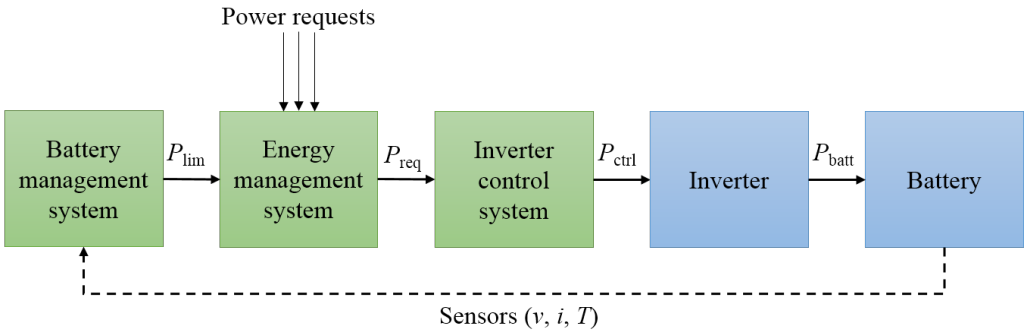

Figure 6.1: Block schedule of the feedback system for power limitation. Due to the time-delay introduced from networked controllers this loop may become unstable if the resistance of the battery is under-estimated.

system containing several networked controllers is formed (see Figure 6.1). The stability of the closed-loop system is examined in Paper 4, where it is concluded that a combination of communication delays and uncertain model parameters may impact stability of the system.

Chapter 7

Summary of included papers

Paper 1

> **B. Fridholm**, M. Nilsson and T. Wik, "Robustness comparison of battery state of charge observers for automotive applications", *19th IFAC World Congress 2014*, August 2014, Cape Town, South Africa.

At the time of this work, several different methods to estimate SOC had been proposed in the literature. The results were inconclusive and no thorough comparison between the different methods had been done. This paper compares the robustness of three different battery SOC estimation algorithms: the Extended Kalman Filter (EKF), the Unscented Kalman Filter (UKF) and the H_∞-filter. Their performance when subject to disturbances such as parameter uncertainties, different sensor noise characteristics and sensitivity to tuning are examined. Simulations show that the appropriate choice of observer algorithm will depend on battery chemistry as well as on the intended application. For batteries with a strong correlation between SOC and OCV, the UKF is robust to disturbances such as sensor bias. The H_∞-filter shows performance on par with the UKF but the variability of the estimation errors are larger. The EKF is found to be a good all-round choice.

Paper 2

> **B. Fridholm**, T. Wik, and M. Nilsson, "Kalman filter for adaptive learning of look-up tables with application to battery ohmic resistance estimation", *Control Engineering Practice*, 48, 2016.

In on-line automotive applications, look-up tables are often used to model non-linearities in component models that are to be valid over large

operating ranges. If the component characteristics change with ageing or wear, these look-up tables must be updated on-line. In this paper, a method is presented where a Kalman filter is used to update the entire look-up table based on local estimation at the current operating conditions. The method is based on the idea that the parameter changes observed as a component ages are caused by physical phenomena having effect over a larger part of the operating range that may have been excited. This means that ageing patterns at different operating points are correlated, and these correlations are used to drive a random walk process that models the parameter changes over the entire operating window. To demonstrate properties of the method, it is applied to estimate the ohmic resistance of a lithiumion battery. In simulations the complete look-up table is successfully updated without problems of drift, even in parts of the operating range that are almost never excited. The method is also robust to uncertainties, both in the ageing model and in initial parameter estimates.

Paper 3

> **B. Fridholm**, T. Wik, and M. Nilsson, "Robust recursive impedance estimation for automotive lithium-ion batteries", *Journal of Power Sources*, 304, 2016.

Recursive algorithms, such as recursive least squares (RLS) or Kalman filters, are commonly used in battery management systems to estimate the electrical impedance of the battery cell. However, these algorithms can in some cases run into problems with bias and even divergence of the estimates. This article illuminates problems that can arise in online estimation using recursive methods, and lists modifications to handle these issues. An algorithm is also proposed that estimates the impedance by separating the problem into two parts; one estimating the ohmic resistance with an RLS approach, and another one where the dynamic effects are estimated using an adaptive Kalman filter (AKF), which is novel in the battery field. The algorithm produces robust estimates of ohmic resistance and time constant of the battery cell in closed loop with SOC estimation, as demonstrated both in simulations and with experimental data from a lithium-ion battery cell.

Paper 4

> **B. Fridholm**, T. Wik, H. Kuusisto, and A. Klintberg, "Estimating power capability of aged lithium-ion batteries in presence

of communication delays", *Journal of Power Sources*, 383, 2018.

Efficient control of electrified powertrains requires accurate estimation of the power capability of the battery for the next few seconds into the future. When implemented in a vehicle, the power estimation is part of a control loop that may contain several networked controllers which introduces time delays that may jeopardize stability. In this article, we present and evaluate an adaptive power estimation method that robustly can handle uncertain health status and time delays. A theoretical analysis shows that stability of the closed loop system can be lost if the resistance of the model is underestimated. Stability can, however, be restored by filtering the estimated power at the expense of slightly reduced bandwidth of the signal. The adaptive algorithm is experimentally validated in lab tests using an aged lithium-ion cell subject to a high power load profile in temperatures from -20 to $+25$°C. The upper voltage limit was set to 4.15 V and the lower voltage limit to 2.6 V, where significant non-linearities are occurring and the validity of the model is limited. After an initial transient when the model parameters are adapted, the prediction accuracy is within $\pm 2\%$ of the actually available power.

Paper 5

B. Fridholm, T. Wik, C. Zou, and A. Klintberg, "Long-term voltage prediction for lithium-ion batteries using an extended equivalent circuit model and moving horizon estimation", *Submitted for publication in Journal of Power Sources.*

Equivalent circuit models are commonly used for predicting the current–voltage response in algorithms for battery management. One example is prediction of power capability where a voltage model can be used to estimate the maximum allowed power for different time-horizons into the future. For long prediction horizons (e.g. 30s or more) the battery characteristics may, however, change considerably. This is in particular a problem for high discharge power in cold temperatures and can then result in significant prediction errors. In this article an extended equivalent circuit model is proposed, where states related to local state-of-charge (concentration) on the particle surface are added. The voltage prediction accuracy is improved compared to the regular equivalent circuit model, which is demonstrated on laboratory data collected in temperatures ranging from -20 to $+25$°C.

Paper 6

B. Fridholm, M. Hedegrd, and T. Wik, "An analytic estimate of available battery energy considering thermal effects", *Submitted for publication in Journal of Power Sources.*

The electrical range of electrified vehicles is limited by the energy available from the battery system. The available energy differs from the total energy stored in the battery due to resistive losses that are highly nonlinear w.r.t. temperature and drawn current. This introduces a dependency on future operating conditions that must be accounted for to get accurate estimates of the available energy. Based on statistical measures of the future driving profile, together with an electro-thermal battery model, an approximate analytical expression for the available energy that considers the temperature trajectory of the battery is derived. The expression is evaluated in simulations using a battery pack model with a thermal system calibrated to laboratory data. The approximation error is within 1% for the tested temperature range -15 to $+30$°C.

Chapter 8

Concluding remarks and future research directions

A main objective of automotive battery management is to address the trade-off between usage and degradation. This problem was here defined as that of translating measurement information (current, voltage, and temperature) into estimations of battery characteristics (cell model parameters), internal states (SOC and SOH), and energy and power capability. A system of adaptive algorithms was proposed to solve the on-line battery estimation problem and was demonstrated on both laboratory cell data and in simulations.

While this thesis aims at describing major parts of the on-line battery estimation problem, there are of course still open research questions. A first example, directly applicable to the work here, is related to formalising the coordination of the different estimators for parameters and SOC. Here, a heuristic approach utilizing how parameters and states affects the frequency response of the voltage model was proposed. Another extension is to treat the problem of inhomogeneous battery packs, i.e. when the cells of the pack are not equal in terms of capacity, impedance, and/or temperature. This work was focused on cell level, and the conversion to pack poses some questions on how to translate cell level results in a computationally efficient way.

Here we focused mainly on cells using NMC chemistry, but should be transferable also to other chemistries. The main prerequisite is that all algorithms requires that the current–voltage characteristics can be described sufficiently well using an equivalent circuit model (ECM). If future cell chemistries, e.g. solid-state or lithium-sulphur, are not behaving as described by an ECM the choice of algorithms may therefore have to be re-evaluated.

An interesting topic, not covered in this thesis, is how data-driven methods can be used for better understanding of ageing phenomena. Today cars

have the possibility to collect huge amounts of statistical data that can be used for this purpose. Cloud-connected vehicles also enables parts of the battery control problem to be handled off-line and generic strategies for this are needed.

Electrochemical control is already a topic of the battery research field. However, it is still difficult to utilize in practical applications due to limited measurement information and high computational complexity. New sensor concepts measuring chemical characteristics inside the cell together with increased computational power can open new opportunities in this field in the coming years. For this to be a feasible direction for the automotive industry, the benefits provided by these methods must, however, be further researched. An example is to quantify how much additional energy, power, and/or life-time that can be expected using electrochemical rather than electrical constraints.

References

[1] "McKinsey." [Online]. Available: https://www.mckinsey.com/industries/automotive-and-assembly/our-insights/the-global-electric-vehicle-market-is-amped-up-and-on-the-rise

[2] U.S. Department of Energy, "Cost and Price Metrics for Automotive Lithium-Ion Batteries," Tech. Rep., 2017.

[3] M. N. Eisler, "A Tesla in every garage?" *IEEE Spectrum*, vol. 53, no. 2, pp. 34–55, 2016.

[4] G. Berckmans, M. Messagie, J. Smekens, N. Omar, L. Vanhaverbeke, and J. V. Mierlo, "Cost projection of state of the art lithium-ion batteries for electric vehicles up to 2030," *Energies*, vol. 10, no. 9, 2017.

[5] W. Fang, O. J. Kwon, and C.-Y. Wang, "Electrochemicalthermal modeling of automotive Li-ion batteries and experimental validation using a three-electrode cell," *International Journal of Energy Research*, vol. 34, pp. 7107–115, 2010.

[6] W. Waag, C. Fleischer, and D. U. Sauer, "Critical review of the methods for monitoring of lithium-ion batteries in electric and hybrid vehicles," *Journal of Power Sources*, vol. 258, pp. 321–339, 2014.

[7] F. Sun, R. Xiong, and H. He, "Estimation of state-of-charge and state-of-power capability of lithium-ion battery considering varying health conditions," *Journal of Power Sources*, vol. 259, pp. 166–176, 2014.

[8] A. Farmann and D. Uwe, "Review article A comprehensive review of on-board State-of-Available-Power prediction techniques for lithium-ion batteries in electric vehicles," *Journal of Power Sources*, vol. 329, pp. 123–137, 2016.

[9] M. Alamgir, "Lithium Has Transformed Vehicle Technology," *IEEE Electrification Magazine*, vol. 5, no. 1, pp. 43–52, 2017.

[10] G. K. Prasad and C. D. Rahn, "Model based identification of aging parameters in lithium ion batteries," *Journal of Power Sources*, vol. 232, pp. 79–85, 2013.

[11] K. A. Smith, "Electrochemical Control of Lithium-Ion Batteries [Applications of Control]," *IEEE Control Systems Magazine*, vol. 30, no. 2, pp. 18–25, 2010.

[12] T.-K. Lee, Y. Kim, A. Stefanopoulou, and Z. S. Filipi, "Hybrid electric vehicle supervisory control design reflecting estimated lithium-ion battery electrochemical dynamics," *Proceedings of the 2011 American Control Conference*, pp. 388–395, 2011.

[13] J. Vetter, P. Novák, M. R. Wagner, C. Veit, K. C. Möller, J. O. Besenhard, M. Winter, M. Wohlfahrt-Mehrens, C. Vogler, and A. Hammouche, "Ageing mechanisms in lithium-ion batteries," *Journal of Power Sources*, vol. 147, no. 1-2, pp. 269–281, 2005.

[14] M. Broussely, P. Biensan, F. Bonhomme, P. Blanchard, S. Herreyre, K. Nechev, and R. J. Staniewicz, "Main aging mechanisms in Li ion batteries," *Journal of Power Sources*, vol. 146, no. 1-2, pp. 90–96, 2005.

[15] J. Groot, "State-of-Health Estimation of Li-ion Batteries: Ageing Models," PhD Thesis, Chalmers University of Technology, 2014.

[16] M. Swierczynski, "Lithium ion battery energy storage system for augmented wind power plants," PhD Thesis, Aalborg University, 2012.

[17] G. Liu, M. Ouyang, L. Lu, J. Li, and X. Han, "Analysis of the heat generation of lithium-ion battery during charging and discharging considering different influencing factors," *Journal of Thermal Analysis and Calorimetry*, vol. 116, no. 2, pp. 1001–1010, 2014.

[18] A. Klintberg, E. Klintberg, B. Fridholm, H. Kuusisto, and T. Wik, "Statistical modeling of OCV-curves for aged battery cells," *IFAC-PapersOnLine*, vol. 50, no. 1, pp. 2164–2168, 2017.

[19] A. Jossen, "Fundamentals of battery dynamics," *Journal of Power Sources*, vol. 154, no. 2, pp. 530–538, 2006.

[20] Y. Zhu and C. Wang, "Strain accommodation and potential hysteresis of LiFePO4cathodes during lithium ion insertion/extraction," *Journal of Power Sources*, vol. 196, no. 3, pp. 1442–1448, 2011.

[21] M. A. Roscher, O. Bohlen, and J. Vetter, "OCV Hysteresis in Li-Ion Batteries including Two-Phase Transition Materials," *International Journal of Electrochemistry*, vol. 2011, pp. 1–6, 2011.

[22] G. L. Plett, "Extended Kalman filtering for battery management systems of LiPB-based HEV battery packs - Part 2. Modeling and identification," *Journal of Power Sources*, vol. 134, no. 2, pp. 262–276, 2004.

[23] X. Tang, X. Mao, J. Lin, and B. Koch, "Li-ion battery parameter estimation for state of charge," *American Control Conference (ACC), 2011*, pp. 941 – 946, 2011.

[24] G. J. Offer, V. Yufit, D. A. Howey, B. Wu, and N. P. Brandon, "Module design and fault diagnosis in electric vehicle batteries," *Journal of Power Sources*, vol. 206, pp. 383–392, 2012.

[25] M. Brandl, M. Wenger, V. Lorentz, M. Giegerich, L. Fanucci, R. Roncella, R. Saletti, and S. Saponara, "Batteries and Battery Management Systems for Electric Vehicles," *2012 Design, Automation & Test in Europe Conference & Exhibition*, 2012.

[26] T. Horiba, "Lithium-ion battery systems," *Proceedings of the IEEE*, vol. 102, no. 6, pp. 1–12, 2014.

[27] H. Rahimi-Eichi, U. Ojha, F. Baronti, and M. Chow, "Battery Management System: An Overview of Its Application in the Smart Grid and Electric Vehicles," *Industrial Electronics Magazine, IEEE*, vol. 7, no. June, pp. 4–16, 2013.

[28] D. Andrea, *Battery Management Systems for Large Lithium Ion Battery Packs*. Artech House, 2010.

[29] Y. Xing, E. W. M. Ma, K. L. Tsui, and M. Pecht, "Battery Management Systems in Electric and Hybrid Vehicles," *Energies*, vol. 4, no. 12, pp. 1840–1857, 2011.

[30] M. U. Cuma and T. Koroglu, "A comprehensive review on estimation strategies used in hybrid and battery electric vehicles," *Renewable and Sustainable Energy Reviews*, vol. 42, pp. 517–531, 2015.

[31] Q. Wang, P. Ping, X. Zhao, G. Chu, J. Sun, and C. Chen, "Thermal runaway caused fire and explosion of lithium ion battery," *Journal of Power Sources*, vol. 208, pp. 210–224, 2012.

[32] S. Wang, L. Shang, Z. Li, H. Deng, and J. Li, "Online dynamic equalization adjustment of high-power lithium-ion battery packs based on the state of balance estimation," *Applied Energy*, vol. 166, pp. 44–58, 2016.

[33] Y. Hua, A. Cordoba-Arenas, N. Warner, and G. Rizzoni, "A multi time-scale state-of-charge and state-of-health estimation framework using nonlinear predictive filter for lithium-ion battery pack with passive balance control," *Journal of Power Sources*, vol. 280, pp. 293–312, 2015.

[34] F. Altaf, "On Modeling and Optimal Control of Modular Batteries," PhD Thesis, Chalmers University of Technology, 2016.

[35] S. Bashash, S. Moura, and H. Fathy, "Charge trajectory optimization of plug-in hybrid electric vehicles for energy cost reduction and battery health enhancement," *American Control Conference (ACC), 2010*, pp. 5824–5831, 2010.

[36] C. Zou, X. Hu, Z. Wei, and X. Tang, "Electrothermal dynamics-conscious lithium-ion battery cell-level charging management via state-monitored predictive control," *Energy*, vol. 141, pp. 250–259, 2017.

[37] L. Ljung, *System Indentification - Theory for the User*, 2nd ed. Prentice Hall, 1999.

[38] K. J. Åström and B. Wittenmark, *Adaptive Control*. Dover Publication Inc, 2008.

[39] F. Gustafsson, *Adaptive Filtering and Change Detection*. John Wiley & Sons, Ltd, 2000.

[40] X. Hu, F. Sun, and Y. Zou, "Online model identification of lithium-ion battery for electric vehicles," *J. Cent. South Univ. Technol.*, vol. 18, pp. 1525–1531, 2011.

[41] C. Zou, A. G. Kallapur, C. Manzie, and D. Nesic, "PDE battery model simplification for SOC and SOH estimator design," *Proceedings of the IEEE Conference on Decision and Control*, vol. 54rd IEEE, no. Cdc, pp. 1328–1333, 2015.

[42] L. Ljung, "Asymptotic Behavior of the Extended Kalman Filter as a Parameter Estimator for Linear Systems," *IEEE Transactions on Automatic Control*, vol. 24, no. 1, pp. 36–50, 1979.

[43] G. Welch and G. Bishop, "An Introduction to the Kalman Filter," Ph.D. dissertation, University of North Carolina at Chapel Hill, 1995.

[44] D. Simon, *Optimal state estimation.* John Wiley Sons Ltd, 2006.

[45] A. J. Laub, *Matrix Analysis for Scientists and Engineers.* Siam, 2005.

[46] P. G. Kaminski, A. E. Bryson, and S. F. Schmidt, "Discrete Square Root Filtering: A Survey of Current Techniques," *IEEE Transactions on Automatic Control*, vol. 16, no. 6, pp. 727–736, 1971.

[47] G. L. Plett, "Sigma-point Kalman filtering for battery management systems of LiPB-based HEV battery packs. Part 1: Introduction and state estimation," *Journal of Power Sources*, vol. 161, no. 2, pp. 1356–1368, 2006.

[48] F. Sun, X. Hu, Y. Zou, and S. Li, "Adaptive unscented Kalman filtering for state of charge estimation of a lithium-ion battery for electric vehicles," *Energy*, vol. 36, no. 5, pp. 3531–3540, 2011.

[49] P. Abbeel, A. Coates, M. Montemerlo, A. Y. Ng, and S. Thrun, "Discriminative Training of Kalman Filters," *Proceedings of Robotics: Science and Systems I*, pp. 289–296, 2005.

[50] A. Sakai and Y. Kuroda, "Discriminatively Trained Unscented Kalman Filter for Mobile Robot Localization," *Journal of Advanced Research in Mechanical Engineering*, vol. 1, no. 3, pp. 153–161, 2010.

[51] J. Seo, M. J. Yu, C. G. Park, and J. G. Lee, "An extended robust H infinity filter for nonlinear uncertain systems with constraints," *Proceedings of the 44th IEEE Conference on Decision and Control, and the European Control Conference, CDC-ECC '05*, vol. 2005, pp. 1935–1940, 2005.

[52] P. Ni and S. Li, "Unscented H_infinity filter based simultaneous localization and mapping," *IEEE Chinese Control Conf. (CCC'11)*, no. 1, pp. 3942–3946, 2011.

[53] J. Yan, G. Xu, H. Qian, and Y. Xu, "Robust state of charge estimation for hybrid electric vehicles: Framework and algorithms," *Energies*, vol. 3, no. 10, pp. 1654–1672, 2010.

[54] B. Hassibi, A. H. Sayed, and T. Kailath, "Linear estimation in Krein Spaces-Part I: Theory," *IEEE Transactions on Automatic Control*, vol. 41, no. 1, pp. 18–33, 1996.

[55] P. Kühl, M. Diehl, T. Kraus, J. P. Schlöder, and H. G. Bock, "A real-time algorithm for moving horizon state and parameter estimation," *Computers and Chemical Engineering*, vol. 35, no. 1, pp. 71–83, 2011.

[56] S. Ungarala, "Computing arrival cost parameters in moving horizon estimation using sampling based filters," *Journal of Process Control*, vol. 19, no. 9, pp. 1576–1588, 2009.

[57] X. Hu, D. Cao, and B. Egardt, "Condition Monitoring in Advanced Battery Management Systems: Moving Horizon Estimation Using a Reduced Electrochemical Model," *IEEE/ASME Transactions on Mechatronics*, vol. 23, no. 1, pp. 167–178, 2018.

[58] J. B. Rawlings and D. Q. Mayne, *Model Predictive Control Theory and Design*. Madison, WI, USA: Nob Hill Publishing, 2009.

[59] Y. Hu and S. Yurkovich, "Battery state of charge estimation in automotive applications using LPV techniques," *2010 American Control Conference, ACC 2010, June 30, 2010 - July 2, 2010*, pp. 5043–5049, 2010.

[60] E. A. Misawa and J. K. Hedrick, "Nonlinear Observers A State-of-the-Art Survey," *Transactions of AMSE*, vol. 111, no. 344, 1989.

[61] I.-S. Kim, "The novel state of charge estimation method for lithium battery using sliding mode observer," *Journal of Power Sources*, vol. 163, no. 1, pp. 584–590, 2006.

[62] M. Doyle, T. Fuller, and J. Newman, "Modeling of Galvanostaic Charge and Discharge of the Lithium/Polymer/Insertion Cell," *Journal of The Electrochemical Society*, vol. 6, 1993.

[63] N. A. Chaturvedi, R. Klein, J. Christensen, J. Ahmed, and A. Kojic, "Algorithms for advanced battery-management systems," *IEEE Control Systems Magazine*, vol. 30, no. 3, pp. 49–68, 2010.

[64] X. Han, M. Ouyang, L. Lu, and J. Li, "Simplification of physics-based electrochemical model for lithium ion battery on electric vehicle. Part II : Pseudo-two-dimensional model simplification and state of charge estimation," *Journal of Power Sources*, vol. 278, pp. 814–825, 2015.

[65] K. A. Smith, C. D. Rahn, and C.-y. Wang, "Model-Based Electrochemical Estimation of Lithium Ion Batteries," *Control Systems Technology,*, vol. 18, no. 1, pp. 714–719, 2008.

[66] D. Di Domenico, A. Stefanopoulou, and G. Fiengo, "Lithium-Ion Battery State of Charge and Critical Surface Charge Estimation Using an Extended Kalman Filter," *Journal of Dynamic Systems, Measurement, and Control*, vol. 132, no. November 2010, pp. 1–11, 2010.

[67] H. Fang, Y. Wang, Z. Sahinoglu, T. Wada, and S. Hara, "Adaptive Estimation of State of Charge for Lithium-ion Batteries," in *American Control Conference*, 2013.

[68] L. Cai and R. E. White, "Reduction of Model Order Based on Proper Orthogonal Decomposition for Lithium-Ion Battery Simulations," *Journal of The Electrochemical Society*, vol. 156, no. 3, p. A154, 2009.

[69] K. A. Smith, C. D. Rahn, and C.-Y. Wang, "Model Order Reduction of 1D Diffusion Systems Via Residue Grouping," *Journal of Dynamic Systems, Measurement, and Control*, vol. 130, no. 1, p. 011012, 2008.

[70] V. R. Subramanian, V. Boovaragavan, V. Ramadesigan, and M. Arabandi, "Mathematical Model Reformulation for Lithium-Ion Battery Simulations: Galvanostatic Boundary Conditions," *Journal of The Electrochemical Society*, vol. 156, no. 4, p. A260, 2009.

[71] C. Speltino, D. D. Domenico, G. Fiengo, and A. Stefanopoulou, "Comparison of reduced order lithium-ion battery models for control applications," *Proceedings of the 48h IEEE Conference on Decision and Control (CDC) held jointly with 2009 28th Chinese Control Conference*, pp. 3276–3281, 2009.

[72] X. Hu, S. Li, and H. Peng, "A comparative study of equivalent circuit models for Li-ion batteries," *Journal of Power Sources*, vol. 198, pp. 359–367, 2012.

[73] M. Chen, S. Member, and G. A. Rinc, "Accurate Electrical Battery Model Capable of Predicting Runtime and I V Performance," *IEEE Transactions on Energy Conversion*, vol. 21, no. 2, pp. 504–511, 2006.

[74] M. Verbrugge, "Adaptive, multi-parameter battery state estimator with optimized time-weighting factors," *Journal of Applied Electrochemistry*, vol. 37, no. 5, pp. 605–616, 2007.

[75] J. Jaguemont, L. Boulon, and Y. Dube, "Characterization and Modeling of a Hybrid-Electric-Vehicle Lithium-Ion Battery Pack at Low Temperatures," *IEEE Transactions on Vehicular Technology*, vol. 65, no. 1, pp. 1–14, 2015.

[76] M. Debert, G. Colin, G. Bloch, and Y. Chamaillard, "An observer looks at the cell temperature in automotive battery packs," *Control Engineering Practice*, vol. 21, no. 8, pp. 1035–1042, 2013.

[77] M. Ouyang, G. Liu, L. Lu, J. Li, and X. Han, "Enhancing the estimation accuracy in low state-of-charge area: A novel onboard battery model through surface state of charge determination," *Journal of Power Sources*, vol. 270, pp. 221–237, 2014.

[78] K. Makinejad, R. Arunachala, S. Arnold, H. Ennifar, H. Zhou, and A. Jossen, "A Lumped Electro - Thermal Model for Li - Ion Cells in Electric Vehicle Application," in *EVS28, Kintex, Korea*, 2014, pp. 1–14.

[79] Z. He, M. Gao, C. Wang, L. Wang, and Y. Liu, "Adaptive state of charge estimation for Li-ion batteries based on an unscented kalman filter with an enhanced battery model," *Energies*, vol. 6, no. 8, pp. 4134–4151, 2013.

[80] D. Haifeng, W. Xuezhe, and S. Zechang, "State and parameter estimation of a HEV li-ion battery pack using adaptive kalman filter with a new SOC-OCV concept," *2009 International Conference on Measuring Technology and Mechatronics Automation, ICMTMA 2009*, vol. 2, pp. 375–380, 2009.

[81] Y. Zou, X. Hu, H. Ma, and S. E. Li, "Combined State of Charge and State of Health estimation over lithium-ion battery cell cycle lifespan for electric vehicles," *Journal of Power Sources*, vol. 273, pp. 793–803, 2015.

[82] D. V. Do, C. Forgez, K. El Kadri Benkara, and G. Friedrich, "Impedance observer for a Li-ion battery using Kalman filter," *IEEE Transactions on Vehicular Technology*, vol. 58, no. 8, pp. 3930–3937, 2009.

[83] G. L. Plett, "Extended Kalman filtering for battery management systems of LiPB-based HEV battery packs - Part 3. State and parameter estimation," *Journal of Power Sources*, vol. 134, no. 2, pp. 277–292, 2004.

[84] Y. H. Chiang, W. Y. Sean, and J. C. Ke, "Online estimation of internal resistance and open-circuit voltage of lithium-ion batteries in electric vehicles," *Journal of Power Sources*, vol. 196, no. 8, pp. 3921–3932, 2011.

[85] X. Tang, X. Mao, J. Lin, and B. Koch, "Capacity estimation for Li-ion batteries," *Proceedings of the 2011 American Control Conference*, 2011.

[86] L. Wang, C. Pan, L. Liu, Y. Cheng, and X. Zhao, "On-board state of health estimation of LiFePO4 battery pack through differential voltage analysis," *Applied Energy*, vol. 168, pp. 465–472, 2016.

[87] M. Ouyang, S. Gao, L. Lu, X. Feng, D. Ren, J. Li, Y. Zheng, and P. Shen, "Determination of the battery pack capacity considering the estimation error using a CapacityQuantity diagram," *Applied Energy*, vol. 177, pp. 384–392, 2016.

[88] N. A. Samad, Y. Kim, J. B. Siegel, and A. G. Stefanopoulou, "Battery Capacity Fading Estimation Using a Force-Based Incremental Capacity Analysis," *Journal of The Electrochemical Society*, vol. 163, no. 8, pp. A1584–A1594, 2016.

[89] A. Klintberg, T. Wik, and B. Fridholm, "Theoretical Bounds on the Accuracy of State and Parameter Estimation for Batteries," *Proceedings of the 2017 American Control Conference*, pp. 4035–4041, 2017.

[90] Y. Hu and S. Yurkovich, "Linear parameter varying battery model identification using subspace methods," *Journal of Power Sources*, vol. 196, no. 5, pp. 2913–2923, 2011.

[91] E. Höckerdal, E. Frisk, and L. Eriksson, "EKF-based adaptation of look-up tables with an air mass-flow sensor application," *Control Engineering Practice*, vol. 19, no. 5, pp. 442–453, 2011.

[92] C. Guardiola, B. Pla, D. Blanco-Rodriguez, and P. Cabrera, "A learning algorithm concept for updating look-up tables for automotive applications," *Mathematical and Computer Modelling*, vol. 57, no. 7-8, pp. 1979–1989, 2013.

[93] J. C. Peyton Jones and K. R. Muske, "Identification and adaptation of linear look-up table parameters using an efficient recursive least-squares technique," *ISA Transactions*, vol. 48, no. 4, pp. 476–483, 2009.

[94] H. Blanke, O. Bohlen, S. Buller, R. W. De Doncker, B. Fricke, A. Hammouche, D. Linzen, M. Thele, and D. U. Sauer, "Impedance measurements on lead-acid batteries for state-of-charge, state-of-health and cranking capability prognosis in electric and hybrid electric vehicles," *Journal of Power Sources*, vol. 144, no. 2, pp. 418–425, 2005.

[95] A. Klintberg, C. Zou, B. Fridholm, and T. Wik, "Kalman filter for adaptive learning of two-dimensional look-up tables applied to OCV-curves for aged battery cells," *Control Engineering Practice*, vol. 84, no. May 2018, pp. 230–237, 2019.

[96] Y. Wang, C. Zhang, and Z. Chen, "An adaptive remaining energy prediction approach for lithium-ion batteries in electric vehicles," *Journal of Power Sources*, vol. 305, pp. 80–88, 2016.

[97] W. Zhang, W. Shi, and Z. Ma, "Adaptive unscented Kalman filter based state of energy and power capability estimation approach for lithium-ion battery," *Journal of Power Sources*, vol. 289, pp. 50–62, 2015.

[98] L. Zheng, J. Zhu, G. Wang, T. He, and Y. Wei, "Novel methods for estimating lithium-ion battery state of energy and maximum available energy," *Applied Energy*, vol. 178, pp. 1–8, 2016.

[99] T. Wik, B. Fridholm, and H. Kuusisto, "Implementation and robustness of an analytically based battery state of power," *Journal of Power Sources*, vol. 287, pp. 448–457, 2015.

[100] T. Feng, L. Yang, X. Zhao, H. Zhang, and J. Qiang, "Online identification of lithium-ion battery parameters based on an improved equivalent-circuit model and its implementation on battery state-of-power prediction," *Journal of Power Sources*, vol. 281, pp. 192–203, 2015.

[101] R. Xiong, F. Sun, H. He, and T. D. Nguyen, "A data-driven adaptive state of charge and power capability joint estimator of lithium-ion polymer battery used in electric vehicles," *Energy*, vol. 63, pp. 295–308, 2013.

[102] C. Burgos-Mellado, M. E. Orchard, M. Kazerani, R. Cárdenas, and D. Sáez, "Particle-filtering-based estimation of maximum available power state in Lithium-Ion batteries," *Applied Energy*, vol. 161, pp. 349–363, 2016.

[103] C. Fleischer, W. Waag, Z. Bai, and D. Uwe, "On-line self-learning time forward voltage prognosis for lithium-ion batteries using adaptive neuro-fuzzy inference system," *Journal of Power Sources*, vol. 243, pp. 728–749, 2013.

Part II

Included Papers

Paper 1

Robustness comparison of battery state-of-charge observers for automotive applications

Björn Fridholm, Magnus Nilsson, and Torsten Wik

19th IFAC World Congress, August 2014, Cape Town, South Africa

Comment: The layout of this paper has been reformatted in order to comply with the rest of the thesis.

Robustness comparison of battery state-of-charge observers for automotive applications

Björn Fridholm, Magnus Nilsson, and Torsten Wik

Abstract

This paper compares the robustness of three different battery State of Charge (SoC) estimation algorithms: the Extended Kalman Filter (EKF), the Unscented Kalman Filter (UKF) and the H_∞ filter. Their performance when subject to disturbances such as parameter uncertainties, different sensor noise characteristics and sensitivity to tuning of the filter are examined.

Simulations show that the appropriate choice of observer algorithm will depend on battery chemistry as well as on the intended application. For batteries with a strong correlation between SoC and OCV, the UKF is robust to disturbances such as sensor bias. The H_∞ observer shows performance on par with the UKF but the variability of the estimation errors are larger. The EKF is a good all-round choice.

1 Introduction

To secure safety, reliability and performance of an electrified vehicle, it is important to monitor the State of Charge (SoC) of the battery system [1]. Batteries are electrochemical components and there are currently no sensors that can measure SoC directly. Instead, electrical signals, such as current and voltages of the battery are used to estimate the SoC via some algorithm. There are several approaches to model based SoC estimation available in literature, such as the Extended Kalman Filter (EKF) [2], the Unscented Kalman Filter (UKF) [3], Luenberger Observers (LO) [4], Sliding Mode Observers (SMO) [5] and H_∞ observers [6].

There are also several types of Li-Ion batteries in production today. These differ in electrode materials, leading to different electrical behaviour when subject to a charging or discharging current. Due to these differences, the model used in the observers are not necessarily the same for different cell chemistries [7].

Another aspect to consider when evaluating SoC estimators is that the battery usage is different depending on vehicle application. In a Battery Electric Vehicle (BEV), the battery is the only energy source and thus a large part of the SoC range will be used. In a Hybrid Electric Vehicle (HEV), the electric system is mainly used to boost power in accelerations and thus the battery will be designed to handle large charge and discharge power, but the used SoC range is normally rather small. A Plug-In Hybrid Electric Vehicle (PHEV) can be used as either a BEV or HEV or any combination in between.

Comparative studies of SoC estimators have been performed before, [8] compare EKF, UKF and LO while [9] focus on LO compared to SMO. The main focus in those papers are on the algorithms and implementation aspects of the observers. In [10], the robustness of an EKF is analysed with respect to temperature and ageing for two different battery types. However, there has been no thorough comparison of the performance of different observers for different battery chemistries.

This paper compares the performance of the EKF to that of the UKF and the H_∞ filter for two different battery chemistries. Using a Monte Carlo simulation approach, robustness to problems such as parameter uncertainties, sensor noise characteristics and observer tuning is analysed. The choice of observers is based on promising results shown in [2], [3] and [6]. These observers can also be implemented by simple and efficient recursive algorithms. In [5], Kim show the potential of the SMO. The implementation is, however, complex compared to the chosen observers, and it is thus left out of the evaluation.

The paper is structured as follows: Section 2 presents the test environment used in the evaluation with battery model, observers and the considered use cases. In Section 3, the robustness evaluation is presented. In Section 4 some conclusions of the tests are drawn and the results are discussed.

2 Experiment Setup

This section describes the test setup used, i.e. the simulation environment consisting of battery and sensor models and the evaluated observers. Also the drive cycles used in the tests are presented, together with metrics to evaluate the observers.

2.1 Battery Model

The observers evaluated are all model based and require a model of the process. The general nonlinear discrete time state space form

$$\begin{aligned} x_{k+1} &= f(x_k, u_k, w_k) \\ y_k &= h(x_k, u_k, v_k) \\ w_k &\sim \mathcal{N}(\bar{w}_k, \Sigma_{w,k}) \\ v_k &\sim \mathcal{N}(\bar{v}_k, \Sigma_{v,k}) \end{aligned} \tag{1}$$

is used, where $\mathcal{N}(\bar{\nu}, \Sigma)$ denotes normally distributed noise with mean $\bar{\nu}$ and variance Σ.

Two different batteries are considered in the study; one lithium iron phosphate (LFP) and one lithium nickel manganese cobalt oxide (NMC). Equivalent circuit models, see Figure 1, were fitted to lab data for both batteries. While it was concluded that both batteries can be suitably modelled by single RC-circuit models, the LFP battery needed a hysteresis state, u_h, to improve the fit to measured data.

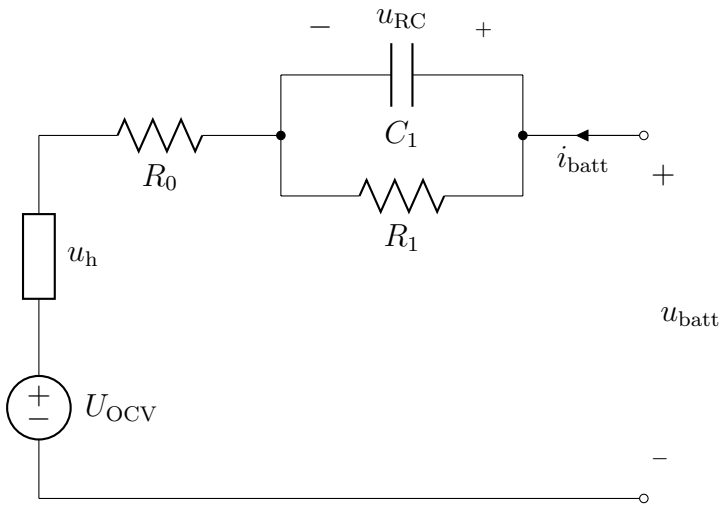

Figure 1: Equivalent circuit battery model

The model equations for both batteries are given in the following sections. For further descriptions of the models, see [2] and [7].

NMC

In room temperature, the NMC battery can be modelled with sufficient accuracy using the following model:

$$\begin{cases} u_{\mathrm{RC},k+1} = e^{-\frac{\Delta t}{\tau_{1,k}}} u_{\mathrm{RC},k} + R_{1,k}\left(1 - e^{-\frac{\Delta t}{\tau_{1,k}}}\right) i_{\mathrm{batt},k} \\ z_{k+1} = z_k + \dfrac{\eta_i \Delta t}{C_{\mathrm{n}}} i_{\mathrm{batt},k} \\ u_{\mathrm{batt},k} = U_{\mathrm{OCV}}(z_k) + u_{\mathrm{RC},k} + R_0(z_k) i_{\mathrm{batt},k} \end{cases}$$

Here, u_{RC}, R_1 and $\tau_1 = R_1 C_1$ are the voltage, resistance and time constant of the RC network, Δt is the sampling time, i_{batt} and u_{batt} are battery current and voltage, z is the battery SoC, η_i is the Coulombic efficiency, C_{n} is the nominal capacity of the battery, U_{OCV} is the open circuit voltage and R_0 is the internal resistance of the battery. Note that the circuit parameters are varying with SoC, i.e. τ_1, R_1, R_0 and U_{OCV} are all functions of SoC.

LFP

The LFP battery needs an additional hysteresis state. The model used is

$$\begin{cases} u_{\mathrm{RC},k+1} = e^{-\frac{\Delta t}{\tau_{1,k}}} u_{\mathrm{RC},k} + R_{1,k}\left(1 - e^{-\frac{\Delta t}{\tau_{1,k}}}\right) i_{\mathrm{batt},k} \\ u_{\mathrm{h},k+1} = e^{-\kappa_k \Delta t} u_{\mathrm{h},k} + \left(1 - e^{-\kappa_k \Delta t}\right) U_{\mathrm{h,max}}(z_k) \\ z_{k+1} = z_k + \dfrac{\eta_i \Delta t}{C_{\mathrm{n}}} i_{\mathrm{batt},k} \\ u_{\mathrm{batt},k} = U_{\mathrm{OCV}}(z_k) + u_{\mathrm{RC},k} + u_{h,k} + R_0(z_k) i_{\mathrm{batt},k} \end{cases}$$

where u_{h} is the hysteresis voltage, κ is the time constant of the hysteresis which is a function of the battery current and $U_{\mathrm{h,max}}$ is the maximum hysteresis. For the LFP battery, also variations with respect to current and charge/discharge are needed, and thus τ_k and R_1 are functions of battery current as well as SoC.

2.2 State of Charge Observers

Three SoC observers were implemented, sharing battery model and parameters according to Section 2.1.

Extended Kalman Filter

The EKF treats the nonlinearities by linearizing the state space representation (1) at each time step. It is a two-step procedure where the *a priori*

state and covariance estimates, $\hat{x}^-$ and $\Sigma_{\tilde{x}}^-$, are first calculated using the state space model. Based on the predicted and measured system output, the estimates are then corrected by the *Kalman gain* K to form the *a posteriori* estimate, $\hat{x}^+$ and $\Sigma_{\tilde{x}}^+$.

A recursive algorithm suited for real-time implementation is described by

$$\begin{aligned}
\hat{x}_k^- &= f\left(\hat{x}_{k-1}^+, u_{k-1}, \bar{w}_{k-1}\right) \\
\Sigma_{\tilde{x},k}^- &= \hat{A}_{k-1}\Sigma_{\tilde{x},k-1}^+\hat{A}_{k-1}^T + \hat{W}_{k-1}\Sigma_{w,k}\hat{W}_{k-1}^T \\
\hat{y}_k &= h\left(\hat{x}_k^-, u_k, \bar{v}_k\right) \\
K_k &= \Sigma_{\tilde{x},k}^-\hat{C}_k^T\left[\hat{C}_k\Sigma_{\tilde{x},k}^-\hat{C}_k^T + \hat{V}_k\Sigma_{v,k}\hat{V}_k^T\right]^{-1} \\
\hat{x}_k^+ &= \hat{x}_k^- + K_k\left(y_k - \hat{y}_k\right) \\
\Sigma_{\tilde{x},k}^+ &= \left(I - K_k\hat{C}_k\right)\Sigma_{\tilde{x},k}^-
\end{aligned} \tag{2}$$

where $\hat{A}_k$, $\hat{W}_k$, $\hat{C}_k$ and $\hat{V}_k$ are the Jacobians:

$$\begin{aligned}
\hat{A}_k &= \frac{\partial f\left(x_k, u_k, w_k\right)}{\partial x_k}\Big|_{x_k=\hat{x}_k^+} \\
\hat{W}_k &= \frac{\partial f\left(x_k, u_k, w_k\right)}{\partial w_k}\Big|_{w_k=\bar{w}_k} \\
\hat{C}_k &= \frac{\partial h\left(x_k, u_k, v_k\right)}{\partial x_k}\Big|_{x_k=\hat{x}_k^-} \\
\hat{V}_k &= \frac{\partial h\left(x_k, u_k, v_k\right)}{\partial v_k}\Big|_{v_k=\bar{v}_k}
\end{aligned}$$

Note that in (2), the Jacobians $\hat{A}_{k-1}$ and $\hat{W}_{k-1}$ from the previous time step are used. For more information on how to derive the EKF, the user is referred to e.g. [2], [11] and [12].

Unscented Kalman Filter

The UKF uses a similar predict/correct procedure as the EKF, but rather than using the Jacobians to linearize the system, the UKF lets several perturbed versions of the current state vector, called sigma points, pass the nonlinear system (1). The estimated state is calculated as a weighted mean of the result, in general providing a better approximation for strong nonlinearities [11].

The recursive algorithm is more complex than the EKF. First, define

the augmented state and sigma point vectors

$$x_k^a = \left[x_k^T, w_k^T, v_k^T\right]^T$$
$$\chi_k^a = \left[\left(\chi_k^x\right)^T, \left(\chi_k^w\right)^T, \left(\chi_k^v\right)^T\right]^T$$

State and covariance estimate predictions are given by

$$\chi_{k-1}^{a,+} = \left\{\hat{x}_{k-1}^{a,+}, \hat{x}_{k-1}^{a,+} + \gamma\sqrt{\Sigma_{\tilde{x},k-1}^{a,+}}, \hat{x}_{k-1}^{a,+} - \gamma\sqrt{\Sigma_{\tilde{x},k-1}^{a,+}}\right\}$$
$$\chi_{k,i}^{x,-} = f\left(\chi_{k-1,i}^{x,+}, u_{k-1}, \chi_{k-1,i}^{w,+}\right)$$
$$\hat{x}_k^- = \sum_{i=0}^{p} \alpha_i^{(m)} \chi_{k,i}^{x,-}$$
$$\Sigma_{\tilde{x},k}^- = \sum_{i=0}^{p} \alpha_i^{(c)} \left(\chi_{k,i}^{x,-} - \hat{x}_k^-\right)\left(\chi_{k,i}^{x,-} - \hat{x}_k^-\right)^T$$

An estimate of the output is calculated from the predicted state

$$\mathcal{Y}_{k,i} = h\left(\chi_{k,i}^{x,-}, u_k, \chi_{k-1,i}^{v,+}\right)$$
$$\hat{y}_k = \sum_{i=0}^{p} \alpha_i^{(m)} \mathcal{Y}_{k,i}$$

The gain of the estimator is

$$\Sigma_{\tilde{y},k} = \sum_{i=0}^{p} \alpha_i^{(c)} \left(\mathcal{Y}_{k,i} - \hat{y}_k\right)\left(\mathcal{Y}_{k,i} - \hat{y}_k\right)^T$$
$$\Sigma_{\tilde{x}\tilde{y},k}^- = \sum_{i=0}^{p} \alpha_i^{(c)} \left(\chi_{k,i}^{x,-} - \hat{x}_k^-\right)\left(\mathcal{Y}_{k,i} - \hat{y}_k\right)^T$$
$$K_k = \Sigma_{\tilde{x}\tilde{y},k}^- \Sigma_{\tilde{y},k}^{-1}$$

Finally, the state and covariance estimates are corrected according to

$$\hat{x}_k^+ = \hat{x}_k^- + K_k\left(y_k - \hat{y}_k\right)$$
$$\Sigma_{\tilde{x},k}^+ = \Sigma_{\tilde{x},k}^- - K_k \Sigma_{\tilde{y},k} K_k^T$$

A thorough background to the unscented transformation and derivation of the UKF can be found in [11] and [3].

Extended H_∞ Filter

H_∞ filters have close similarities to Kalman filters, as pointed out by [11]. They are just like Kalman filters for linear systems, but can also be used

for nonlinear systems by extended [13] and unscented [14] transformations. In the SoC estimation field, [6] promotes the use of the H_∞ filter, based on the fact that it does not require information on noise characteristics.

In [15], the sub-optimal H_∞ filtering problem is formulated as that of finding an estimate $\hat{x}$ such that

$$\sup_{x_0, w \in H_2, v \in H_2} = \frac{\|L_k x_k - L_k \hat{x}_k\|_2^2}{\|x_0 - \hat{x}_0\|_{P_0^{-1}}^2 + \|w_k\|_2^2 + \|v_k\|_2^2} < \gamma^2 \tag{3}$$

for some predefined error bound γ and state weight matrix L. A solution to the problem is given by the recursion

$$\begin{aligned}
\hat{x}_k^- =& f\left(\hat{x}_{k-1}^+, u_{k-1}, \bar{w}_{k-1}\right) \\
R_k =& \begin{bmatrix} I & 0 \\ 0 & -\gamma^2 I \end{bmatrix} + \begin{bmatrix} \hat{C}_k \\ L_k \end{bmatrix} P_{k-1} \begin{bmatrix} \hat{C}_k^T L_k^T \end{bmatrix} \\
P_k =& \hat{A}_k P_{k-1} \hat{A}_k^T + \hat{W}_k \hat{W}_k^T \\
& - \hat{A}_k P_{k-1} \begin{bmatrix} \hat{C}_k^T & L_k^T \end{bmatrix} R_k^{-1} \begin{bmatrix} \hat{C}_k \\ L_k \end{bmatrix} P_{k-1} \hat{A}_k^T \\
K_k =& P_k \hat{C}_k^T \left[\hat{V}_k \hat{V}_k^T + \hat{C}_k P_k \hat{C}_k^T\right]^{-1} \\
\hat{x}_k^+ =& \hat{x}_k^- + K_k \left(y_k - h\left(\hat{x}_k^-, u_k, \bar{v}_k\right)\right)
\end{aligned}$$

For the solution to actually solve the sub-optimal H_∞ filtering problem, the following condition must also hold:

$$P_k^{-1} + \hat{C}_k^T \hat{C}_k - \gamma^{-2} L_k^T L_k > 0 \tag{4}$$

2.3 Filter Tuning

The H_∞ filter is not relying on the noise covariance estimates, Σ_w and Σ_v. The only parameters chosen by the user is the state weight matrix L and error bound γ. They must be chosen such that (4) is fulfilled, but otherwise the estimate is rather insensitive to tuning, as will be shown later in Section 3.

The performance of the EKF and UKF observers depend on the tuning of the covariance matrices Σ_w and Σ_v. To make a fair comparison, an automatic procedure for tuning the covariance matrices was implemented. The procedure, presented by [16], uses information from an improved set of measurements, y^*, compared to the final application. Here, it is assumed that the improved output has a linear relation to the state, i.e. $y^* = Hx$. The prediction likelihood is maximized by solving the optimization problem

$$\langle \Sigma_w, \Sigma_v \rangle = \arg\max_{\Sigma_w, \Sigma_v} \sum_{k=0}^{N} -\log|2\pi\Omega_k| - \tilde{y}_k^{*T} \Omega_k^{-1} \tilde{y}_k^* \tag{5}$$

with $\Omega_k = H_k \Sigma_{\tilde{x},k} H_k^T + \Sigma_{y^*}$, where Σ_{y^*} is the variance of the improved measurement, N is the number of samples in the test and $\tilde{y}_k^* = (y_k^* - \hat{y}_k)$.

This work is simulation based, and thus the true SoC is available to use as y^*. For the u_{RC} and u_{h} voltages, no individual measurements are available. However, they are related to the SoC via circuit parameters and the output equation, so it is possible to get an estimate of the complete covariance matrix.

Having only the SoC as y^*, (5) can be simplified. First note that $H_k = 1$ in this case and secondly that Σ_{y^*} was assumed small compared to the variance of the SoC estimate $\Sigma_{\hat{z}}$, and was discarded. The optimization problem (5) then simplifies to the scalar expression

$$\langle \Sigma_w, \Sigma_v \rangle = \arg \max_{\Sigma_w, \Sigma_v} \sum_{k=0}^{N} -\log|2\pi\Sigma_{\hat{z},k}| - \frac{(y_k^* - \hat{z}_k)^2}{\Sigma_{\hat{z},k}}$$

which was solved using a simple search algorithm presented in [16].

The two main difficulties found using the method were:

- The result is sensitive to initial estimates. This was overcome by using several different initial estimates.
- The improved SoC signal uses Coulomb counting, as do the estimators. In order to find a trade-off between Coulomb counting and the information from the measured cell voltage, an initial SoC estimation error was needed.

2.4 Use Cases

Depending on the level of electrification of the target vehicle, the use of the battery will be different. An HEV using only a small part of the SoC range will have fewer possibilities to calibrate the estimation, while a PHEV or BEV must handle larger SoC ranges and may also need higher precision in their estimates. In the evaluation, two cycles were used, see Figure 2. One for HEV where the SoC swing is approximately 10 % and one PHEV cycle starting from a fully charged battery and then slowly draining it to empty with a charge sustaining part in the middle. BEV is considered to be similar to PHEV with the exception of the charge sustaining portion of the cycle and thus no additional cycle was added for this case.

2.5 Performance Indicators

In order to assess the performance of the different observers, a set of metrics is needed. The evaluations are based on 100 Monte Carlo simulations and

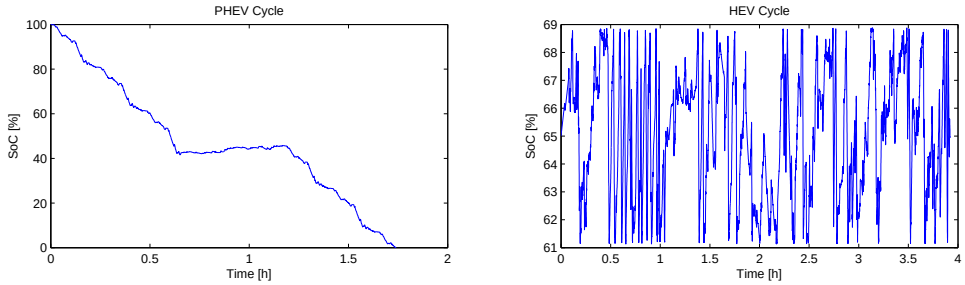

(a) PHEV (b) HEV

Figure 2: Drive cycles for the PHEV and HEV use case, note the different scaling of the y-axis

the performance indicators used must give a representative value over all these simulations. In [17], several aspects of the choice of performance indicators are discussed. In this evaluation, the following were selected:

Mean Absolute Percentage Error

The average error in percent was considered an appropriate measure since it has a direct interpretation. The MAPE is given by

$$\text{MAPE} = \frac{1}{MN} \sum_{j=1}^{M} \sum_{i=1}^{N} |\tilde{z}_{i,j}|$$

where M is the number of Monte Carlo simulations, N is the number of samples in one simulation and $\tilde{z} = z - \hat{z}$ is the SoC error in percent.

Max Percentage Error

The max error gives an important worst case measure. It is taken over all simulations according to

$$\text{MAX} = \max_{i,j} |\tilde{z}_{i,j}|$$

Note that the first n samples of each simulation is left out in order to reduce the influence of the initial error. In this work, $n = 1000$ seconds was used.

2.6 Limitations

There are some limitations imposed on the test setup and evaluation.

Tuning

To reduce the time needed for tuning of the observers, the procedure presented in Section 2.3 is used to optimize the covariance matrix over the whole SoC range. Improved estimates may be achieved using matrices that depend on SoC. The same tuning is also used for both the HEV and PHEV cycles.

Unmodelled Behaviour

The performance of the observers is highly dependent on the quality of the model used. To minimize the influence of unmodelled behaviour in the evaluation, the same model is used to provide the reference SoC as is used in the observers.

3 Robustness Analysis

This section presents the different test cases and the results of the robustness evaluation.

3.1 Benchmark Test

The first test uses correct model and observer parameters and only adds Gaussian noise on the current and voltage sensors. Also, based on this noise, an initial SoC error is imposed on the observers. The results from this test provide an indication on the best performance that can be expected from each observer type.

In Figure 3 the results of 100 Monte Carlo simulations are plotted. It can be seen that the errors are small in almost all cases. Only the UKF for the LFP battery has trouble finding the correct SoC due to the flat OCV curve, see Figure 4a. Note that the tuning used is a compromise between the HEV and PHEV cycles. The UKF can be tuned to produce slightly better estimates for HEV, but that negatively impacts the performance for PHEV case.

3.2 Model Parameter Uncertainties

The characteristics of a battery depends on several factors, e.g. SoC, temperature and age. Even if the battery model parameters are calibrated on-line, the algorithm must be robust to deviations from optimal parameters in the model. In the evaluation, the reasons for a deviation in parameter values are not considered. Instead, it is the algorithms' ability to handle the

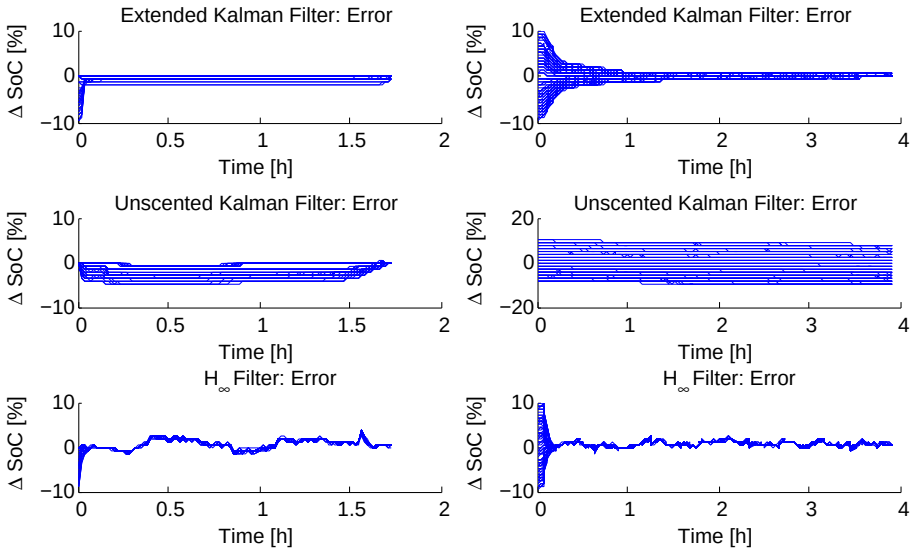

(a) LFP, PHEV

(b) LFP, HEV

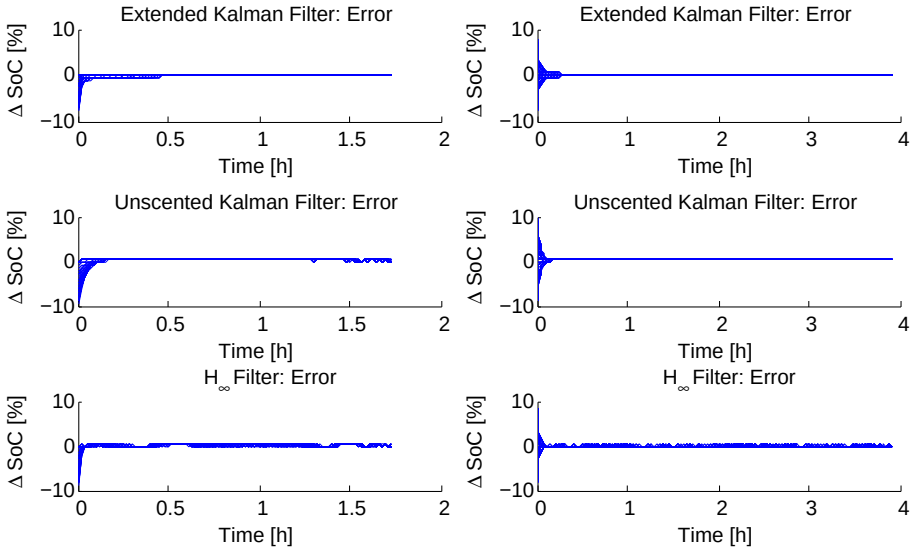

(c) NMC, PHEV

(d) NMC, HEV

Figure 3: Benchmark simulation only adding Gaussian noise with small variance to current and voltage sensor values. Most simulated cases are acceptable from a SoC accuracy perspective, but the UKF estimate for the LFP battery on the HEV cycle shows an almost constant offset depending on the initial estimation error.

erroneous model parameters that is in focus. The parameters of the battery model used in the observers were randomly distorted from the values used in the reference model. Gaussian noise was also added to the measurement signals as in the benchmark test.

For the analysis, the case where the OCV is uncertain was separated from the other parameter variations since the impact of an erroneous OCV can be severe.

OCV Errors

In Figure 4, the OCV curves of the two batteries are shown. The OCV robustness tests evaluate how the observers handle perturbations of magnitudes up to 0.01V compared to the nominal OCV curve.

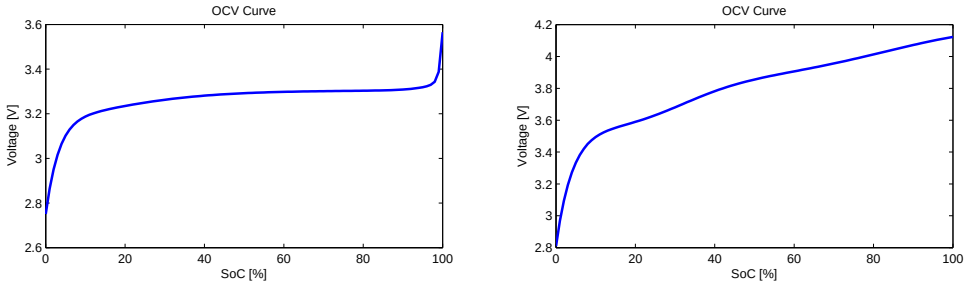

(a) LFP (b) NMC

Figure 4: OCV curve of the evaluated batteries

In Figure 5, the results of 100 Monte Carlo simulations are shown for all four combinations of battery and use case. In general, the impact of an uncertain OCV curve is most severe for the NMC battery. The reason for this is that the observers use the OCV curve more for the NMC battery compared to the LFP battery. For the NMC battery all three estimators show similar results, both for HEV and PHEV cycles. For the LFP battery the UKF have trouble converging with a more or less constant estimation error for most part of the SoC range. The impact of this is most severe on the HEV cycle. The estimation error of the H_∞ filter is varying a lot during the cycle, but the convergence rate is fast also for the combination of LFP battery and HEV cycle, which is the most difficult combination.

Parameter Errors

The parameters of the battery model used by the observer will vary with SoC, temperature, age, etc. This test is designed to examine the ability of the respective observer to handle uncertainties in the model parameters.

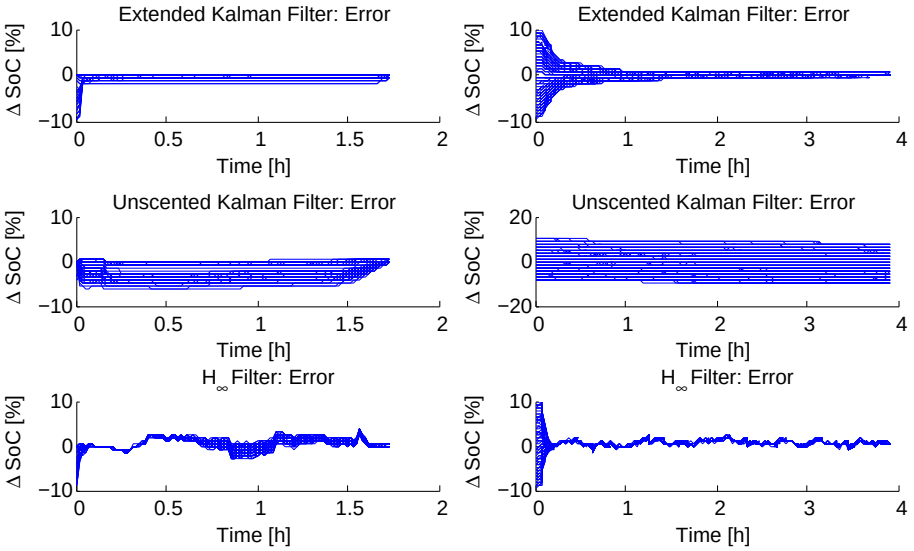

(a) LFP, PHEV

(b) LFP, HEV

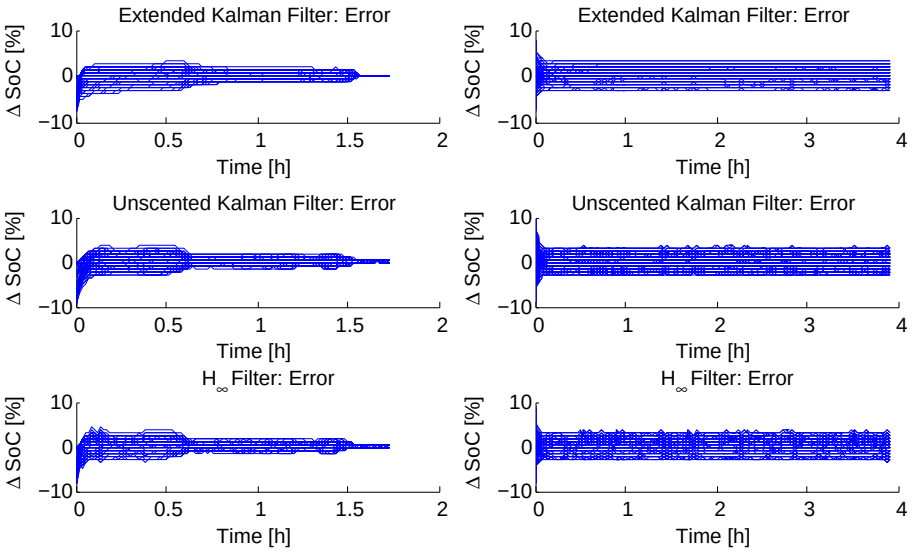

(c) NMC, PHEV

(d) NMC, HEV

Figure 5: Results from Monte Carlo simulations for with perturbations of OCV curve

Random perturbations are added to the resistances R_0 and R_1, to the time constant τ_1 and to the capacity of the battery C_n. The worst-case errors are rather large in order to push the observers to the limits of what they can handle. The results of the simulations are shown in Figure 6.

The H_∞ observer is most sensitive to errors in model parameters for both batteries. The differences between observers are, however, rather small for all but the PHEV cycle with the LFP battery.

3.3 Sensor Noise

Gaussian noise is added to the sensors in all the tests in this evaluation. Two tests were specifically designed to evaluate the robustness to erroneous assumptions of noise characteristics, one adding bias to the current sensor estimate and the other increasing the variance of the voltage measurement.

Current Sensor Bias

In this test, the bias of the current sensor is chosen as a normally distributed random variable with variance chosen to give a maximum deviation over the realizations of approximately 1A. The results are shown in Figure 7. For the LFP battery, the H_∞ filter shows no drift of the estimation. However, just as in all other cases, the variability of the estimates are large. The EKF performance is on par with H_∞ for the whole cycle, but is also constantly drifting which means that it is not suitable for a long-term drive with biased current sensor. The UKF also shows drift and is further set back by its poor performance for the LFP battery. When the OCV curve provides the observer with more information, like in the case of the NMC battery, the UKF handles the bias well for both the HEV and PHEV cycles. We may also note that the H_∞ estimate is slightly better than the EKF estimate for the NMC battery.

Voltage Sensor Variance

In this test, the variance of the voltage sensor is varied. The standard deviation of the voltage sensor used in the simulations are 0.1-1mV, compared to 0.3mV used in the other simulations. The main observation in this test is the poor performance of the H_∞ filter, particularly for the NMC battery, see Figure 8. This makes the H_∞ filter less suited if the uncertainty of the voltage measurement is large. This result can seem surprising, given that the H_∞ filter does not use any information on the noise characteristics of the measurement signals. For this reason, it is easy to assume that it is robust to differences in variance. However, a closer study of the robustness

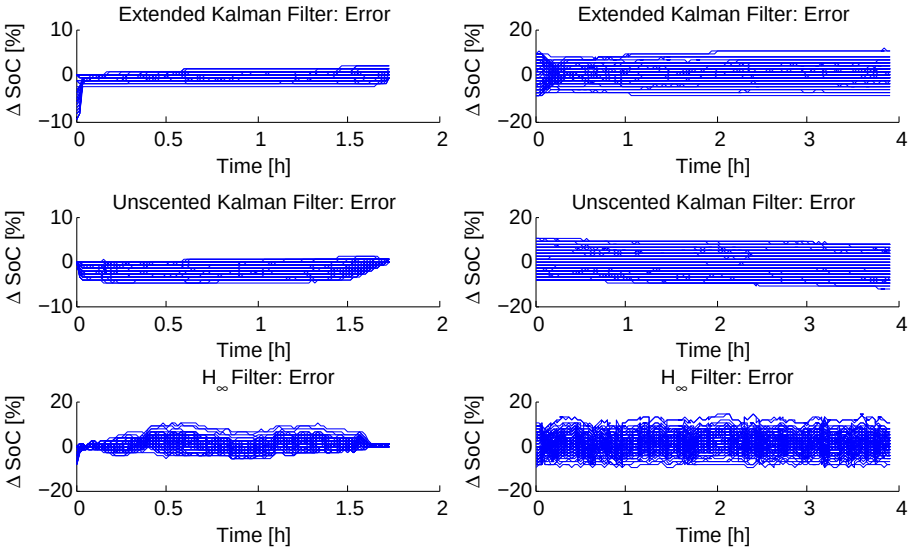

(a) LFP, PHEV (b) LFP, HEV

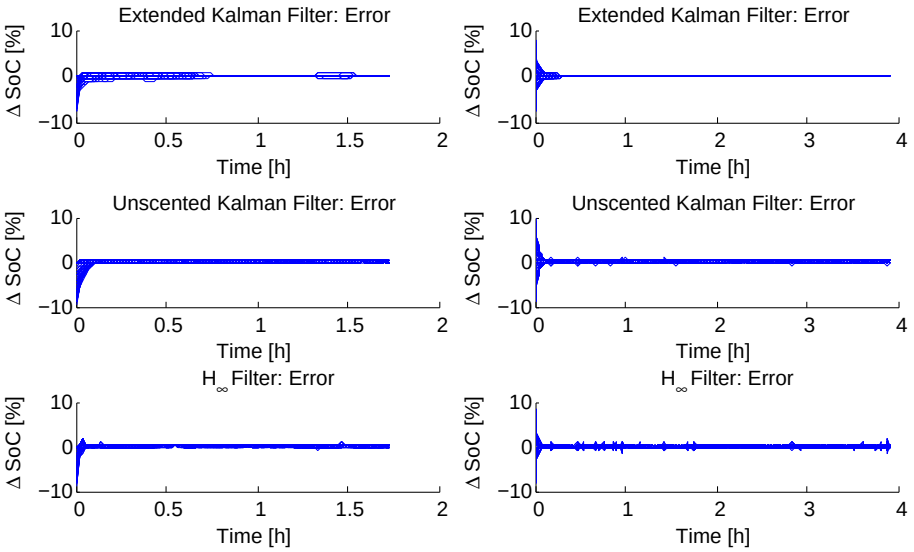

(c) NMC, PHEV (d) NMC, HEV

Figure 6: Results from Monte Carlo simulations with perturbations of model parameters.

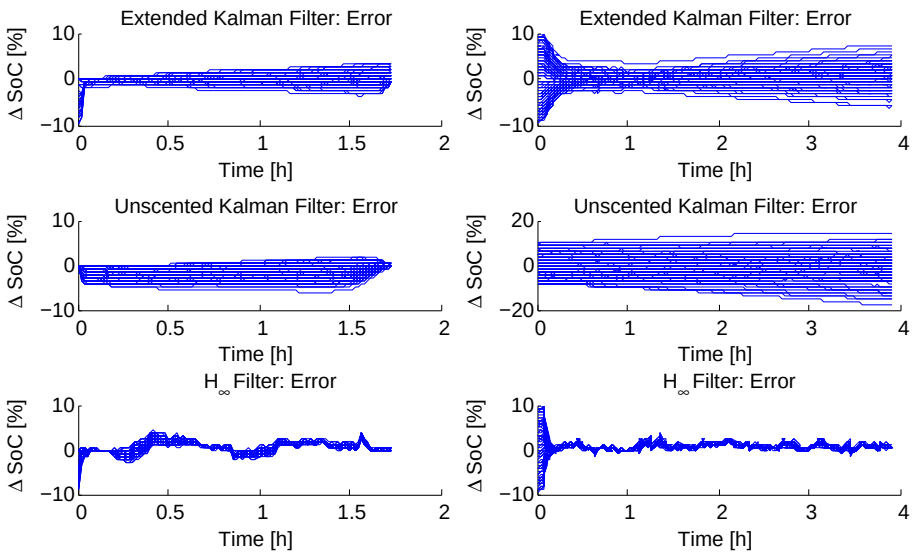

(a) LFP, PHEV

(b) LFP, HEV

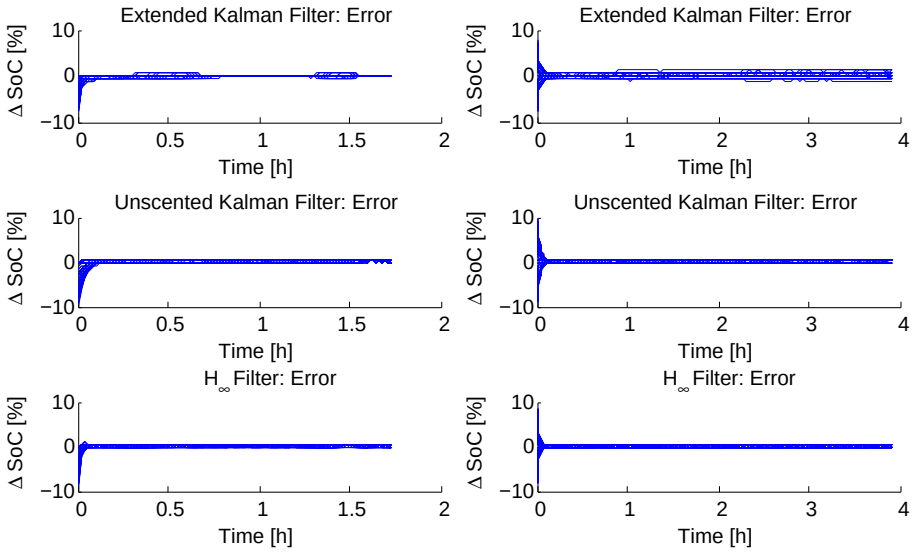

(c) NMC, PHEV

(d) NMC, HEV

Figure 7: Results from Monte Carlo simulations with biased current sensor

bound (3) using the actual values for L and γ, gives a bound that is actually larger than the full SoC range.

3.4 Sensitivity to Observer Tuning

The EKF and UKF have covariance matrix parameters, Σ_w and Σ_v, that must be tuned. Tuning is expensive and in real world applications it is not feasible to expect that an optimal set of observer parameters is used. For this reason it is interesting to see how sensitive the algorithms are to perturbations in parameter tuning.

In this test, two versions of the observers using the same measurement signals and battery models were run. A reference observer using parameters from the procedure in Section 2.3 was compared to an observer where uniformly distributed noise was added to the covariance matrices, Σ_w and Σ_v. For the UKF, also the parameter controlling the distance and weight of the sigma points was changed. For the H_∞ observer, the L matrix was changed in the same manner.

The results are shown in Figure 9, where the differences between the reference observer estimates and the estimates using the perturbed covariances are plotted. The results are similar for all simulations. H_∞ produces the same estimate as long as the requirement of positive definitiveness of (4) is met. For the EKF, it is mainly the convergence rate that is affected by the tuning and the estimation converged for all simulations. The UKF is most sensitive to tuning, and especially the tuning of the parameter controlling the distance and weight of the sigma points. Also note that the UKF estimation diverges for some simulations on the HEV cycle with the LFP battery.

3.5 Comparison

Figure 10 provides an overview of the performance of the different observers. The main findings are:

- For the NMC battery, with strong correlation between OCV and SoC, the UKF outperforms the other observers. On the other hand, when the SoC–OCV relation is flat, the UKF is not a good option since it has convergence problems in several test cases.

- The EKF shows robust behaviour in most cases, except for biased current sensor readings. The impact of the drift is not so obvious in Figure 10, but is best studied in Figure 7.

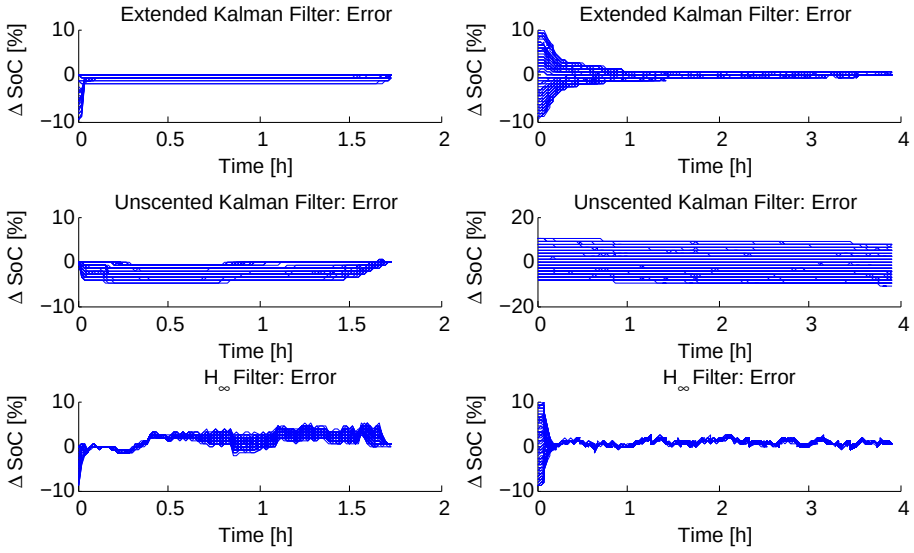

(a) LFP, PHEV (b) LFP, HEV

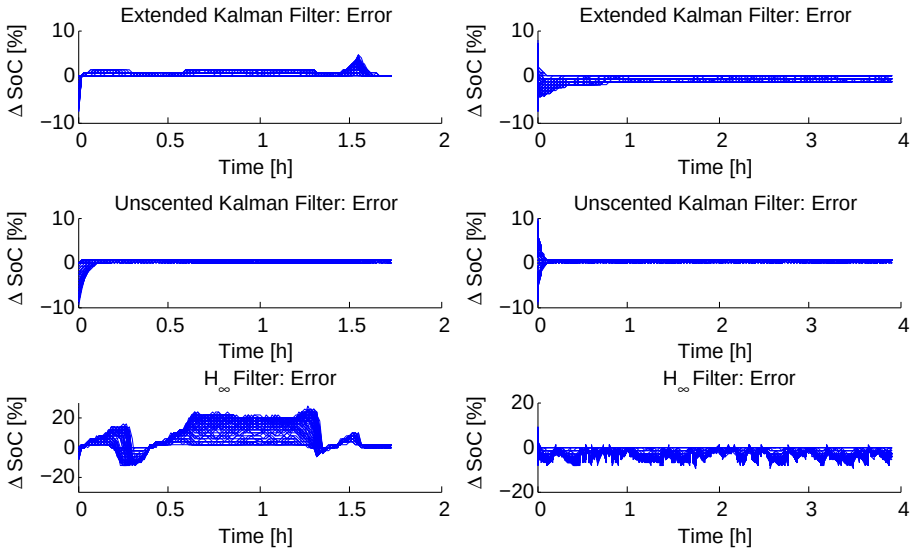

(c) NMC, PHEV (d) NMC, HEV

Figure 8: Results from Monte Carlo simulations with different variance on the voltage sensor. Note the scaling on the H_∞ filter for NMC and PHEV cycle.

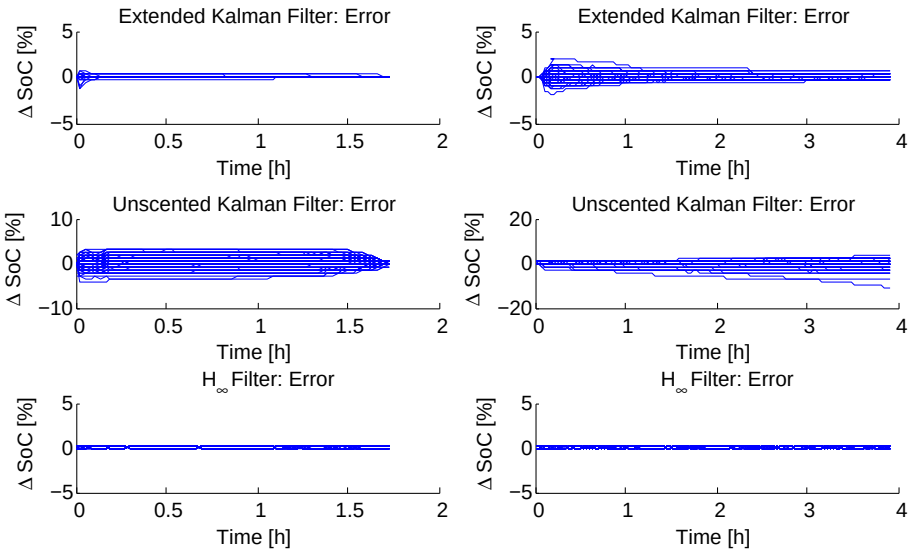

(a) LFP, PHEV (b) LFP, HEV

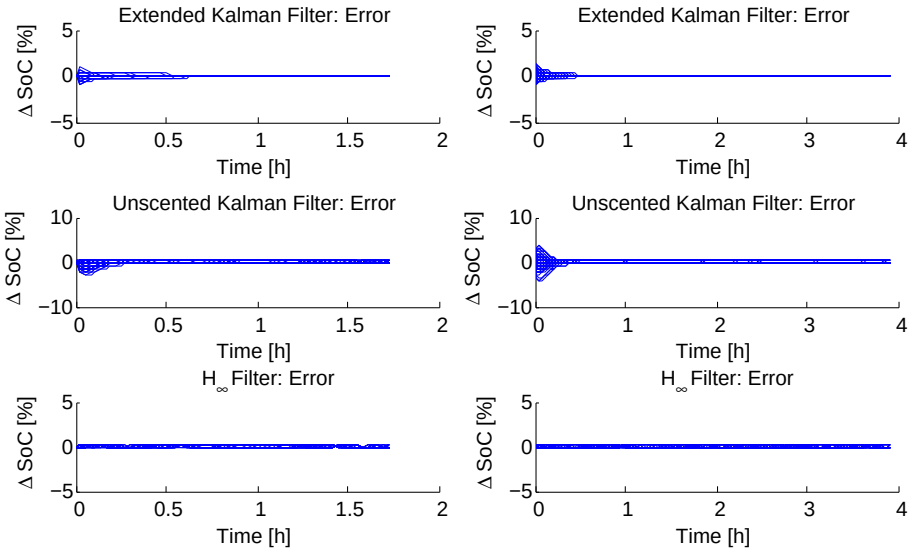

(c) NMC, PHEV (d) NMC, HEV

Figure 9: Difference between reference observer estimation and estimation using perturbed covariance matrices

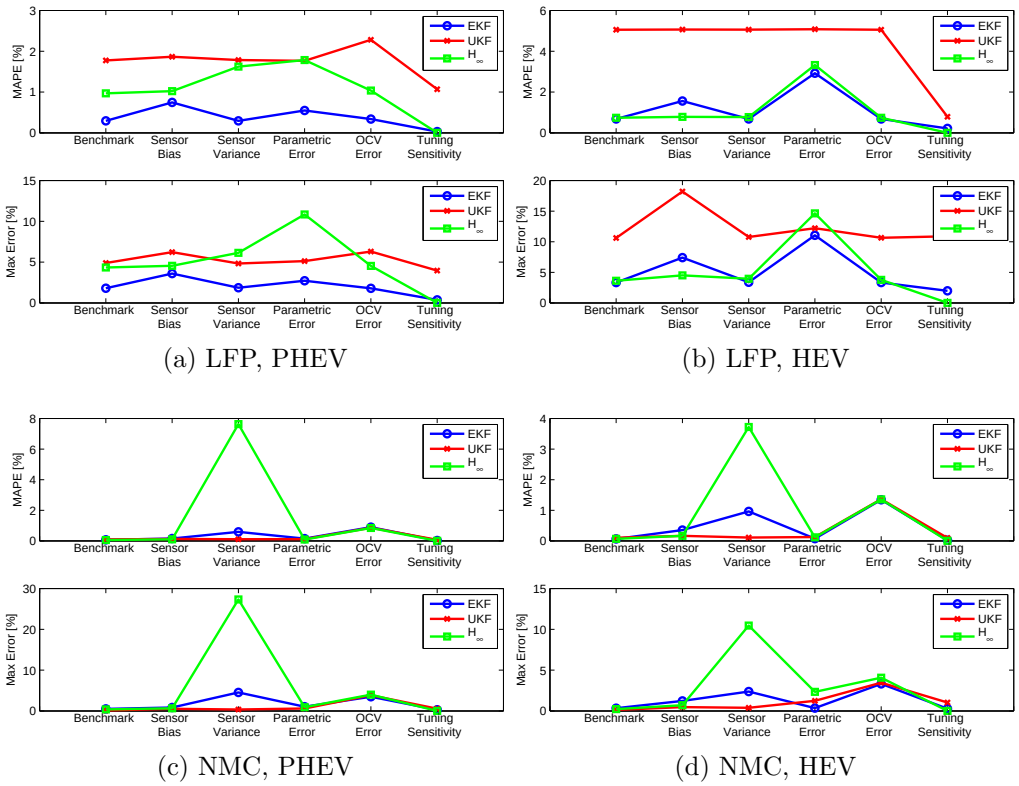

(a) LFP, PHEV (b) LFP, HEV

(c) NMC, PHEV (d) NMC, HEV

Figure 10: Comparison of the performance in the different cases. Caution should be taken when looking at the absolute values of the estimator performance. It is the relative differences that are in focus here.

- The H_∞ observer performs very well considering that there are basically no tuning parameters. However, the estimates for the H_∞ observer are somewhat unpredictable, sometimes giving large errors.

4 Conclusions

The simulation study reveals significant differences in observer performance that can not be purely attributed to tuning of the observers. Some influence of the tuning can, however, not be ruled out.

The general finding is that when the observability of the system is poor, e.g. on the flat part of OCV curve for the LFP chemistry, it is important that the observer can do controlled Coulomb counting. EKF proved to be best at this task. When the observability is stronger, e.g. for the NMC chemistry, the choice of observer will affect the performance. In this study, UKF performed best for most cases, while H_∞ provided the most consistent

estimates with respect to different uncertainties.

The guaranteed robustness bounds of the H_∞ filter are too generous for practical use in SoC estimation. However, the performance of the observer was good in the case of good observability.

References

[1] L. Lu, X. Han, J. Li, J. Hua, and M. Ouyang, "A review on the key issues for lithium-ion battery management in electric vehicles," *Journal of Power Sources*, vol. 226, pp. 272–288, 2013.

[2] G. L. Plett, "Extended Kalman filtering for battery management systems of LiPB-based HEV battery packs - Part 3. State and parameter estimation," *Journal of Power Sources*, vol. 134, no. 2, pp. 277–292, 2004.

[3] G. L. Plett, "Sigma-point Kalman filtering for battery management systems of LiPB-based HEV battery packs. Part 1: Introduction and state estimation," *Journal of Power Sources*, vol. 161, no. 2, pp. 1356–1368, 2006.

[4] Y. Hu and S. Yurkovich, "Battery state of charge estimation in automotive applications using LPV techniques," *2010 American Control Conference, ACC 2010, June 30, 2010 - July 2, 2010*, pp. 5043–5049, 2010.

[5] I.-S. Kim, "The novel state of charge estimation method for lithium battery using sliding mode observer," *Journal of Power Sources*, vol. 163, no. 1, pp. 584–590, 2006.

[6] J. Yan, G. Xu, H. Qian, and Y. Xu, "Robust state of charge estimation for hybrid electric vehicles: Framework and algorithms," *Energies*, vol. 3, no. 10, pp. 1654–1672, 2010.

[7] X. Hu, S. Li, and H. Peng, "A comparative study of equivalent circuit models for Li-ion batteries," *Journal of Power Sources*, vol. 198, pp. 359–367, 2012.

[8] J. Li, L. Wang, C. Lyu, W. Luo, K. Ma, and L. Zhang, "A method of remaining capacity estimation for lithium-ion battery," *Advances in Mechanical Engineering*, vol. 2013, 2013.

[9] X. Chen, W. Shen, Z. Cao, and A. Kapoor, "A Comparative Study of Observer Design Techniques for State of Charge Estimation in Electric

Vehicles," *7th IEEE Conference on Industrial Electronics and Applications*, pp. 102–107, 2012.

[10] X. Hu, S. Li, H. Peng, and F. Sun, "Robustness analysis of State-of-Charge estimation methods for two types of Li-ion batteries," *Journal of Power Sources*, vol. 217, pp. 209–219, 2012.

[11] D. Simon, *Optimal state estimation.* John Wiley Sons Ltd, 2006.

[12] G. Welch and G. Bishop, "An Introduction to the Kalman Filter," Technical report, University of North Carolina at Chapel Hill, 1995.

[13] J. Seo, M. J. Yu, C. G. Park, and J. G. Lee, "An extended robust H infinity filter for nonlinear uncertain systems with constraints," *Proceedings of the 44th IEEE Conference on Decision and Control, and the European Control Conference, CDC-ECC '05*, vol. 2005, pp. 1935–1940, 2005.

[14] P. Ni and S. Li, "Unscented H_infinity filter based simultaneous localization and mapping," *IEEE Chinese Control Conf. (CCC'11)*, no. 1, pp. 3942–3946, 2011.

[15] B. Hassibi, A. H. Sayed, and T. Kailath, "Linear estimation in Krein Spaces-Part I: Theory," *IEEE Transactions on Automatic Control*, vol. 41, no. 1, pp. 18–33, 1996.

[16] P. Abbeel, A. Coates, M. Montemerlo, A. Y. Ng, and S. Thrun, "Discriminative Training of Kalman Filters," *Proceedings of Robotics: Science and Systems I*, pp. 289–296, 2005.

[17] X. Li and Z. Zhao, "Measures of performance for evaluation of estimators and filters," *Proc. 2001 SPIE Conf. on Signal and Data Processing*, no. July-August, pp. 1–12, 2001.

Paper 2

Kalman filter for adaptive learning of look-up tables with application to battery ohmic resistance estimation

Björn Fridholm, Torsten Wik, and Magnus Nilsson

Control Engineering Practice, 48, 2016

Comment: The layout of this paper has been reformatted in order to comply with the rest of the thesis.

Kalman filter for adaptive learning of look-up tables with application to battery ohmic resistance estimation

Björn Fridholm, Torsten Wik, and Magnus Nilsson

Abstract

In online automotive applications, look-up tables are often used to model nonlinearities in component models that are to be valid over large operating ranges. If the component characteristics change with ageing or wear, these look-up tables must be updated online. Here, a method is presented where a Kalman filter is used to update the entire look-up table based on local estimation at the current operating conditions. The method is based on the idea that the parameter changes observed as a component ages are caused by physical phenomena having effect over a larger part of the operating range than may have been excited. This means that ageing patterns at different operating points are correlated, and these correlations are used to drive a random walk process that models the parameter changes. To demonstrate properties of the method, it is applied to estimation of the ohmic resistance of a lithium-ion battery. In simulations the complete look-up table is successfully updated without problems of drift, even in parts of the operating range that are almost never excited. The method is also robust to uncertainties, both in the ageing model and in initial parameter estimates.

Keywords: Kalman filter; Parameter estimation; Automotive battery; Li-ion battery; Battery resistance estimation.

1 Introduction

The characteristics of many physical systems vary with both operating conditions and age. These variations typically occur on very different timescales and can thus be treated separately in parameter estimators. Parameter variations due to operating conditions are often modelled explicitly, e.g. using look-up tables, while ageing is typically handled by robust design or by an adaptive scheme acting on a slower time scale.

An example of such a system is automotive lithium-ion batteries, where the ohmic resistance changes considerably both with temperature, State-of-Charge, and age [1, 2, 3]. Variations with age are much slower than changes with operating conditions [4], which motivates handling these two types of variations separately. In the literature, there are several articles focusing on building models valid over the operating range, using look-up tables [5, 6, 7, 8] and elementary functions [9, 10, 11, 12]. To handle variations due to ageing, recursive algorithms such as recursive least squares (RLS) [13, 12] or Kalman filters [6, 14] are commonly used for online estimation of parameters at the current operating conditions.

Within the battery community, there appears to be no published methods for updating look-up tables. Some previous work on updating look-up tables can, however, be found in other fields using Kalman filters [15, 16] and recursive least squares [17], though the focus is then on an update of the look-up table only at the operating points closest to the current operating conditions. This means that the parameter estimate in operating points that have not been visited for a long time may be far from the true value. For vehicle batteries, this can cause a problem, for instance when cold cranking in operating conditions that have not been updated for a long time [18].

In this work, we present a novel method for updating an entire look-up table based on information only at the current operating conditions. This is made possible by modelling correlations between changes in parameter values at different operating points over ageing and include them in a Kalman filter that handles the update of the look-up table.

This article is structured such that Section 2 introduces some notation used in the article. Section 3 presents look-up tables and Section 4 the ageing model. In Section 5, the proposed algorithm is presented and in Section 6, it is tested in a simulation study. Eventually, Section 7 summarizes the results.

2 Notation

Some terms used in the paper have specific meaning that are important to keep in mind and are therefore listed in Table 1 with a short description. Some other important non-standard notations are listed in Table 2. Note that subscripts k always is a time index, i.e. $\Theta_k = \Theta(k)$, while indices i and j always refers to an element of the vector containing the operating points. More standardised notation are described when introduced.

Table 1: Abbreviations and nomenclature

BoL	Beginning-of-Life, i.e. a new battery where SoH = 100%.
EoL	End-of-Life, i.e. when a battery is considered useless for the application, SoH = 0%.
MoL	Middle-of-Life, not always well defined in literature, but here we mean SoH around 50%.
Operating condition	Currently active conditions. In this document, the operating condition is always temperature.
Operating points	Discretization of the operating range into a vector.
Operating range	The expected range that must be handled by the model, e.g. highest to lowest temperature.
SoC	State-of-Charge.
SoH	State-of-Health, in this work only defined by number of charge/discharge cycles the battery has been exposed to.
Spilling effect	Refers to when information from one operating condition is used to update operating points related to other operating conditions.

3 Look-up tables

In Fig. 1, a one dimensional look-up table is depicted. Denote by x_i, $i = 1, \ldots, n$, the operating points defining the look-up table break-points. Let $\Theta \in \mathbb{R}^n$ be the corresponding vector of look-up table values, and define the time varying index, $i(k)$, as

$$i(k) = \max \{j = 1, \ldots, n | x_j \leq x(k)\},$$

where $x(k)$ is the current operating condition, which in general is between the break-points of the look-up table. Define the scalar value $\eta \in [0, 1]$ as

$$\eta(k) = \frac{x(k) - x_{i(k)}}{x_{i(k)+1}(k) - x_{i(k)}}, \quad x_1 \leq x(k) \leq x_n,$$

where η is limited to be 0 if $x(k) < x_1$ and 1 if $x(k) > x_n$. With linear interpolation, the current parameter value is given by (cf. Fig. 1)

$$\theta^x(k) = (1 - \eta(k))\theta_{i(k)}(k) + \eta(k)\theta_{i(k)+1}(k).$$

In the following, the vector $C_k = [c_1(k), \ldots, c_n(k)]$ will be defined by the elements

$$c_j(k) = \begin{cases} 1 - \eta(k), & j = i(k) \\ \eta(k), & j = i(k) + 1 \\ 0, & \text{otherwise} \end{cases}$$

Table 2: Notation

Θ	Look-up table parameter vector with elements corresponding to the operating points. Note that it is always the same physical parameter, e.g. ohmic resistance, but at different operating points, e.g. different temperatures.
θ_i	Parameter value at operating point i.
Θ_k	Parameter vector at current time step, i.e. short notation for $\Theta(k)$.
θ^x	Parameter value at current operating condition.
x	Operating condition.
x_i	Operating point i.
i, j	Index of operating point.
k	Time index in discrete time.
η	Interpolation variable.
w, v, e	Realizations of Gaussian random variables.
Σ	Covariance matrix used to model ageing.
μ_i	Expected value for parameter θ_i.
σ_i	Standard deviation for parameter θ_i.
$\rho_{i,j}$	Correlation coefficient between parameter θ_i and θ_j.

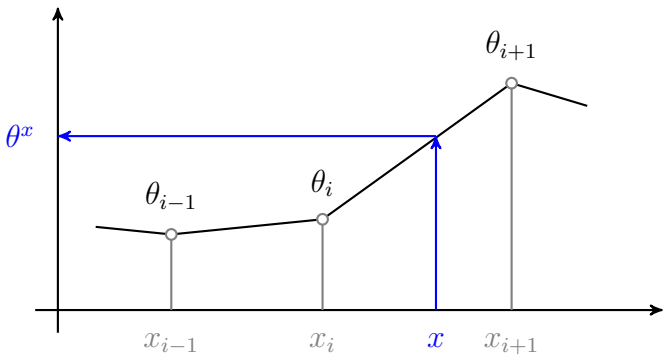

Figure 1: Example of 1-D look-up table. Here $\eta = 0.6$

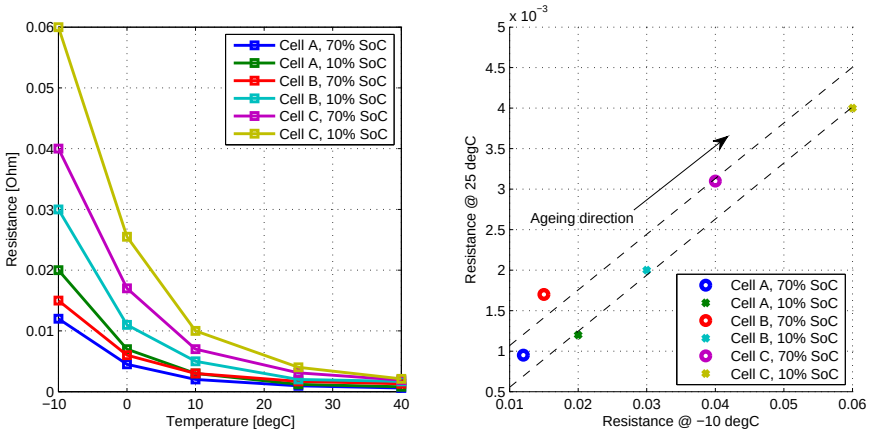

Figure 2: (Left) The ohmic resistance for three different battery cells of the same type but at different stages of ageing, cell A is new, cell B was aged 200 cycles and cell C was aged 1900 cycles. (Right) An X–Y scatter plot of all battery data at −10°C and +25°C together with line-fits for 10% and 70% SoC respectively. The data has been extracted from the experimental results presented in [20].

which means that the look-up table output can be written in matrix notation as

$$\theta^x(k) = C_k\Theta(k). \tag{1}$$

4 Ageing model

The ageing model proposed here builds on the idea that the changes observed due to ageing has an underlying physical cause and will thus affect the parameters values at all operating points. This leads to a long-term trend in the changes that can be utilized to improve estimation at parts of the look-up table where data have not been collected for a long time. In [19], several reasons for an increase in battery impedance as the battery ages are presented, such as conductor corrosion and loss of active electrode surface. It is reasonable to assume that these effects are visible across the entire operating range. Such a correlation is also observed in the data presented in [20], where data from three different cells at two stages of ageing are shown for five different temperatures and two SoC levels. The data are reproduced in Fig. 2, where cell A is new, cell B was aged 200 cycles and cell C was aged 1900 cycles.

In Fig. 2, the resistance for all three batteries at two different operating points, −10°C and 25°C, are shown in an x–y plot. It indicates strong correlation between changes in parameter values at different operating points

over ageing, where an increase in resistance at one temperature correlates well with an increase at other temperatures.

4.1 Assumptions

In the derivation of the model used for ageing, there are three important assumptions made:

- First, it is assumed that the parameter vector Θ can be seen as a stochastic process with a multivariate normal distribution. This means that all linear combinations of θ_i are normally distributed, and consequently θ^x is normally distributed.

- For the look-up table adaptation presented in the next section to work, the break-point grid must be dense enough to consider linear interpolation to be a sufficiently good approximation of the values between the grid points. If this fails to be fulfilled, convergence problems may occur.

- Finally, the initial parameter vector and its variance are assumed to be known. This is often the case in battery management applications, where the characteristics of new cells are thoroughly investigated.

4.2 Resulting ageing model

Slowly time-varying parameters can often be modelled as a random walk process, such as

$$\Theta(k+1) = \Theta(k) + w(k), \tag{2}$$

where $w \in \mathbb{R}^n$, $w \sim \mathcal{N}(0, Q)$ is a white Gaussian noise term that induces the variations. $Q \in \mathbb{R}^{n \times n}$ is a symmetric and positive definite covariance matrix, where the diagonal entries contain the parameter variances while correlations between parameters appear as non-zero off-diagonal entries. The ageing model proposed in this article includes the correlations observed in Fig. 2 in the covariance matrix Q.

Now, assume we have a set of m batteries at different stages of ageing, from beginning-of-life (BoL) to end-of-life (EoL). Denote the parameter vector for each battery by $\Theta_l \in \mathbb{R}^n$, $l = 1, \ldots, m$ and form the sample mean $\bar{\Theta} \in \mathbb{R}^n$ for all batteries at each operating point as

$$\bar{\Theta} = \frac{1}{m} \sum_{l=1}^{m} \Theta_l. \tag{3}$$

Then the unbiased sample covariance is given by

$$\Sigma = \frac{1}{m-1}\sum_{i=1}^{m}\left(\Theta_i - \bar{\Theta}\right)\left(\Theta_i - \bar{\Theta}\right)^T. \tag{4}$$

The contents of Σ will be

$$\Sigma = \begin{bmatrix} \sigma_1^2 & \rho_{12}\sigma_1\sigma_2 & \dots & \rho_{1n}\sigma_1\sigma_n \\ \rho_{12}\sigma_1\sigma_2 & \sigma_2^2 & \dots & \rho_{2n}\sigma_2\sigma_n \\ \vdots & \vdots & \ddots & \vdots \\ \rho_{1n}\sigma_1\sigma_n & \rho_{2n}\sigma_2\sigma_n & \dots & \sigma_n^2 \end{bmatrix}, \tag{5}$$

where σ_i^2 is the sample variance for operating point i, and ρ_{ij} is the correlation coefficient between parameters at operating points i and j.

5 Look-up table adaptation

Based on local estimation of the parameter value at the current operating conditions, the goal is to construct an algorithm that produces the best possible estimate of the parameter value at all operating points of the look-up table. In this context, "best" means finding an unbiased estimate $\hat{\Theta}$ of Θ with the least variance, under the model assumptions made in Section 4.1.

5.1 Method outline

The block scheme in Fig. 3 illustrates the two main parts of the look-up table adaptation system. First, the parameter value θ_k^x and its corresponding error variance P_k^x are estimated under the current operating conditions using a Kalman filter, see [6, 21, 14] for examples on how this can be done. Given θ_k^x and P_k^x, the look-up table adaptation block updates the parameters of the look-up table at all operating points. It turns out that a Kalman filter can be used also for this update. In this work, focus is on the look-up table adaptation, and hereafter, the local parameter estimator is assumed to provide the look-up table adaptation with the estimate $\hat{\Theta}_k^x$ and its time varying estimation error variance P_k^x.

5.2 Kalman filter

Using Kalman filters for parameter estimation requires a model of how the parameters are expected to change. Assume that the slowly varying parameters can be modelled as random walk processes, i.e.

$$\Theta_{k+1} = \Theta_k + w_k \tag{6}$$

$$\theta_k^x = C_k\Theta_k + v_k, \tag{7}$$

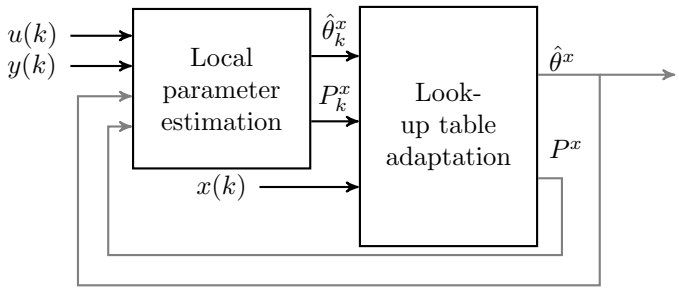

Figure 3: Block scheme of the combined parameter estimation and look-up table adaptation. $\hat{\theta}^x$ and P^x from the look-up table adaptation block are used to initialize the local parameter estimation, which in turn provides the look-up table adaptation with updated estimates of the parameter vector and its variance.

where $w_k \sim \mathcal{N}(0, \Sigma)$ is a white noise term that model the slow variations, Σ is the covariance matrix described in Section 4, $v_k \sim \mathcal{N}(0, P_k^x)$ where P_k^x is the estimation variance of the parameter estimate at the current operating point, and finally C_k is defined by (1).

The Kalman filter equations used to update the look-up table parameter vector $\hat{\theta}$ are then

$$P_k^- = P_{k-1}^+ + \gamma\Sigma \tag{8}$$

$$K_k = P_k^- C_k^T \left(C_k P_k^- C_k^T + P_k^x\right)^{-1} \tag{9}$$

$$\hat{\Theta}_k = \hat{\Theta}_{k-1} + K_k \left(\hat{\theta}_k^x - C_k \hat{\Theta}_{k-1}\right) \tag{10}$$

$$P_k^+ = P_k^- - K_k C_k P_k^-, \tag{11}$$

where γ is a design parameter that can be used to tune the rate of adaptation.

The use of γ is similar to how Kalman filters are often tuned, where the covariance matrices are used to tune the filter to a desired behaviour rather than reflect the uncertainties directly. In the simulations presented here, a scalar-valued γ was used. If more flexibility is needed, for instance the possibility to control the rate of adaptation in the current operating condition and "spill-over" separately, a matrix-valued γ can be used. Note in that case that a Hadamard product, i.e. element-wise multiplication, must be used rather than normal matrix multiplication.

5.3 Observability analysis

For stochastic systems, observability is often defined in terms of a strict reduction of the conditional state covariance given the outputs (see e.g.

[22] or [23]). A necessary, but not sufficient condition for the stochastic system to be observable is that the corresponding deterministic system is observable.

The deterministic time-varying discrete-time system

$$x(k+1) = A_k x(k) \tag{12}$$

$$y(k) = C_k x(k) \tag{13}$$

is said to be observable on the time frame $[k_0, k_f]$ if the observability matrix

$$\mathcal{O}(k_0, k_f) = \begin{bmatrix} C_{k_0} \\ C_{k_0+1}\Phi(k_0+1, k_0) \\ \vdots \\ C_{k_f-1}\Phi(k_f-1, k_0) \end{bmatrix}, \tag{14}$$

where $\Phi(k_f - 1, k_0) = A_{k_f-1}A_{k_f-2}\cdots A_{k_0}$ is the transition matrix, has full rank.

Using the random walk parameter update (6)–(7) means that the system matrix A is the identity matrix, and consequently also the transition matrix is the identity matrix. Observability of the system then turns into

$$\mathcal{O}(k_0, k_f) = \begin{bmatrix} C_{k_0} \\ C_{k_0+1} \\ \vdots \\ C_{k_f} \end{bmatrix} \tag{15}$$

and we can see that this matrix has full rank only in the special case when the entire operating region has been covered. In all other cases, the observability matrix is rank deficient and thus the system is not observable.

5.4 Analysis of non-observable parameters

Since all parameters are updated by the algorithm, it is important to examine what happens to the non-observable parts of the parameter vector. This is done by examining the one-step prediction for an example with only two parameters. Extension to the general case is straightforward.

Assume that the parameter vector is $\Theta_k = [\,\theta_{1,k} \quad \theta_{2,k}\,]^T$ and that the current operating conditions are such that only parameter $\theta_{1,k}$ is estimated[1]. This means that $C_k = [\,1 \quad 0\,]$. Let $\hat{\Theta}_{k-1}$ be the estimate at time step $k-1$ having a covariance

$$P^+_{k-1} = \begin{bmatrix} P^+_{11,k-1} & P^+_{12,k-1} \\ P^+_{12,k-1} & P^+_{22,k-1} \end{bmatrix}. \tag{16}$$

[1]Cf. the example depicted in Fig. 2 and let data be collected for -10°C while also the resistance value in $+25$°C is updated based on this information.

Assuming that the covariance model (5) holds at time-step k, (8)–(9) becomes

$$P_k^- = \begin{bmatrix} P_{11,k-1}^+ + \gamma\sigma_1^2 & P_{12,k-1}^+ + \gamma\rho_{12}\sigma_1\sigma_2 \\ P_{12,k-1}^+ + \gamma\rho_{12}\sigma_1\sigma_2 & P_{22,k-1}^+ + \gamma\sigma_2^2 \end{bmatrix} \equiv \tag{17}$$

$$\equiv \begin{bmatrix} P_{11,k}^- & P_{12,k}^- \\ P_{12,k}^- & P_{22,k}^- \end{bmatrix} \tag{18}$$

$$K_k = \begin{bmatrix} P_{11,k-1}^+ + \gamma\sigma_1^2 \\ P_{12,k-1}^+ + \gamma\rho_{12}\sigma_1\sigma_2 \end{bmatrix} \left(P_{11,k-1}^+ + \gamma\sigma_1^2 + P_k^x\right)^{-1} \equiv \tag{19}$$

$$\equiv \begin{bmatrix} P_{11,k}^- \\ P_{12,k}^- \end{bmatrix} \left(P_{11,k}^- + P_k^x\right)^{-1}, \tag{20}$$

which means that (10) gives the estimate of the unobserved state $\hat{\theta}_2$ as

$$\hat{\theta}_{2,k} = \hat{\theta}_{2,k-1} + \frac{P_{12,k}^-}{P_{11,k}^- + P_k^x}\left(\hat{\theta}_k^x - \hat{\theta}_{1,k-1}\right), \tag{21}$$

which we recognise as the conditional expectation of θ_2 given a noisy observation of θ_1, i.e.

$$\hat{\theta}_{2,k} = \mathbb{E}\left\{\theta_{2,k} \middle| \hat{\theta}_{1,k} = \hat{\theta}_k^x\right\}. \tag{22}$$

In [24], Anderson and Moore prove that this is a general property of the Kalman filter. Furthermore, the Kalman filter is the minimum variance estimator. This means that the proposed algorithm will produce an estimate of the look-up table parameters that reflects the expected value of the parameter vector conditioned on all previous observations, i.e.

$$\hat{\Theta}_k = \mathbb{E}\left\{\Theta_k \middle| \hat{\theta}_0^x, \hat{\theta}_1^x, \ldots, \hat{\theta}_k^x\right\}. \tag{23}$$

The lack of observability will, however, come at the price of a potentially unbounded state covariance. For parameters with weak correlation to the currently excited operating range, the term $K_k C_k P_k^-$ in (11) is close to zero, which in turn means that the covariance for those parameters increase linearly according to (8). One way to avoid this problem, is to introduce anti-windup by covariance saturation, i.e. replacing (11) with for example

$$P_k^+ = \begin{cases} P_k^- - K_k C_k P_k^- & P_k^- < P_{\max} \\ P_{k-1}^+ & \text{otherwise} \end{cases}$$

where the choice of $P_{\max}$ is a trade-off between robustness and alertness to changes when an operating point is visited.

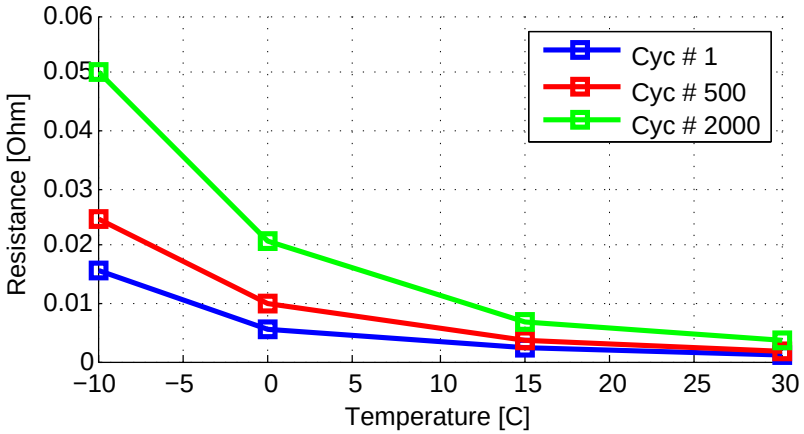

Figure 4: Resistance over all operating points for three stages of aging from the validation realization of the model.

6 Simulation study

A simulation study was designed to demonstrate the methods ability to update parts of the look-up table that are infrequently excited. Due to lack of experimental data with sufficiently many ageing points[2] to build the model and method entirely on real data, the results presented in [20] are used together with the assumptions from Section 4.1 to generate the input data.

The basic behaviour that we want to capture with the algorithm can be seen in Fig. 4. The parameter's value at four different temperatures is plotted for three different stages of ageing.

6.1 Data generation model

Data for the ageing model and a virtual validation dataset were created using the model

$$\theta_i(z_{\text{soh}}) = \mu_i(z_{\text{soh}}) + w_i(z_{\text{soh}}) \tag{24}$$

where θ_i, $i = 1, \ldots, n$, are the parameter values at the operating points, μ_i is the expected value of the parameters at different stages of ageing based on [20], z_{soh} is a measure of the age of the battery often referred to as State-of-Health (SoH), and $w_i \sim \mathcal{N}(0, \sigma_i(z_{\text{soh}}))$ is a white noise term that reflects the fact that not all batteries are equal. Using the model (24), data for 10

[2]Note that to accurately test the algorithm on real-world data requires data to be stored during each cycle, or that the algorithm runs in parallel with the tests from BoL to EoL, a process that will take several years to complete.

Table 3: Parameter values used in data generation. Mean values are approximated from [20].

Operating Point	°C	-10	0	15	30	Std dev
Res @ BOL	mΩ	16	6	2	1	0.1
Res @ MOL	mΩ	23	9	3	2	0.2
Res @ EOL	mΩ	50	21	7	3	0.3

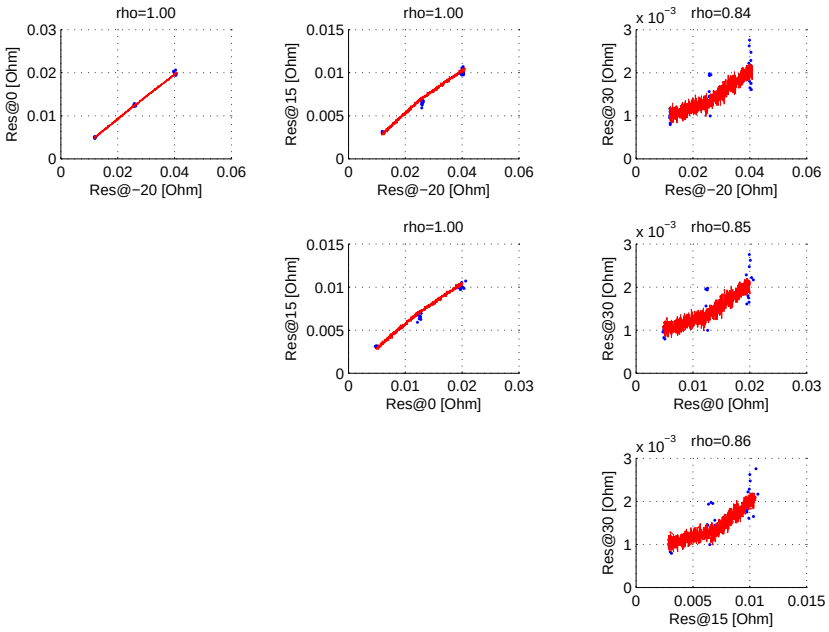

Figure 5: Data used for correlation model (blue dots) and validation (red line) in X–Y plots for all combinations of four data points. There are three clusters of blue dots corresponding to BoL, MoL and EoL from left to right. The algorithm assumes that the red line passes through the centre of each cluster. This is not the case for the validation data here, which means that there are discrepancies between model and validation data, as can be expected in reality.

different batteries were generated with settings according to Table 3. The resulting data are illustrated as blue dots in Fig. 5, where the operating points are plotted in an x–y plot for each of the operating points and age points. From these data, the covariance matrix used to model the ageing correlations was calculated.

The virtual validation battery was also generated using data from Table 3, and its resistance was assumed to change linearly from BoL to MoL

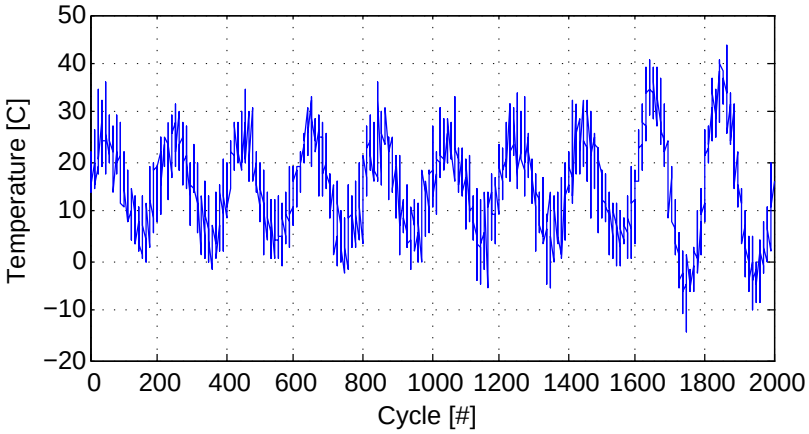

Figure 6: Temperature used in simulations. Note that for the first 1600 cycles, the temperature is mostly above 0°C. For the final 400 cycles the complete operating range is covered, which means that the convergence properties of the algorithm can be studied when actual data are collected for the operating point in −10°C.

and from MoL to EoL. In the intended application, the parameter value used by the look-up table adaptation algorithm will come from an estimation of the true parameter value at the current operating conditions. To reflect this, an additional uncertainty was added to the virtual validation battery, implemented by

$$\hat{\theta}_k^x = \theta_k^x + v_k, \tag{25}$$

where $v_k \sim \mathcal{N}(0, P_k^x)$. The validation data can be seen as red lines in Fig. 5. $\hat{\theta}_k^x$ and the noise statistics P_k^x, are known to the look-up table adaptation Kalman filter but not the realization, i.e. the actual value of v_k is not known. In simulations, a constant value $P_k^x = 10^{-4}$ was used for all operating points.

To define the operating conditions for each cycle, the temperature was assumed to vary according to a sine wave with ten evolutions overlaid with white noise

$$x(k) = 15 + A(k)\sin(\pi/100) + e \ [^\circ\mathrm{C}]\,, \tag{26}$$

where $e \sim \mathcal{N}(0, 3)$, and $A(k)$ is 10 for $k \leq 1600$ and 26 for $k > 1600$. This could be seen as representing 1900 drive cycles performed over 10 years. However, the important aspect here is that the operating point −10°C is not excited until the 400 last cycles uses a sine wave with larger amplitude to make sure the entire operating range is covered (see Fig. 6).

6.2 Simulation results

In Fig. 7 the parameter evolutions for the four different temperature operating points, as defined in Table 3, are shown together with a reference simulation not using the correlation over ageing, i.e. without "spill-over". With only a few exceptions, data are collected for temperatures above 0°C and before cycle 1700 actual data for the operating point in −10°C is never received. For the estimation without "spill-over", the resistance in the operating point in −10°C is only updated on the occasions when the temperature is below 0°C. With the correlation model of the ageing, this operating point is updated at all temperatures and, hence, the changes are tracked continuously. As can be seen in Fig. 7, the estimation using the correlation model performs very well compared to the case of no "spill-over", and a significant improvement is seen for the operating points that are seldom excited. In regions that are frequently excited, the behaviour is more or less the same as for the case when no correlation model is used, which is a desired property.

The covariance matrix estimated by the Kalman filter is plotted in Fig. 8 for both diagonal and cross terms. It can be seen how the elements change with temperature such that the variances decrease in operating points close to the current operating conditions and increase in operating points further away. Because of this, there may be reason to include some kind of covariance anti-windup mechanism in a practical application, see Section 5.4.

When the complete range is excited, there are some fluctuations in the estimation in the −10°C operating point where the estimate is actually changed in the wrong direction. The reason for this is that the validation battery does not fully follow the covariance model and when the Kalman filter updates the −10°C operating point based on data from warmer temperatures, the changes can be in the wrong direction. This is an inherent risk using a feed-forward update like this, and to reduce the impact of this the tuning parameter γ was introduced.

6.3 Sensitivity to ageing model

Next, the sensitivity to the ageing model was investigated by imposing uncertainties to σ_i of the covariance model (5), where the parameters were randomly perturbed by up to ±20% from the correct value. A set of 100 Monte Carlo simulations were run and the results can be seen in Fig. 9. The algorithm behaves well in all these cases and even though the uncertainties results in decreased performance, it is still slightly better than the update without "spill-over" in Fig. 7. Note that also the case of no "spill-over" would have been affected by these uncertainties since it uses the σ_i terms

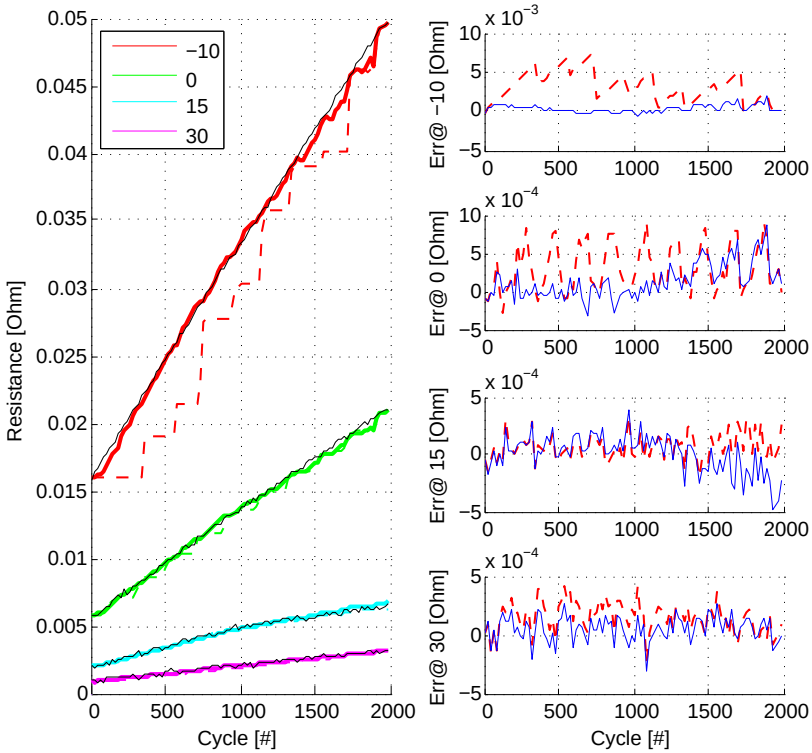

Figure 7: (Left) Illustration of the evolution of the resistance for the four temperature operating points over 1900 cycles. Black lines are the true parameter values as generated by the model, thick lines are the estimates using the proposed algorithm with $\gamma = 0.1$ and dashed lines are estimations without "spill-over". (Right) The errors in the individual estimations; blue is the estimate using the ageing model, while red dashed uses no "spill-over". Note that before cycle 1700, no data were collected for the operating point at $T = -10°\mathrm{C}$.

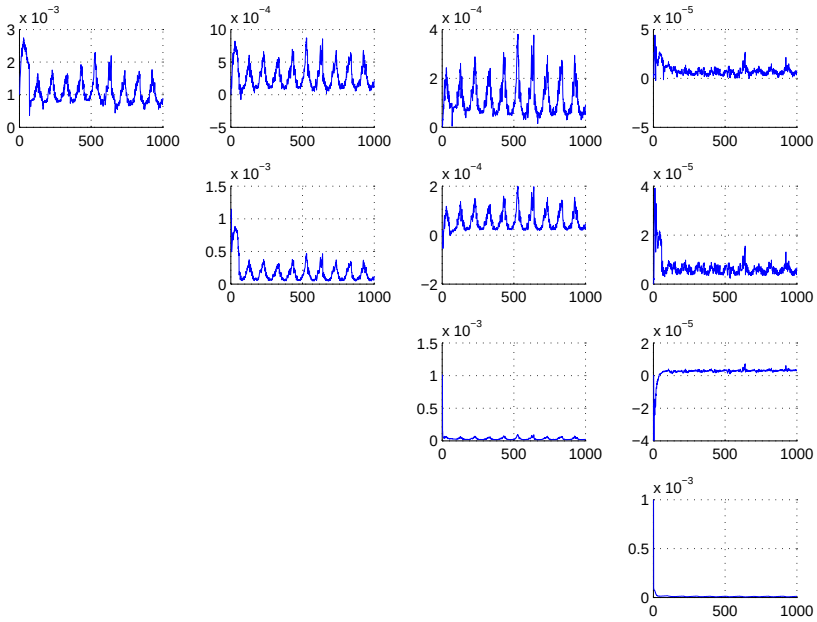

Figure 8: Variance and cross terms for all operating points as estimated by the Kalman filter. The variance decreases when the temperature is close to an operating point and vice versa. Note the different scaling on the y-axes.

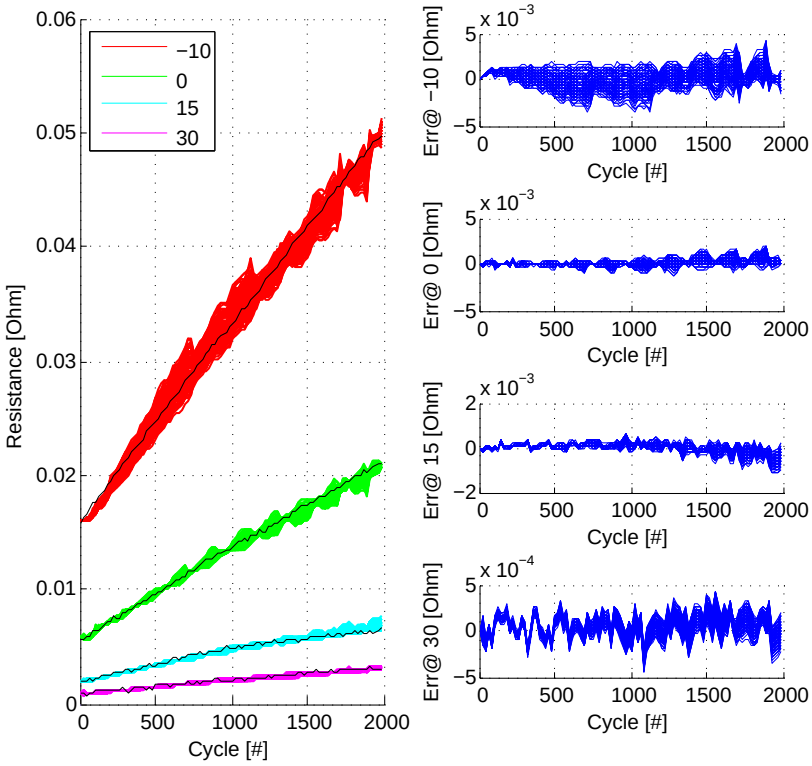

Figure 9: Overview of look-up table update when uncertainty is imposed on the ageing model. Black lines represent the true parameter values generated by the model. Note that there is no constant drift in the estimate in -10°C, even though the feed-forward update is based on an erroneous model.

for its update. It should also be clarified that these results are positive since the feed-forward update based on erroneous model does not lead to a significant parameter drift in the infrequently excited operating point -10°C.

6.4 Robustness to erroneous initialization

In the regions of the operating range that have not been excited, the look-up table adaptation will provide a feed-forward update of the parameters. For the update to behave correctly, the initial parameters must thus be accurate. To assess the robustness to erroneous initialization, 100 simulations varying the resistance uniformly within $\pm 50\%$ from the true values were performed. The initial error is independent between operating points, which basically means that the algorithm updates the resistance at non-excited operating points based on incorrect assumptions.

As can be seen in Fig. 10, also this case is handled well but it takes

some time before the operating point −10°C, which is hardly excited at all, converges to a reasonable estimate.

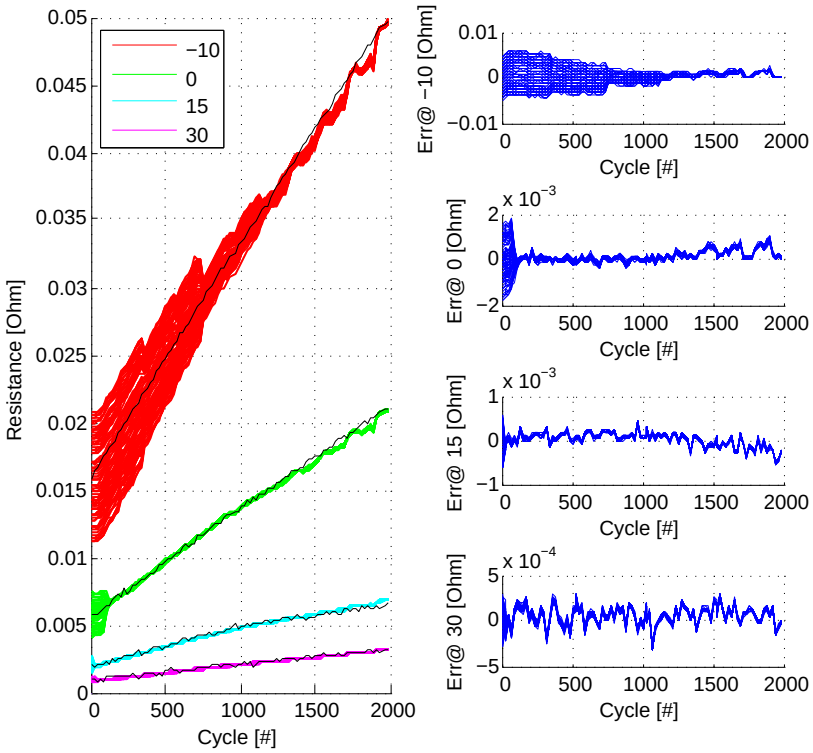

Figure 10: Overview of look-up table update when the initial resistance is incorrect. Black lines represent the true parameter values generated by the model.

7 Summary and future work

A method for updating look-up tables to reflect changed characteristics as a component ages has been proposed. In the method, a Kalman filter is used to update an entire look-up table based on local estimation at current operating conditions by utilizing correlations between changes in parameter values at different operating points. While the system in the general case is unobservable, a feed-forward update is still performed in non-excited regions that reflect the expected value of the complete look-up table conditioned on the observations.

The correlations, that are estimated offline, are included in the noise covariance matrix in the Kalman filter to introduce a "spill-over" of information between different regions of the look-up table. One tuning parameter

γ is included in the algorithm to tune the amount of "spill-over" and rate of parameter adaptation.

In a simulation study, the method was applied to estimation of the ohmic resistance of a lithium-ion battery. The entire look-up table was successfully updated without problems of drift, even in parts of the operating range that were seldom excited. Robustness to uncertainties both in the ageing model and errors in the initial parameter estimates was assessed, and even though the performance decreased, the method performed better than updating the look-up table without "spill-over".

Future work includes validating the method on a larger set of battery measurements. Also, extensions to higher dimensions in order to handle variations in both temperature and SoC is ongoing.

8 Acknowledgements

This work was supported by Volvo Car Corporation and Chalmers University of Technology, and sponsored by the Swedish Energy Agency through the project Batman.

References

[1] M. Broussely, P. Biensan, F. Bonhomme, P. Blanchard, S. Herreyre, K. Nechev, and R. J. Staniewicz, "Main aging mechanisms in Li ion batteries," *Journal of Power Sources*, vol. 146, no. 1-2, pp. 90–96, 2005.

[2] J. Remmlinger, M. Buchholz, M. Meiler, P. Bernreuter, and K. Dietmayer, "State-of-health monitoring of lithium-ion batteries in electric vehicles by on-board internal resistance estimation," *Journal of Power Sources*, vol. 196, no. 12, pp. 5357–5363, 2011.

[3] J. Vetter, P. Novák, M. R. Wagner, C. Veit, K. C. Möller, J. O. Besenhard, M. Winter, M. Wohlfahrt-Mehrens, C. Vogler, and A. Hammouche, "Ageing mechanisms in lithium-ion batteries," *Journal of Power Sources*, vol. 147, no. 1-2, pp. 269–281, 2005.

[4] A. Jossen, "Fundamentals of battery dynamics," *Journal of Power Sources*, vol. 154, no. 2, pp. 530–538, 2006.

[5] M. Debert, G. Colin, G. Bloch, and Y. Chamaillard, "An observer looks at the cell temperature in automotive battery packs," *Control Engineering Practice*, vol. 21, no. 8, pp. 1035–1042, 2013.

[6] D. V. Do, C. Forgez, K. El Kadri Benkara, and G. Friedrich, "Impedance observer for a Li-ion battery using Kalman filter," *IEEE Transactions on Vehicular Technology*, vol. 58, no. 8, pp. 3930–3937, 2009.

[7] X. H. X. Hu and F. S. F. Sun, "Fuzzy Clustering Based Multi-model Support Vector Regression State of Charge Estimator for Lithium-ion Battery of Electric Vehicle," *2009 International Conference on Intelligent Human-Machine Systems and Cybernetics*, vol. 1, pp. 1–5, 2009.

[8] J. Jaguemont, L. Boulon, and Y. Dube, "Characterization and Modeling of a Hybrid-Electric-Vehicle Lithium-Ion Battery Pack at Low Temperatures," *IEEE Transactions on Vehicular Technology*, vol. 65, no. 1, pp. 1–14, 2015.

[9] M. Chen, S. Member, and G. A. Rinc, "Accurate Electrical Battery Model Capable of Predicting Runtime and I V Performance," *IEEE Transactions on Energy Conversion*, vol. 21, no. 2, pp. 504–511, 2006.

[10] X. Hu, S. Li, H. Peng, and F. Sun, "Robustness analysis of State-of-Charge estimation methods for two types of Li-ion batteries," *Journal of Power Sources*, vol. 217, pp. 209–219, 2012.

[11] L. Lam, P. Bauer, and E. Kelder, "A practical circuit-based model for Li-ion battery cells in electric vehicle applications," *INTELEC, International Telecommunications Energy Conference (Proceedings)*, 2011.

[12] C. Zou, A. G. Kallapur, C. Manzie, and D. Nesic, "PDE battery model simplification for SOC and SOH estimator design," *Proceedings of the IEEE Conference on Decision and Control*, vol. 54rd IEEE, no. Cdc, pp. 1328–1333, 2015.

[13] X. Hu, F. Sun, and Y. Zou, "Online model identification of lithium-ion battery for electric vehicles," *J. Cent. South Univ. Technol.*, vol. 18, pp. 1525–1531, 2011.

[14] G. L. Plett, "Extended Kalman filtering for battery management systems of LiPB-based HEV battery packs - Part 3. State and parameter estimation," *Journal of Power Sources*, vol. 134, no. 2, pp. 277–292, 2004.

[15] E. Höckerdal, E. Frisk, and L. Eriksson, "EKF-based adaptation of look-up tables with an air mass-flow sensor application," *Control Engineering Practice*, vol. 19, no. 5, pp. 442–453, 2011.

[16] C. Guardiola, B. Pla, D. Blanco-Rodriguez, and P. Cabrera, "A learning algorithm concept for updating look-up tables for automotive applications," *Mathematical and Computer Modelling*, vol. 57, no. 7-8, pp. 1979–1989, 2013.

[17] J. C. Peyton Jones and K. R. Muske, "Identification and adaptation of linear look-up table parameters using an efficient recursive least-squares technique," *ISA Transactions*, vol. 48, no. 4, pp. 476–483, 2009.

[18] H. Blanke, O. Bohlen, S. Buller, R. W. De Doncker, B. Fricke, A. Hammouche, D. Linzen, M. Thele, and D. U. Sauer, "Impedance measurements on lead-acid batteries for state-of-charge, state-of-health and cranking capability prognosis in electric and hybrid electric vehicles," *Journal of Power Sources*, vol. 144, no. 2, pp. 418–425, 2005.

[19] M. Swierczynski, "Lithium ion battery energy storage system for augmented wind power plants," PhD Thesis, Aalborg University, 2012.

[20] W. Waag, C. Fleischer, and D. U. Sauer, "On-line estimation of lithium-ion battery impedance parameters using a novel varied-parameters approach," *Journal of Power Sources*, vol. 237, pp. 260–269, 2013.

[21] B. Fridholm, T. Wik, and M. Nilsson, "Robust recursive impedance estimation for automotive lithium-ion batteries," *Journal of Power Sources*, vol. 304, pp. 33–41, 2016.

[22] H. F. Chen, "On stochastic observability and controllability," *Automatica*, vol. 16, no. 2, pp. 179–190, 1980.

[23] A. R. Liu and R. R. Bitmead, "Stochastic observability in network state estimation and control," *Automatica*, vol. 47, no. 1, pp. 65–78, 2011.

[24] B. D. O. Anderson and J. B. Moore, *Optimal Filtering*, T. Kailath, Ed. Englewood Cliffs, New Jersey: Prentice-Hal, Inc., 1979, vol. 1.

Paper 3

Robust recursive impedance estimation for automotive lithium-ion batteries

Björn Fridholm, Torsten Wik, and Magnus Nilsson

Journal of Power Sources, 304, 2016

Comment: The layout of this paper has been reformatted in order to comply with the rest of the thesis.

Robust recursive impedance estimation for automotive lithium-ion batteries

Björn Fridholm, Torsten Wik, and Magnus Nilsson

Abstract

Recursive algorithms, such as recursive least squares (RLS) or Kalman filters, are commonly used in battery management systems to estimate the electrical impedance of the battery cell. However, these algorithms can in some cases run into problems with bias and even divergence of the estimates. This article illuminates problems that can arise in the online estimation using recursive methods, and lists modifications to handle these issues. An algorithm is also proposed that estimates the impedance by separating the problem in two parts; one estimating the ohmic resistance with an RLS approach, and another one where the dynamic effects are estimated using an adaptive Kalman filter (AKF) that is novel in the battery field. The algorithm produces robust estimates of ohmic resistance and time constant of the battery cell in closed loop with SoC estimation, as demonstrated by both in simulations and with experimental data from a lithium-ion battery cell.

Highlights:

- Identifies potential problems encountered in recursive parameter estimation
- Methods to improve performance and robustness of recursive parameter estimators
- Robust algorithm for estimation of battery cell impedance parameters

Keywords: Recursive parameter estimation; Kalman filter; Adaptive estimation; Battery impedance estimation; Robustness; Lithium-ion battery.

1 Introduction

The electrical impedance of the battery cell is used when estimating for instance State of Charge (SoC), State of Energy (SoE), State of Power (SoP)

and State of Health (SoH). As the battery ages, its impedance increases due to e.g. loss of electrode surface area and conductor corrosion [1, 2], and in order to maintain accuracy in all the estimations, it is vital to continuously monitor and update the impedance [3, 4, 5, 6].

In the literature, several different approaches to impedance estimation have been presented. Most common are offline system identification methods using some type of lab tests. Two such approaches are frequency domain identification using electrochemical impedance spectroscopy (EIS), and time domain identification using pulse tests [7, 8]. These methods rely on specialized equipment, test cycles and processing of large amounts of data, and are thus not suited for online implementation on low-cost processors used in automotive applications.

Focusing attention to methods suitable for online implementation, most of these rely on using an equivalent circuit model of the battery. The parameters are then estimated using primarily current and voltage information. Three conceptually different approaches are presented in the literature:

- *Recursive methods* store only data needed to perform one re-calculation of the model (see e.g. [9, 10, 11, 12]). The parameter estimates are then updated based on the new information in each time step. Low computational and storage costs have made this a popular choice for online parameter estimation.

- *Non-recursive methods* estimates parameters based on batches of data and thus requires larger amounts of data to be stored. While often used in offline system identification methods, the storage requirements means that they are less suitable for online applications. There can, however, be cases when non-recursive methods are needed (see e.g. [3, 13, 14]).

- *Machine learning algorithms* such as structured neural networks (SNN) (see e.g. [15]) and support vector machines (SVM) (see e.g. [16]) are useful when the battery characteristics cannot be accurately described by a simple model. Using training data, the algorithms learn how the system works. Problems such as large storage requirements and risk of overfitting reduces their applicability in online automotive tasks.

A comprehensive review of methods used in the literature, can be found in [17].

The rest of this article will focus on recursive methods with three main contributions; (i) a set of examples illustrating when recursive algorithms can fail; (ii) modifications to handle these issues; and (iii) design and experimental evaluation of an algorithm for estimation of battery impedance.

The structure is such that in Section 2, the recursive methods in focus are presented. In Section 3, the test environment and battery model used for evaluation of the estimators are described. Section 4 highlights issues that can be encountered in recursive estimators and proposes solutions to these problems. An algorithm is proposed in Section 5 and then evaluated using both simulations and experimental data in Section 6. Finally, Section 7 summarizes the results.

2 Recursive parameter estimation

In the following sections, two frequently used recursive parameter estimators are presented; the recursive least squares (RLS) and the Kalman filter. These algorithms are related and both use a linear regression model of the system in generic form,

$$y(k) = \varphi^T(k)\theta(k) + e(k), \tag{1}$$

where y is the observed output, φ is the regressor, θ is the parameter vector to be estimated and e is a noise term.

2.1 Recursive least squares

The method of solving an over-determined set of equations using least squares is well known to most engineers. In mathematical terms, the method determines the parameter vector $\hat{\theta}$ that minimizes the squared error between the measured output and the output predicted by the model (1), i.e.

$$\hat{\theta}(k) = \arg\min_{\theta} \frac{1}{2} \sum_{i=1}^{k} \lambda^{k-i} \left(y(i) - \varphi^T(i)\theta\right)^2, \tag{2}$$

where $0 \ll \lambda \leq 1$ is a forgetting factor introduced to weigh recent data more than old. This minimization problem has an analytic solution that can be implemented as a recursive algorithm:

$$\hat{\theta}(k) = \hat{\theta}(k-1) + K(k)\varepsilon(k) \tag{3}$$

$$K(k) = P(k-1)\varphi(k)\left(\lambda + \varphi^T(k)P(k-1)\varphi(k)\right)^{-1} \tag{4}$$

$$P(k) = \left(I - K(k)\varphi^T(k)\right)P(k-1)/\lambda, \tag{5}$$

where K is the estimator gain, P is the covariance estimate and $\varepsilon(k) = y(k) - \varphi^T(k)\hat{\theta}(k-1)$ is the residual between measured and estimated output.

In the literature, there are several versions of recursive least squares estimators [18, 19, 20]. By simplifications, reformulations of the cost function

or avoiding estimation of the covariance estimate, they can be tailored to system requirements. In this work, the regular RLS algorithm with exponential forgetting factor (3)–(5) is used. In the battery estimation field, RLS has been used for parameter estimation in e.g. [10, 12].

2.2 Kalman filter

The Kalman filter can be seen a special case of the RLS algorithm, where the parameter variations are modelled as random walks, i.e.

$$\theta(k+1) = \theta(k) + w(k),$$

where $w(k) \sim \mathcal{N}(0, R_w)$ is a Gaussian white noise. Like in (1), the measurement is distorted by additive noise,

$$y(k) = \varphi^T(k)\theta(k) + v(k), \tag{6}$$

but now it is assumed that $v(k) \sim \mathcal{N}(0, R_v)$ is a Gaussian white noise. The Kalman filter algorithm then becomes

$$\hat{\theta}(k) = \hat{\theta}(k-1) + K(k)\varepsilon(k) \tag{7}$$

$$K(k) = P(k-1)\varphi(k)\left(R_v(k) + \varphi^T(k)P(k-1)\varphi(k)\right)^{-1} \tag{8}$$

$$P(k) = P(k-1) - K(k)\varphi^T(k)P(k-1) + R_w(k), \tag{9}$$

where we note that the noise covariances, R_w and R_v, which represents the noise statistics, often are considered as tuning parameters. Derivation of the linear Kalman filter can be found in several sources, for instance the original paper [21] or more recent descriptions, such as [22]. In the battery estimation field, Kalman filters are used for parameter estimation in e.g. [9, 11].

3 Test environment

In the upcoming discussions, a test environment is used to evaluate the algorithms and to highlight potential problems.

3.1 Equivalent circuit battery model

In online battery management systems, it is common to use a model of the current–voltage response in form of an equivalent circuit like the one

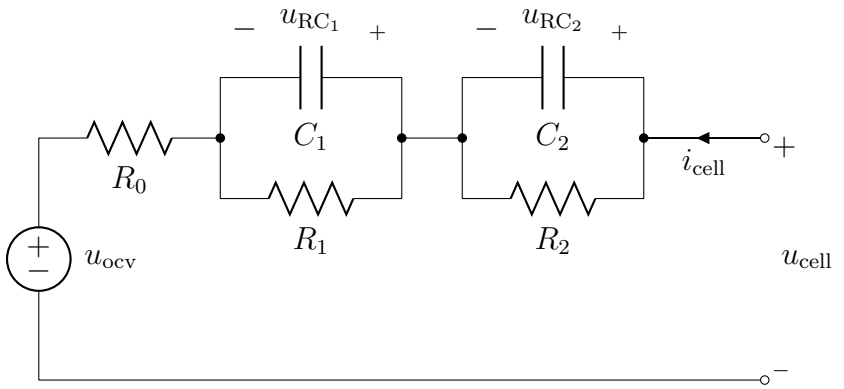

Figure 1: Equivalent circuit model with two RC-pairs.

in Fig. 1. Discretized with sampling time Δt and zero order hold, it is described by

$$u_{\mathrm{RC}_1}(k+1) = e^{-\frac{\Delta t}{C_1 R_1}} u_{\mathrm{RC}_1}(k) + R_1 \left(1 - e^{-\frac{\Delta t}{C_1 R_1}}\right) i_{\mathrm{cell}}(k) \tag{10}$$

$$u_{\mathrm{RC}_2}(k+1) = e^{-\frac{\Delta t}{C_2 R_2}} u_{\mathrm{RC}_2}(k) + R_2 \left(1 - e^{-\frac{\Delta t}{C_2 R_2}}\right) i_{\mathrm{cell}}(k) \tag{11}$$

$$u_{\mathrm{cell}}(k) = u_{\mathrm{ocv}}(z_{\mathrm{soc}}(k)) + u_{\mathrm{RC}_1}(k) + u_{\mathrm{RC}_2}(k) + R_0 i_{\mathrm{cell}}(k), \tag{12}$$

where z_{soc} is the SoC of the battery, and the rest of the parameters and signals are defined in Fig. 1. Note that the notation is slightly simplified, since all impedance parameters are varying with respect to operating conditions such as temperature, SoC, current and age (z_{soh}). As an example, this means that the ohmic resistance should be denoted $R_0(T(k), z_{\mathrm{soc}}(k), i_{\mathrm{cell}}(k), z_{\mathrm{soh}}(k))$. It is also common to report the time constant $\tau_i = R_i C_i$ instead of the individual values for the dynamic part of the model. In the upcoming discussions, the model (10)–(12) is referred to as the dual RC model. Also a first order version of the model, referred to as the single RC model, is used where (11) is omitted and u_{RC_2} in (12) is set to zero.

A dual RC reference model with parameters that are non-linear with respect to temperature and SoC was identified offline from lab tests of a commercially available lithium ion cell of nickel manganese cobalt oxide (NMC) type intended for use in a plug-in hybrid electric vehicle (PHEV). The voltage prediction accuracy of the model is within 20mV for the validation cycles used in Section 6.2. It should be noted that the non-linear dual RC model is a simplification of a real battery cell, which means that the reference parameters reported are not "true" parameters. However, the accuracy of the voltage prediction indicates that the found parametrization is a good approximation, and thus the parameters estimated by the recursive

algorithms are expected to be close to the reference parameters.

3.2 SoC estimator

For SoC estimation an extended Kalman filter (EKF) was used (see e.g. [4, 7]). There are two different versions using single and dual RC models respectively. In both cases, R_0, R_1 and C_1 are coming from the parameter estimator, while R_2 and C_2 for the dual RC model uses fixed values based on an offline system identification. Tuning of the SoC estimator, to get a trade-off between Coulomb counting and voltage feedback, was done manually. The same tuning was used for all parameter estimators to enable a fair comparison between them.

3.3 Setup used in simulations

In Fig. 2a, a block scheme of the setup used in the simulation studies in Sections 4 and 6.1 is presented. The dual RC reference model is used to calculate SoC and voltage from the current. The parameter estimator can use either true SoC from the battery model, i.e. z_{soc}, referred to as open loop estimation, or use estimated SoC, $\hat{z}_{\text{soc}}$, from an EKF using a single RC model with the estimated parameters. This is referred to as closed loop estimation.

3.4 Setup used with experimental data

In Section 6.2, the algorithm proposed in the article is tested on experimental data from lab tests. The impedance parameters (R_0, R_1, C_1) are estimated in closed loop with a SoC estimation algorithm based on an EKF. In order to produce accurate SoC estimates in cold temperatures, the SoC EKF needed a dual RC model. Since the algorithm proposed here focus on estimating only a single RC model, the SoC EKF uses a fixed time constant for the slower dynamics (R_2, C_2). A block scheme of this setup is shown in Fig. 2b.

3.5 Load profile

The load profile used in the simulations is based on a complete vehicle simulation of a charge sustaining drive cycle. The current and voltage of a single cell can be seen in Fig. 3.

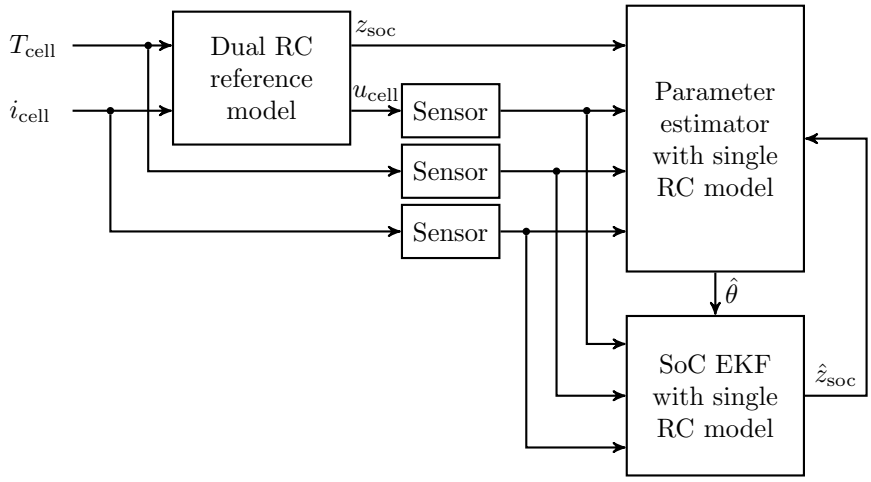

(a) Setup for simulations

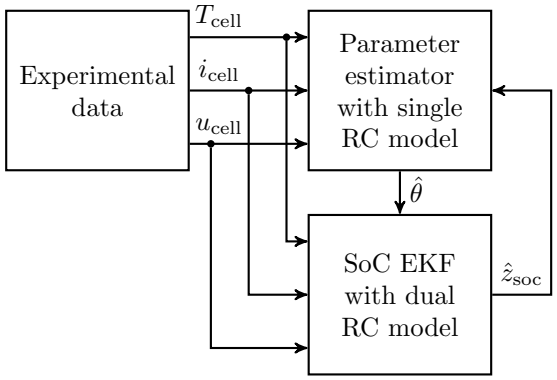

(b) Setup for experiment data

Figure 2: (a): Block scheme of the setup used in simulations. A reference battery model with parameters estimated offline from lab tests is used to generate the cell voltage given current and temperature test vectors. The estimators, i.e. RLS or Kalman filter, estimates a single RC model either in open loop using the true SoC from the battery model, i.e. z_{soc}, or in closed loop using estimated SoC from the EKF, i.e. $\hat{z}_{\text{soc}}$. Sensor noises are assumed to be white and Gaussian. (b): Block scheme of the setup used when examining performance on experimental data. The parameter estimator has a single RC model while the EKF uses a dual RC model with fixed time constant for the slower dynamics.

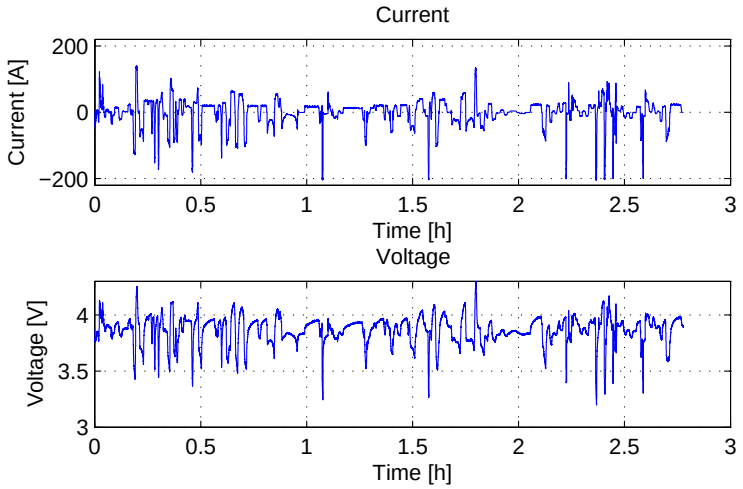

Figure 3: Current and voltage load profiles used in the evaluation.

4 Potential problems in recursive estimators

Both the RLS and the Kalman filter algorithms assume some special properties of the problem formulation, such as a correct model and known noise statistics. In a real application, these assumptions are generally not met and the impact of violating them are in the best case biased estimates and in the worst case diverging estimates. The following section will present some examples of situations when these algorithms can fail and propose modifications from the literature to handle these problems. Most of the discussions are kept general but some application specific motivations are used.

4.1 A motivating example

Two estimators, one RLS (3)–(5) and one Kalman filter (7)–(9) were implemented to estimate R_0, R_1 and C_1 of the single RC model. For the open loop simulation case presented in Section 3.3, it is straightforward to tune both estimators to achieve performance according to solid lines in Fig. 4 when there is no noise added to the current or voltage sensors. However, when the estimation is performed in closed loop with SoC estimation, the results with dashed lines are obtained. In the example, Gaussian white noise was also added to the current and voltage signals with standard deviations of 3A and 1.5mV, respectively. As can be seen, the performance is no longer acceptable since the Kalman filter has problems with convergence on both ohmic resistance and SoC estimates, and the RLS shows undesired behaviour around 2 hours into the cycle when the time constant estimation

suddenly increases. In the upcoming sections, some of the reasons for the poor performance will be examined together with solutions to handle the problems.

4.2 Amount of parameters to estimate

The first and most obvious problem when estimating impedance in batteries is that there are several parameters to estimate based on relatively few measured variables. Here, we want to estimate ohmic resistance and one or two time constants with two parameters each, leading to 3–5 parameters based on only current and voltage information. In some papers, e.g. [9, 3], even more complex implementations of the diffusion time constant is proposed. In [3], however, the estimation task is handled by using a non-recursive estimation of the diffusion parameters. Parameters also vary non-linearly with for instance temperature and if this effect is also to be included in the estimation, there will be even more parameters to estimate introducing risk of insufficient excitation.

4.3 Noise effects

The RLS is good at handling Gaussian noise since it will perform an averaging of the data. However, Gaussian noise on the regressor variable can lead to biased estimates [23], as can be seen by the dotted blue line in the estimation of R_0 presented in Fig. 4. The size of the bias will depend on the signal to noise ratio (SNR) of the regressor. In this example, amplitude dependent noise is added to the current sensor, where the standard deviation of the noise is increased linearly from 0 to 5A as the current goes from 0 to 100A. Note that the noise added in this example is more extreme than in the other simulations in order to illustrate the effect.

Dead-zones

An effective way to guarantee high SNR is to use a dead-zone. The idea behind dead-zones is to allow parameter adaptation only when the estimation residual, ε, is significantly larger than the noise term e. In [18], the following bound is suggested:

$$|\varepsilon(k)| \geq 2 \sup|e(k)|$$

Since it may be difficult to know the upper bound of the noise term, knowledge about the application is often used to set the size of the dead-zone.

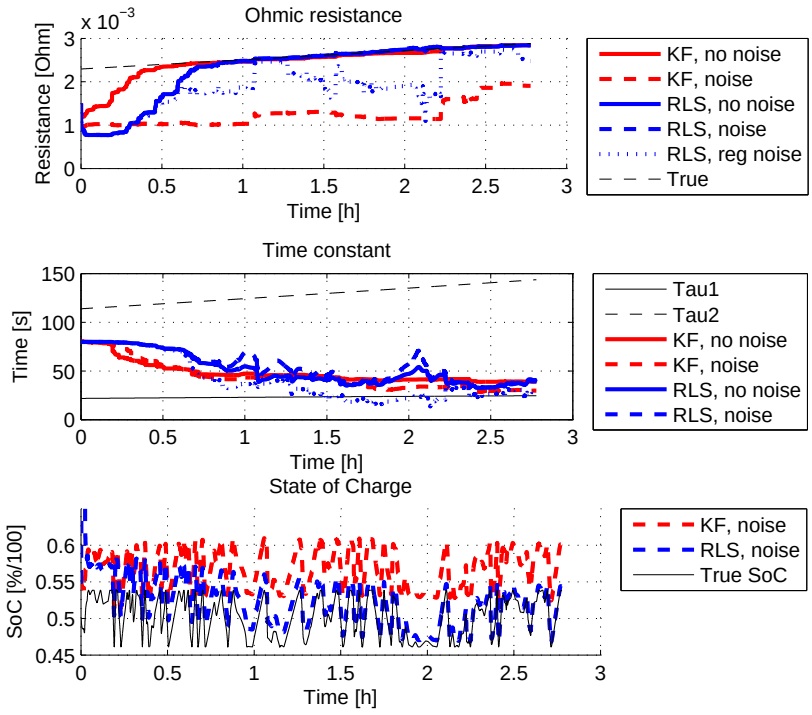

Figure 4: Estimation of parameters R_0, R_1 and C_1 using both Kalman filter and RLS. (Solid) No noise is added to the sensor signals and estimation is done in open loop, i.e. based on true SoC. Both estimators handle the task, though the RLS must be tuned for slower adaptation than the Kalman filter. (Dashed): Noise is added to the sensor signals and estimation is done in closed loop with SoC estimation. Here we see that both estimators have problems. The Kalman filter estimates of ohmic resistance and SoC does not converge, and all attempts to improve this by tuning failed. The RLS also have some undesired behaviour when the time constant estimate suddenly increase at around 2h. (Dotted): RLS estimation of ohmic resistance when signal to noise ratio of the regressor, i.e. current, is low. Note that $\tau_1 = R_1 C_1$ is plotted instead of the individual estimates of R_1 and C_1.

Pre-filtering

When the estimated parameters are time-varying, a forgetting factor is often used to weigh recent data more than older. This will reduce the noise suppression since the contribution to the averaging is gradually reduced by the age of the data. There will thus be a trade-off between noise suppression and ability to adapt the parameters to actual changes.

A way to reduce this problem is to apply a pre-filter to the sensor signals. The pre-filter may be of low-pass, high-pass or band-pass type, depending on the noise characteristics. It is important though, to use the same filtering on all inputs and outputs to reduce the risk of biased estimates.

4.4 Model errors

To guarantee convergence to the correct set of parameters, the algorithms must use a correct model description. Failing to provide the correct model means that the parameters becomes biased and the bias depends on the excitation [18]. In the battery application, a "grey-box" model based on physical insights is used. As already discussed, this is not a complete description of processes inside the battery and for this reason, it is important to retain caution in the adaptation task.

Three of the main contributors to uncertainties in the single RC model used for parameter estimation are:

- Gaussian sensor noise on both current and voltage measurements.
- Unmodelled slow dynamics.
- Error in OCV from the fact that estimated SoC is used.

Since unmodelled slower dynamics and OCV uncertainties are effects that change slowly, the error in (12) will not be white noise, but correlated to the regressor vector, i.e.

$$\mathbb{E}\left\{\varphi^T(k)e(k)\right\} \neq 0. \tag{13}$$

Modelling correlated noise

One way of handling effects not explained by the chosen model structure is to include a noise model, where additional parameters are used to estimate the noise colour. From the assumptions in the previous section, one can conclude that the error may be an almost constant offset with a rapid measurement noise superimposed. A reasonable model for this is a first order system, with a long time constant, driven by white noise, that is

$$e(k) = ce(k-1) + v(k), \tag{14}$$

where c is an unknown parameter defining the correlation of the error and v is white noise. Since the noise term is not known, it cannot be directly included in the regression model. The way to overcome this is to approximate it by the estimation residual, $\varepsilon(k) = y(k) - \varphi^T(k)\hat{\theta}(k-1)$.

Note that reducing the bias with a noise model generally comes at the cost of increased variance in all estimates, as well as increased storage and computational requirements due to the additional parameter(s).

Robust estimation

Least squares estimation rely on Gaussian estimation residuals, which means that the probability of having large residuals is small. This may not be the case in reality and one way of reducing the influence of large errors suggested by [18] is to normalize the error by, for instance, replacing (5) with

$$\hat{\theta}(k) = \hat{\theta}(k-1) + K(k)\frac{\varepsilon(k)}{1+|\varepsilon(k)|}.$$

4.5 Time-varying parameters

The main reason for using an adaptive system for battery impedance estimation is to handle parameter variations due to ageing effects. If the RLS is to be alert to changes in the parameters, old data must be discarded. The simplest way to include this in a recursive manner, is to introduce an exponential forgetting factor, λ, as in the cost function (2). The forgetting factor is always between zero and one, where a value of one means that old data is given the same importance as recent data, and decreasing λ corresponds to a shorter historic time-horizon influencing the estimate. Most often, λ is chosen to be very close to one.

When the excitation of the system is poor, the forgetting factor may cause a phenomenon called covariance windup, which refers to an increase in the estimated covariance. The reason for this is that the term $K(k)\varphi^T(k)$ in this case is close to zero, which for the RLS implies that (5) becomes

$$P(k) \approx P(k-1)/\lambda, \quad \lambda < 1$$

and the covariance thus grows exponentially. When there is information in the signals again, the estimator gain may become very large, causing large jumps in estimated parameter values. In Fig. 4 this effect can be seen both after 1 hour and around 2 hours, when the time constant estimation is increasing rapidly for the RLS estimate. This is due to covariance windup, which can be seen by red lines in Fig. 5 that includes a plot of the estimated covariance for the time constant estimate.

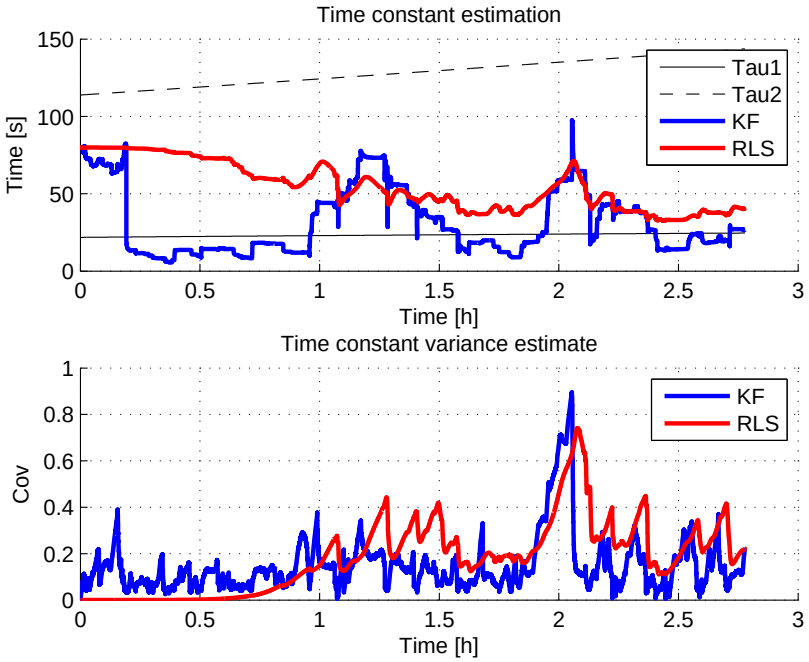

Figure 5: Examples of covariance windup from simulation of the RLS algorithm with forgetting factor (red) and the Kalman filter when fast adaptation is allowed (blue).

In the Kalman filter, the random walk model introduces an alertness to time-varying parameters via the matrix R_w that is added to the estimated covariance. Just like the RLS algorithm, poor excitation (small $K(k)\varphi^T(k)$) may cause covariance windup in the Kalman filter, since the covariance estimate becomes

$$P(k) \approx P(k-1) + R_w(k).$$

In the example above, this problem was not so obvious because the adaptation is relatively slow. However, as can be seen by blue lines in Fig. 5, faster adaptation can lead to problems of the same type as for the RLS algorithm. This is admittedly a rather extreme example, but it reveals a potential problem of the regular Kalman filter in this application.

Time-varying forgetting factor

To handle the problem of covariance windup for poorly exciting inputs, as exhibited by the RLS algorithm, the forgetting factor can be made time-varying. Most of the approaches presented in literature are ad-hoc solutions limiting the covariance estimate in some way. In [24], use of a time-varying

forgetting factor is suggested by modifying the RLS algorithm according to:

$$\begin{aligned}
\hat{\theta}(k) &= \hat{\theta}(k-1) + K(k)\varepsilon(k) \\
K(k) &= P(k-1)\varphi(k)\left(1 + \varphi^T(k)P(k-1)\varphi(k)\right)^{-1} \\
\lambda(k) &= 1 - \frac{\varepsilon^2(k)}{\sigma\left(1 + \varphi^T(k)P(k-1)\varphi(k)\right)} \\
W(k) &= \left(I - K(k)\varphi^T(k)\right)P(k-1) \\
P(k) &= \begin{cases} W(k)/\lambda(k), & \operatorname{tr}\left(W(k)/\lambda(k)\right) \leq C \\ W(k), & \text{otherwise} \end{cases}
\end{aligned}$$

where two new tuning parameters are introduced; a gain of the forgetting factor (σ) and an upper bound to the trace of the estimation covariance matrix.

Adaptive Kalman filters

One method to avoid covariance windup for Kalman filters is to use an adaptive Kalman filter as proposed by [25]. Rather than viewing R_w as a matrix chosen by the designer, it is actively used to drive the covariance estimate P to a user-defined desired covariance P_d. This is achieved by choosing

$$R_w(k) = \frac{P_d\varphi(k)\varphi^T(k)P_d}{R_v(k) + \varphi^T(k)P_d\varphi(k)}. \tag{15}$$

In [26], Evestedt and Medvedev show that this alternative method provides good anti-windup properties in the parameter estimator.

4.6 Numerical issues

Both RLS and Kalman filters involves matrix computations that may exhibit poor numerical properties when implemented on microprocessors [27]. To quantify numerical properties, the condition number of the covariance matrix can be used as an indicative measure. In Fig. 6, the condition number of the estimated covariance is plotted for RLS and Kalman filters together with the result from the algorithm proposed in Section 5. It can be seen how the proposed algorithm successfully reduce the condition number by a factor of 10^4 compared to the regular Kalman filter by use of scaling and square root implementation. Even if the condition number contains no information about the performance of the estimator, poor numerical conditioning may lead to instability of the estimator.

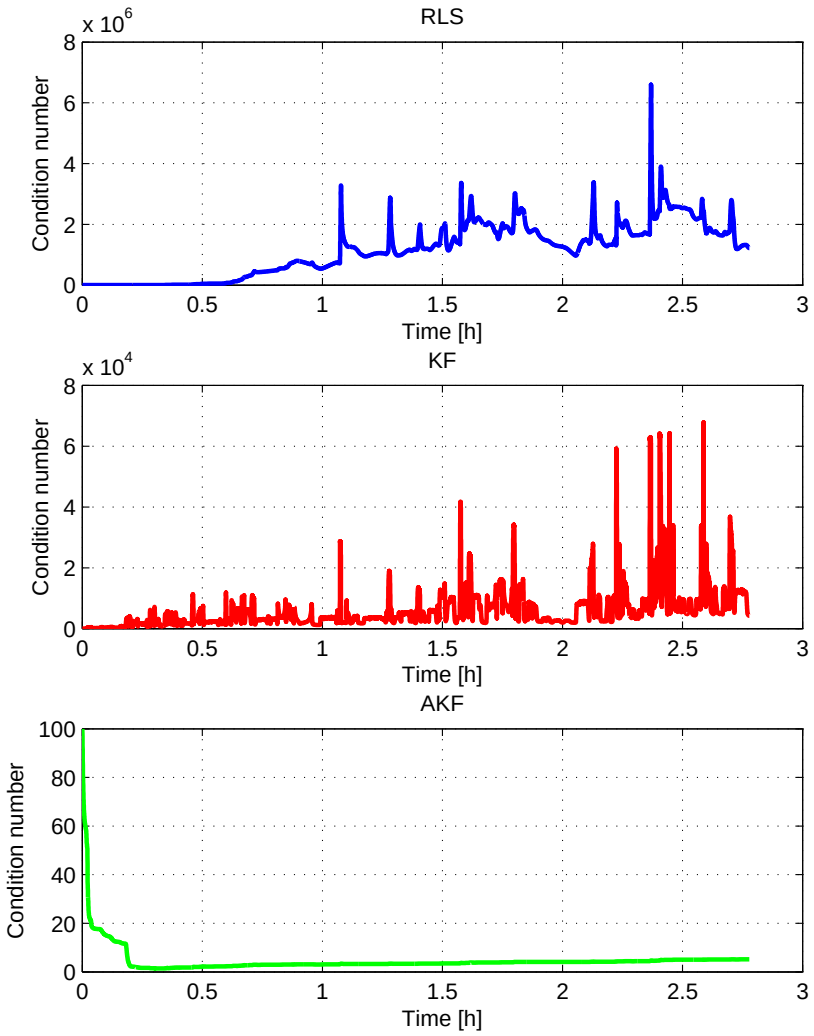

Figure 6: Condition number of the covariance estimate produced by the RLS, Kalman filter and AKF. It can be seen how signal scaling and square root implementation are two very successful techniques to reduce the condition number of the covariance estimate.

Signal scaling

The first measure to take in trying to avoid numerical issues is to scale the signals such that they are in the same order of magnitude. In an automotive battery system, the current can be several hundred amperes, while the voltages are in the order of a few volts and the interesting deviations of the voltage are in the order of tens of millivolts. Based on this, it is wise to scale the input current and voltage with their maximum values.

Square root implementation

As seen in Fig. 6, straightforward implementation of the RLS and Kalman filter according to equations (3)–(5) and (7)–(9) can result in algorithms with poor numerical properties because of the recursive propagation of the error covariances from one time-step to the next. To reduce this issue, and improve the condition number of the covariance matrix, the algorithm can be modified to propagate the square root of the error covariance instead [28]. Algebraically the implementations are equivalent, but the numerical properties are significantly improved.

4.7 SoC and parameter estimation interaction

One important aspect to consider when designing the adaptation algorithm is that there is an interaction between impedance and SoC estimation. As described in Section 4.4, errors in SoC introduces uncertainty in the OCV voltage, and the time constant estimation is then based on biased voltage information. Fortunately, the bias decreases when the OCV curve is flat, which is contrary to SoC uncertainty which increases in that case. In Fig. 4, it can be seen how the SoC estimation fails to produce accurate estimates when the parameters are estimated using the Kalman filter. This problem is even more prominent when the algorithms are subject to real-world data.

Convergence of combined state and parameter estimators normally rely on separation of time constants, implying that the parameters vary much slower than the states of the system. In a battery, the impedance change on very different time-scales [29], and since it depends statically on SoC, temperature and current, this jeopardizes the assumption that parameters and states can be separated. For instance, having unmodelled current dependency may lead to parameter values changing faster than SoC itself.

5 Proposed estimation method

Based on the descriptions in previous sections, a novel algorithm for estimating R_0, R_1 and C_1 is proposed. The algorithm splits estimation of ohmic resistance from the estimation of the dynamic part of the model in order to improve robustness. It also uses a type of adaptive Kalman filter that has, to the best of the authors' knowledge, not been proposed for battery parameter estimation before. A similar approach to separate the problem is also suggested in [9], but the chosen algorithms for each part are different compared to this work.

5.1 Estimation of ohmic resistance

Using a sufficiently short sampling time, we can assume that both the voltages u_{ocv} and u_{RC1} of (12) are almost constant. R_0 is a slowly varying parameter and it can thus be approximated by

$$R_0 = \frac{u_{\text{cell}}(k) - u_{\text{cell}}(k-1)}{i_{\text{cell}}(k) - i_{\text{cell}}(k-1)}, \tag{16}$$

providing that the denominator is non-zero. Introducing the notation $\Delta u_{\text{cell}}(k) = u_{\text{cell}}(k) - u_{\text{cell}}(k-1)$ and $\Delta i_{\text{cell}}(k) = i_{\text{cell}}(k) - i_{\text{cell}}(k-1)$, the ohmic resistance can be estimated using the RLS algorithm, i.e.

$$\hat{R}_0(k) = \hat{R}_0(k-1) + K_R(k)\left(\Delta u_{\text{cell}}(k) - \hat{R}_0(k-1)\Delta i_{\text{cell}}(k)\right), \tag{17}$$

where

$$K_R(k) = \begin{cases} \dfrac{P_R(k-1)\Delta i_{\text{cell}}(k)}{\lambda + \Delta i_{\text{cell}}^2(k) P_R(k-1)}, & \text{if } \|\Delta i_{\text{cell}}\| > \delta_{\text{deadzone}} \\ 0, & \text{otherwise} \end{cases} \tag{18}$$

$$P_R(k) = \left(1 - K_R(k)\Delta i_{\text{cell}}(k)\right) P_R(k-1)/\lambda. \tag{19}$$

The dead-zone reduces the risk for covariance windup by acting as a noise suppressor and makes sure that the system has been sufficiently excited before using data for identification. It should be noted that R_0 estimated this way will not be a pure ohmic resistance, it will also include dynamic effect that are faster than the used sampling time. For the purpose of e.g. SoC estimation, this is wanted since

5.2 Estimation of time constant

To simplify notation, the following symbols are used in the forthcoming:

$$\alpha = e^{-\frac{\Delta t}{C_1 R_1}}$$
$$\beta = R_1 \left(1 - e^{-\frac{\Delta t}{C_1 R_1}}\right).$$

The single RC model can then be written as

$$\begin{aligned} u_{\mathrm{RC}_1}(k+1) &= \alpha u_{\mathrm{RC}_1}(k) + \beta i_{\mathrm{cell}}(k) \\ u_{\mathrm{cell}}(k) &= u_{\mathrm{ocv}}(z_{\mathrm{soc}}(k)) + R_0 i_{\mathrm{cell}}(k) + u_{\mathrm{RC}_1}(k) + e(k), \end{aligned}$$

where a noise term $e(k)$ is introduced to model errors in the voltage prediction as described in Section 4.4.

By introducing

$$y(k) \triangleq u_{\mathrm{cell}}(k) - u_{\mathrm{ocv}}(\hat{z}_{\mathrm{soc}}(k)) - R_0 i_{\mathrm{cell}}(k),$$

the model can be expressed in terms of the backwards time-shift operator q^{-1}, defined by $q^{-1}x(k) = x(k-1)$, as

$$y(k) = \frac{\beta q^{-1}}{1 - \alpha q^{-1}} i_{\mathrm{cell}}(k) + e(k).$$

Transforming back to the time domain we have

$$y(k) = \alpha y(k-1) + \beta i_{\mathrm{cell}}(k-1) + e(k) - \alpha e(k-1) \tag{20}$$

Finally, the noise model (14) and introduction of scaling variables k_u and k_i to the voltage and current, respectively, yields

$$\tilde{y}(k) = \alpha \tilde{y}(k-1) + \beta \frac{k_u}{k_i} \tilde{i}_{\mathrm{cell}}(k-1) + k_u(c-\alpha)\varepsilon(k-1) \tag{21}$$

where $\tilde{y}(k) = k_u y(k)$, $\tilde{i}(k) = k_i i(k)$ and ε is the estimation residual used as an approximation of e.

In the generic form of (1), this gives the regression and parameter vector

$$\begin{aligned} \varphi(k) &= \begin{bmatrix} k_u y(k-1) & k_i i_{\mathrm{cell}}(k-1) & \varepsilon(k-1) \end{bmatrix}^T \\ \theta(k) &= \begin{bmatrix} \theta_1 & \theta_2 & \theta_3 \end{bmatrix}^T = \begin{bmatrix} \alpha & \frac{k_u}{k_i}\beta & k_u(c-\alpha) \end{bmatrix}^T, \end{aligned}$$

which means that the parameters of interest can be recalled from the expressions

$$\begin{aligned} R_1 &= \frac{k_i}{k_u} \frac{\theta_2}{1-\theta_1} \\ C_1 &= \frac{k_u}{k_i} \frac{\Delta t(\theta_1 - 1)}{\theta_2 \log(\theta_1)}. \end{aligned} \tag{22}$$

Note that the only use of the parameter c is to reduce bias in the other terms.

Estimation of R_1 and C_1, is then based on the AKF algorithm (7)–(9) and (15), where the design variables are R_v and the desired covariance estimate P_d. The algorithm tested in the next section also applies linear, first order low-pass filters to current and voltage measurements to remove high frequency content.

6 Evaluation

The proposed algorithms will now be used to estimate the values of R_0, R_1 and C_1 in Fig. 1, both in simulations and on lab data from an commercially available NMC battery intended for use in a PHEV. The simulated case, which is identical to the motivating example of Section 4.1, is mainly used to visualize the robustness to different initial values. The lab data cases are combined with an initial estimation error in SoC to see how the combined uncertainty in both SoC and parameters is handled.

6.1 Simulation study

To evaluate robustness of the parameter estimation algorithm, the convergence properties for different initial parameter values are investigated in a simulation study, using the setup presented in Section 3.3. Estimation is done in closed loop with SoC estimation, starting from an initial SoC error of 5%. The results in Fig. 7 show that even for rather large initial errors, both parameter and SoC estimates converges. These results can be compared to Fig. 4, where neither RLS nor Kalman filter, in their standard form, managed to produce reliable estimates. The fast adaptation that occurs after approximately 15 minutes is because that is the first time the current is large enough to provide sufficient excitation of the system. The single time constant converges close to the shorter of the time constants of the dual RC model. The reason for this is the frequency content of the excitation signal.

6.2 Algorithm applied to lab data

To further evaluate the algorithm, it was subjected to lab data for two different temperatures. The combined estimation task was also complicated by introducing initial errors to both SoC and parameters. As seen in Fig. 8, the performance of the combined SoC and impedance estimator is good in both validation temperatures. SoC converges to within 1% from reference

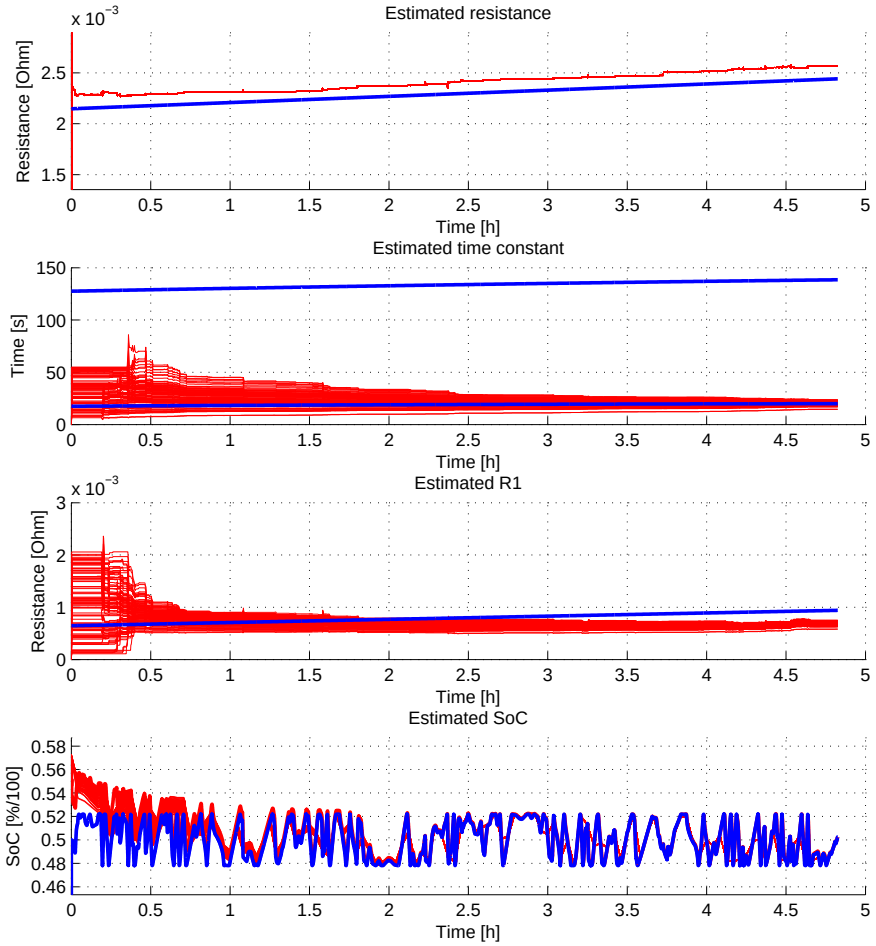

Figure 7: Robustness analysis. The ohmic resistance R_0 and time constant $\tau_1 = R_1 C_1$ as estimated in 100 Monte Carlo simulations where the initial estimate was chosen randomly. Note that the reference model (black lines) uses the non-linear dual RC model, while only a single RC model is estimated. The convergence rate of the estimation is very dependent on initial value, but it still converges to a region around the expected value, which should be between the short and long time constant of the model. The reason for convergence closer to the short time constant is due to the frequency content of the input signal, which excites the fast dynamics more than the slower.

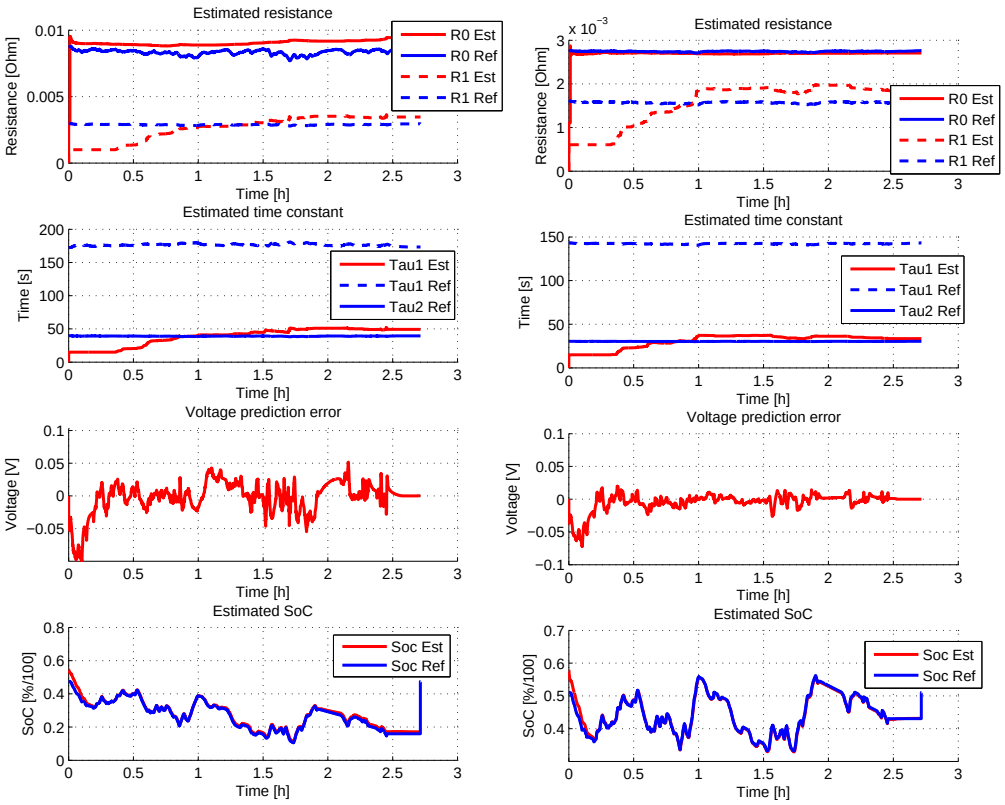

(a) 0°C (b) 22°C

Figure 8: Parameter convergence of ohmic resistance and time constant together with voltage prediction accuracy and resulting SoC estimation based on identified parameters for (a) 0°C and (b) +22°C. Reference parameters are from simulation of the dual RC reference model.

SoC given by Coulomb counting in test rig and the parameter estimates also converge to close to the reference model. Voltage prediction based on the estimated parameters is within 50mV in 0°C and 20°C after parameters are adapted, which allows strong voltage feedback in the SoC estimation.

7 Summary and Future Work

When using recursive estimators such as Kalman filters or RLS to estimate parameters in battery cell models there are some potential pitfalls to consider. An example was shown where both Kalman filter and RLS exhibited problems with sensor noise, covariance windup and poor numerical stability.

Several actions proposed in the literature to handle these issues were presented leading up to a novel algorithm for estimation of battery impedance in closed loop with SoC estimation.

In the algorithm, the estimation of ohmic resistance is separated from the estimation of the time constant in order to improve robustness. Ohmic resistance is then estimated using an RLS algorithm with a dead-zone to ensure proper excitation and signal to noise ratio. The time constant is estimated with an adaptive Kalman filter that handles poor excitation and include features such as pre-filtering and signal scaling to further improve robustness.

The performance of the algorithm was demonstrated by successfully estimating the ohmic resistance and time constant of the battery cell in closed loop with SoC estimation for data recorded in lab.

Future work includes extending the algorithm to also estimate the second time constant needed to get an accurate SoC estimate in colder temperatures.

8 Acknowledgements

This work was supported by Volvo Cars, AB Volvo, Intertek, Viktoria Swedish ICT and Chalmers, and partly financed by the Swedish Energy Agency through the project State of Function.

References

[1] M. Broussely, P. Biensan, F. Bonhomme, P. Blanchard, S. Herreyre, K. Nechev, and R. J. Staniewicz, "Main aging mechanisms in Li ion batteries," *Journal of Power Sources*, vol. 146, no. 1-2, pp. 90–96, 2005.

[2] J. Vetter, P. Novák, M. R. Wagner, C. Veit, K. C. Möller, J. O. Besenhard, M. Winter, M. Wohlfahrt-Mehrens, C. Vogler, and A. Hammouche, "Ageing mechanisms in lithium-ion batteries," *Journal of Power Sources*, vol. 147, no. 1-2, pp. 269–281, 2005.

[3] C. Fleischer, W. Waag, H. M. Heyn, and D. U. Sauer, "On-line adaptive battery impedance parameter and state estimation considering physical principles in reduced order equivalent circuit battery models estimation," *Journal of Power Sources*, vol. 262, pp. 457–482, 2014.

[4] B. Fridholm, M. Nilsson, and T. Wik, "Robustness comparison of battery state of charge observers for automotive applications," *IFAC Proceedings Volumes (IFAC-PapersOnline)*, vol. 19, pp. 2138–2146, 2014.

[5] S. Sepasi, R. Ghorbani, and B. Y. Liaw, "A novel on-board state-of-charge estimation method for aged Li-ion batteries based on model adaptive extended Kalman filter," *Journal of Power Sources*, vol. 245, pp. 337–344, 2014.

[6] T. Wik, B. Fridholm, and H. Kuusisto, "Implementation and robustness of an analytically based battery state of power," *Journal of Power Sources*, vol. 287, pp. 448–457, 2015.

[7] G. L. Plett, "Extended Kalman filtering for battery management systems of LiPB-based HEV battery packs - Part 2. Modeling and identification," *Journal of Power Sources*, vol. 134, no. 2, pp. 262–276, 2004.

[8] W. Waag, C. Fleischer, and D. U. Sauer, "On-line estimation of lithium-ion battery impedance parameters using a novel varied-parameters approach," *Journal of Power Sources*, vol. 237, pp. 260–269, 2013.

[9] D. V. Do, C. Forgez, K. El Kadri Benkara, and G. Friedrich, "Impedance observer for a Li-ion battery using Kalman filter," *IEEE Transactions on Vehicular Technology*, vol. 58, no. 8, pp. 3930–3937, 2009.

[10] X. Hu, F. Sun, and Y. Zou, "Online model identification of lithium-ion battery for electric vehicles," *J. Cent. South Univ. Technol.*, vol. 18, pp. 1525–1531, 2011.

[11] G. L. Plett, "Extended Kalman filtering for battery management systems of LiPB-based HEV battery packs - Part 3. State and parameter estimation," *Journal of Power Sources*, vol. 134, no. 2, pp. 277–292, 2004.

[12] C. Zou, A. G. Kallapur, C. Manzie, and D. Nesic, "PDE battery model simplification for SOC and SOH estimator design," *Proceedings of the IEEE Conference on Decision and Control*, vol. 54rd IEEE, no. Cdc, pp. 1328–1333, 2015.

[13] L. P. Mandal and R. W. Cox, "A transient-based approach for estimating the electrical parameters of a lithium-ion battery model," *2011 IEEE Energy Conversion Congress and Exposition*, pp. 2635–2640, 2011.

[14] P. J. van Bree, A. Veltman, W. H. A. Hendrix, and P. P. J. van den Bosch, "Prediction of battery behavior subject to high-rate partial state of charge," *IEEE Transactions on Vehicular Technology*, vol. 58, no. 2, pp. 588–595, 2009.

[15] D. Andre, A. Nuhic, T. Soczka-Guth, and D. U. Sauer, "Comparative study of a structured neural network and an extended Kalman filter for state of health determination of lithium-ion batteries in hybrid electricvehicles," *Engineering Applications of Artificial Intelligence*, vol. 26, no. 3, pp. 951–961, 2013.

[16] V. Klass, M. Behm, and G. Lindbergh, "A support vector machine-based state-of-health estimation method for lithium-ion batteries under electric vehicle operation," *Journal of Power Sources*, vol. 270, pp. 262–272, 2014.

[17] W. Waag, C. Fleischer, and D. U. Sauer, "Critical review of the methods for monitoring of lithium-ion batteries in electric and hybrid vehicles," *Journal of Power Sources*, vol. 258, pp. 321–339, 2014.

[18] K. J. Åström and B. Wittenmark, *Adaptive Control*. Dover Publication Inc, 2008.

[19] F. Gustafsson, *Adaptive Filtering and Change Detection*. John Wiley & Sons, Ltd, 2000.

[20] L. Ljung, *System Indentification - Theory for the User*, 2nd ed. Prentice Hall, 1999.

[21] R. E. Kalman, "A New Approach to Linear Filtering and Prediction Problems," *Journal of Basic Engineering*, vol. 82, no. 1, p. 35, 1960.

[22] G. Welch and G. Bishop, "An Introduction to the Kalman Filter," Ph.D. dissertation, University of North Carolina at Chapel Hill, 1995.

[23] R. Pintelon and J. Schoukens, *System Identification - A Frequency Domain Approach*, 2nd ed. Wiley IEEE Press, 2012.

[24] S. L. Shah and W. R. Cluett, "Recursive Least Suuares Based Estimation Schemes for self-Tuning Control," *Canadian Journal of Chemical Engineering*, vol. 69, no. 3, 1991.

[25] B. Stenlund and F. Gustafsson, "Avoiding windup in recursive parameter estimation," *Preprints of reglermöte 2002*, pp. 148–153, 2002.

[26] M. Evestedt and A. Medvedev, "Stationary behavior of an anti-windup scheme for recursive parameter estimation under lack of excitation," *Automatica*, vol. 42, pp. 151–157, 2006.

[27] A. J. Laub, *Matrix Analysis for Scientists and Engineers*. Siam, 2005.

[28] P. G. Kaminski, A. E. Bryson, and S. F. Schmidt, "Discrete Square Root Filtering: A Survey of Current Techniques," *IEEE Transactions on Automatic Control*, vol. 16, no. 6, pp. 727–736, 1971.

[29] A. Jossen, "Fundamentals of battery dynamics," *Journal of Power Sources*, vol. 154, no. 2, pp. 530–538, 2006.

Paper 4

Estimating power capability of aged lithium-ion batteries in presence of communication delays

Björn Fridholm, Torsten Wik, Hannes Kuusisto, and Anton Klintberg

Journal of Power Sources, 304, 2016

Comment: The layout of this paper has been reformatted in order to comply with the rest of the thesis.

Estimating power capability of aged lithium-ion batteries in presence of communication delays

Björn Fridholm, Torsten Wik, Hannes Kuusisto, and Anton Klintberg

Abstract

Efficient control of electrified powertrains requires accurate estimation of the power capability of the battery for the next few seconds into the future. When implemented in a vehicle, the power estimation is part of a control loop that may contain several networked controllers which introduces time delays that may jeopardize stability. In this article, we present and evaluate an adaptive power estimation method that robustly can handle uncertain health status and time delays. A theoretical analysis shows that stability of the closed loop system can be lost if the resistance of the model is under-estimated. Stability can, however, be restored by filtering the estimated power at the expense of slightly reduced bandwidth of the signal.

The adaptive algorithm is experimentally validated in lab tests using an aged lithium-ion cell subject to a high power load profile in temperatures from -20 to +25°C. The upper voltage limit was set to 4.15V and the lower voltage limit to 2.6V, where significant non-linearities are occurring and the validity of the model is limited. After an initial transient when the model parameters are adapted, the prediction accuracy is within ±2% of the actually available power.

Keywords: Adaptive estimation; lithium-ion; power capability; batterymanagement; time-delay systems; state of power.

1 Introduction

The energy management system (EMS) of a plug-in hybrid electric vehicle (PHEV) uses information about the power available from the electric system to optimize efficiency, performance, and driving experience [1, 2, 3]. To avoid premature ageing, the battery power must be limited by specifying

regions of safe use in terms of limits on voltage, current, and temperature. Power capability of the battery cannot be measured directly and the battery management system (BMS) must therefore estimate the power available for the next few seconds into the future [4]. This can be achieved using model-based techniques where the current–voltage characteristics are used to predict the voltage response to a given constant current. A major difficulty in this task is that the characteristics of the battery changes considerably with both operating conditions and age [5, 6, 7]. However, on-line parameter estimation techniques such as recursive least squares or Kalman filter can be used to maintain accuracy in the power estimation, by keeping the battery model updated over time.

State-of-power (SoP) can be divided into two separate parts; (i) predicting the maximum charge and discharge power that is available without violating constraints on voltage, current, etc., and (ii) limiting the power if the request of the vehicle exceeds the available power. A typical set-up in a vehicle application is shown if Fig. 1. The BMS measures current, voltage and temperature of the battery cells and estimates the maximum power that the battery pack can deliver. This is sent over the controller area network (CAN) to the EMS. The EMS collects power requests from all subsystems connected to the battery and communicates how much power each component may use. The consumers (here represented by the power controller) then actuates the power out-take from the battery. In the limiting case, closed-loop control of the power containing several networked controllers is formed. As will be shown later in this article, a combination of communication delays and uncertain model parameters may impact stability of the system. Similar observations are also presented in [8].

Adaptive power estimation has been analysed before, see for instance [9, 10] for two recent review articles on the subject of power prediction. In summary, different approaches have been considered, such as:

- Analytic expressions based on an equivalent circuit model (see e.g. [11, 12])
- Kalman filter based estimation (see [13, 14, 15])
- Particle filter based estimation (see [16])
- Neural networks (see [17])

This article extends the work in [11], where an analytical calculation of the battery SoP was presented. The method was analysed for stability and performance in simulations, and the main contributions in this article are (i) stability analysis of adaptive maximum (minimum) current estimation in the presence of parametric uncertainty and communication delays;

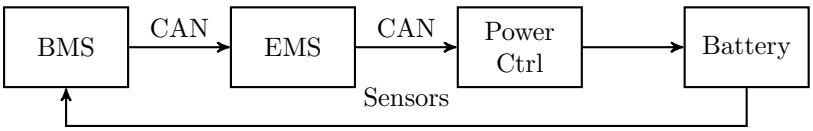

Figure 1: Typical controller configuration in vehicle application.

and (ii) experimental validation in battery lab using an aged cell in cold temperatures.

The article is structured as follows; in Section 3 the models and algorithms are introduced. Section 4 presents a robustness analysis together with an extension to the power limit algorithm that handles parameter uncertainty. In Section 5, a laboratory validation of the adaptive system is presented. Section 6 summarizes the results.

2 Nomenclature

In Table 1, the notation used in this article is listed.

3 Adaptive state-of-power algorithm

An adaptive state-of-power algorithm consists of three major parts, (i) a battery model, (ii) parameter estimator, and (iii) a prediction of the power that can be delivered or absorbed without violating battery constraints. This section presents these parts by reviewing some previous results.

3.1 Battery model

In battery estimation applications, equivalent circuit models are often used to predict voltage as a function of current (see e.g. [18, 5, 19]). The prediction horizons of interest for the SoP considered here are in the range of 1–5 seconds, which means that slower dynamics of the cell can be discarded. Here, a first-order equivalent circuit model, where the voltage v_1 models diffusion effects (see Fig. 2), is considered suitable for the purpose. In continuous time, the equivalent circuit model is described by

$$\dot{v}_1(t) = -\frac{1}{T}v_1(t) + \frac{1}{C}i(t) \tag{1}$$

$$v(t) = v_{\text{oc}}(z_{\text{soc}}(t)) + v_1(t) + R_0 i(t), \tag{2}$$

where z_{soc} is the state-of-charge, v_{ocv} is the open circuit voltage, $T = R_1 C$ is the time constant, and $\dot{v}_1 = dv_1/dt$. The parameters $R_0, R_1, C \in \mathbb{R}^+$ and

Table 1: Nomenclature

Symbol	Description
v	Cell voltage
i	Current
p	Power
v_1	Voltage over RC pair in equivalent circuit model
T	Time constant of RC pair in equivalent circuit model
C	Capacitance in equivalent circuit model
R_0, R_1	Resistances in equivalent circuit model
z_{soc}	State of charge
v_{oc}	Open circuit voltage function
y	Output in linear regression model
φ	Regression vector in linear regression model
θ	Parameter vector in linear regression model
e	Noise term
Δt	Prediction horizon of SoP algorithm
v_{lim}	Voltage limit used in SoP algorithm, either v_{max} or v_{min}
v_{max}	Upper voltage limit
v_{min}	Lower voltage limit
i_{lim}	Current limit used in SoP algorithm, either i_{max} or i_{min}
$i_{\text{lim,v}}$	Current limit based on voltage
$i_{\text{lim,c}}$	Fixed current limit
i_{max}	Maximum current
i_{min}	Minimum current (i.e. maximum discharge current)
Δv	Voltage margin from v to v_{lim}
I, V	Laplace transform of i and v respectively
K	Gain of SoP algorithm
G	Transfer function representation of equivalent circuit model
F, F_0	Transfer functions describing the SoP algorithm
τ	Time delay from CAN communication
SoC	State of charge
SoP	State of power
PHEV	Plug-in hybrid electric vehicle
BMS	Battery management system
EMS	Energy management system
CAN	Controller area network
OCV	Open circuit voltage

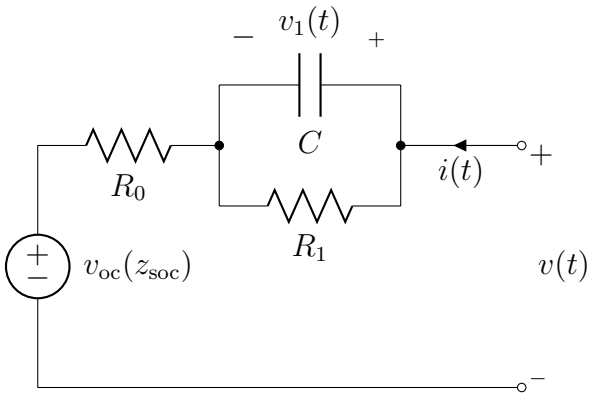

Figure 2: Equivalent circuit battery model.

variables $v, v_1, i \in \mathbb{R}$ are defined in Fig. 2. The sign convention is such that a positive current (power) charges the battery.

3.2 Recursive parameter estimation

Since the battery characteristics change significantly with both operating conditions and age, it is common to include some kind of parameter adaptation in the algorithms of the BMS. There are several alternatives to this, both in continuous time [12, 20], and in discrete time [21, 22, 23].

For parameter estimation, models are often formulated in regressor form, i.e.

$$y(t) = \varphi^T(t)\theta(t) + e(t),$$

where $y \in \mathbb{R}$ is the output, $\varphi \in \mathbb{R}^n$ is the regression vector, $\theta \in \mathbb{R}^n$ is the parameter vector, $e \in \mathbb{R}$ is a noise term, and n is the number of parameters. Given recorded data at discrete times t_k, $k = 1, \ldots, N$, the parameter vector θ can then be estimated using the least squares solution

$$\hat{\theta} = \left[\sum_{k=1}^{N} \varphi^T(t_k)\varphi(t_k)\right]^{-1} \sum_{i=k}^{N} \varphi^T(t_k)y(t_k).$$

Assuming that the OCV remains constant during the time-horizon considered, the battery model (1–2), can be described in regressor form by

$$\begin{aligned} y(t) &= \dot{v}(t) \\ \varphi^T(t) &= \left[v_{oc} - v(t), \quad \tfrac{di(t)}{dt}, \quad i(t)\right] \\ \theta^T &= \left[\tfrac{1}{T}, R_0, \tfrac{R_0+R_1}{T}\right]. \end{aligned}$$

For more details on how the above procedure can be implemented in a practical application, the reader is referred to [20, 22].

3.3 Power limit estimation

The power limit algorithm contains two parts, one for calculating the limiting current (i.e. the current that will drive the voltage to its limit at the end of the defined time horizon), and one for calculating the power. The algorithm was originally presented in [11], and only the main results are described here.

Limiting current

The polarization voltage (v_1) in Eq. (1) is a linear ordinary differential equation, which has the analytical solution

$$v_1(t) = e^{\frac{t_0-t}{T}} v_1(t_0) + \frac{1}{C}\int_{t_0}^{t} e^{\frac{\tau-t}{T}} i(\tau)d\tau.$$

Thus, if a constant current $i(t^+)$ is applied to the RC-circuit on the time interval $(t, t+\Delta t]$ we get an analytical expression for the future voltage:

$$v_1(t+\Delta t) = v_1(t)e^{-\frac{\Delta t}{T}} + R_1 i(t^+)(1-e^{-\frac{\Delta t}{T}}).$$

Assuming that the OCV is unchanged on this time interval, and that the constant (but yet unknown) limiting current $i_{\text{lim,v}}(t)$ is applied to the system on the time interval $(t, t+\Delta t]$, then by definition, the voltage at time $t+\Delta t$ will be

$$\begin{aligned} v_{\text{lim}} &= v_{\text{oc}} + R_0 i_{\text{lim,v}}(t) + v_1(t+\Delta t) \\ &= v_{\text{oc}} + R_0 i_{\text{lim,v}}(t) + v_1(t)e^{-\frac{\Delta t}{T}} + R_1 i_{\text{lim,v}}(t)(1-e^{-\frac{\Delta t}{T}}). \end{aligned}$$

Here it is worth noting that the current $i_{\text{lim,v}}$ is considered constant during the prediction horizon. However, a new calculation of $i_{\text{lim,v}}$ is done at each time step and for this reason it is given an explicit time dependency.

The margin between the measured voltage $v(t)$ and the limit voltage v_{lim} is:

$$\begin{aligned} \Delta v(t) &= v_{\text{lim}} - v(t) \\ &= R_0(i_{\text{lim,v}}(t) - i(t)) + v_1(t)(e^{-\frac{\Delta t}{T}} - 1) + \\ &\quad R_1 i_{\text{lim,v}}(t)(1-e^{-\frac{\Delta t}{T}}) \\ &= (R_0 + R_1 - R_1 e^{-\frac{\Delta t}{T}}) i_{\text{lim,v}}(t) - R_0 i(t) + \\ &\quad v_1(t)(e^{-\frac{\Delta t}{T}} - 1), \end{aligned}$$

where we have used the assumption that v_{oc} is constant during the prediction horizon. Solving this equation for the limiting current $i_{\text{lim,v}}(t)$, we get:

$$i_{\text{lim,v}}(t) = \frac{\Delta v(t) + \hat{R}_0 i(t) + \hat{v}_1(t)(1 - e^{-\frac{\Delta t}{\hat{T}}})}{\hat{R}_0 + \hat{R}_1(1 - e^{-\frac{\Delta t}{\hat{T}}})}, \tag{3}$$

where the notation $\hat{(\cdot)}$ was introduced to stress that these parameters and states are not available as measurements, but are estimated. Note also that the limitation pair (v_{lim}, $i_{\text{lim,v}}$) will appear once for charging (v_{max}, $i_{\text{max,v}}$) and once for discharging (v_{min}, $i_{\text{min,v}}$).

In addition to the voltage based limits on current, there are normally also system dependent constraints on the current ($i_{\text{lim,c}}$) that must not be violated[1]. As a consequence, the final limit will be $i_{\text{max}}(t) = \min(i_{\text{max,c}}, i_{\text{max,v}}(t))$ for charging and $i_{\text{min}}(t) = \max(i_{\text{min,c}}, i_{\text{min,v}}(t))$ for discharging.

Predicted maximum power

In a vehicle application it is the power rather than the current that is of interest, and hence also what is limited. To calculate the power, predicted voltage at time $t+\Delta t$ given the constant current $i_{\text{lim}}(t)$ during the prediction horizon is used. Note that this will be a conservative estimate for the discharge case since the actual voltage will be higher than v_{lim} for most of the pulse.

The voltage at time $t + \Delta t$ can be estimated as previously by

$$\hat{v}(t + \Delta t) = v_{\text{oc}} + \hat{R}_0 i_{\text{lim}}(t) + \hat{v}_1(t) e^{-\frac{\Delta t}{\hat{T}}} + \hat{R}_1 i_{\text{lim}}(t)(1 - e^{-\frac{\Delta t}{\hat{T}}}).$$

If the OCV is unavailable or uncertain, a similar approach as for the calculation of $i_{\text{lim,v}}(t)$ can be used, i.e.

$$\begin{aligned}\hat{v}(t + \Delta t) = v(t) + \hat{R}_0(i_{\text{lim}}(t) - i(t)) + \hat{v}_1(t)(e^{-\frac{\Delta t}{\hat{T}}} - 1) + \\ \hat{R}_1 i_{\text{lim}}(t)(1 - e^{-\frac{\Delta t}{\hat{T}}}).\end{aligned}$$

The reader can verify that inserting the current from (3) will indeed give $\hat{v}(t + \Delta t) = v_{\text{lim}}$.

Finally, the power limit is calculated as

$$p_{\text{lim}}(t) = \hat{v}(t + \Delta t) i_{\text{lim}}(t). \tag{4}$$

[1]It should also be mentioned that additional limitations from battery SoC and temperature are sometimes included in the current limitation, but they were not considered in this work.

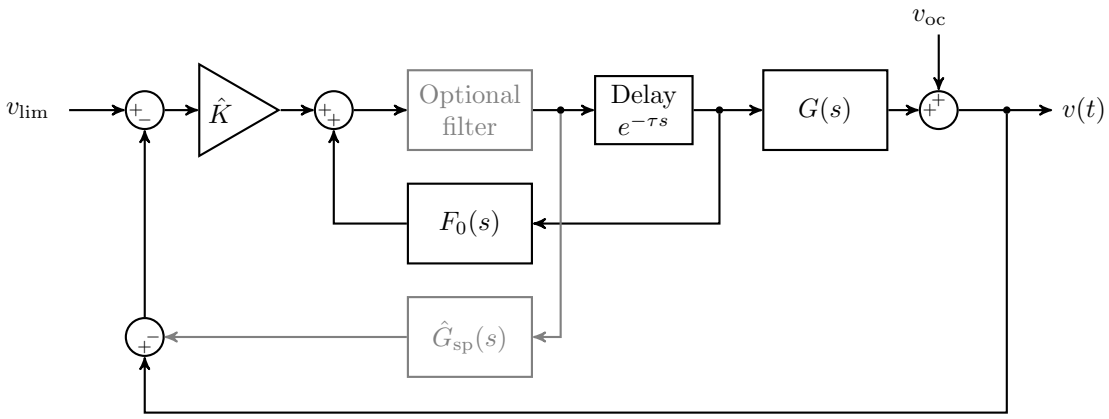

Figure 3: Feedback system where the power is limited by the BMS. Time delay on CAN is represented by the Delay block. Optional blocks to improve robustness are marked in grey.

4 Robustness analysis

The power actuated in the vehicle will be limited by the power from Eq. (4). Assuming that the requested power exceeds this limit, the algorithm acts as a closed-loop system controlling the voltage to v_{lim}. In [11] the stability of this closed loop system was examined. The result was that, assuming correct model description, the closed loop system is always stable. In this work we extend the analysis by relaxing the assumptions of correct model to allow parametric errors (since the parameters are estimated) and we also examine the impact of communication delays.

4.1 Feedback system

It should be noted that the true system is nonlinear due to power being the communicated signal. However, assuming that we are close to the voltage limit v_{lim}, and that the actuation from battery power to current is fast, the system can be approximated by the linear version in Fig. 3, where we have also included two block in grey that will be described shortly.

To derive the transfer functions in Fig. 3, start from the limitation on

current in Eq. (3) that in the Laplace domain can be rewritten as

$$\begin{aligned} I_{\text{lim}}(s) &= \hat{K}\left(\Delta V(s) + \hat{R}_0 I(s) + \frac{\hat{R}_1(1-e^{-\Delta t/\hat{T}})}{1+\hat{T}s} I(s)\right) \\ &= \hat{K}\Delta V(s) + \frac{1+\hat{K}\hat{R}_0\hat{T}s}{1+\hat{T}s} I(s) \\ &\triangleq \hat{K}\Delta V(s) + F_0(s)I(s), \end{aligned}$$

where s is the Laplace variable, $I(s) = \mathcal{L}\{i(t)\}$, $I_{\text{lim}}(s) = \mathcal{L}\{i_{\text{lim}}(t)\}$, $\Delta V(s) = \mathcal{L}\{\Delta v(t)\}$, and

$$\hat{K} = \frac{1}{\hat{R}_0 + \hat{R}_1(1-e^{-\frac{\Delta t}{\hat{T}}})}.$$

Noting that $i(t) = i_{\text{lim}}(t-\tau)$, which in the Laplace domain corresponds to $I(s) = e^{-\tau s} I_{\text{lim}}(s)$, the transfer function $F(s)$ from $\Delta V(s)$ to $I(s)$ is

$$F(s) = \frac{\hat{K}e^{-\tau s}}{1 - F_0(s)e^{-\tau s}}.$$

Deriving a transfer function for the battery model, i.e. Eq. (1–2) is not possible due to the nonlinear function v_{oc}. However, v_{oc} changes slowly compared to the system dynamics and it can thus be regarded as a low frequent load disturbance. This means that it will not impact the stability analysis and, for this purpose, the battery model can therefore be written as

$$G(s) = R_0 + \frac{R_1}{1+Ts}.$$

4.2 Stability under uncertainty

The stability properties of the closed loop system are determined by the loop gain $L(j\omega) = F(j\omega)G(j\omega)$. Sensitivity analysis based on parameter perturbations identified that under-estimation of R_0 have the greatest impact on closed loop stability. For this reason, using the parameters of Tab. 2, the Nyquist and Bode diagrams are plotted for two different cases (i) the parameters of F are correct, and (ii) R_0 is under-estimated ($\hat{R}_0 = 0.4R_0$). The results are presented as dashed lines in Fig. 4.

Under the assumption that the model and parameters are correct, the system is stable, however, with under-estimated R_0 the system becomes unstable. The limit according to the theoretical analysis is just below $\hat{R}_0 < 0.5R_0$. It should be noted that this bound will most probably be optimistic since the equivalent circuit model is a simplification of the true battery, and thus, for a real application instability may occur even if $\hat{R}_0 > 0.5R_0$.

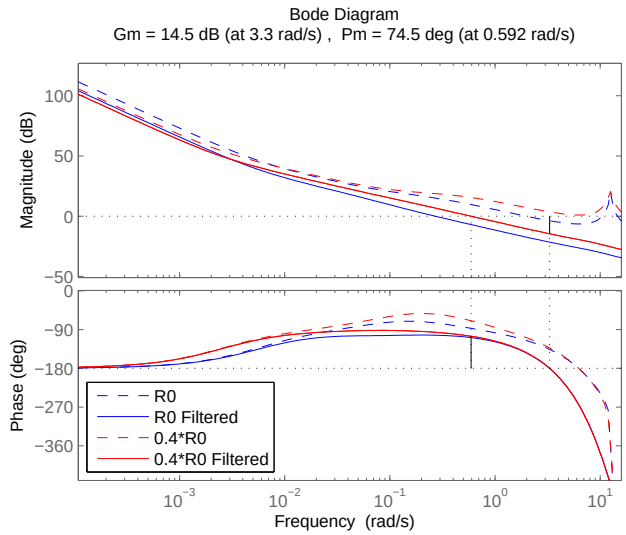

(a)

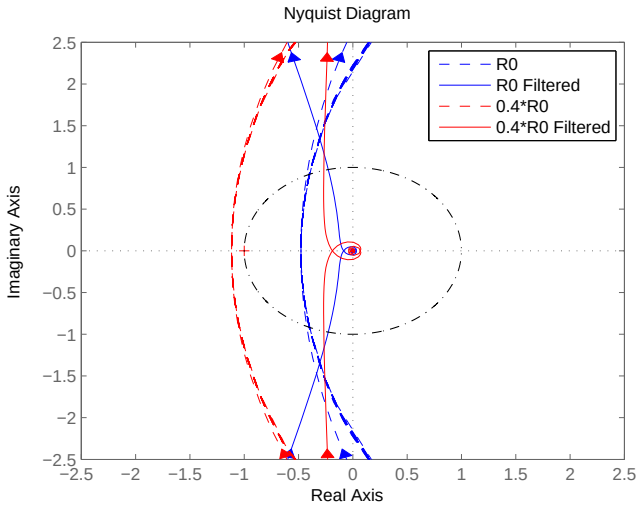

(b)

Figure 4: (a) Bode, and (b) Nyquist diagrams for the loop gain of the closed loop system in presence of delay. Depending on accuracy of $\hat{R}_0$ estimation at limit, the system may become unstable. Dashed lines are for system without filter and solid lines are with the filter proposed in Section 4.3.

Table 2: Settings used in the stability analysis.

Prediction horizon	Δt	2 s
Time delay	τ	0.5 s
Battery model	R_0	1 mΩ
	R_1	1 mΩ
	T	20 s
LP filter	a	3

4.3 Improving robustness

To improve the robustness of the system, several alternative solutions were considered, as described below. The method finally chosen for implementation was to use the low-pass filter. The motivation behind this choice was the simplicity of implementation and the effectiveness to remove the unwanted behaviour.

Low-pass filter of power limit

The chosen method used in the laboratory tests was to introduce a first order low-pass filter to the predicted power (see grey block in Fig. 3). The transfer function is

$$F_{\text{lp}} = \frac{1}{1+as}.$$

From a stability perspective, this is not the obvious choice since it introduces an additional negative phase shift up to 90°. However, the reduced bandwidth stabilizes the system. The effect of the low-pass filter can be seen as solid lines in Fig. 4. We can see that the system is successfully stabilized also in the case of under-estimated R_0.

Lead-lag compensator

Time-delays only affect the phase of the system. In automatic control it is common to use lead-lag filters to affect the phase characteristics. The transfer function of the lead-lag filter can be described by

$$F_{ll}(s) = \frac{1+k_1\tau_1 s}{1+\tau_1 s}\frac{1+k_2\tau_2 s}{1+\tau_2 s},$$

where $k_1 > 1$, $0 < k_2 < 1$ and $\tau_1 < \tau_2$. For this application, one lead filter followed by dual lag filters were needed to achieve the desired effect. This was significantly more complex than the low-pass filter previously described. It did, however, have less effect on system bandwidth and should that be important for the application, the lead-lag filter could be a better solution.

Smith predictor

Another common technique for handling time delays is to use a so called "Smith predictor" where a model of the system is used to compensate for the time delay. In this application, the standard solution is a feedback of the current before the communication delay trough the transfer function

$$\hat{G}_{\text{sp}}(s) = (1 - e^{-\tau s})\hat{G}(s),$$

as the grey block in Fig. 3. For this application, the Smith predictor had problems to handle the combination of battery model inaccuracies, estimated parameters, and uncertain time delays, sometimes causing severely degraded performance of the power limits. For this reason it was not considered a good solution here. For more information on Smith predictor the reader is referred to [24, 25].

Separate control law for feedback case

It is of course also possible to switch from one structure for the power prediction case to another function for controlling the voltage to v_{lim} when the requested power is limited. This would require some form of bumpless transfer between prediction and limitation. There is also the matter of actually identifying when the power is limited if the time delay is not known exactly.

5 Experimental validation

The proposed algorithm was evaluated at Volvo Cars battery testing facilities using a rapid prototyping environment that mimics the system in Fig. 3. The tests were performed on an aged NMC lithium-ion cell with approximately 90% capacity retention. The cell is intended for use in plug-in HEV applications.

5.1 Rapid prototyping environment

The rapid prototyping environment (see Fig. 5(a)) is based around a dSpace hardware-in-the-loop (HIL) rig running the adaptive power limit algorithm. Configurable time delays are used to model the CAN communication and the inputs to the algorithm are measured by sensors used in the Volvo XC90 T8 Twin Engine vehicles. The power is then actuated by a Bitrode battery cell cycler, and the cell is in a climatic test chamber where the ambient temperature can be varied. Forced cooling of the cell provided by fans is

Table 3: Settings used in the validation. Note: current direction is positive for charging.

Prediction horizon	Δt	2 s
Maximum voltage	$v_{\max}$	4.15 V
Minimum voltage	$v_{\min}$	2.6 V
Maximum current	$i_{\max,c}$	100 A
Minimum current	$i_{\min,c}$	-250 A
Time delay	τ	0.5 s

used to keep its surface temperature close to the chamber temperature also when subjected to high charge and discharge power.

Test cycle

The test cycle used to represent the driver request is based on the standard drive cycles Hyzem and US06. The battery starts at approximately 80% SoC and is then depleted using a repeated Hyzem rural cycle down to approximately 20% followed by a charge sustain part using the US06 cycle (see Fig. 5(b)). The overall power profile is highly dynamic, causing significant polarization of the cell. Total test time is 2800 seconds. Based on this cycle two tests are performed, one to evaluate the prediction accuracy of the algorithm and one for the adaptation to the voltage limit.

5.2 Closed loop stability

Before evaluating system accuracy, robustness to parameter uncertainties was examined by intentionally adding a bias to the estimate of R_0. As the results of the theoretical analysis predicted, the algorithm becomes unstable without the proposed filter, see Fig. 6(a). In the tests, $\hat{R}_0$ was approximately $0.8R_0$ as estimated without bias. The power limit when the request exceeds the available power, exhibit serious oscillations in the power. The filter successfully removed the oscillation just as expected from the theoretical analysis (Fig. 6(b)). Since R_0 is under-estimated we can observe significant under voltage in this case. For results with unbiased R_0, see Section 5.4.

5.3 Power prediction

The purpose of this test was to investigate the predictive ability of the algorithm. The test cycle in Fig. 5(b) was run for +25, +10, 0, −10, and −20°C. At irregular intervals the maximum (minimum) power predicted by the algorithms was actuated for $\Delta t = 2$s. In order to evaluate the accuracy,

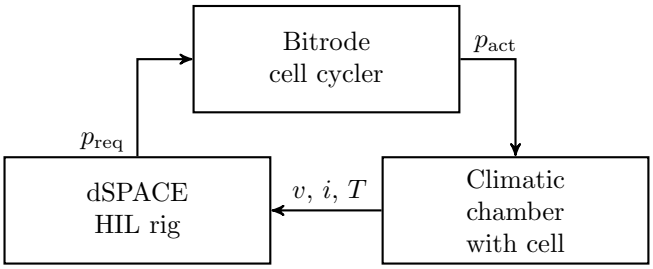

(a) Schematics of experimental setup with HIL rig, cell cycler and climatic chamber with cell. The signal flow is such that the HIL rig sends out a power request that the cell cycler actuates. The resulting cell voltage, current and temperature are measured using sensors that could typically be used in on-board BMS application and fed back to the HIL rig.

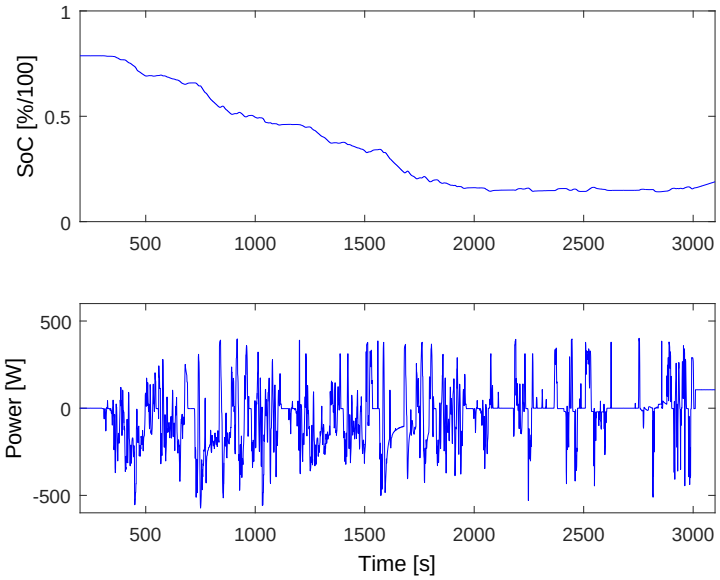

(b) Test cycle used in the evalutation based on the standard drive cycles Hyzem rural and US06.

Figure 5: Test setup in battery lab.

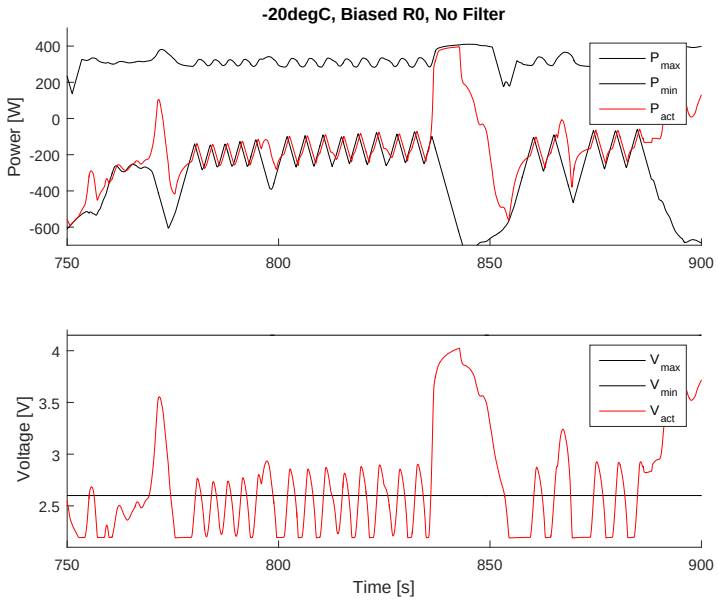

(a)

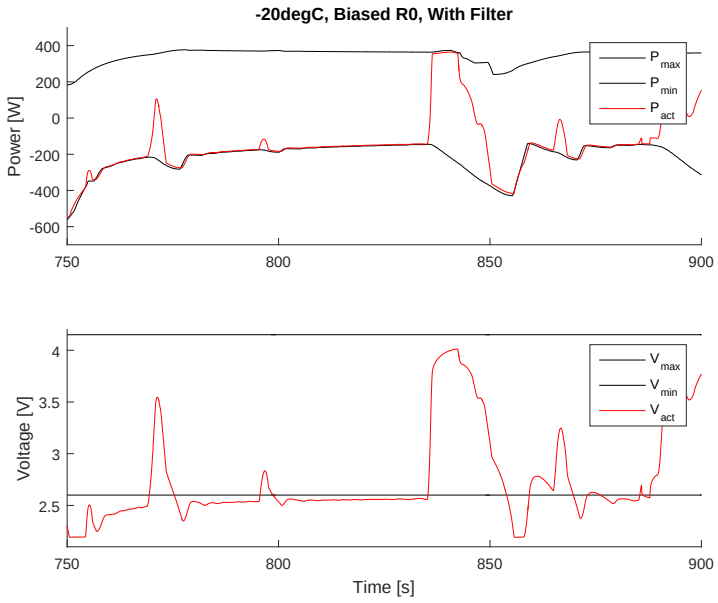

(b)

Figure 6: Test with under estimated R_0 (a) without and (b) with the proposed filter on power.

the limitation at v_{lim} was inactive during this test, thus allowing the voltage to go outside of the range v_{min} – v_{max} if the power was over-estimated. Note that the pulses occur at slightly different SoC levels for the different temperatures. This is because of charging constraints over temperature and also that the power and energy of the test pulses are different.

Depending on the limiting factor (current or voltage), the margin to the limit after prediction horizon was recorded and documented in Table 4. The measures used in the table are

$$\Delta V = \begin{cases} v(t) - v_{\text{max}} & \text{Charging} \\ v_{\text{min}} - v(t) & \text{Discharging} \end{cases}$$

$$\Delta I = \begin{cases} i(t) - i_{\text{max}} & \text{Charging} \\ i_{\text{min}} - i(t) & \text{Discharging} \end{cases}$$

which means that a negative value always relate to under-estimated power and vice versa.

The overall results are within ±2% of the actually available power, which is good considering the extreme use case with high power for an aged cell at cold temperatures. In the first pulse of the test the prediction is rather poor because the parameters are still adapting (see Fig. 7 for an example of the parameter adaptation). Also, the accuracy of the equivalent circuit model is sometimes poor in the tested cases, typically when significant polarization is built up in the cell after repeated pulses. The accuracy then degrades due to the inability of the equivalent circuit model to predict voltage, see e.g. pulse 11 and 12 in Table 4. Pulse 9 of the test in +10°C occurs just after a heavy discharge of the cell and the power is then under-estimated due to the filter described in Section 4.3.

5.4 Adaptation to voltage limit

To validate the behaviour of the algorithms when the power request exceeds the available power, the same test cycle as before was used, but with the modification that the predicted available power was actuated for 15s. This time the limitation was not overridden and instead it was examined how the power was ramped down to keep the voltage within the allowed limits. In Fig. 8, a zoom of one of the pulses at −20°C is shown. The behaviour is typical for the application when a time delay is present. First a small undershoot in the order of 10mV occurs at around 6915s but it quickly recovers and converges to v_{lim}. Note that none of the stability issues described in Section 5.2 were present in the tests.

Table 4: Test results for power prediction. It will be either voltage or current that limits the power. In the table '–' is reported for the signal that was not limiting, '*' is used for pulses that was not actuated due to battery power already being limited. 'C' is charge and 'D' is discharge. Positive sign is used if power was over-estimated and negative is used for under-estimation (this applies to both charge and discharge cases).

Pulse	Nr	1	2	3	4	5	6	7	8	9	10	11	12	13
Time	s	449	559	866	1032	1200	1341	1506	1559	1731	2185	2247	2816	2955
Type	-	D	C	D	D	C	D	C	C	D	C	D	D	C
+25°C														
SoC	%	89	85	69	66	64	57	53	54	40	28	28	22	22
ΔV	V	–	0.0	–	–	–	–	–	–	–	–	–	–	–
ΔI	A	-2	–	-2	-4	-1	-3	-1	-1	+4	-1.5	-1	+0.5	-2
+10°C														
SoC	%	85	82	64	62	59	51	47	49	33	21	22	22	22
ΔV	V	–	-0.01	–	–	–	–	–	–	-0.1	–	+0.02	–	–
ΔI	A	-5	–	+4	-3	0	+3	-1.5	-1	–	-1.5	–	-0.5	-1.5
0°C														
SoC	%	80	77	60	57	53	46	42	42	28	19	19	18	20
ΔV	V	–	+0.01	-0.08	–	–	-0.04	–	–	-0.05	–	–	–	–
ΔI	A	-20	–	–	-15	-2	–	-4	-2	–	-3	-7	-3	-3
−10°C														
SoC	%	75	71	52	49	46	38	34	35	24	23	23	23	24
ΔV	V	-0.3	+0.01	+0.05	-0.05	–	+0.1	–	–	*	–	+0.15	-0.02	–
ΔI	A	–	–	–	–	-1	–	-5	-1	*	-2	–	–	-3
−20°C														
SoC	%	75	71	54	50	49	41	37	38	31	25	25	23	24
ΔV	V	-0.2	+0.05	+0.02	-0.12	-0.05	0.0	–	–	*	–	+0.35	+0.3	-0.07
ΔI	A	–	–	–	–	–	–	-4	-3	*	-10	–	–	–

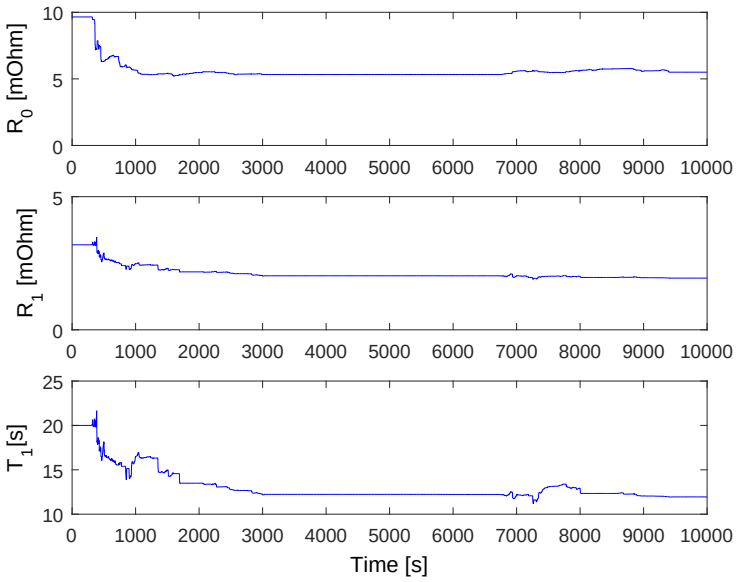

Figure 7: Parameter adaptation for test in −20°C.

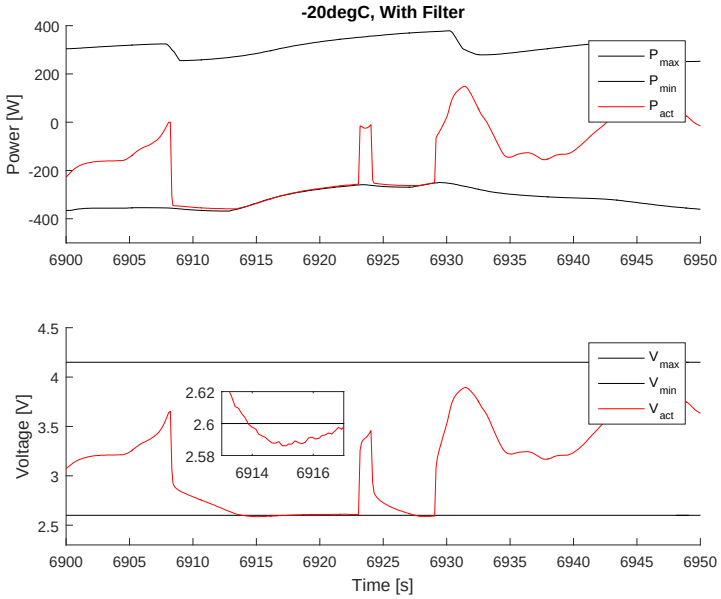

Figure 8: Example of voltage adaptation to $v_{\min}$ in test in $-20°$C.

6 Conclusions and future work

An adaptive power estimation algorithm was implemented, analysed and tested to evaluate its suitability for on-line implementation on a vehicle battery management system. The algorithm was designed to handle changed battery characteristics and also time delays caused by network control of vehicle power distribution.

The algorithm performs as expected in laboratory tests and estimation accuracy is normally within 2% of the actually available power. However, there are occasional outliers when parameters are not fully adapted and for discharge cases at low state-of-charge.

Focus of this work was on short term power estimation (i.e. 1-5 seconds prediction horizon). The algorithm was also tested for longer prediction horizons (up to 30 seconds). For that task, significantly degraded performance was noted. The indication is that this is due to poor model validity for long, high power pulses in cold temperatures. Further work is needed to improve the algorithm also for long term power estimation.

7 Acknowledgements

This work was supported by Volvo Cars and Chalmers, and financed by the Swedish Energy Agency through the project "Life-long battery control".

References

[1] S. J. Moura, J. L. Stein, and H. K. Fathy, "Battery-Health Conscious Power Management in Plug-In Hybrid Electric Vehicles via Electrochemical Modeling and Stochastic Control," *IEEE Transactions on Control Systems Technology*, vol. 21, no. 3, pp. 679–694, 2013.

[2] E. Kim, J. Lee, and K. G. Shin, "Real-time prediction of battery power requirements for electric vehicles," in *2013 ACM/IEEE International Conference on Cyber-Physical Systems, ICCPS 2013*, 2013, pp. 11–20.

[3] J. L. Mathieu and J. A. Taylor, "Controlling nonlinear batteries for power systems: Trading off performance and battery life," *2016 Power Systems Computation Conference (PSCC)*, pp. 1–7, 2016.

[4] L. Lu, X. Han, J. Li, J. Hua, and M. Ouyang, "A review on the key issues for lithium-ion battery management in electric vehicles," *Journal of Power Sources*, vol. 226, pp. 272–288, 2013.

[5] J. Jaguemont, L. Boulon, and Y. Dube, "Characterization and Modeling of a Hybrid-Electric-Vehicle Lithium-Ion Battery Pack at Low Temperatures," *IEEE Transactions on Vehicular Technology*, vol. 65, no. 1, pp. 1–14, 2015.

[6] A. Jossen, "Fundamentals of battery dynamics," *Journal of Power Sources*, vol. 154, no. 2, pp. 530–538, 2006.

[7] Y. Ji, Y. Zhang, and C.-Y. Wang, "Li-Ion Cell Operation at Low Temperatures," *Journal of the Electrochemical Society*, vol. 160, no. 4, pp. A636–A649, 2013.

[8] Z. Jin, Z. Zhang, and P. Wyatt, "Integrating Feedback Control Algorithms with the Lithium- Ion Battery Model to Improve the Robustness of Real Time Power Limit Estimation," in *SAE Technical Paper*, vol. 2017-01, no. 1206, 2017.

[9] A. Farmann and D. Uwe, "Review article A comprehensive review of on-board State-of-Available-Power prediction techniques for lithium-ion batteries in electric vehicles," *Journal of Power Sources*, vol. 329, pp. 123–137, 2016.

[10] M. U. Cuma and T. Koroglu, "A comprehensive review on estimation strategies used in hybrid and battery electric vehicles," *Renewable and Sustainable Energy Reviews*, vol. 42, pp. 517–531, 2015.

[11] T. Wik, B. Fridholm, and H. Kuusisto, "Implementation and robustness of an analytically based battery state of power," *Journal of Power Sources*, vol. 287, pp. 448–457, 2015.

[12] T. Feng, L. Yang, X. Zhao, H. Zhang, and J. Qiang, "Online identification of lithium-ion battery parameters based on an improved equivalent-circuit model and its implementation on battery state-of-power prediction," *Journal of Power Sources*, vol. 281, pp. 192–203, 2015.

[13] F. Sun, R. Xiong, and H. He, "Estimation of state-of-charge and state-of-power capability of lithium-ion battery considering varying health conditions," *Journal of Power Sources*, vol. 259, pp. 166–176, 2014.

[14] W. Zhang, W. Shi, and Z. Ma, "Adaptive unscented Kalman filter based state of energy and power capability estimation approach for lithium-ion battery," *Journal of Power Sources*, vol. 289, pp. 50–62, 2015.

[15] R. Xiong, F. Sun, H. He, and T. D. Nguyen, "A data-driven adaptive state of charge and power capability joint estimator of lithium-ion polymer battery used in electric vehicles," *Energy*, vol. 63, pp. 295–308, 2013.

[16] C. Burgos-Mellado, M. E. Orchard, M. Kazerani, R. Cárdenas, and D. Sáez, "Particle-filtering-based estimation of maximum available power state in Lithium-Ion batteries," *Applied Energy*, vol. 161, pp. 349–363, 2016.

[17] C. Fleischer, W. Waag, Z. Bai, and D. Uwe, "On-line self-learning time forward voltage prognosis for lithium-ion batteries using adaptive neuro-fuzzy inference system," *Journal of Power Sources*, vol. 243, pp. 728–749, 2013.

[18] X. Hu, S. Li, and H. Peng, "A comparative study of equivalent circuit models for Li-ion batteries," *Journal of Power Sources*, vol. 198, pp. 359–367, 2012.

[19] S. Nejad, D. T. Gladwin, and D. A. Stone, "A systematic review of lumped-parameter equivalent circuit models for real-time estimation of lithium-ion battery states," *Journal of Power Sources*, vol. 316, pp. 183–196, 2016.

[20] B. Xia, X. Zhao, R. de Callafon, H. Garnier, T. Nguyen, and C. Mi, "Accurate Lithium-ion battery parameter estimation with continuous-time system identification methods," *Applied Energy*, vol. 179, pp. 426–436, 2016.

[21] W. Waag, C. Fleischer, and D. U. Sauer, "On-line estimation of lithium-ion battery impedance parameters using a novel varied-parameters approach," *Journal of Power Sources*, vol. 237, pp. 260–269, 2013.

[22] B. Fridholm, T. Wik, and M. Nilsson, "Robust recursive impedance estimation for automotive lithium-ion batteries," *Journal of Power Sources*, vol. 304, pp. 33–41, 2016.

[23] H. Wu, S. Yuan, X. Zhang, C. Yin, and X. Ma, "Model parameter estimation approach based on incremental analysis for lithium-ion batteries without using open circuit voltage," *Journal of Power Sources*, vol. 287, pp. 108–118, 2015.

[24] L. Dongkwon, "Robust PID tuning for Smith predictor in the presence of model uncertainty," *Journal of Process Control*, vol. 9, no. 1, pp. 79–85, 1999.

[25] W. Zhang, Y. Sun, and X. Xu, "Two Degree-of-Freedom Smith Predictor for Processes with Time Delay," *Automatica*, vol. 34, no. 10, pp. 1279–1282(4), 1998.

Paper 5

Long-term voltage prediction for lithium-ion batteries using an extended equivalent circuit model and moving horizon estimation

Björn Fridholm, Torsten Wik, Changfu Zou, and Anton Klintberg

Submitted for publication in Journal of Power Sources

Comment: The layout of this paper has been reformatted in order to comply with the rest of the thesis

Long-term voltage prediction for lithium-ion batteries using an extended equivalent circuit model and moving horizon estimation

Björn Fridholm, Torsten Wik, Changfu Zou, and Anton Klintberg

Abstract

Equivalent circuit models are commonly used for predicting the current–voltage response in algorithms for battery management. One example is prediction of power capability where a voltage model can be used to estimate the maximum allowed power for different time-horizons into the future. For long prediction horizons (e.g. 30s or more) the battery characteristics may, however, change considerably. This is in particular a problem for high discharge power in cold temperatures and can then result in significant prediction errors. In this article an extended equivalent circuit model is proposed, where states related to local state-of-charge (concentration) on the particle surface are added. The voltage prediction accuracy is improved compared to the regular equivalent circuit model, which is demonstrated on laboratory data collected in temperatures ranging from −20 to +25°C.

Keywords: Adaptive estimation; power capability; battery management; state of power; battery modelling; moving horizon estimation.

1 Introduction

Algorithms for predicting power capability of batteries often use equivalent circuit models to relate current and voltage constraints (see e.g. [1, 2, 3]). As an example, the model can be used to calculate the voltage response to a known maximum current, and similarly to calculate the current that would cause the voltage to reach a predefined limit. To deliver consistent behaviour of the electric vehicle, it is often the power that can be provided during some time into the future that is sought, rather than the instantaneous power, and then the voltage response must be predicted. The accuracy of power prediction is thus directly related to the accuracy of the voltage prediction.

When a short-term prediction of the voltage response is sufficient (typically less than 5s), a first or second order equivalent circuit model (ECM) can be used [4, 5, 6]. With constant parameters the ECM is, however, only valid for a limited operating window (charge level, temperature, age, etc.). To extend the accuracy to a wider operating range the ECM can be improved by estimating its parameters online [7]. Parameter adaptation inevitably relies on the assumption that the parameter variations are slow in comparison to both the system dynamics and the prediction horizons of interest. If the characteristics change too fast, the adaptation will not be able to track the changes and the recent past is not representative for predicting the near-term future. In some cases, such as low state-of-charge (SOC) or low temperature operation, the battery behaviour as described by a traditional ECM changes considerably. The ECM can then produce significant errors as illustrated in Figure 1, where the assumption of slowly time-varying parameters is violated at around 1600s. The failure to capture this voltage-drop will limit the models applicability for estimation tasks. The consequences may be that SOC is under-estimated, while the power capability is over-estimated.

An alternative to online estimation of the parameters is to use parameter-varying techniques such as gain-scheduling, where the parameters are varied w.r.t. scheduling parameters, e.g. SOC, temperature, and current (see e.g. [8, 9, 10]). By visual inspection of the error in Figure 1, it seems reasonable to assume that the observed behaviour cannot be captured by scheduling the parameters this way. Temperature and SOC remains relatively constant for the considered time-horizon, while the response to current is very different at e.g. 1570s compared to 1620s. To improve the voltage prediction, a new or improved model is needed.

Ouyang et al. [11] captured the voltage drop in low SOC ranges by introducing additional states to the ECM related to electrode surface concentration. Similar effects of low surface concentration were noted by [12] in operation at high power and low temperatures. Then slow diffusion dynamics lead to low local concentrations even in cases when the bulk SOC was not particularly low. In this article, results from [11] and [12] are combined to form an extended equivalent circuit model for improved voltage prediction.

Voltage prediction online requires correct model parameters and initial state. In the battery example, neither of those are directly measurable, and it is therefore common to use an observer to estimate them. There are several algorithms available for this task, and in the battery research field different types of Kalman filters [13, 14, 15] and moving horizon estimation (MHE) [16, 17, 18] have been proposed.

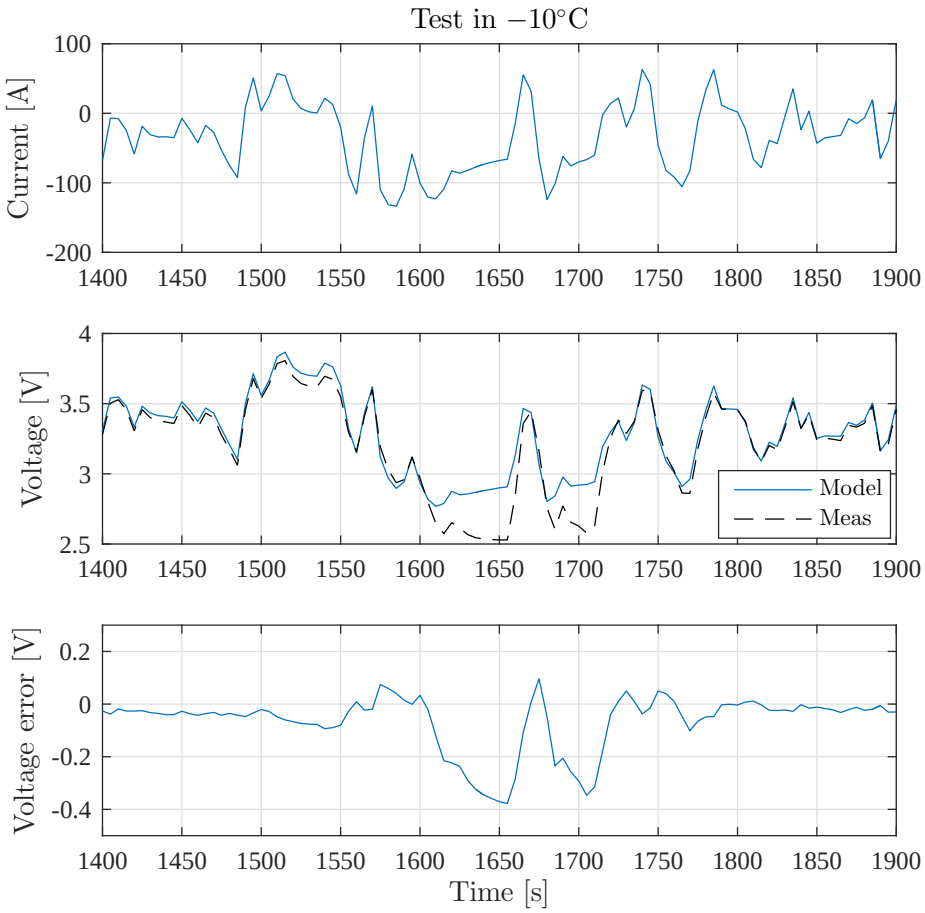

Figure 1: Example of simulation result of a first order RC equivalent circuit model tuned to a lithium-ion cell. For the major part of the test, the model produces accurate voltage predictions, but for extended high power discharge pulses between 1600–1720s the prediction is far off. If this voltage model is used for power prediction, the available power will be significantly over-estimated, which in a vehicle application can impact driveability.

The contributions of the article are:

- An extended ECM for low temperature, high discharge power cases inspired by [11] and [12].
- A formulation and evaluation of MHE for online estimation of parameters and states of the extended ECM.
- A validation of voltage prediction accuracy on laboratory data in a wide temperature range.

The rest of this article is structured such that Section 2 presents the extended ECM. Section 3 describes the parameter and state estimation. In Section 4 the accuracy of the voltage prediction is evaluated on laboratory battery cell data. Section 5 concludes the article by summarizing the findings and proposing future work.

2 Extended equivalent circuit model

The aim of this section is to derive a "grey-box" model structure to handle the observed current–voltage response for low temperatures. For this purpose, a comparison between physics based single particle models and ECMs is used to motivate an extended ECM.

Remark. The model uses insights from electrochemistry, but the intention is not to give a detailed description of the internal dynamics of a battery.

2.1 Generic model structure

There are several models used throughout this article. To enhance readability of the upcoming algorithms, a generic nonlinear state-space model in discrete time is used, according to

$$x_{k+1} = f(x_k, u_k, \theta_k) \tag{1}$$
$$y_k = h(x_k, u_k, \theta_k), \tag{2}$$

where $x \in \mathbf{R}^{n_x}$ are the internal states, $u \in \mathbf{R}$ is the input (current), $y \in \mathbf{R}$ is the output (terminal voltage), and $\theta \in \mathbf{R}^{n_\theta}$ are the parameters.

Remark. The parameters will normally be considered constant and then the time index k is excluded.

2.2 Single particle model

Most electrochemical models of lithium-ion batteries stems from the model proposed in [19]. By imposing a series of assumptions, this non-linear model based on partial-differential equations can be simplified to a system of non-linear differential-algebraic equations called a single particle model (SPM). SPMs use only one particle for each electrode, and depending on the assumptions and methods used for the simplification, the resulting model becomes slightly different (see e.g. [20, 21, 22]). For the purpose of this article, we will only consider the description of the terminal voltage, and then all the models are conceptually similar. Discarding electrolyte dynamics, the terminal voltage depends on surface concentration, over-potentials, and an ohmic drop, i.e.

$$v(t) = U_p(c_p^{(s)}(t)) - U_n(c_n^{(s)}(t)) + \eta_p(t) - \eta_n(t) + R_0 i(t),$$

where $c_p^{(s)}$ and $c_n^{(s)}$ are the surface concentrations in the positive (p) and negative (n) electrodes, $U_p, U_n : \mathbf{R} \to \mathbf{R}$ are nonlinear material dependent functions that maps the surface concentrations to potentials, η_p and η_n are over potentials, and R_0 is a lumped resistive term.

2.3 Equivalent circuit model

In equivalent circuit models (ECM) electrical circuit elements are used to mimic the current–voltage response of the battery cell. In discrete time the ECM can be described by

$$\begin{aligned}
v_1(k+1) &= \alpha_1 v_1(k) + \beta_1 i(k) \\
&\vdots \\
v_{n_v}(k+1) &= \alpha_{n_v} v_{n_v}(k) + \beta_{n_v} i(k) \\
z(k+1) &= z(k) + \Delta t Q_{\text{nom}}^{-1} i(k) \\
v_{\text{ecm}}(k) &= h_{\text{ocv}}(z(k)) + \sum_{j=1}^{n_v} v_j(k) + R_0 i(k),
\end{aligned}$$

where z is the SOC related to the average (bulk) concentration of lithium in solid phase, $h_{\text{ocv}} : \mathbf{R} \to \mathbf{R}$ is a nonlinear function that maps z to open circuit voltage (see Figure 2), v_j are polarization voltages describing diffusion dynamics, Δt is the sampling time, R_0 is a lumped resistive term, $\alpha_j = \exp(-\Delta t/R_j C_j)$ and $\beta_j = R_j(1 - \exp(-\Delta t/R_j C_j))$ are parameters related to the circuit parameters, Q_{nom} is the capacity, and $j = 1, \ldots, n_v$ is an integer index.

The parameters and states of the ECM are then

$$x_{\text{ecm}} = [v_1, \ldots, v_{n_v}, z]^T \in \mathbf{R}^{n_v+1}$$
$$\theta_{\text{ecm}} = [\alpha_1, \ldots, \alpha_{n_v}, \beta_1, \ldots, \beta_{n_v}, Q_{\text{nom}}^{-1}, R_0]^T \in \mathbf{R}^{2n_v+2}.$$

In the following sections, the ECM will be referred to as ECM1, ECM2, and ECM4, where the number refers to n_v, i.e. the number of polarization voltages (RC-circuits) included in the model.

2.4 Extended equivalent circuit model

As described in [11], a major conceptual difference between the ECM and SPM is the use of open circuit voltage (OCV) based on cell average SOC versus individual open circuit potential (OCP) based on surface concentration. The polarization voltages v_j in the ECM, thus, models both the over potentials and the diffusion dynamics in the solid phase, a simplification that works well as long as the OCV-curve is relatively linear. In areas where the derivative changes fast, such as below 10% SOC in Figure 2, the ECM needs to compensate for this nonlinear effect by using a different set of parameters. The idea in the extended ECM (XECM) is to approximate surface SOC (z_{s}) by

$$z_{\text{s}}(k) = z(k) + \sum_{l=1}^{n_z} \Delta z_l(k),$$

where Δz_l represents the difference between bulk and surface concentrations and is governed by first order dynamics that in discrete time can be written as

$$\Delta z_l(k+1) = \alpha_l \Delta z_l(k) + \beta_l i(k),$$

where α_l and β_l are constants. It is then the surface SOC that is fed through the OCV curve rather than bulk SOC. The output equation can then be written as

$$v_{\text{xecm}}(k) = h_{\text{ocv}}\left(z_s(k)\right) + \sum_{j=1}^{n_v} v_j(k) + R_0 i(k),$$

where the parameters and states are

$$x_{\text{xecm}} = [v_1, \ldots, v_{n_v}, \Delta z_1, \ldots, \Delta z_{n_z}, z]^T \in \mathbf{R}^{n_v+n_z+1}$$
$$\theta_{\text{xecm}} = [\alpha_1, \ldots, \alpha_{n_v+n_z}, \beta_1, \ldots, \beta_{n_v+n_z}, Q_{\text{nom}}^{-1}, R_0]^T \in \mathbf{R}^{2n_v+2n_z+2}.$$

The models are referred to as XECM1 when $n_v = n_z = 1$ and XECM2 when $n_v = n_z = 2$.

Remark. The number of states for polarization voltages (v_j) and local SOC (Δz_l) can be selected independently, but in the forthcoming they are always set to the same number.

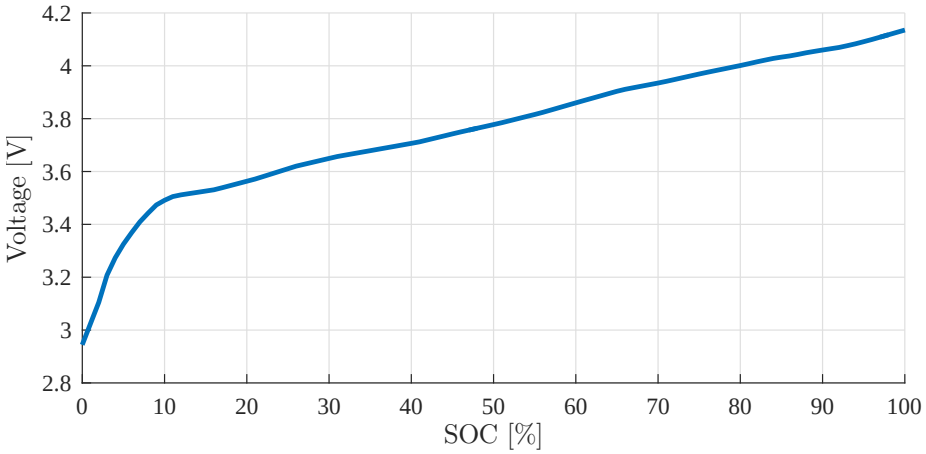

Figure 2: Open circuit voltage of the battery used in the laboratory tests.

2.5 Model structure evaluation

To assess the potential of the proposed model structures, laboratory data from an NMC cell tested in temperatures from −20 to +25°C were used. The current cycle is the same as in Figure 1 for all temperatures, except the part between 1600–1720s where the current is selected so that the voltage approaches the lower voltage limit 2.5V.

Initial state x_0 and constant parameters θ of the five models ECM1, ECM2, ECM4, XECM1, and XECM2 were identified by minimizing the prediction error subject to the model dynamics, i.e.

$$\begin{aligned} \min_{x_0,\theta} \quad & \sum_{k=0}^{N} \left(y_k - h(x_k, u_k, \theta)\right)^2 \\ \text{s.t.} \quad & x_{k+1} = f(x_k, u_k, \theta),\ k = 0, \ldots, N-1 \\ & \theta \in \mathcal{P}, \end{aligned}$$

where y_k and u_k are measured voltage and current respectively, and $\mathcal{P}$ is the set of feasible values for the parameters.

The optimization was implemented and solved in Matlab using the function `fmincon` and the results of simulating the models using their optimal solutions of x_0 and θ are illustrated in Figure 3. The first conclusion to draw is that the results are very similar most of the time. In temperatures above 0°C the ECM performance is very similar to XECM, except for ECM1. When the temperature is below 0°C and the voltage drops below 3V in high power discharge, the XECM provides a better fit. This can be seen in Figure 4, where details of the results for ECM4 and XECM2 are plotted (these models were selected since they have the same number

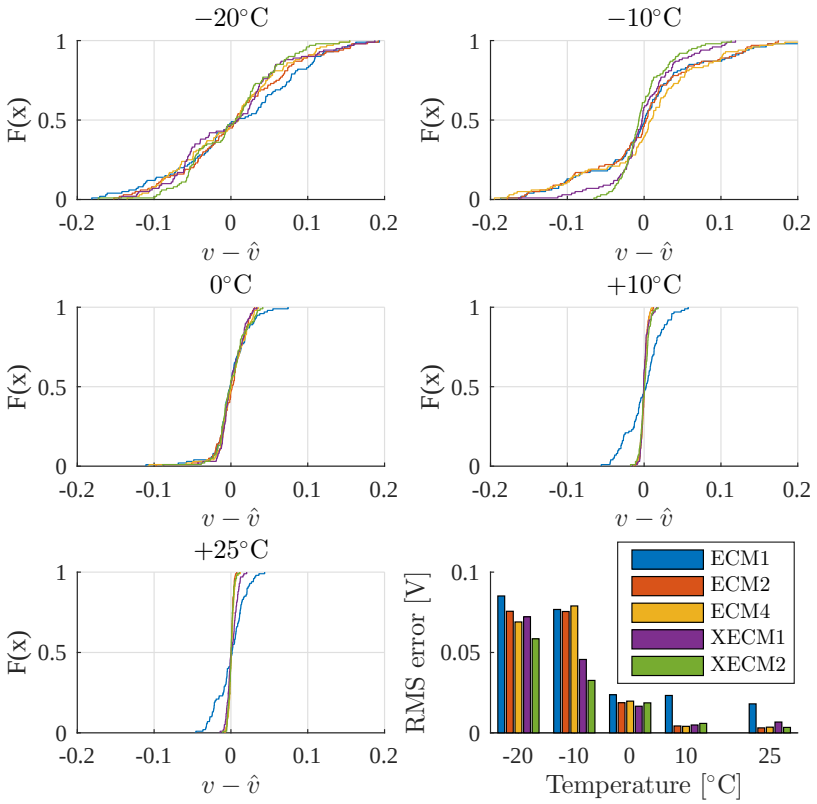

Figure 3: (a)–(e) Cumulative distribution function of the voltage error when simulating the models using optimized parameters. Note how similar the results are except for ECM1 and low temperatures where the estimation error of the ECMs are larger on the negative side, i.e. voltage is over-estimated. (f) RMS error for each temperature and model structure. Note, the colour coding is the same in all sub-figures.

of free parameters). The ECM4 fails to capture the high current part between 1600–1720s, even though the initial state and parameters have been optimized. The XECM2 provides an improved fit, and this coincides with when the estimated local SOC drops below the "knee" of the OCV curve. The performance of ECM2 and ECM4 is very similar (see Figure 3) and therefore it was concluded that adding more dynamics to the ECM does not solve the problem, instead, non-linear dynamic effects must be taken into consideration, which is what the XECM provides.

3 State and parameter estimation

To maintain accuracy during operation, for instance in an electric vehicle, the parameters and unmeasurable internal states must be tracked. This

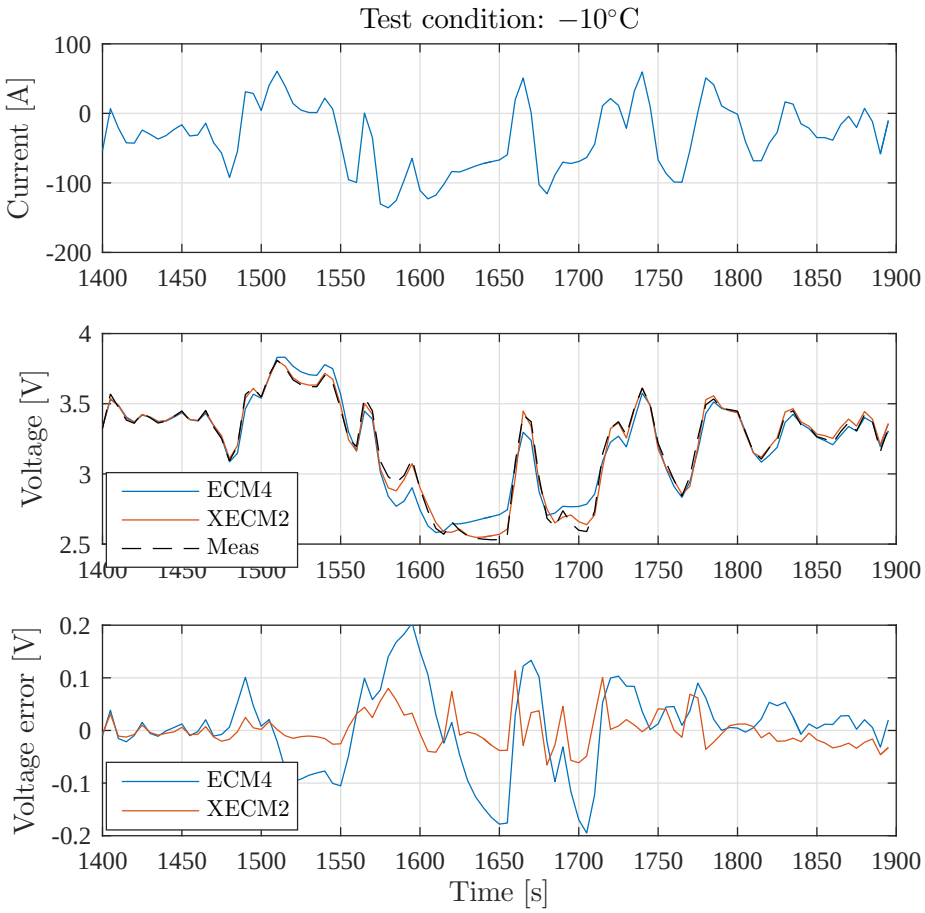

Figure 4: Laboratory data and simulations of the ECM4 and XECM2 using optimal parameters and initial state for data collected at -10°C. Note that both models have the same number of parameters and states. The parameters are optimized for the data in the example, illustrating that the XECM is possible to tune to the desired behaviour better than the ECM, which fails to capture the voltage response in spite of an optimal set of parameters and initial state.

is normally achieved by an observer and in this work a moving horizon estimation scheme was selected. The motivation behind that choice is its flexibility to handle joint estimation of parameters and states, and that it can handle constraints.

3.1 Moving horizon estimation

Moving horizon estimation (MHE) is an optimization-based method that uses a receding time-horizon covering a limited number of past measurements. A dynamic optimization problem is repeatedly solved online in each time-step. Disturbances in the form of unknown and slowly time-varying parameters can be estimated along with the states in a consistent way by adding them as additional variables to the optimization problem. Letting k be present time, N be the time horizon, and defining $L = k - N$, the MHE considering states (x), parameters (θ) and state noise (w) can be described by

$$\begin{aligned}
&\min_{x_j, w_j, \theta} \left\| \begin{matrix} x_L - \bar{x}_L \\ \theta - \bar{\theta}_L \end{matrix} \right\|^2_{P_L^{-1}} + \sum_{j=L}^{k} \left\| y_j - h(x_j, u_j, \theta) \right\|^2_R + \sum_{j=L}^{k-1} \left\| w_j \right\|^2_Q \\
&\text{s.t.} \quad x_{j+1} = f(x_j, u_j, \theta) + w_j, \ j = L, \ldots, k-1 \\
&\qquad \theta \in \mathcal{P}, x_j \in \mathcal{X}, w_j \in \mathcal{W}, \ j = L, \ldots, k,
\end{aligned}$$

where $P_L \in \mathbf{R}^{n_x+n_\theta}$, $R \in \mathbf{R}$, and $Q \in \mathbf{R}^{n_x}$ are positive definite weighting matrices, $\mathcal{P}$, $\mathcal{X}$, and $\mathcal{W}$ define the constraints, and the notation $\|a\|_A^2 = a^T A a$ is used.

There are three parts of this objective function, (i) the arrival cost, (ii) the prediction error, and (iii) the state noise. They all have their individual weighting matrices. The prediction error and state noise were here given static weights while the arrival cost, described next, must be updated in each iteration.

For the parameters and states estimated at time k to actually be optimal, all data from time $-\infty$ to present time k must be considered in the optimization. Even if the problem is truncated to start at time 0, this means that the optimization problem to solve grows unbounded with time. To overcome this, the arrival cost is used to sum up the information prior to the current time window, thereby transforming the problem to an equivalent one of fixed size. In general, the exact arrival cost cannot be calculated but there are numerous approximations available (see e.g. [23, 24]). Usually, it is assumed that some prior information is available in the form of the initial state and parameter estimates ($\bar{x}_L$, $\bar{\theta}_L$) with a corresponding covariance matrix P_L. Hence, letting the inverse of P_L determine the weight relative to

the other terms in the objective, results in a large (small) cost of choosing (x_L, θ_L) far away from $(\bar{x}_L, \bar{\theta}_L)$ when the confidence in the estimate is high (low).

One strategy for computing an approximate arrival cost is to use a first-order Taylor expansion around the trajectory of past estimates. This is equivalent to applying an EKF recursion for the covariance update [18, 25]. The weighting of the arrival cost can be calculated as the smoothed Kalman filter estimate using the following recursion:

$$
\begin{aligned}
K_L &= P_L C_L^T \left(C_L P_L C_L^T + \tilde{R} \right)^{-1} \\
h_L &= h(x_L, u_L, \theta_L) \\
\begin{bmatrix} \bar{x}_{L+1}^- \\ \bar{\theta}_{L+1}^- \end{bmatrix} &= \begin{bmatrix} \bar{x}_L \\ \bar{\theta}_L \end{bmatrix} + K_L \left(y_L - h_L - C_L \begin{bmatrix} \bar{x}_L - x_L \\ \bar{\theta}_L - \theta_L \end{bmatrix} \right) \\
\begin{bmatrix} \bar{x}_{L+1} \\ \bar{\theta}_{L+1} \end{bmatrix} &= \begin{bmatrix} f(x_L, u_L, \theta_L) \\ \theta_L \end{bmatrix} + A_L \begin{bmatrix} \bar{x}_{L+1}^- - x_L \\ \bar{\theta}_{L+1}^- - \theta_L \end{bmatrix} \\
P_{L+1}^- &= (I - K_L C_L) P_L \\
P_{L+1} &= A_L P_{L+1}^- A_L^T + Q \\
P_{L+1} &= A_L (I - K_L C_L) P_L A_L^T + \tilde{Q}
\end{aligned}
$$

where $\tilde{R} \in \mathbf{R}$ and $\tilde{Q} \in \mathbf{R}^{n_x + n_\theta}$ are tuning matrices, and A_L and C_L are Jacobians of the state dynamics and output equation respectively.

4 Voltage prediction

The concept of future voltage prediction is explained in Figure 5. Based on current and voltage measurements up to present time, the MHE is used to estimate parameters and states. In the prediction step, the model is simulated 30s forward, assuming that the current is known, and the predicted voltage is then compared to the true measured voltage.

To reduce the size of both the estimation and prediction steps the data, which were originally sampled with a step-time of 1s, were down-sampled to 5s by averaging. This also has the advantage of focusing the estimation on the dominating dynamics. To further limit the amount of free parameters, only XECM1 and ECM2 are evaluated. The optimization is implemented and solved in Matlab using the CasADi framework [26].

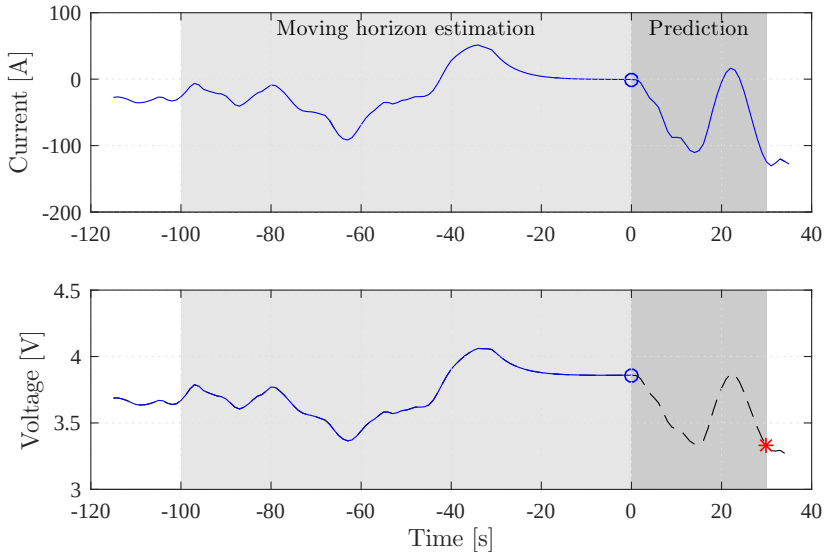

Figure 5: Example of how voltage prediction is done. Based on data up to time $t = 0$ the state and parameters are estimated using the MHE algorithm. Based on the estimated parameters, final state, and future current, the model is simulated 30s ahead to predict what the voltage should be. This is then compared to the actual voltage at that point in time.

4.1 Horizon in MHE

First, the impact of the estimation horizon length was investigated on the XECM1 by testing various setting from $N = 1$ (EKF) up to $N = 60$ (i.e. 300s of data). Note that $N = 1$ uses a regular EKF instead of MHE. The results are illustrated in Figure 6. It can be seen that the RMS error is significantly reduced when including more historic data for the estimation. However, using too long horizons increases the RMS error somewhat, and the minimum error was achieved with $N = 30$ (150s of data). While more careful calibration may have changed the RMS error, it was considered unlikely that the overall results would have changed significantly. The reason that the estimator benefits from an extended time-horizon is that the linearised system is almost unobservable due to similar dynamics of the v_1 and Δz_1 states.

4.2 XECM vs ECM

Next the performance of the XECM1 is compared to the ECM2 in an online setting using the same data as in Section 2.5. Manual calibration of Q and R matrices of the MHE was done for a horizon of $N = 30$ using a training data set in -10°C. The same calibration was then used for all

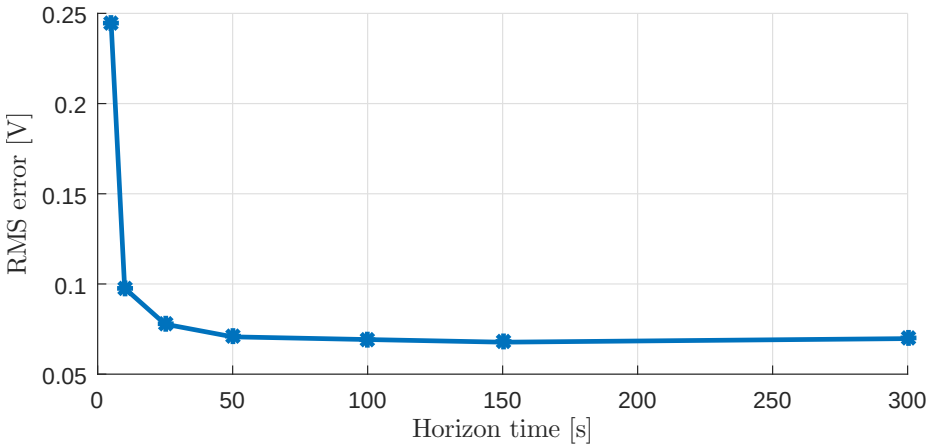

Figure 6: RMS prediction error for different horizons of past data included in the MHE algorithm. The data for N=1 (5s), uses a regular EKF.

temperatures, except for parameter initialization that was taken from the offline optimizations presented in Section 2.

The results for ECM2 and XECM1 in -10°C are illustrated in Figure 7, where it can be seen how the prediction accuracy is improved using XECM1 in longer periods of high discharge power. In Figure 8, the state trajectories of XECM1 are plotted. Note the extremely low local SOC estimated at around 1300s, which coincides with the part of the cycle that ECM2 fails to capture.

An overview of the performance for all tested temperatures is given in Figure 9, which depicts the cumulative distribution function of the prediction errors for both models. The accuracy of the XECM1 model is overall better in all temperatures. The full potential as compared to offline optimization (Figure 3) is, however, not achieved. Future work is needed to further investigate the reasons, but it is either due to that the optimal set of parameters cannot be found using historic data, and in that case some gain-scheduling technique might be needed, or it might be that the joint estimation of parameters and states is difficult due to different excitation conditions, and in that case dual estimation of parameters and states might be needed.

5 Conclusions and future work

Equivalent circuit models (ECM) are often used in algorithms for predicting power capability of batteries. When operated at low SOC and/or low temperatures, ECMs may, however, fail to capture the voltage response of the battery. An extended ECM that includes additional states related to

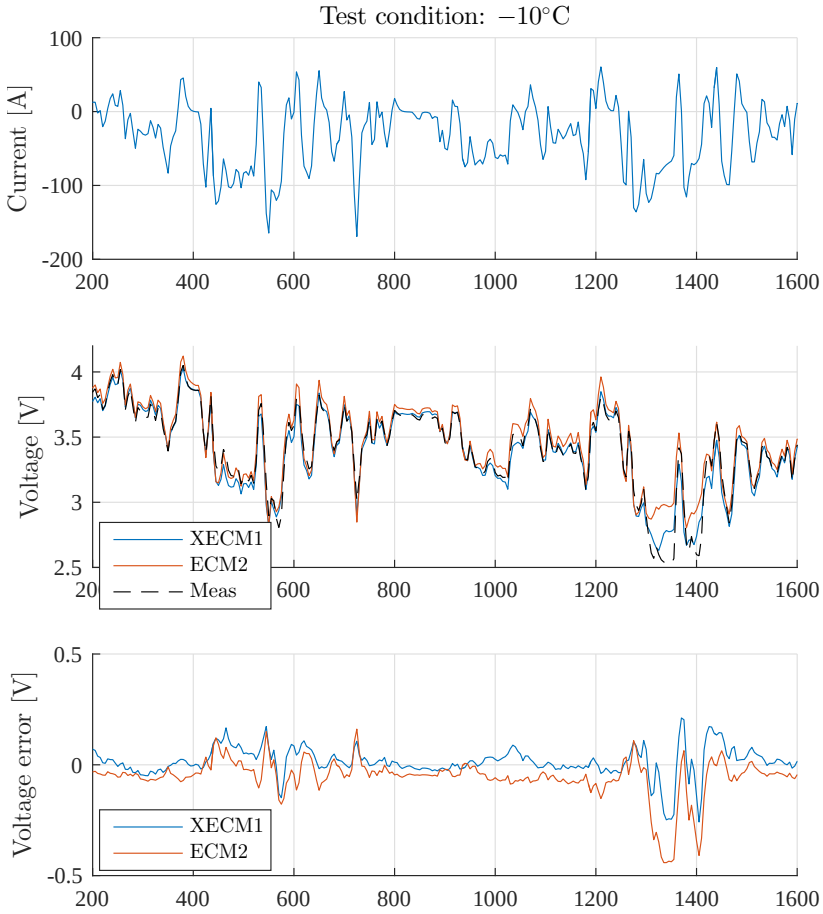

Figure 7: Voltage prediction based on 30s simulation using initial state and parameters from moving horizon estimation.

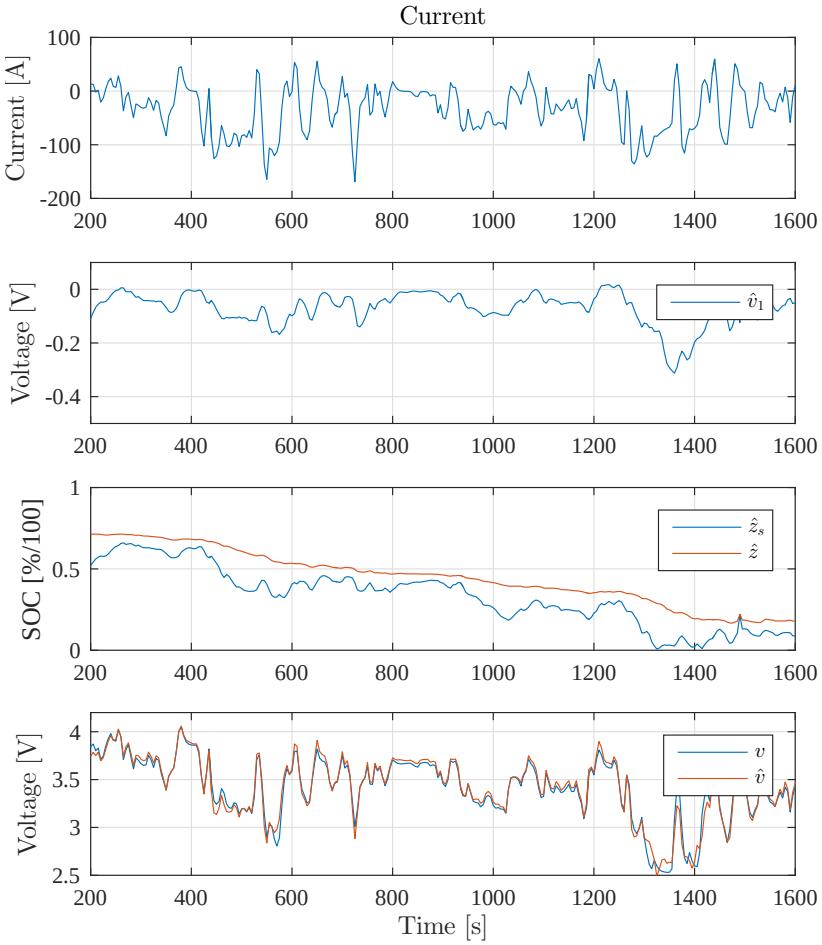

Figure 8: Estimated state trajectories of the XECM1 for the test in -10°C.

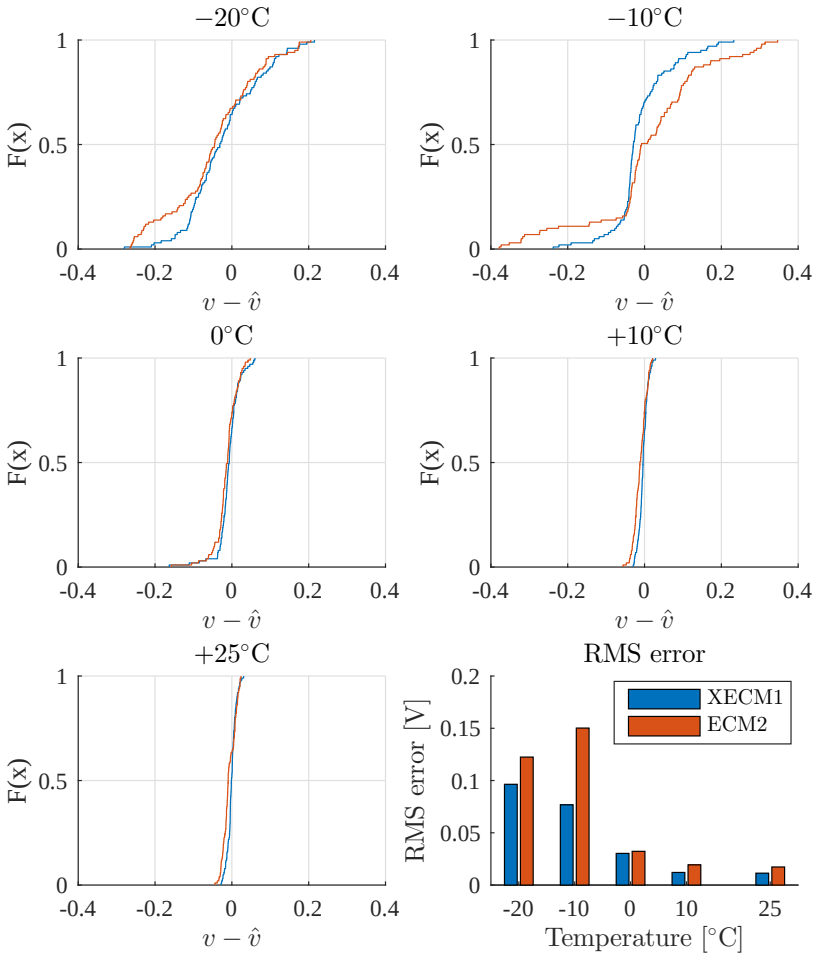

Figure 9: Cumulative distribution of prediction errors for all tested temperatures together with RMS error. The evaluated part of the drivecycle is the same as in previous examples. In the CDF plots, it is in particular the negative errors that are interesting since they lead to an over-estimation of voltage (and hence also available power).

local SOC was proposed to improve the prediction accuracy. To estimate parameters and states of the model online, a moving horizon estimation scheme was used. The improvement of the extended model was demonstrated by comparing it to the standard ECM using laboratory data from a wide temperature range. Future research directions are to further improve the online estimation accuracy of the MHE by e.g. dual estimation of parameters and states, and to incorporate the extended model in a power prediction algorithm.

Acknowledgements

This work was supported by Volvo Cars and Chalmers, and financed by the Swedish Energy Agency through the project "Life-long battery control" (P39786-1).

References

[1] T. Wik, B. Fridholm, and H. Kuusisto, "Implementation and robustness of an analytically based battery state of power," *Journal of Power Sources*, vol. 287, pp. 448–457, 2015.

[2] B. Fridholm, T. Wik, H. Kuusisto, and A. Klintberg, "Estimating power capability of aged lithium-ion batteries in presence of communication delays," *Journal of Power Sources*, vol. 383, pp. 24–33, 2018.

[3] T. Feng, L. Yang, X. Zhao, H. Zhang, and J. Qiang, "Online identification of lithium-ion battery parameters based on an improved equivalent-circuit model and its implementation on battery state-of-power prediction," *Journal of Power Sources*, vol. 281, pp. 192–203, 2015.

[4] S. Nejad, D. T. Gladwin, and D. A. Stone, "A systematic review of lumped-parameter equivalent circuit models for real-time estimation of lithium-ion battery states," *Journal of Power Sources*, vol. 316, pp. 183–196, 2016.

[5] G. Liu, M. Ouyang, L. Lu, J. Li, and J. Hua, "A highly accurate predictive-adaptive method for lithium-ion battery remaining discharge energy prediction in electric vehicle applications," *Applied Energy*, vol. 149, pp. 297–314, 2015.

[6] F. Sun, R. Xiong, and H. He, "Estimation of state-of-charge and state-of-power capability of lithium-ion battery considering varying health conditions," *Journal of Power Sources*, vol. 259, pp. 166–176, 2014.

[7] B. Fridholm, T. Wik, and M. Nilsson, "Robust recursive impedance estimation for automotive lithium-ion batteries," *Journal of Power Sources*, vol. 304, pp. 33–41, 2016.

[8] B. Fridholm, T. Wik, and M. Nilsson, "Kalman filter for adaptive learning of look-up tables with application to automotive battery resistance estimation," *Control Engineering Practice*, vol. 48, pp. 78–86, 2016.

[9] J. Jaguemont, L. Boulon, and Y. Dube, "Characterization and Modeling of a Hybrid-Electric-Vehicle Lithium-Ion Battery Pack at Low Temperatures," *IEEE Transactions on Vehicular Technology*, vol. 65, no. 1, pp. 1–14, 2015.

[10] M. Debert, G. Colin, G. Bloch, and Y. Chamaillard, "An observer looks at the cell temperature in automotive battery packs," *Control Engineering Practice*, vol. 21, no. 8, pp. 1035–1042, 2013.

[11] M. Ouyang, G. Liu, L. Lu, J. Li, and X. Han, "Enhancing the estimation accuracy in low state-of-charge area: A novel onboard battery model through surface state of charge determination," *Journal of Power Sources*, vol. 270, pp. 221–237, 2014.

[12] H. Ekström, B. Fridholm, and G. Lindbergh, "Comparison of lumped diffusion models for voltage prediction of a lithium-ion battery cell during dynamic loads," *Journal of Power Sources*, vol. 402, no. August, pp. 296–300, 2018.

[13] G. L. Plett, "Extended Kalman filtering for battery management systems of LiPB-based HEV battery packs - Part 3. State and parameter estimation," *Journal of Power Sources*, vol. 134, no. 2, pp. 277–292, 2004.

[14] D. Di Domenico, E. Prada, and Y. Creff, "An adaptive strategy for Li-ion battery internal state estimation," *Control Engineering Practice*, vol. 21, no. 12, pp. 1851–1859, 2013.

[15] C. Zou, C. Manzie, D. Nešić, and A. G. Kallapur, "Multi-time-scale observer design for state-of-charge and state-of-health of a lithium-ion battery," *Journal of Power Sources*, vol. 335, pp. 121–130, 2016.

[16] B. Suthar, V. Ramadesigan, P. Northrop, B. Gopaluni, S. Santhanagopalan, R. Braatz, and V. Subramanian, "Optimal control and state estimation of lithium-ion batteries using reformulated models," *Proceedings of the American Control Conference*, pp. 5350–5355, 2013.

[17] J. N. Shen, Y. J. He, Z. F. Ma, H. B. Luo, and Z. F. Zhang, "Online state of charge estimation of lithium-ion batteries: A moving horizon estimation approach," *Chemical Engineering Science*, vol. 154, pp. 42–53, 2016.

[18] X. Hu, D. Cao, and B. Egardt, "Condition Monitoring in Advanced Battery Management Systems: Moving Horizon Estimation Using a Reduced Electrochemical Model," *IEEE/ASME Transactions on Mechatronics*, vol. 23, no. 1, pp. 167–178, 2018.

[19] M. Doyle, T. F. Fuller, and J. Newman, "Modeling of Galvanostatic Charge and Discharge of the Lithium/Polymer/Insertion Cell," *Journal of The Electrochemical Society*, vol. 140, no. 6, pp. 1526–1533, 1993.

[20] K. A. Smith, C. D. Rahn, and C. Y. Wang, "Control oriented 1D electrochemical model of lithium ion battery," *Energy Conversion and Management*, vol. 48, no. 9, pp. 2565–2578, 2007.

[21] X. Han, M. Ouyang, L. Lu, and J. Li, "Simplification of physics-based electrochemical model for lithium ion battery on electric vehicle. Part I: Diffusion simplification and single particle model," *Journal of Power Sources*, vol. 278, pp. 802–813, 2015.

[22] C. Zou, C. Manzie, and D. Nesic, "A Framework for Simplification of PDE-Based Lithium-Ion Battery Models," *IEEE Transactions on Control Systems Technology*, vol. 24, no. 5, pp. 1594–1609, 2016.

[23] P. Kühl, M. Diehl, T. Kraus, J. P. Schlöder, and H. G. Bock, "A real-time algorithm for moving horizon state and parameter estimation," *Computers and Chemical Engineering*, vol. 35, no. 1, pp. 71–83, 2011.

[24] S. Ungarala, "Computing arrival cost parameters in moving horizon estimation using sampling based filters," *Journal of Process Control*, vol. 19, no. 9, pp. 1576–1588, 2009.

[25] J. B. Rawlings and D. Q. Mayne, *Model Predictive Control Theory and Design*. Madison, WI, USA: Nob Hill Publishing, 2009.

[26] J. Andreasson, "A general purpose software framework for dynamic optimization," PhD thesis, KU Leuven, 2013.

Paper 6

An analytic estimate of available battery energy considering thermal effects

Björn Fridholm, Marcus Hedegärd, and Torsten Wik

Submitted for publication in Journal of Power Sources

Comment: The layout of this paper has been reformatted in order to comply with the rest of the thesis

An analytic estimate of available battery energy considering thermal effects

Björn Fridholm, Marcus Hedegärd, and Torsten Wik

Abstract

The electrical range of electrified vehicles is limited by the energy available from the battery system. The available energy differs from the total energy stored in the battery due to resistive losses that are highly nonlinear w.r.t. temperature and drawn current. This introduces a dependency on future operating conditions that must be accounted for to get accurate estimates of the available energy. Based on statistical measures of the future driving profile, together with an electro-thermal battery model, an approximate analytical expression for the available energy that considers the temperature trajectory of the battery is derived. The expression is evaluated in simulations using a battery pack model with a thermal system calibrated to laboratory data. The error introduced by the approximate expression is within 1% for the tested temperature range −15 to +30°C.

Keywords: Lithium-ion; energy estimation; battery management; state of energy; battery modelling; thermal modelling.

1 Introduction

Information about the energy available from the battery system is important for electrified vehicles, both to enable optimal energy management and for calculating remaining driving range [1, 2]. In the literature, energy estimation is often described in terms of state-of-energy (SOE), where the remaining energy is related to the energy for a fully charged battery. The problem can then be approached analogous to state-of-charge (SOC) estimation by e.g. model-based estimators, such as different types of Kalman filters [3, 4], neural networks [5], and H_∞ filters [6], or by introducing direct relationships between SOC and SOE [7]. While there is a clear relationship between SOC and the energy stored in the battery, the energy that the vehicle can use (hereafter referred to as available energy) will differ from the stored energy due to losses, which depend primarily on the drawn current

and the internal resistance [2]. Theoretically, the available energy is given by integrating the battery power over the remaining drive cycle, i.e.

$$E_{\text{avail}}(t) = \int_t^{t_{\text{end}}} v(\tau)i(\tau)d\tau, \tag{1}$$

where v is battery terminal voltage, i is current, and t_{end} is the instant when the battery reaches its minimum allowed charge level ($z_{\min}$).

Calculating the available energy thus requires knowledge about future operating conditions of the battery, information that is normally unavailable in online vehicle applications. Still, Liu et al. [8] demonstrated accurate estimates of the available energy by solving (1) for an assumed future current profile together with an equivalent circuit model. Full knowledge of the future driving profile may not be realistic to expect in online applications, but historical data on driver behaviour together with route information can provide statistical information about the future driving profile [9, 10]. Barai et al. [2] utilize this to solve (1) for an assumed future average current. However, one important aspect that is not considered in [2, 8] is how the battery temperature impacts available energy.

It is well established that the resistance of lithium-ion batteries is highly nonlinear w.r.t. temperature, where lower temperature causes significantly increased resistance [11] and thus also increased losses. Therefore, it is important to also consider the temperature trajectory of the battery when estimating available energy. For SOE estimation, temperature dependencies have been dealt with by using a definition the energy for a fully charged battery that varies with temperature (see e.g. [3, 4, 5]). Validation of SOE estimation accuracy has then in general focused on constant temperatures, even though [3] also considered linearly varying temperature and constant discharge current. Literature review for this work revealed no contributions on modelling the future temperature trajectory of the battery.

One motivation for studying the energy in a thermal steady-state may be that the battery pack is normally controlled to some reference operating temperature using a cooling system. To reduce cost it is, however, quite common to exclude actuators for heating the battery. Instead, the battery heating is left to rely on the internal heat-generation caused by resistive losses [11]. When starting from a low temperature, there will thus be a transient phase when the losses are significantly higher compared to operation in a thermal steady-state. As an example, the available energy is approximately 95% of the total stored energy for a battery that is operated constantly close to a reference temperature of +30°C, whereas it may drop below 90% when the battery is heated by losses from an initial temperature below 0°C (see Section 6).

This article falls into the category of solving the power integral (1), but extends the existing results by providing (i) an analytic expression of available energy, (ii) including the thermal dynamics of the battery pack, and (iii) using the future current statistics instead of a given current profile.

The remainder of this article is structured such that Section 2 introduces the vehicle application considered. Section 3 describes an electro-thermal battery model suitable for energy estimation. Section 4 presents a derivation of the proposed analytic expression for available energy. Section 5 gives the algorithm for implementation, which is evaluated in simulations in Section 6. Finally, Section 7 concludes the article and suggests future research directions.

2 Vehicle system

Before moving into the main results of the work, it must be noted that an exact calculation of available energy is not possible in online vehicle applications. However, based on assumptions presented in this section, an expression for estimating the available energy can be derived.

2.1 Future driving conditions

In online applications it is not feasible to have full knowledge of the future driving profile. However, given the extensive efforts and rapid development of data-driven methods (see e.g. [10, 12]), improved predictions of driver intent and future traffic situations can be expected. Here, we assume that statistical information is available according to:

Assumption 1. *The average (i_{avg}) and standard deviation (i_{std}) of the future current are known.*

2.2 Battery pack

An automotive battery pack contains hundreds of battery cells that are all slightly different due to variations in manufacturing, uneven ageing, etc. [13]. However, this variability is not considered here where it is presumed that

Assumption 2. *all cells of the battery pack are identical.*

Remark. By this assumption, the battery pack can be regarded as one single cell.

The upcoming calculations rely on a battery model, where the parameters and states are not directly measurable in the vehicle. This problem has been thoroughly investigated (see e.g. [14]) and to focus on energy estimation, it is assumed that

Assumption 3. *all needed model parameters and state-of-charge (SOC) are available.*

Remark. The parameters and states are also needed for other tasks of the battery management system. The energy estimation therefore does not introduce any additional needs.

2.3 Thermal system

To calculate a temperature trajectory of the battery pack, also thermal management must be considered. There are many configurations available (see [11]) but here it is assumed that

Assumption 4. *no external heating is applied to the battery.*

Remark. The thermal management can, thus, be divided into two parts; (i) uncontrolled heating by internal heat generation, and (ii) controlled cooling to a reference temperature.

3 Simplified electro-thermal battery model

This section introduces an electro-thermal battery model suitable for available energy estimation. Based on the limited information about future operating conditions provided by Assumption 1, a first order equivalent circuit model (see Figure 1) with temperature dependent parameters is simplified to a purely resistive model that can be used to calculate the power integral (1).

3.1 Electrical dynamics

Our estimation approach requires a capacity definition that remains constant over a charge cycle. This is achieved by relating measures to the open circuit voltage.

Remark. There might be small variations in the open circuit voltage (OCV) w.r.t. temperature, but this effect is negligible for the cells and temperature range considered in this work, as was also found in [15].

The following definitions will then lead to an (almost) temperature independent capacity definition:

Definition 15. *A battery cell is fully charged, i.e. state-of-charge $z = 1$, when its open circuit voltage is $v_{\max}$.*

Definition 16. *A battery cell is fully discharged, i.e. state-of-charge $z = 0$, when its open circuit voltage is $v_{\min}$.*

Definition 17. *The nominal capacity (Q_{nom}) is the number of ampere seconds between fully charged and fully discharged.*

Definition 18. *The minimum state-of-charge ($z_{\min}$) is the minimum allowed charge level of the battery.*

Remark. Normally the battery is not used down to $z = 0$ for both safety and durability reasons and therefore $z_{\min}$ is often set to some value above 0, typically $z_{\min} = 0.1$.

In continuous time the temperature dependent equivalent circuit model in Figure 1 can be described by

$$\dot{v}_1(t) = -\frac{1}{\tau_1(T(t))}v_1(t) + \frac{1}{C_1(T(t))}i(t) \tag{2}$$

$$\dot{z}(t) = \frac{1}{Q_{\text{nom}}}i(t) \tag{3}$$

$$v(t) = h_{\text{oc}}(z(t)) + v_1(t) + R_0(T(t))i(t), \tag{4}$$

where z is SOC, v_1 is dynamic voltage, h_{oc} is a non-linear function that maps SOC to open circuit voltage, T is temperature, and R_0, C_1 and $\tau_1 = R_1C_1$ are temperature dependent parameters (see Figure 1).

Remark. It is assumed that the parameters are fairly constant over the used SOC range, and the model therefore does not depend explicitly on SOC. Yet, the parameters of the simulation model used for evaluation in later sections do depend on SOC.

3.2 Thermal dynamics

For the thermal dynamics, a simplified lumped mass model based on energy balance is used. Only Joule heating is considered, while entropy effects are neglected [16]. Convective cooling is assumed, but only considered via a cooling power directly on the battery. It is assumed that the heat is only generated in the resistances R_0 and R_1 of Figure 1 such that the energy balance for the battery becomes

$$mc\dot{T}(t) = R_0(T(t))i^2(t) + R_1(T(t))i_1^2(t) + P_{\text{cool}}(t), \tag{5}$$

where m is the thermal mass, c is the corresponding specific heat capacity, and P_{cool} is the cooling power applied to the battery. Similar models have previously been used in [16, 17, 18].

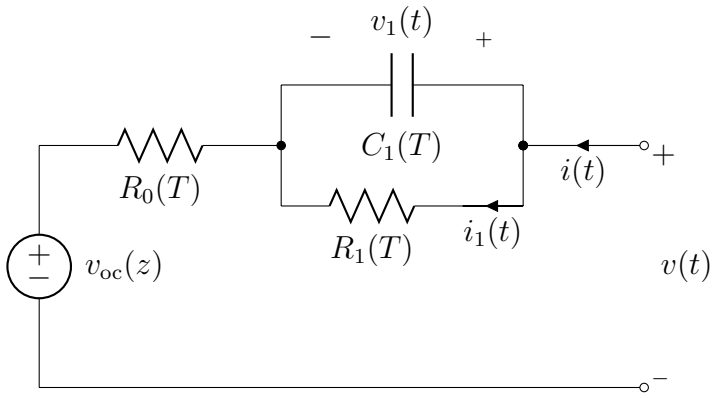

Figure 1: Equivalent circuit model.

3.3 Simplification of resistance

Based on the limited information about the future current from Assumption 1, the dynamic voltage (2) cannot be resolved in time. Instead, a simplified resistive model for $v(t)$, i.e.

$$v(t) \approx v_{\text{oc}}(z(t)) + R(T)i(t), \tag{6}$$

with the same statistical properties as (4) is sought.

First let

$$R_0(T^*) = R_0,\, R_1(T^*) = R_1, \text{ and } \tau_1(T^*) = \tau_1,$$

for an arbitrary fixed temperature T^*. Also note that by Assumption 1,

$$\mathrm{E}[i(t)] = i_{\text{avg}} \tag{7}$$
$$\mathrm{E}[i^2(t)] = i_{\text{avg}}^2 + i_{\text{std}}^2 = i_{\text{rms}}^2. \tag{8}$$

The derivation is more straight-forward using the discrete-time equivalent of (2), which with sampling time t_s can be described as

$$v_1(k+1) = \underbrace{e^{-t_s/\tau_1}}_{\alpha} v_1(k) + \underbrace{R_1(1 - e^{-t_s/\tau_1})}_{\beta = R_1(1-\alpha)} i(k). \tag{9}$$

Since it is unrealistic that the current can be modelled as white noise, it is assumed that

$$i(k) = i_{\text{avg}} + \Delta i(k), \tag{10}$$

where Δi is filtered white noise according to

$$\Delta i(k+1) = \gamma \Delta i(k) + w(k), \tag{11}$$

with $w \sim \mathcal{N}(0, \sigma_w^2)$ and $\gamma < 1$ is the time-correlation of the current.

Studying the correlation between v_1 and i using (9–11) it can be shown that

$$\mathrm{E}[v_1^2] = R_1^2 \underbrace{\frac{(1-\alpha)(1+\gamma\alpha)}{(1+\alpha)(1-\gamma\alpha)}}_{\varphi} i_{\mathrm{std}}^2 + R_1^2 i_{\mathrm{avg}}^2.$$

Returning to (5) we see that the approximation

$$R = R_0 + \frac{i_{\mathrm{avg}}^2 + \varphi i_{\mathrm{std}}^2}{i_{\mathrm{rms}}^2} R_1, \tag{12}$$

leads to

$$\mathrm{E}[R_0 i^2(t) + R_1 i_1^2(t)] = \mathrm{E}[R i^2(t)]. \tag{13}$$

Since the temperature T^* is arbitrary, this holds for all temperatures.

3.4 Temperature dependent resistance

Inspired by [19], an explicit expression for the temperature dependence of the resistance is introduced on the form

$$R(T) = \bar{R} e^{-\kappa(T - T_{\mathrm{ref}})}, \tag{14}$$

where $\bar{R}$ is the resistance at the reference temperature T_{ref}, and κ is a tuning parameter to handle the temperature dependence.

Remark. Here we have implicitly assumed that the temperature dependence for both R_0 and R_1 can also be described by (14) using the same κ. While this may seem questionable the impact on the final results is small, as will be seen in Section 6.

The future temperature can now be calculated for cases without cooling ($P_{\mathrm{cool}} = 0$) using (5). However, it will be based on statistical information of the future current, and the temperature and current are thus not independent. Motivated by the fact that the temperature variations are significantly slower than the variations in current, we will ignore this dependency and use the approximation:

$$mc \frac{d}{dt} \mathrm{E}[T(t)] \approx \bar{R} e^{-\kappa(\mathrm{E}[T(t)] - T_{\mathrm{ref}})} i_{\mathrm{rms}}^2,$$

which is a separable differential equation that can be solved by

$$\begin{aligned} \frac{mc}{\bar{R}} \int_{T_0}^{T_1} e^{\kappa(\mathrm{E}[T] - T_{\mathrm{ref}})} dT &= \int_{t_0}^{t_1} i_{\mathrm{rms}}^2 dt \\ \frac{mc}{\kappa \bar{R}} \left(e^{\kappa(T_1 - T_{\mathrm{ref}})} - e^{\kappa(T_0 - T_{\mathrm{ref}})} \right) &= i_{\mathrm{rms}}^2 \left(t_1 - t_0 \right). \end{aligned} \tag{15}$$

Remark. From here on all variables related to future operating conditions should be considered in terms of their expected values, for readability this is, however, left out of the equations.

4 Available energy calculation

Based on (1) and (6), the available energy can be calculated as

$$\begin{aligned} E_{\text{avail}}(t) &\approx \int_t^{t_{\text{end}}} v_{\text{oc}}(z(\tau))i(\tau) + R(T)i^2(\tau)d\tau \\ &= \underbrace{\int_t^{t_{\text{end}}} v_{\text{oc}}(z(\tau))i(\tau)d\tau}_{E_{\text{nom}}(t)} + \underbrace{\int_t^{t_{\text{end}}} R(T)i^2(\tau)d\tau}_{E_{\text{loss}}(t)}, \end{aligned}$$

where E_{nom} is the nominal (total) energy, E_{loss} is the temperature dependent losses, and t_{end} is defined as the instant when SOC is at $z_{\min}$, which can be calculated by solving (3)

$$\begin{aligned} z_{\min} &= z(t) + \frac{1}{Q_{\text{nom}}} \int_t^{t_{\text{end}}} i(\tau)d\tau \\ &\approx z(t) + \frac{1}{Q_{\text{nom}}} \int_t^{t_{\text{end}}} \mathrm{E}[i(\tau)]d\tau \end{aligned}$$

which gives

$$t_{\text{end}} \approx t + \frac{Q_{\text{nom}}(z_{\min} - z(t))}{i_{\text{avg}}}. \tag{16}$$

4.1 Nominal energy

For the nominal energy, the integral can be solved using the variable substitution $d\tau = dz/\dot{z}$ together with (3), which gives

$$E_{\text{nom}}(t) = Q_{\text{nom}} \int_{z(t)}^{z_{\min}} v_{\text{oc}}(z)dz. \tag{17}$$

The nominal energy is thus independent of the operating conditions and the integral can therefore be solved offline and stored in the battery management system.

4.2 Resistive losses

Consider the case when the battery starts at a temperature below the reference, which is the hard case since the transient temperature initially leads to increased losses. Equations (5), (6), and (13) gives

$$R(T)i_{\text{rms}}^2 = mc\dot{T}(t) - P_{\text{cool}}(t).$$

Now, assume that the temperature is allowed to increase freely until a reference temperature T_{ref} is reached, after which we have perfect cooling, i.e. all of the generated heat is cooled away. The expected value of the cooling is then

$$\mathrm{E}[P_{\text{cool}}(t)] = \begin{cases} 0, & T(t) < T_{\text{ref}} \\ \bar{R}i_{\text{rms}}^2, & T(t) \geq T_{\text{ref}}. \end{cases} \tag{18}$$

so that

$$R(T(t))i_{\text{rms}}^2 = \begin{cases} mc\dot{T}(t), & T(t) < T_{\text{ref}} \\ \bar{R}i_{\text{rms}}^2, & T(t) \geq T_{\text{ref}}. \end{cases}$$

There are now two cases depending on whether T_{ref} is reached during the cycle or not. Referring back to (15) we define

$$t_{\text{ref}} = t + \frac{mc}{\kappa \bar{R} i_{\text{rms}}^2} \left(1 - e^{\kappa(T(t) - T_{\text{ref}})}\right), \tag{19}$$

and consequently T_{ref} is reached if $t_{\text{ref}} < t_{\text{end}}$.

4.3 Case 1: T_{ref} is reached

Assuming that T_{ref} is reached it follows that

$$\begin{aligned} E_{\text{loss}}(t) &= \mathrm{E}\left[\int_t^{t_{\text{end}}} R(T(\tau))i^2(\tau)d\tau\right] \\ &= \int_t^{t_{\text{end}}} mc\dot{T}(\tau) - \mathrm{E}[P_{\text{cool}}(\tau)]d\tau \\ &= \int_t^{t_{\text{ref}}} mc\dot{T}(\tau)d\tau - \bar{R}i_{\text{rms}}^2 \int_{t_{\text{ref}}}^{t_{\text{end}}} 1 d\tau \\ &= \underbrace{mc(T_{\text{ref}} - T(t))}_{\text{heat-up}} - \underbrace{\bar{R}i_{\text{rms}}^2(t_{\text{end}} - t_{\text{ref}})}_{\text{running loss}}. \end{aligned} \tag{20}$$

Combining equations (16), (19), and (20) yields the final expression for the energy losses

$$E_{\text{loss}}(t) = mc\Delta T(t) + \frac{mc}{\kappa}\left(1 - e^{-\kappa\Delta T(t)}\right) - \frac{\bar{R}i_{\text{rms}}^2 Q_{\text{nom}}\Delta z(t)}{i_{\text{avg}}}, \tag{21}$$

where $\Delta T(t) = T_{\text{ref}} - T(t)$ and $\Delta z(t) = z_{\min} - z(t)$.

4.4 Case 2: T_{ref} is not reached

If the reference temperature is not reached before the battery is fully discharged, we have to solve (15) with $t_1 = t_{\text{end}}$, i.e.

$$T_{\text{end}} = T_{\text{ref}} + \frac{1}{\kappa}\ln\left(\frac{\kappa\bar{R}i_{\text{rms}}^2}{mc}\left(t_{\text{end}} - t + e^{\kappa(T(t)-T_{\text{ref}})}\right)\right),$$

and the final expression for energy losses then becomes

$$\begin{aligned} E_{\text{loss}}(t) = {} & mc\left(T_{\text{ref}} - T(t)\right) + \\ & + \frac{mc}{\kappa}\ln\left(\frac{\kappa\bar{R}i_{\text{rms}}^2}{mc}\left(t_{\text{end}} - t + e^{\kappa(T(t)-T_{\text{ref}})}\right)\right). \end{aligned} \tag{22}$$

5 Algorithm for energy estimation

The previous sections have presented several steps to calculate the available energy. Here the needed steps are summarised into an algorithm.

Initialization

Input the states ($z(t)$ and $T(t)$),
and load-cycle statistics (i_{avg}, i_{std}, and γ)

Step 1

Calculate t_{end} using (16).
Calculate t_{ref} using (19).

Step 2

Calculate E_{nom} using (17).
If $t_{\text{ref}} < t_{\text{end}}$ then calculate E_{loss} using (21),
else calculate E_{loss} using (22).

Output

Output $E_{\text{avail}} = E_{\text{nom}} + E_{\text{loss}}$.

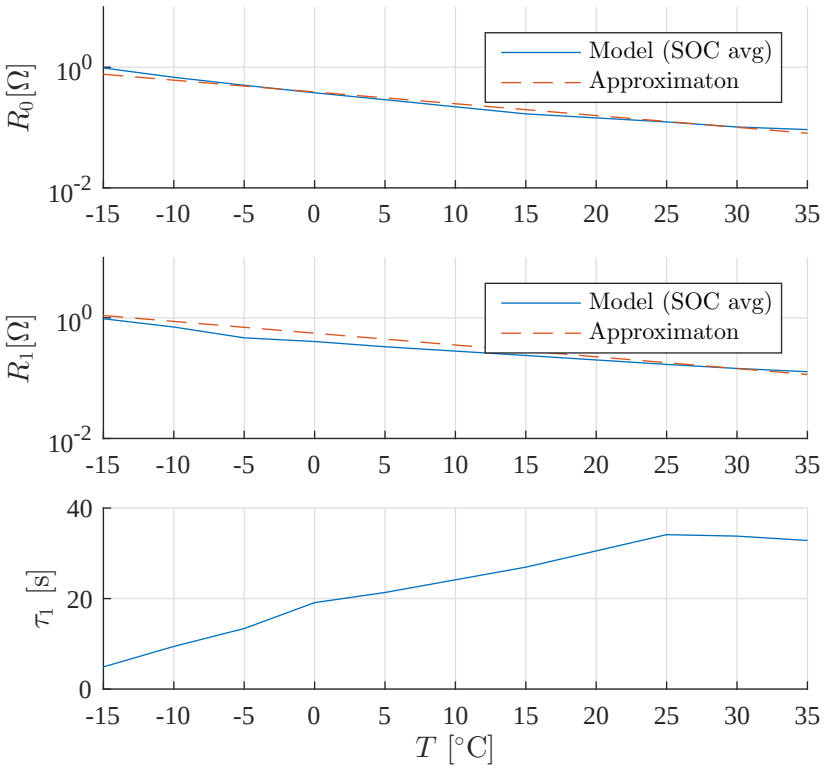

Figure 2: Equivalent circuit parameters used for model together with approximate values used in energy calculation.

6 Simulation study

The validity of the proposed expression is now demonstrated in a simulation study using two different drive cycles and initial temperatures ranging from −15 to +30°C. The simulated model is of a complete battery system, calibrated to vehicle tests. The temperature dependence for the parameters of the model is illustrated in Figure 2 together with the approximations used in the energy calculation. Since the resistances vary a lot over the temperature range, they are plotted using a logarithmic y-axis. In the model R_0 also varies with SOC, but here the average value over the SOC range 10–95% is illustrated. The values of the remaining model parameters are detailed in Table 1.

6.1 Thermal management

A simple thermal control law provides a realistic temperature trajectory of the battery pack. When the battery temperature exceeds 31°C, cooling with constant power is activated until the temperature drops below 28°C. These limits were chosen in order to keep the average temperature close to

Table 1: Parameters used in the energy calculation.

Parameter	Unit	Value
Q_{nom}	[As]	95040
m	[kg]	62
c	[J/(kg K)]	1330
$z_{\min}$	[%]	15
T_{ref}	[°C]	30
$\bar{R}_0$	[Ω]	0.101
$\bar{R}_1$	[Ω]	0.144
κ	[1/K]	0.043

the reference $T_{\text{ref}} = 30$°C. As already mentioned, no heating is applied. In Figure 3 the temperature trajectories for all tested cases are shown.

Remark. This deviates from the ideal control law assumed in (18).

6.2 Drive cycles

Two drive cycles are used to test the accuracy of the energy estimation, Hyzem rural (Hybrid zero emission) and UDDS (Urban Dynamometer Driving Schedule), both commonly used to evaluate energy consumption of electrified vehicles. The drive cycles are scaled so that Hyzem rural discharges the battery in one hour, while the UDDS takes approximately two hours. In Figure 4 both current profiles are shown together with the statistical measures based on Assumption 1.

6.3 Energy estimation accuracy

The energy efficiency of the battery pack, defined as

$$\eta = \frac{E_{\text{avail}}}{E_{\text{nom}}},$$

is illustrated in Figure 5 for true and estimated energies. When started at the reference temperature +30°C, resistive losses are approximately 4% of the total energy stored in the battery. When the initial temperature is -15°C, the losses are over 11%. The error of the approximate expression is within 0.7% in all tested cases -15, 0, 15, 25, and 30°C.

Since E_{avail} can be recalculated during the drive cycle, the accuracy is improved as the battery is drained. An example can be seen in Figure 6 where the full trajectory of true and estimated available energy are plotted for the Hyzem rural cycle with an initial battery temperature of -15°C,

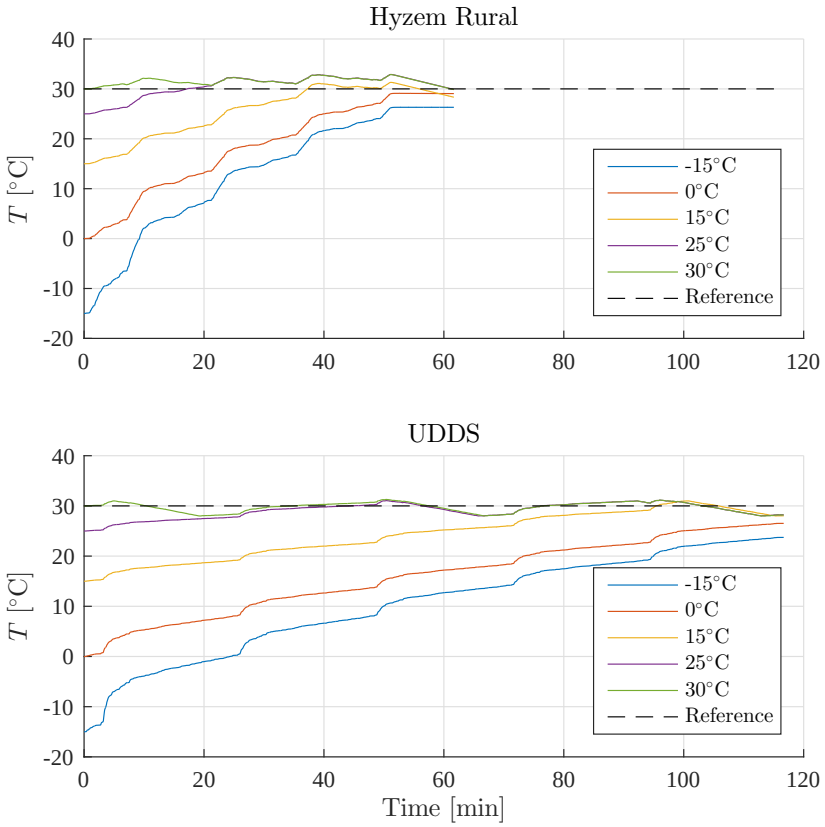

Figure 3: The temperature as a function of time for the two drive cycles.

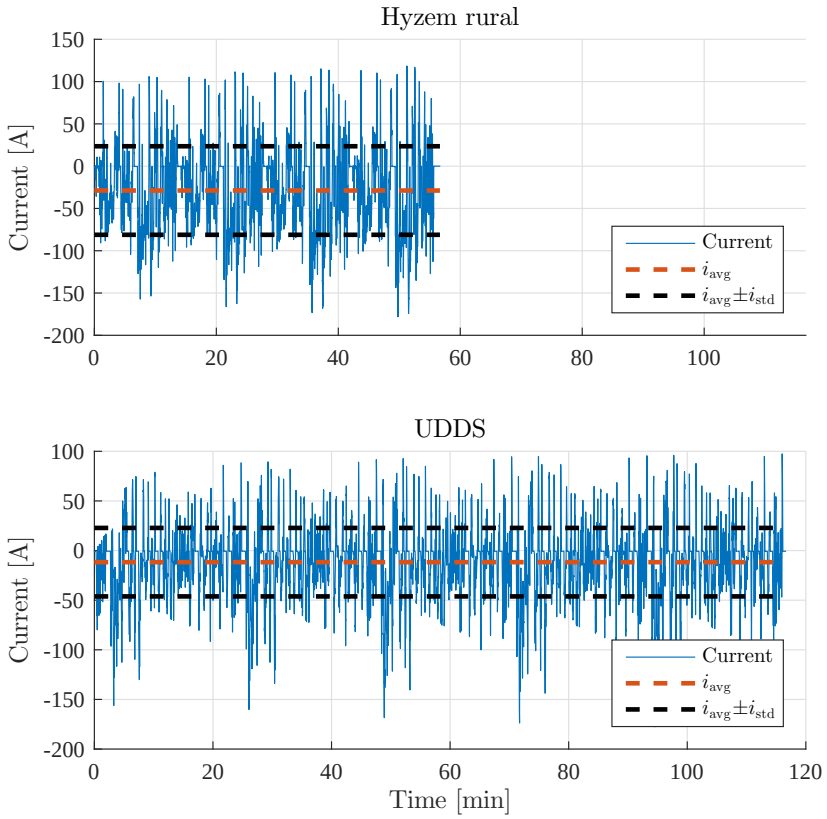

Figure 4: Current profiles used in the evaluation

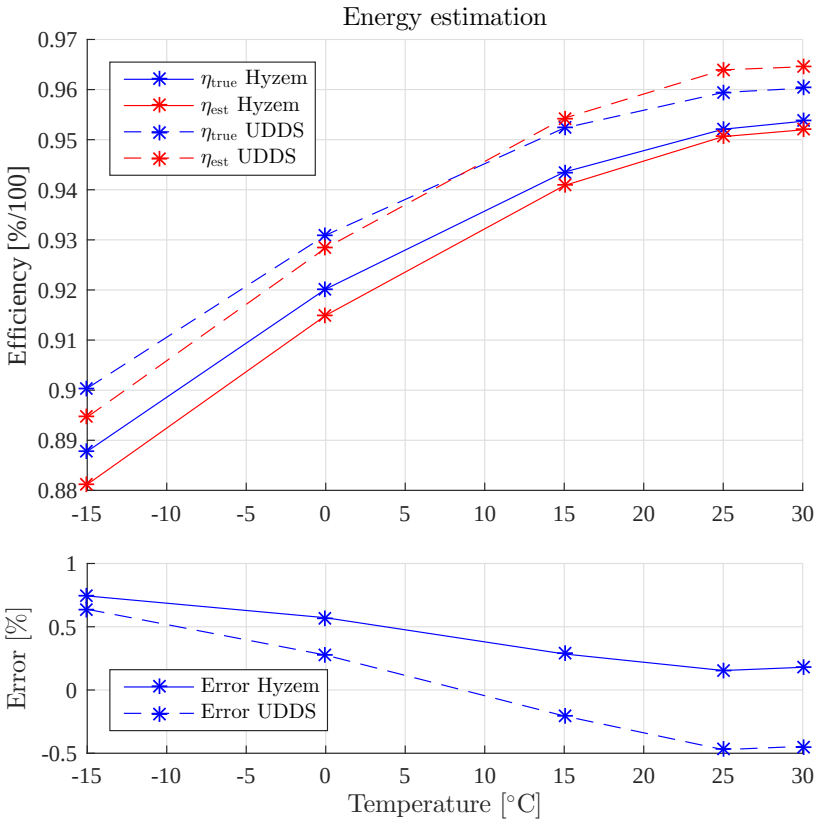

Figure 5: Actual and estimated energy efficiency as a function of temperature for the two drive cycles.

i.e. the case with largest error. The main reason for the convergence is that the temperature increases and, thus, comes closer to the reference temperature where the used approximations of the resistances are better.

7 Conclusions and future work

Estimating the remaining available energy in a battery pack is an important function for electrified vehicles. We have derived an analytic expression for the available energy that relies on statistical information about the future drive cycle, and which handles temperature transients after starting with a cold battery.

The accuracy is within 0.7% of the true energy when evaluated using a highly accurate battery pack model calibrated to vehicle data, which can be considered very good. In a real-world application the accuracy may be reduced because of larger uncertainties of parameters, states, and the future drive cycle.

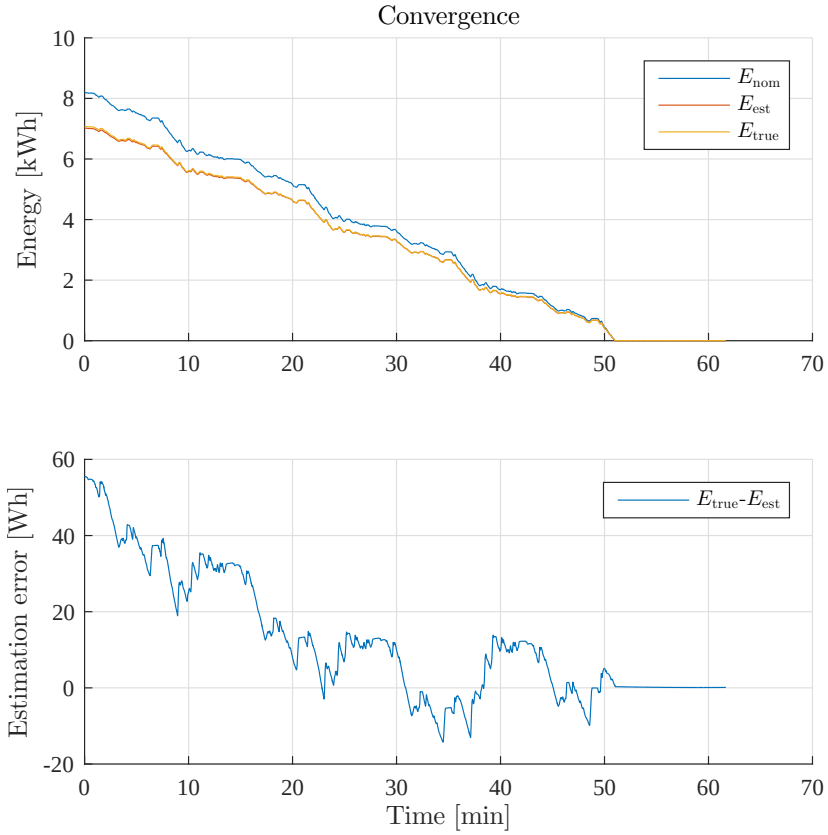

Figure 6: Trajectory of true and estimated energy for Hyzem rural with initial temperature of -15°C. The initial error in energy estimation is reduced as the temperature of the battery increases, and for the lower SOC region they are almost identical.

Some of the assumptions were introduced to simplify the expressions and improve readability of the article. Better approximations of e.g. resistances can be included. Future work is needed to handle heating when starting with a cold battery. Another interesting work is to consider the case when the future power, rather than future current, is known. This introduces difficulties since the current will then depend on the voltage response of the battery system and an analytic expression can most likely no longer be derived.

Acknowledgements

This work was supported by Volvo Cars and Chalmers, and financed by the Swedish Energy Agency through the project "Life-long battery control" (P39786-1).

References

[1] Y. Zhang, W. Wang, Y. Kobayashi, and K. Shirai, "Remaining Driving Range Estimation of Electric Vehicle," *2012 IEEE International Electric Vehicle Conference*, pp. 1–7, 2012.

[2] A. Barai, K. Uddin, W. D. Widanalage, A. McGordon, and P. Jennings, "The effect of average cycling current on total energy of lithium-ion batteries for electric vehicles," *Journal of Power Sources*, vol. 303, pp. 81–85, 2016.

[3] Y. Wang, C. Zhang, and Z. Chen, "An adaptive remaining energy prediction approach for lithium-ion batteries in electric vehicles," *Journal of Power Sources*, vol. 305, pp. 80–88, 2016.

[4] W. Zhang, W. Shi, and Z. Ma, "Adaptive unscented Kalman filter based state of energy and power capability estimation approach for lithium-ion battery," *Journal of Power Sources*, vol. 289, pp. 50–62, 2015.

[5] G. Dong, X. Zhang, C. Zhang, and Z. Chen, "A method for state of energy estimation of lithium-ion batteries based on neural network model," *Energy*, vol. 90, pp. 879–888, 2015.

[6] C. Lin, H. Mu, R. Xiong, and J. Cao, "Multi-model probabilities based state fusion estimation method of lithium-ion battery for electric vehicles: State-of-energy," *Applied Energy*, vol. 194, pp. 560–568, 2017.

[7] L. Zheng, J. Zhu, G. Wang, T. He, and Y. Wei, "Novel methods for estimating lithium-ion battery state of energy and maximum available energy," *Applied Energy*, vol. 178, pp. 1–8, 2016.

[8] G. Liu, M. Ouyang, L. Lu, J. Li, and J. Hua, "A highly accurate predictive-adaptive method for lithium-ion battery remaining discharge energy prediction in electric vehicle applications," *Applied Energy*, vol. 149, pp. 297–314, 2015.

[9] R. Wang and S. M. Lukic, "Review of driving conditions prediction and driving style recognition based control algorithms for hybrid electric vehicles," *2011 IEEE Vehicle Power and Propulsion Conference, VPPC 2011*, 2011.

[10] J. Park, Y. L. Murphey, R. McGee, J. G. Kristinsson, M. L. Kuang, and A. M. Phillips, "Intelligent trip modeling for the prediction of an origin-destination traveling speed profile," *IEEE Transactions on Intelligent Transportation Systems*, vol. 15, no. 3, pp. 1039–1053, 2014.

[11] J. Jaguemont, L. Boulon, and Y. Dubé, "A comprehensive review of lithium-ion batteries used in hybrid and electric vehicles at cold temperatures," *Applied Energy*, vol. 164, pp. 99–114, 2016.

[12] Q. Gong, Y. Li, and Z. Peng, "Power management of plug-in hybrid electric vehicles using neural network based trip modeling," *American Control Conference*, pp. 4601–4606, 2009.

[13] J. Kim, J. Shin, C. Jeon, and B. Cho, "High accuracy state-of-charge estimation of Li-Ion battery pack based on screening process," *Conference Proceedings - IEEE Applied Power Electronics Conference and Exposition - APEC*, pp. 1984–1991, 2011.

[14] B. Fridholm, T. Wik, and M. Nilsson, "Robust recursive impedance estimation for automotive lithium-ion batteries," *Journal of Power Sources*, vol. 304, pp. 33–41, 2016.

[15] G. Liu, M. Ouyang, L. Lu, J. Li, and X. Han, "Analysis of the heat generation of lithium-ion battery during charging and discharging considering different influencing factors," *Journal of Thermal Analysis and Calorimetry*, vol. 116, no. 2, pp. 1001–1010, 2014.

[16] K. Makinejad, R. Arunachala, S. Arnold, H. Ennifar, H. Zhou, and A. Jossen, "A Lumped Electro - Thermal Model for Li - Ion Cells in Electric Vehicle Application," in *EVS28, Kintex, Korea*, 2014, pp. 1–14.

[17] J. Jaguemont, L. Boulon, and Y. Dube, "Characterization and Modeling of a Hybrid-Electric-Vehicle Lithium-Ion Battery Pack at Low Temperatures," *IEEE Transactions on Vehicular Technology*, vol. 65, no. 1, pp. 1–14, 2015.

[18] M. Debert, G. Colin, G. Bloch, and Y. Chamaillard, "An observer looks at the cell temperature in automotive battery packs," *Control Engineering Practice*, vol. 21, no. 8, pp. 1035–1042, 2013.

[19] J. Remmlinger, M. Buchholz, M. Meiler, P. Bernreuter, and K. Dietmayer, "State-of-health monitoring of lithium-ion batteries in electric vehicles by on-board internal resistance estimation," *Journal of Power Sources*, vol. 196, no. 12, pp. 5357–5363, 2011.